



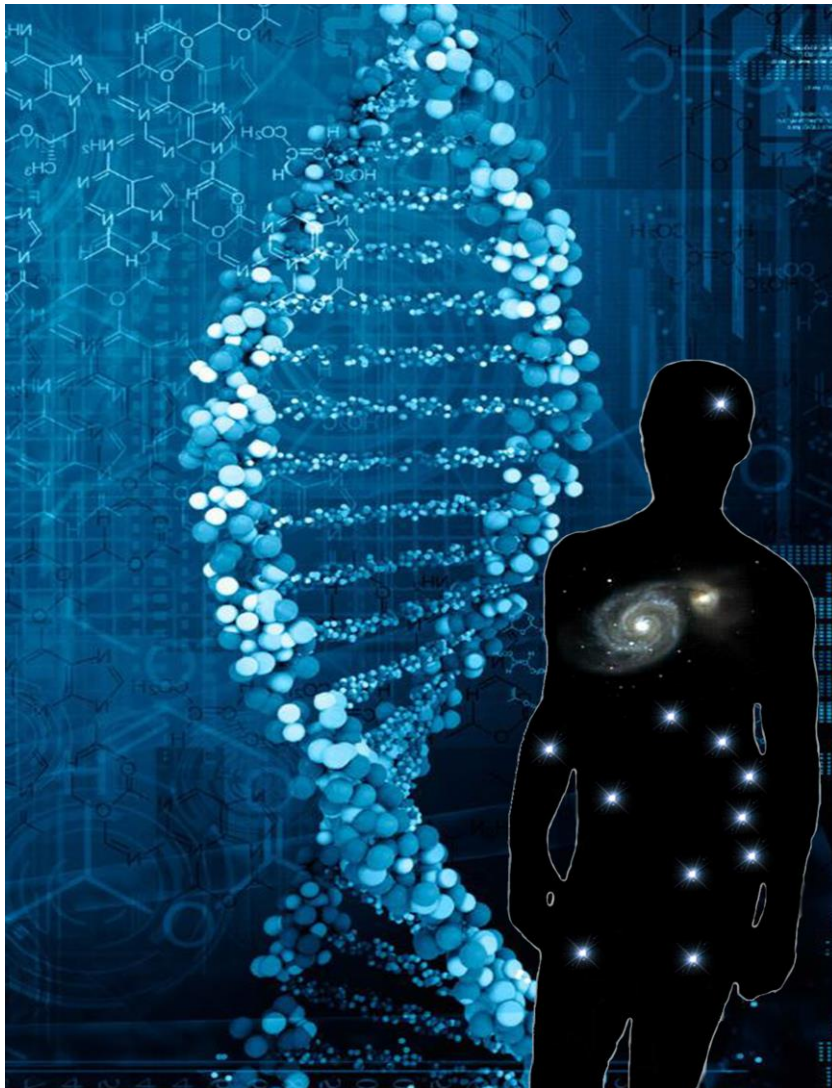
**UniversitätsSpital
Zürich**

Direktion Forschung und Lehre

Programm

16th Day of Clinical Research
Georg-Friedrich-Götz-Preisverleihung 2017

Zurich, February 9, 2017



**Universität
Zürich**^{UZH}

Assoziierte Kliniken

Universitätsklinik Balgrist

Kinderspital Zürich

Psychiatrische Universitätsklinik Zürich

Zentrum für Zahnmedizin

Committee Day of Clinical Research

Prof. Dr. A. Aguzzi
Prof. Dr. O. Distler
Prof. Dr. S. Gay
Prof. Dr. R. Graf
Prof. Dr. H. Moch
Prof. Dr. G. Senti
Prof. Dr. R. Speck
Prof. Dr. M. Weller
Prof. Dr. A. von Eckardstein
PD Dr. Mira Katan Kahles
PD Dr. Paolo Cinelli
Robin Schneider, MBA

Table of contents

Program	1 - 3
List of Abstracts	4. - 17
Abstracts	18 - 174

Programm

Donnerstag, 9. Februar 2017

Grosser Hörsaal Ost

08.15 **Eröffnung**

Prof. Dr. med. Gabriela Senti
Direktorin Forschung und Lehre, UniversitätsSpital Zürich

08.20 **Begrüssung**

Prof. Dr. med. Gregor Zünd
Vorsitzender der Spitaldirektion

08.25 **Begrüssung**

Prof. Dr. med. Rainer Weber
Dekan der Medizinischen Fakultät der Universität Zürich

Session 1: Cardiovascular/Metabolics/Endocrinology

Chairpersons: Dr. med. Jelena-Rima Templin-Ghadri, Prof. Dr. med. Felix Tanner

08.35 Wissenschaftliches Hauptreferat

“Gender in Cardiovascular Disease: Back to Basics”

Prof. Dr. med. Cathérine Gebhard, Oberärztin, Klinik für Nuklearmedizin, UniversitätsSpital Zürich

08.55 **VEGF-A regulates endothelial HDL transcytosis**

S. Velagapudi, L. Roher, A. von Eckardstein

09.05 **Heart dysfunction in systemic sclerosis: involvement of a novel fibrogenic stromal cell subset**

M. Stellato, M. Rudinik, F. Renoux, E. Pachera, K. Soltar, K. Klingel, J. Hennes, P. Blyszczuk, O. Distler, G. Kania

09.15 **Small pericardial effusions predict outcome in heart transplant recipients**

S. F. Stämpfli, T. Özkartal, N. Hagenbuch, S. Bernhart, A. J. Flammer, A. Vecchiati, G. M. Fröhlich, F. Ruschitzka, L. Held, F. C. Tanner

09.25 **Coffee Break**

Session 2: Hematology/Oncology

Chairpersons: Prof. Dr. Peter J. Wild, Prof. Dr. Felix Niggli

09.40 Wissenschaftliches Hauptreferat

“Molecular pathogenesis of diffuse large B-cell lymphoma: opportunities for personalized treatment strategies“

Prof. Dr. rer. nat. Anne Müller, Gruppenleiterin, Institut für Molekulare Krebsforschung, Universität Zürich

10.00 **Synergistic activity of NKG2D-based chimeric antigen receptor (CAR)-T cells and radiotherapy against glioma**

T. Weiss, M. Weller, M. Pruschy, Ch. Sentman, P. Roth

10.10 **Role of SUV39H1 in ADAM17-mediated radioresistance**

S. Bender, A. Sharma, A. Brogini-Tenzer, M. Pruschy

10.20 **Improved cancer immunotherapy by a CD25-mimobody conferring selectivity to human interleukin-2**

N. Arenas-Ramirez, C. Zou, S. Popp, D. Zingg, B. Brannetti, E. Wirth, Th. Calzascia, J. Kovarik, L. Sommer, G. Zenke, J. Woytschak, C. H. Regnier, A. Katopodis, O. Boyman

Session 3: Regenerative Medicine and Advanced Technologies

Chairpersons: Prof. PhD Lukas Sommer, Prof. Dr. Dr. med. Maximilian Emmert

- 10.35 Wissenschaftliches Hauptreferat
“CRISPR/Cas9 and organoids: Tools for disease-modeling and gene-therapy”
Prof. Dr. Gerald Schwank, Forschungsgruppenleiter, Stem Cell Biology & Diseases Modeling, Institute for Molecular Health Sciences, ETH Zürich
- 10.55 **Exogenous Melatonin Rescues Small-for-Size Liver Graft Failure**
Z. Song, E. Maurizio, B. Humar, N. Borgeaud, R. Graf, P.-A. Clavien, Y. Tian
- 11.05 **Deciphering hematopoietic stem cell niche factors in bioengineered human bone marrow models in vivo**
Q. Vallmajó-Martin, M. Lütolf, M. Ehrbar
- 11.15 **Systemic Application of Adipose Derived Stem Cells Accelerates Functional Peripheral Nerve Regeneration in a Rodent Transection and Repair Model**
R. Schweizer, J. Schnider, P. Fanzio, W. Tsuji, M. Solari, K. Marra, J.P. Rubin, J. Plock, V. Gorantla
- 11.30 Lunch/Poster viewing

Session 4: Infection/Immunity/Inflammation

Chairpersons: Prof. Dr. med. Dr. phil. nat. Jana Pachlopnik, PD Dr. med. Jan S. Fehr

- 13.25 Wissenschaftliches Hauptreferat
“Targeted therapies in systemic sclerosis: challenges in translation from bench to bedside in fibrotic diseases”
Prof. Dr. med. Oliver Distler, Klinikdirektor, Klinik für Rheumatologie, UniversitätsSpital Zürich
- 13.45 **PTPN2 controls intestinal inflammation and promotes colitis-associated tumor formation via control of inflammasome activation and IL-1 α release**
M. Spalinger, L. Hering, R. Manzini, J. Riggs, C. Gottier, K. Atrott, T. Raselli, A. Fettelschoss, Th. Kündig, G. Rogler, M. Scharl
- 13.55 **Targeted Nuclear Imaging for the Early Detection of Lung Involvement in Systemic Sclerosis**
J. Schniering, S. Haller, M. Benesova, Z. Guo, C. Feghali-Bostwick, R. Schibli, O. Distler, C. Müller, B. Maurer
- 14.05 **Optimizing STI Screening Among HIV positive MSM using a Simple Risk Evaluation**
D. Braun, A. Marzel, D. Bircher, P. Schreiber, C. Grube, A. Scherrer, R. Kouyos, H. Günthard

Session 5: Neurosciences/Pharmacology

Chairpersons: PD Dr. med. Mira Katan Kahles, Prof. Dr. med. Gerd-Achim Kullak-Ublick

- 14.20 Wissenschaftliches Hauptreferat
“Basic research insights into neurodevelopmental disorders”
Prof. Dr. med. Theofanis Karayannis, Assistenzprofessor, Institut für Hirnforschung, Universität Zürich
- 14.40 **Progressive cone degeneration in a chronic hypoxia-like situation can be rescued by targeting Hif1 α**
M. Barben, C. Schori, M. Samardzija, C. Grimm
- 14.50 **Rational design of anti-PrP antibodies to block prion induced neurodegeneration**
A. Senatore, C. Tiberi, G. Horny, S. Fels, N. George, T. Pietzonka, S. Hornemann, A. Aguzzi
- 15.00 **Electrophysiological changes in mice devoid of cellular prion protein**
M.-A. Wulf, M. Nuvolone, A. Senatore, A. Aguzzi
- 15.15 Coffee Break

Session 6: Klinische Forschungsschwerpunkte KFSP

- 15.30 **Präsentation**
KFSP: Multiple Sklerose
Prof. Dr. med. Roland Martin, Leitender Arzt, Klinik für Neurologie, UniversitätsSpital Zürich
- 15.50 **Präsentation**
KFSP: Hemato-Lymphatic Diseases
Prof. Dr. med. Markus Manz, Klinikdirektor, Klinik für Hämatologie, UniversitätsSpital Zürich
- 16.10 **Präsentation**
KFSP: Liver Tumors
Prof. Dr. phil. Rolf Graf, Abteilungsleiter Wissenschaft, Zentrum Forschung Chirurgie
UniversitätsSpital Zürich
- 16.35 **Verleihung Day of Clinical Research Preis**
- 17.00 **Verleihung Georg Friedrich Götz-Preis 2017**
- 18.15 **Apéro**

Cardiovascular Diseases / Metabolics / Endocrinology

Basic Research

3630

I. Alecu, A. Von Eckardstein, T. Hornemann
Elucidating Novel Metabolic Pathways of the Cytotoxic 1-Deoxysphingolipids

3631

R. Steiner, A. Von Eckardstein, T. Hornemann
Elucidating the metabolic pathway of atypical deoxymethylsphingolipids

3661

M. Stellato, M. Rudnik, F. Renoux, E. Pachera, K. Sotlar, K. Klingel, J. Henes, P. Blyszczuk, O. Distler, G. Kania
Heart dysfunction in systemic sclerosis: involvement of a novel fibrogenic stromal cell subset

3662

G. Karsai, T. Hornemann, A. Von Eckardstein
The role of 1-deoxy-sphingolipids in cell migration and wound healing

3684

S. Velagapudi, L. Rohrer, A. Von Eckardstein
VEGF-A regulates endothelial HDL transcytosis

3689

P. Zanoni, S. Velagapudi, M. Keel, R. Meier, S. Stoma, S. Nørrelykke, L. Rohrer, A. Von Eckardstein
A genome-wide siRNA screen as a tool to unveil new players in hepatic High Density Lipoprotein metabolism

3711

A. Zhakupova, N. Debeuf, M. Krols, I. Alecu, A. Von Eckardstein, B.N. Lambrecht, S. Janssens, T. Hornemann
The Role of ORMDL Proteins as Regulators of Mammalian Serine Palmitoyltransferase

3717

ML. Lone, Tho. Hornemann
Structural and Functional Characterization of Serine Palmitoyl Transferase in Mammals

3721

S. Suriyanarayanan, T. Hornemann, A. Von Eckardstein
Elucidating the pathomechanism of neurotoxic 1-deoxysphingolipids

3785

T. Skaria, J. Vogel
 α CGRP suppresses the proliferation and Angiotensin II induced myofibroblast differentiation of cardiac fibroblasts

Clinical Trials

3617

DC. Benz, F. Mikulicic, C. Gräni, D. Moret, M. Possner, OF. Clerc, AA. Studer Bruengger, O. Gaemperli, RR. Buechel, AP. Pazhenkottil, PA. Kaufmann
CT-derived Corrected Contrast Opacification Decrease Predicts Long-Term Outcome in Patients With Coronary Stenosis

3639

J. Schneider, V. Lapierre-Fetaud, F. Fluri, A. Luft, JC. Sanchez, M. Katan
Serum Amyloid A - a novel predictor of stroke associated infections

3690

SF. Stämpfli, T. Özkartal, N. Hagenbuch, B. Bernhart, AJ. Flammer, A. Vecchiati, GM. Fröhlich, F. Ruschitzka, L. Held, FC. Tanner
Small pericardial effusions predict outcome in heart transplant recipients

3692

SF. Stämpfli, L. Erhart, N. Hagenbuch, BE. Stähli, C. Gruner, M. Greutmann, M. Niemann, BA. Kaufmann, R. Jenni, L. Held, FC. Tanner

proBNP is strong predictor of outcome in left ventricular non-compaction cardiomyopathy

3732

K. Slankamenac, G. Haberkorn, O. Meyer, H.A. Bischoff-Ferrari, D.I. Keller

Geriatric Assessment May Reduce Re-Visits in the Emergency Department in Older Patients with Positive Identification of Senior at Risk (ISAR) Screening

Hematology / Oncology

Basic Research

3670

R. Myburgh, J. Jonathan, S. Surema, M. Michal, S. Isringhausen, E. Edo, AA. Müller, D. Neri, B. Becher, M. Van den Broek, MG. Manz
Treatment of Acute Myeloid Leukemia (AML) with Immunotherpaies

3695

MS. Silginer, SN. Nagy, CH. Happold, HS. Schneider, MW. Weller, PR. Roth
Autocrine activation of the IFN signaling pathway modulates the immunogenicity of glioma cells

3703

C. Yang, O. Shakhova
The Metastatic Role of SOX9 in Neuroblastoma

3734

P-A. Ahorner, I-E. Symeonidou, D. Fink, M. Stucki
The role of TopBP1 in the cellular response to DNA double-strand breaks

3735

T. Weiss, M. Weller, M. Pruschy, C. Sentman, P. Roth
Synergistic activity of NKG2D-based chimeric antigen receptor (CAR)-T cells and radiotherapy against glioma

3739

A. Krättli, O. Shakhova
The role of SOX10 in melanoma resistance

3743

JH. Jang, F. Janker, S. Arni, N. Borgeaud, Y. Yamada, W. Weder, W. Jungraithmayr
NK cell recruitment via CD26/DPP4 inhibition decreased lung cancer growth

3746

M. Gualandi, O. Shakhova
Identifying the cell of origin of neuroblastoma

3753

I.E. Symeonidou, P.A. Ahorner, D. Bundschuh, D. Fink, M. Stucki
Nucleolar localization of TOPBP1 in response to DNA double strand breaks

3760

MB. Kirschner, B. Vrugt, M. Friess, M. Meerang, PJ. Wild, N. Van Zandwijk, G. Reid, W. Weder, I. Opitz
Refinement of the prognostic miR-Score for use in diagnostic specimens from chemo-naïve malignant pleural mesothelioma patients

3761

J. Kresoja, S. Sulemani, M. Kirchner, M. Ronner, G. Reid, S. Kao, BW. Schwaller, RA. Stahel, W. Weder, E. Felley-Bosco
Post-Transcriptional regulation of mesothelioma marker calretinin

3763

A. Gomariz, S. Isringhausen, P. Helbling, U. Suessbier, G. Paul, G. Szekely, O. Goksel, S. Stoma, S. Nørrelykke, C. Nombela-Arrieta
Applying 3D quantitative microscopy to study global topography and cellular interactions in the bone marrow

3764

S. Steiner, G. Wanner-Seleznik, T. Reding, A. Dittmann, A. Perren, E. Eliane, M. Heikenwälder, R. Graf
Gastrokine as a novel potential biomarker for premalignant pancreatic lesions

3766

L. Wu, W. Blum, L. Pecze, T. Henzi, V. Serre-Beinier, H. Rerhauer, C. Aquino, B. Vrugt, M. De Perrot, B. Schwaller, E. Felley-Bosco
Role of macrophages and mesothelial precursors accumulation in tumor development in asbestos-exposed

mice

3768

M. Meerang, J. Kreienbühl, M. Friess, M. Kirchner, W. Weder, I. Opitz
Targeting cullin ubiquitin ligase leads to growths arrest in malignant pleural mesothelioma cells

3771

R. Zuber, P-K. Bode, C. Matter, U. Camenisch, B. Bode, R. Stupp, O. Shakhova, C. Britschgi
SOX10 as a therapeutic target in Clear Cell Sarcoma

3778

U. Süssbier, HC. Wong, S. Isringhausen, A. Gomariz-Carillo, P. Helbling, T. Nagasawa, AM. Müller, MG. Manz
Functional and structural dynamics of the bone marrow stromal microenvironment after cytoreductive therapies

3779

P. Helbling, S. Isringhausen, T. Nagasawa, C. Nombela-Arrieta
Multidimensional analysis of the hematopoietic microenvironment during embryonic development and early postnatal life.

3783

V. Lysenko, N. Wildner, RA. Flavell, MG. Manz, A. Theocharides
Establishment of a patient-derived myelofibrosis xenograft mouse model

3790

GS. Spaltro
Dissecting mechanisms that drive HSC towards quiescence

Translational Research

3627

E. Bellini, N. Valtcheva, PJ. Wild
Identification of the molecular drivers of endometrial cancer progression

3628

D. Hinger, F. Grossmann, P. Ruiz Sanchez, C. Maake
The novel photoactive nano drug HypLip as early detection and treatment modality for gastric cancer

3682

S. Ehrbar, S. Schmid, S. Klöck, M. Guckenberger, O. Riesterer, S. Tanadini-Lang
Validation of Dynamic Treatment-Couch Tracking for Motion Compensation during Prostate SBRT

3683

K. Oehl, B. Vrugt, U. Wagner, M. Meerang, M.B. Kirschner, W. Weder, I. Opitz, P.J. Wild
Tracking the Clonal Origin and Chemotherapy Resistance of Malignant Pleural Mesothelioma

3719

J. Kraysenbuehl, M. Di Martino, M. Guckenberger, N. Andratschke
Automated VMAT planning for whole brain irradiation with hippocampus sparing: improved target coverage while avoiding unnecessary hot spots in the brain

3723

S. Bender, A. Sharma, A. Brogini-Tenzer, M. Pruschy
Role of SUV39H1 in ADAM17-mediated radioresistance

3741

A. Okonska, R. Parrotta, W. Weder, R. Stahel, L. Lorenza, E. Felley-Bosco
A novel BRCA1-associated protein-1 isoform affects response of mesothelioma cells to drugs impairing BRCA1-mediated DNA repair

3747

I. Grgic, J. Ott, S. Deschoemaeker, A. Heyerick, M. Pruschy
Modulation of tumor hypoxia for hypofractionated radiotherapy

3751

R. Casanova, U. Rulle, H. Moch, A. Soltermann

Prognostic relevance of lung squamous cell carcinoma tumor fragmentation, a histologic marker of increased tumor invasiveness

3752

A. Schindler, A. Courtier, M. Goldinger, F. Jaberg-Bentele, M. Manuel, S. Perez, J. Mouret, T. Nguyen-Kim1, I.G. Raaijmakers, P. Kvistborg, N. Pasqual, B.A. Haanen, R. Dummer, P. Levesque

The peripheral blood TCR repertoire might facilitate patient stratification for immune checkpoint blockade inhibition in metastatic melanoma

3755

M. Nesteruk, O. Riesterer, K. Ikenberg, S. Stieb, H. Moch, G. Studer, M. Guckenberger, S. Tanadini-Lang
Pre-treatment CT radiomics predicts HPV status and local tumor control after definitive radiochemotherapy in head and neck cancer

3774

Ms. Irmisch, Ms. Freiburger, Mr. Cheng, Mr. Pornputtpong, Ms. Singer, Mr. Thurnheer, Mr. Stekhoven, Ms. Halaban, Mr. Beerenwinkel, Mr. Dummer, Mr. Levesque

Whole exome sequencing and a novel gene panel as precision medicine tools for metastatic melanoma patients

3789

N. Arenas-Ramirez, C. Zou, S. Popp, D. Zingg, B. Brannetti, E. Wirth, T. Calzascia, J. Kovarik, L. Sommer, G. Zenke, J. Woytschak, C.H. Regnier, A. Katopodis, O. Boyman

Improved cancer immunotherapy by a CD25-mimobody conferring selectivity to human interleukin-2

Clinical Trials

3626

O. Lauk, M. Friess, M. Meerang, M. Kirschner, C. Bommeli, RA. Stahel, W. Weder, I. Opitz

Is toxicity increased by adding intraoperative chemotherapy to preoperative induction chemotherapy for mesothelioma patients?

3648

I. Opitz, M. Friess, M. Meerang, M. Kirschner, K. Berard, O. Lauk, W. Weder

Long Term Freedom from Recurrence after Induction Chemotherapy and Extrapleural Pneumonectomy in Mesothelioma Patients

3748

S. Ferrari, U. Schanz, P. Samaras, M. Manz, J. Grassinger

Analysis of the accuracy of a calculation tool to predict the yield of hematopoietic stem cells after leukapheresis

3776

M. Wösle, IF. Ciernik

Relapsing Solitary Brain Metastases Treated with HybridArc™: ICRU 50/62 for Small Volumes

3784

CM. Wilk, I. Weber, K. Seidl, AM. Müller, C. Rachmühl, A. Holzmann-Bürgel, SP. Kuster, U. Schanz, AS. Zinkernagel

Impact of oral gut decontamination on Staphylococcus aureus colonization in patients undergoing hematopoietic stem cell transplantation

Regenerative Medicine and Advanced Technologies

Basic Research

3611

P. Kron, M. Linecker, P. Limani, A. Schlegel, P. Kambakamba, JM. Lehn, C. Nicolau, R. Graf, B. Humar, PA. Clavien

Hypoxia driven Hif 2a coordinates mouse liver regeneration by coupling parenchymal growth to vascular expansion

3636

U. Blache, V. Milleret, M. Ehrbar

Synthetic materials meet 3D cell biology: PEG hydrogels as blank slate to study ECM-formation in 3D

3664

E. Malagola, R. Chen, M. Bombardo Ayats, K. Schlesinger, T. Reding, A. Von Eckardstein, R. Graf, S. Sonda

Role of Thyroid hormone T3 in acinar cell proliferation following cerulein induced acute pancreatitis

3699

A. Bopp, P. Wolint, J. Buschmann, MY. Emmert, Y. Tian, O. Evrova, M. Hilbe, P. Giovanoli, F. Maisano, SP. Hoerstrup

Effects of hcpMSCs seeded as single cells or as 3D-microtissues onto vascularization of a collagen Matricel® scaffold on the CAM assay

3727

M. Langiewicz, A. Schlegel, E. Saponara, M. Linecker, P. Borger, R. Graf, B. Humar, PA. Clavien

Indian hedgehog mediates early acceleration of liver regeneration induced by ALPPS two-staged hepatectomy

3782

M. Schneider, A. Gupta, P. Borger, R. Graf, P-A. Clavien

Adipose tissue-derived mesenchymal stem cells for the treatment of small for size liver

Translational Research

3613

SC. Hess, WJ. Stark, S. Märsmann, P. Giovanoli, P. Cinelli, J. Buschmann

Modulation of gene expression in human adipose-derived stem cells seeded on PLGA or biomimetic nanocomposite: comparison of 2D films and 3D electrospun meshes – the “real” comparison

3614

W. Baumgartner, I. Schneider, SC. Hess, WJ. Stark, S. Märsmann, P. Giovanoli, P. Cinelli, J. Buschmann

Static, dynamic, mechanical loading – different in vitro culture conditions and their impact on the gene expression of human primary adipose-derived stem cells seeded on a biomimetic nanocomposite

3615

SC. Hess, EM. Schneider, WJ. Stark, S. Märsmann, P. Giovanoli, P. Cinelli, J. Buschmann

Influence of amorphous tricalcium phosphate nanoparticles incorporated in PLGA on the gene expression of human adipose-derived stem cells seeded on casted films or electrospun meshes

3616

O. Evrova, G. Meier Bürgisser, C. Ebnöther, C. Scalera, E. Elias, JG. Jess, P. Giovanoli, M. Calcagni, V. Vogel, J. Buschmann

Cellular response towards implant delivering PDGF-BB to fully transected rabbit Achilles tendon three weeks post-operation

3675

R. Schweizer, S. Oksuz, B. Banan, JA. Plock, VS. Gorantla, P. Fontes

Attenuation of Ischemia-Reperfusion Injury after ex vivo Preservation of Vascularized Composite Allografts by Subnormothermic Machine Perfusion with Hemoglobin-based Oxygen Carriers

3676

R. Schweizer, JT. Schnider, PM. Fanzio, W. Tsuji, MG. Solari, KG. Marra, JP. Rubin, JA. Plock, VS.

Gorantla

Systemic Application of Adipose Derived Stem Cells Accelerates Functional Peripheral Nerve Regeneration in A Rodent Transection and Repair Model

3688

L. Ahnen, H. Stachel, S. Kleiser, C. Hagmann, J. Jiang, A. Kalyanov, S. Lindner, M. Wolf, S. Sanchez
Near-Infrared Image Reconstruction of Newborn's Brains: Development and Validation of the Light Sensor Prototype

3698

ZL. Song, E. Maurizio, B. Humar, N. Borgeaud, R. Graf, PA. Clavien, YH. Tian
Exogenous Melatonin Rescues Small-for-Size Liver Graft Failure

3791

Q. Vallmajó-Martín, Q. Vallmajó-Martin, M. Lütolf, M. Ehrbar
Deciphering hematopoietic stem cell niche factors in bioengineered human bone marrow models in vivo

Infection / Immunity / Inflammation

Basic Research

3624

YT. Chang, M. Ziegler, D. Ignatova, P. Ivanov, R. Profanter, K. Kerl, R. Dummer, E. Contassot, F. French, A. Cozzio, S. Misailovic, W. Hoetzenecker, M. Vechev, E. Guenova
Ineffective antibody-dependent cellular cytotoxicity in patients with late stage cutaneous T cell lymphoma

3641

T. Skaria, E. Bachli, G. Schoedon
WIF1 prevents WNT5A-mediated actin cytoskeleton remodeling and monolayer disintegration in human vascular endothelial cells

3645

M. Bombardo Ayats, E. Saponara, H. Malagola, R. Chen, R. Graf, S. Sonda
Inhibition of Class I HDAC ameliorates chronic pancreatitis by reducing leukocyte recruitment, acinar-to-ductal metaplasia and fibrosis

3656

M. Rudnik, M. Stellato, E. Pachera, B. Maurer, J.C. Henes, K. Klingel, K. Sotlar, P. Blyszczuk, O. Distler, G. Kania
Monocytes/Neurotrophins/Myofibroblasts As a Novel Axis in Systemic Sclerosis

3657

F. Renoux, M. Stellato, O. Boyman, D. Impellizzieri, J. Distler, C. Dees, A. Subramaniam, G. Kania, O. Distler
The transcription factor Fra2 is playing a key role in the control of Treg development and autoimmunity

3658

V. Chandrasekar, M. Einsiedler, U. Herrmann, H. Budka, A. Aguzzi
Human iPS stem cell based in vitro modeling and characterization of OPRI genetic prion disease:

3673

J. Cosin-Roger, S. Bengs, S. Lang, M. Turina, A. Rickenbacher, K. Seuwen, P. Ruiz, B. Misselwitz, G. Rogler, C. De Vallière
OGR1 (GPR68) expression is increased in intestinal inflammation and correlates with disease activity in patients with IBD

3674

YL. Kok, S. Schmutz, A. Inderbitzin, M. Shilaih, A. Kelley, C. Berens, HF. Günthard, KJ. Metzner
A Novel HIV-1-based Vector that Reproduces Features of Active and Latent HIV-1 Infections

3678

R. Chen, T. Hornemann, S. Camargo, R. Graf, S. Sonda
1-Deoxy-sphingolipids, novel biomarkers of diabetes, are cytotoxic for exocrine pancreatic cells

3679

R. Chen, E. Malagola, G. Mosca, M. Dietrich, E. Saponara, K. Grabliauskaite, R. Zuellig, O. Tschopp, R. Graf, S. Sonda
Akt1 regulates the development of inflammation and tissue regeneration during acute pancreatitis

3685

J. Cosin-Roger, C. Stanzel, A. Terhalle, L. Wolfram, K. Atrott, PA. Ruiz, H. Melhem, MR. Spalinger, S. Lang, I. Frey-Wagner, M. Scharl, M. Hausmann, G. Rogler
Gp96 deficiency partially affects TLR4 functionality due to an impaired ERK and p38 phosphorylation

3709

D. Impellizzieri, ME. Räber, W. Jungraithmayr, O. Boyman
Characterization of human skin-homing T cells in health and disease.

3710

M. Malehmir, E. Kotsiliti, D. Pfister, V. Leone, C. Deppermann, J. Volz, D. Dauch, B. Nieswandt, L. Zender, A. Weber, M. Heikenwälder
Anti-platelet treatment for metabolically induced NASH and HCC

3714

R. Grindberg, E. Schlaepfer, G. Schreiber, V. Simon, S. Speck
Dose and subtype specific analyses of the anti-HIV effects of IFN-alpha family members

3726

Y. Yamada, D. Impellizzieri, T. Maeyashiki, K. Bruestle, L. Dubs, JH. Jang, U. Karakus, J. Woytschak, I. Inci, W. Weder, O. Boyman, W. Jungraithmayr
Induction of persistent tolerance to lung transplants by IL-2 complex-stimulated regulatory T cells in vivo

3733

I. Tcybarevich, N. Obialo, J. Cosin-Roger, K. Seuwen, G. Rogler, B. Misselwitz, C. De Vallière
The role of the rs8005161 polymorphism on pH-sensing G protein-coupled receptor GPR65(TDAG8) signaling in intestinal inflammation

3744

MRS. Spalinger, HL. Hering, MR. Manzini, JBR. Riggs, GC. Gottier, AK. Atrott, TR. Raselli, AF. Fettelschoss, TMK. Kündig, GR. Rogler, MS. Scharl
PTPN2 controls intestinal inflammation and promotes colitis-associated tumour formation via control of inflammasome activation and IL-1alpha release

3750

CKS. Muller, A. Rockinger, S. Bredl, C. Fenwick, G. Pantaleo, C. Münz, RF. Speck
Antibody based anti-HIV-1 therapy

3759

J. Madon, AG. Franchini, DM. Heuberger, W. Ruf, L. Asmis, RA. Schuepbach
Prolonged incubation of endothelial tissue factor with recombinant clotting factor VIIa reduces tissue factor complex activity

3767

R.S. Bruckner, N. Marsiano, E. Nissim-Eliraz, E. Nir, S. Lang, M.R. Spalinger, G. Rogler, S. Yagel, M. Scharl, N.Y. Shpigel
New human gut xenograft mouse model for intestinal fistulas

3769

EP. Pachera, AS. Assassi, GS. Salazar, MFB. Frank-Bertoncelj, RD. Dobrota, FK. Kurreeman, JVB. De Vries-Bouwstra, TM. Messemaker, CFB. Feghali-Bostwick, JD. Distler, GK. Kania, OD. Distler
Long Noncoding RNA H19X is a Master Regulator of Extracellular Matrix Production in Systemic Sclerosis and Other Fibrotic Diseases

3772

F. Largey, Iv. Jelcic, A. Czaplinski, R. Capaul, M. Sospedra, R. Martin, Il. Jelcic
Fingolimod-induced peripheral lymphopenia leads to expansion of cytomegalovirus-reactive T cells and concomitant attrition of varizella zoster virus-specific immunity

3773

F. Largey, Iv. Jelcic, M. Sospedra, R. Martin, Il. Jelcic
Patterns of Intrathecal Antiviral Antibody Production During Natalizumab-Associated Progressive Multifocal Leukoencephalopathy

3781

DM. Heuberger, AG. Franchini, RA. Schuepbach
The thrombin-thrombomodulin complex cleaves protease-activated receptor 2 in a glycosylation dependent manner

3786

MRS. Spalinger, CG. Gottier, LH. Hering, SL. Lang, GR. Rogler, MS. Scharl
Co-housing DSS treated mice with healthy mice results in faster normalization of the intestinal microbiota and promotes recovery from colitis

3787

MRS. Spalinger, SL. Lang, CG. Gottier, GR. Rogler, MS. Scharl
Reduced inflammasome activation upon loss of PTPN22 is dependent on autophagy-mediated degradation of NLRP3

Translational Research

3640

B. Weder, C. Mamie, M. Hausmann, G. Rogler

Increased lymphocyte apoptosis in a mouse model of spontaneous colitis upon A-1211212 treatment

3660

J. Schniering, S. Haller, M. Benesova, Z. Guo, C. Feghali-Bostwick, R. Schibli, O. Distler, C. Müller, B. Maurer

Targeted Nuclear Imaging for the Early Detection of Lung Involvement in Systemic Sclerosis

3665

F. Ugolini, F. Andreoni, N. Keller, A. Neff, V. Nizet, A. Holland, E. Marques-Maggio, AS. Zinkernagel, RA. Schuepbach

Attenuation of streptokinase-mediated virulence in *Streptococcus disgalactiae* subsp. *equisimilis* necrotizing fasciitis by immunoglobulin

3693

HA. Mbunkah, S. Schmutz, A. Marzel, NN. Ndi, E. Mbu, LM. Besong, BA. Sama, E. Orock, M. Shilaih, NK. Campbell, R. Kouyos, HF. Günthard, KJ. Metzner

Prevalence of transmitted HIV-1 drug resistance in Cameroon in the years 2014/15

3702

U. Siler, S. Romao, E. Tejera, O. Oleksandr, E. Kuzmenko, R.G. Valencia, V. Meda Spaccamela, B.H. Belohradsky, O. Speer, M. Schmutz, E. Kohne, M. Hoenig, J. Freihorst, A.S. Schulz, J. Reichenbach
Severe glucose-6-phosphate dehydrogenase deficiency leads to susceptibility to infection and absent NETosis

3706

D. Lenggenhager, J. Gouttenoire, M. Malehmir, M. Bawohl, H. Honcharova-Biletska, S. Kreuzer, D. Semela, J. Neuweiler, S. Hürlimann, P. Aepli, M. Fraga, R. Sahli, L. Terracciano, L. Rubbia-Brandt, B. Müllhaupt, C. Sempoux, D. Moradpour, A. Weber

Visualization of hepatitis E virus RNA and proteins in the human liver

3713

PW. Schreiber, SP. Kuster, B. Hasse, C. Bayard, C. Rüegg, P. Kohler, PM. Keller, G. Bloemberg, F. Maisano, D. Bettex, M. Halbe, R. Sommerstein, H. Sax

Reemergence of *Mycobacterium chimaera* in Heater-Cooler Units despite Intensified Cleaning and Disinfection Protocol

3715

ME. Raeber, K. Karakus, TT. Nguyen, J. Woytschak, O. Boyman

Low-dose IL-2 and improved IL-2 formulations for Treg-deficient immunopathologies

3718

M. Meerwein, A. Tarnutzer, M. Hombach, A.S. Zinkernagel

Increased azithromycin susceptibility of multi-drug resistant Gram-negative bacteria in eukaryotic growth medium

3725

M. Waldner, W. Zhang, IB. James, K. Allbright, R. Schweizer, JA. Plock, K. Marra, MG. Solari, VS. Gorantla, JP. Rubin

Comparison of the immunomodulating effects of human bone marrow derived mesenchymal stem cells and adipose derived stem cells in vitro across different HLA barriers

3770

L. Hering, JB. Riggs, S. Lang, K. Atrott, B. Becher, G. Rogler, M. Scharl, MR. Spalinger

Loss of PTPN2 in dendritic cells affects expression of pro-inflammatory cytokines but has no major role in the intestine

Clinical Trials

3625

VP. Strouvelle, V. Vongrad, DL. Braun, YL. Kok, R. Kouyos, KJ. Metzner, HF. Günthard

Effects of peg-IFN α on the HIV-1 DNA levels in HIV-1/HCV co-infected individuals

3646

DW. Lewandowska, R. Capaul, S. Prader, O. Zagordi, FD. Geissberger, M. Knorr, C. Berger, T. GÜngör, J. Reichenbach, J. Böni, A. Zbinden, A. Trkola, J. Pachlopnik Schmid, M. Huber
Persistent Mammalian Orthoreovirus, Coxsackievirus and Adenovirus Co-Infection in a Child with a Primary Immunodeficiency Detected by Metagenomic Sequencing

3687

DL. Braun, A. Marzel, D. Bircher, P. Schreiber, C. Grube, A. Scherrer, R. Kouyos, HF. Günthard
Optimizing STI Screening Among HIV positive MSM using a Simple Risk Evaluation

3694

DL. Braun, R. Kouyos, B. Hampel, C. Grube, HF. Günthard, J. Böni, JS. Fehr
A Systematic HCV-RNA Scree in HIV+ MSM Reveals High Number of Potential Transmitters

3705

HJ. Klein, F. Lehner, R. Schweizer, N. Fuchs, P. Steiger, P. Giovanoli, R. Graf, JA. Plock
The Role of Pancreatic Stone Protein as Early Marker for Infection and Mortality in Burns

Neurosciences / Pharmacology

Basic Research

3637

M. Samardzija, B. Landfried, M. Barben, C. Grimm
Digoxin-induced photoreceptor toxicity in the mouse retina

3638

V. Eckhardt, B. Li, E. Schaper, J. Dauvillier, C. Tournaire, P. Goloubninoff, A. Aguzzi
Elucidating the role of chaperones in prion biosynthesis and replication by siRNA mediated high throughput screening

3647

F. Romano, AA. Tarnutzer, S. Ramat, D. Straumann, G. Bertolini
Alcohol-induced effect on gaze holding mechanism

3655

A. Bürgin, C. Bockisch, A. Tarnutzer
Increased uncertainty about the direction of gravity in bilateral vestibulopathy correlates with residual utricular function

3668

AK. Lakkaraju, R. Marpakwar, P. Liberski, A. Aguzzi
Identifying the determinants of spongiform phenotype in prion infections

3671

Y. Zarb, D. Kirschenbaum, A. Aguzzi, A. Keller
Cerebral microvascular calcification in the mouse model for primary familial brain calcification is caused by ossification of capillaries.

3672

M. Sauer, M. Arras, T. Fleischmann, M. Lipiski, A. Tourvieille, P. Cinelli, P. Jirkof
Refined buprenorphine treatment protocols for pain relief in mice

3680

DP. Pease, V. Eckhardt, M. Emmenegger, AA. Aguzzi
Discovery of miRNA-Regulated PrP Synthesis Pathways via a Genome-Wide Human miRNA Screen

3686

M. Barben, C. Schori, M. Samardzija, C. Grimm
Progressive cone degeneration in a chronic hypoxia-like situation can be rescued by targeting Hif1a

3691

MA. Wulf, M. Nuvolone, A. Senatore, A. Aguzzi
Electrophysiological changes in mice devoid of cellular prion protein

3697

A. Senatore, P. Schwarz, A. Aguzzi
Calcium channel subunit $\alpha 2\delta$ -1 as a genetic modifier of prion toxicity

3700

S. Sorce*, M. Nuvolone*, G. Russo, P. Schwarz, A. Aguzzi
Temporal transcriptional changes induced by prions in mice

3701

S. Sorce, M. Nuvolone, P. Schwarz, EJ. Rushing, P. Pelczar, A. Aguzzi
The role of the prion protein in the development of muscular pathology

3704

C. Scheckel, DP. Pease, A. Aguzzi
Systematic Profiling of Molecular Changes during Prion Disease Progression

3707

F. Storti, J. Fingerle, C. Maugeais, E. Nogoceke, L. Rohrer, A. Von Eckardstein, C. Grimm
Lipoprotein genes in the retina: a local role in the development of age-related macular degeneration

(AMD)?

3724

E. Boran, S. Burnos, F. Fedele, N. Krayenbühl, P. Hilfiker, T. Grunwald, J. Sarnthein
Test-retest reliability of the spatial distribution of high frequency oscillations (HFO) in intracranial EEG

3730

D. Kirschenbaum, F. Voigt, D. Laptev, A. Sahin, O. Bichsel, F. Helmchen, J. Buhmann, A. Aguzzi
CRYSTAL & HITS: quantifying Alzheimer's disease pathology in the whole-mount mouse brain

3731

K. Frauenknecht, M. Emmenegger, A. Kerschenmeyer, C. Schiavi, R. Moos, S. Hornemann, A. Aguzzi
Evaluation of human antibodies against microglia related receptors as potential novel biomarkers and immunotherapeutics for targeted therapy in neurodegeneration and neuroinflammation

3736

SC. Ambroz, M. Töteberg-Harms, J. Funk, D. Barthelmes, C. Gerth-Kahlert
Functional and morphological outcome analysis of pediatric cataract surgery

3738

A. Senatore, C. Tiberi, G. Horny, S. Fels, N. George, T. Pietzonka, S. Hornemann, A. Aguzzi
Rational design of anti-PrP antibodies to block prion induced neurodegeneration

3740

M. Pfammatter, M. Andreasen, G. Meisl, R. Mezzenga, T. Knowles, A. Aguzzi, S. Hornemann
Absolute quantification of amyloid aggregates using a digital amyloid amplification assay

3754

TFL. Ting-Feng, DS. Dominik, MYH. Melody Ying-Yu
Modulation of visual response after L-dopa treatment in zebrafish larvae

3757

SY. Bögli, M. Afthinos, MYY. Huang
An in-depth study of the influence of gabapentin and memantine on the infantile nystagmus syndrome in zebrafish: implications for therapy of ocular motor diseases

3758

D. Heinzer, M. Avar, M. Pfammatter, V. Eckhardt, B. Li, B. Kuhn, S. Mauerhofer, U. Rosenberg, S. Hornemann, A. Aguzzi
Establishing Methods to Detect Surface-Bound Scrapie Prion Protein on Surgical Steel

Translational Research

3642

T. Fedele, G. Ramantani, S. Burnos, P. Hilfiker, G. Curio, T. Grunwald, N. Krayenbühl, J. Sarnthein
Prediction of seizure outcome improved by fast ripples detected in low-noise intraoperative corticogram

3651

G. Bertolini, J. Bos, E. Groen, T. Frett, R. Hemmersbach, F. Wuyts, D. Straumann
Visual Reinforcement of Illusory Rotations during Centrifugation: A Novel Habituation Strategy to Motion Sickness

3659

E. Krajnc, Z. Gai, G. Kullak-Ublick
In-vitro model for drug-induced hepatic steatosis

3666

A. Papachristodoulou, K. Hasenbach, M. Janicot, M. Weller, P. Roth
Inhibition of TGF- β 1/2 as a therapeutic approach in experimental gliomas

3677

M. Emmenegger, K. Frontzek, G. Meisl, E. Schaper, K. Frauenknecht, N. Wuillemin, J. Domange, K. Kleffel, L. Saleh, T. Sonati, S. Hornemann, I. Xenarios, A. Von Eckardstein, A. Aguzzi
Large-scale screening for diagnostic and therapeutic autoantibodies in hospital cohorts

3696

M. Visentin, Z. Gai, A. Torozzi, C. Hiller, GA. Kullak-Ublick
Molecular Pharmacology of Colistin Sulfate

3716

P. Baumgartner, M. El Amki, R. Steffen, H. Schneider, A.R. Luft, M. Weller, B. Imthurn, G.S. Merki-Feld, S. Wegener
Neuroprotective effects of new generation progestins in experimental stroke involve upregulation of GABA(A) receptor subunits

3722

RR. Reimann, L. Caflisch, Ah. Varol, V. Chandrasekar, M. Hermann, S. Hornemann, As. Senatore, Asv. Lakkaraju, Ma. Nuvolone, Be. Schneider, Aa. Aguzzi
Depicting the role of the FT functional domains in antiprion mediated neurodegeneration

3737

C. Schori, M. Barben, M. Samardzija, D. Barthelmes, C. Grimm
The vitreous proteome of chronic hypoxic response mediated retinal degeneration.

3742

S. Santos, S. Stantos, Ch. Haslinger, M. Hamburger, M. Mennet, O. Potterat, M. Schnelle, U. Von Mandach, A P. Simões-Wüst
In vitro effect of Bryophyllum pinnatum press juice combined with atosiban on myometrium contractility

3745

JW. Wagner, JK. Klohs, DK. Kirschenbaum, FV. Voigt, LR. Regli, AK. Keller
Microvascular changes after experimental subarachnoid hemorrhage in mice

3780

A. Eckhard, D. Bächinger, V. Wettstein, C. Brühlmann, T. Honegger, B. Schuknecht, A. Huber, A. Monge Naldi
MR-Imaging of the Vestibular Aqueduct in the diagnosis of Meniere's Disease

Clinical Trials

3712

H. Dahmke, A. Jetter, H. Kupferschmidt, GA. Kullak-Ublick, S. Weiler
Retrospective analysis of pharmacokinetic interactions between Tizanidine and Ciprofloxacin

3728

J. Drazen, M. Töteberg-Harms
Micro-pulse Cyclophotocoagulation reduces IOP faster compared to G-probe-Cyclophotocoagulation

3756

SY. Bögli, AA. Tarnutzer, D. Straumann, B. Bertolini
Uncovering the link between gaze evoked and rebound nystagmus

3775

IF. Ciernik, M. Wösle, J. Krayenbuehl
Choroidal Melanoma and Fractionated Radiosurgery (fSRS) with Photons

3777

M. Dysli, M. Dysli, D. Rappoport, T. Schmückle Meier, CJ. Bockisch, CJ. Bockisch, CJ. Bockisch, K. Landau, KP. Weber, KP. Weber
Hess screen testing shows an exodeviation shift compared to the Harms screen test

P. Kron¹, M. Linecker¹, P. Limani¹, A. Schlegel¹, P. Kambakamba¹, JM. Lehn¹, C. Nicolau¹, R. Graf¹, B. Humar¹, PA. Clavien¹

Hypoxia driven Hif 2a coordinates mouse liver regeneration by coupling parenchymal growth to vascular expansion

Viszeralchirurgie, UniversitätsSpital Zürich, Zürich¹

Introduction:

Interaction between sinusoidal endothelial cells (SECs) and hepatocytes is a prerequisite for liver function. Upon tissue loss, both liver cell populations need to be regenerated. Repopulation occurs in a coordinated pattern, first through the regeneration of parenchyme (hepatocytes) which then produces VEGF to enable the subsequent angiogenic phase. The signals that instruct hepatocytes to induce timely VEGF remain unidentified. Given that liver is highly vascularized, we reasoned that fluctuations in oxygenation after tissue loss may contribute to the coordination between hepatocyte and SEC proliferation.

Methods:

To prevent a development of hepatic hypoxia after resection, we applied the novel antihypoxic molecule inositol trispyrophosphate (ITPP). ITTP acts as an allosteric effector of hemoglobin, increasing dissociation of O₂ from heme under low oxygen tension. ITTP efficiently promotes *in vivo* oxygenation of hypoxic tissues, an effect that lasts for about two days following injection. We injected ITTP 30 min. before hepatectomy, a period sufficient to inhibit tumor hypoxia without affecting normoxic tissues. To assess regeneration, liver-to-body-weight ratio (LW/BW) was measured at various times after resection.

Results:

ITTP treatment delayed liver weight gain after hepatectomy. Comparison with controls revealed the presence of a hypoxic period around the peak of hepatocyte mitosis. Inhibition of hypoxia led to deficient hepatocyte mitosis, suppressed the regenerative Vegf wave, and abrogated the subsequent reconstruction of the sinusoidal network. These ITTP effects were ongoing with the reduction in hepatocellular Hif2a. In contrast, Hif1a was unaffected by ITTP. Hif2a knockdown phenocopied all effects of ITTP, including the mitotic deficiencies, Vegf suppression and angiogenic failure.

Conclusion:

Our study identifies oxygen as a key regulator of liver regeneration. Hypoxia - inherent to the expansion of parenchyme - activates Hif2a to couple hepatocyte mitosis with the angiogenic phase. Hif2a acts as a safeguard to initiate sinusoidal reconstruction only upon successful hepatocyte mitosis, thereby enforcing a timely order onto cell-type specific regeneration patterns. These findings portray the hypoxia-driven Hif2a-Vegf axis as a prime node in coordinating SEC-hepatocyte crosstalk during liver regeneration.

Modulation of gene expression in human adipose-derived stem cells seeded on PLGA or biomimetic nanocomposite: comparison of 2D films and 3D electrospun meshes – the “real” comparison

Institute for Chemical and Bioengineering, Department of Chemistry and Applied Biosciences, ETH Zurich, CH-8093 Zurich, Switzerland¹, Division of Plastic and Hand Surgery, University Hospital Zurich, Rämistrasse 100, CH-8091 Zurich, Switzerland², Division of Trauma Surgery, University Hospital Zurich, Rämistrasse 100, CH-8091 Zurich, Switzerland³

Introduction:

Tissue engineering of materials seeded with stem cells is confronted with finding the appropriate cues to trigger the intended stem cell differentiation. In this regard, three-dimensional environments offered to stem cells are often compared to their two-dimensional culture behavior in the plastic culture dish. Here, we compare the gene expression pattern of stem cells seeded in a 3D electrospun mesh compared to cells seeded on a 2D film – of exactly the same material.

Methods:

Electrospun meshes of poly-lactic-co-glycolic acid (PLGA) or nanocomposite disks of PLGA and amorphous calcium phosphate nanoparticles (PLGA/a-CaP) were seeded with primary human adipose-derived stem cells (ASCs) and cultured either in DMEM or in osteogenic medium. Corresponding two-dimensional films were also seeded with ASCs. After two weeks, minimum stem cell criteria markers as well as typical markers for osteogenesis, endothelial cell differentiation, adipogenesis and chondrogenesis were analyzed by quantitative real-time PCR.

Results:

While stem cell markers were overall only slightly affected, osteogenic genes were upregulated when 3D meshes were compared to 2D films, especially osteocalcin. As for angiogenesis, CD31 was upregulated under all conditions. Adipogenic differentiation as assessed by PPAR-g-2 revealed an upregulation for the PLGA/DMEM system, while a clear downregulation was found for the PLGA/aCaP/osteogenic medium system.

Conclusion:

When 3D electrospun fiber meshes are seeded with ASCs and their differentiation is compared to 2D casted films, only few genes are affected with the same trend (CD105, osteocalcin and CD31). Otherwise, gene expression for a 2D/3D change is highly dependent on the material composition as well as the culture medium. The beneficial three-dimensional environment for stem cells found in many studies has therefore not to be interpreted by the third dimension alone and should carefully be compared to 2D films fabricated of the same material.

W. Baumgartner², I. Schneider², SC. Hess¹, WJ. Stark¹, S. Märsmann², P. Giovanoli², P. Cinelli³, J. Buschmann²

Static, dynamic, mechanical loading – different in vitro culture conditions and their impact on the gene expression of human primary adipose-derived stem cells seeded on a biomimetic nanocomposite

Institute for Chemical and Bioengineering, Department of Chemistry and Applied Biosciences, ETH Zurich, CH-8093 Zurich, Switzerland¹, Division of Plastic and Hand Surgery, University Hospital Zurich, Rämistrasse 100, CH-8091 Zurich, Switzerland², Division of Trauma Surgery, University Hospital Zurich, Rämistrasse 100, CH-8091 Zurich, Switzerland³

Introduction:

Bioreactors are used to solve problems in tissue engineering with respect to sufficient nutrient and oxygen supply especially in critical size grafts. Some bioreactors not only act as continuous perfusion systems but also enable mechanical loading of cell-seeded grafts. Hence, cells cultivated under perfusion and compression experience shear stress and mechanical load, which might influence their proliferation and differentiation behavior.

Methods:

Electrospun nanocomposite disks of poly-lactic-co-glycolic acid and amorphous calcium phosphate nanoparticles (PLGA/a-CaP) were seeded with primary human adipose-derived stem cells (ASCs) and eight disks were stacked in a bioreactor running with basal culture medium (no differentiation supplements). Under continuous perfusion or perfusion plus uniaxial cyclic compression for 8 hours/day with 10 min/hour, ASCs were cultivated during 14 days. As a control, ASCs were cultivated under static conditions. The differentiation behavior was analyzed in terms of gene expression; typical stem cells markers CD73, CD90 and CD105; osteogenic markers ALP, RUNX2, collagen I and osteocalcin, endothelial cell markers CD31 and CD34, adipogenic marker PPAR-2 and chondrogenic marker Sox9 were analyzed by quantitative real-time PCR. In addition, biomechanical characteristics of the piled construct (stiffness, dissipation of energy) were analyzed as a function of time.

Results:

Dynamic cultivation of ASCs seeded in a three-dimensional random fiber mesh, both by perfusion and by perfusion plus axial compression, leads to a complete different gene expression pattern when compared to static seeding. Strong downregulation of ALP, CD34, collagen I and CD90 were determined. Furthermore, mild downregulation of RUNX2, Sox 9 and osteocalcin were found.

When the perfusion plus compression-system was compared to the perfusion-only system, an upregulation of ALP, RUNX2 and collagen I was observed, while osteocalcin was downregulated. This implies that the compression of ASCs while cultivated in a perfusion bioreactor slightly retards osteogenic differentiation compared to mere perfusion.

Conclusion:

Dynamic cultivation of stem cells can be used to trigger intended differentiation. Compared to static cultivation, drastic changes in gene expression are observed. Additional mechanical stimulation, for example by compression, can even more modulate the gene expression pattern, offering a supplement-free way of in vitro differentiation.

Influence of amorphous tricalcium phosphate nanoparticles incorporated in PLGA on the gene expression of human adipose-derived stem cells seeded on casted films or electrospun meshes

Institute for Chemical and Bioengineering, Department of Chemistry and Applied Biosciences, ETH Zurich, CH-8093 Zurich, Switzerland¹, Division of Plastic and Hand Surgery, University Hospital Zurich, Rämistrasse 100, CH-8091 Zurich, Switzerland², Division of Trauma Surgery, University Hospital Zurich, Rämistrasse 100, CH-8091 Zurich, Switzerland³

Introduction:

Triggering osteogenesis of mesenchymal stem cells (MSCs) is one key issue in the bone tissue engineering community. Besides supplementation of the culture medium, the use of composite materials as scaffolds is a viable option. Especially nanocomposites with an inorganic and an organic component have been investigated lately – and osteogenesis of MSCs has been attributed to inorganic phases like calcium phosphate under several conditions.

Methods:

Electrospun meshes of poly-lactic-co-glycolic acid (PLGA) or nanocomposite of PLGA and amorphous calcium phosphate nanoparticles (PLGA/a-CaP) in a weight ratio of 60:40 were seeded with primary human adipose-derived stem cells (ASCs) and cultured either in DMEM or in osteogenic medium (OS). Corresponding two-dimensional films were also seeded with ASCs. After two weeks, minimum stem cell criteria markers as well as typical markers for osteogenesis, endothelial cell differentiation, adipogenesis and chondrogenesis were analyzed by quantitative real-time PCR. Concentrations of free Ca ions and phosphate ions standing in equilibrium with the materials were assessed by ICP-OES.

Results:

Typical stem cell markers CD73 and CD105 were not affected by the presence of aCaP nanoparticles, while CD90 was downregulated. Osteogenic markers like ALP and RUNX-2 were slightly downregulated, while collagen I was upregulated for 2D casted films, while it was downregulated for 3D electrospun meshes. Osteocalcin was only upregulated when MSCs were seeded on 2D films in OS; all other conditions were not affected by aCaP nanoparticles. CD31 was not affected, while CD34 was upregulated in DMEM, but not in OS. Adipogenic marker PPAR-g-2 was downregulated by aCaP, especially for 3D meshes, while it was upregulated on films in OS, but not in 3D in OS. Finally, the chondrogenic marker Sox9 was slightly upregulated in DMEM and more in OS.

Conclusion:

The presence of 40 weight % aCaP nanoparticles in PLGA had an impact on the differentiation of human ASCs; in a two-week experiment, chondrogenic rather than osteogenic differentiation was found to be favored in the presence of aCaP nanoparticles. In addition, aCaP in 3D electrospun meshes showed stronger effects on gene expression than in 2D casted films, caused probably by a larger reduction of free calcium and phosphate ion concentration by higher availability of nucleation sites in the nanocomposite compared to pure PLGA.

O. Evrova¹, G. Meier Bürgisser¹, C. Ebnöther¹, C. Scalera³, E. Elias⁴, JG. Jess⁴, P. Giovanoli¹, M. Calcagni¹, V. Vogel², J. Buschmann¹

Cellular response towards implant delivering PDGF-BB to fully transected rabbit Achilles tendon three weeks post-operation

Division of Plastic and Hand Surgery, University Hospital Zurich, Rämistrasse 100, CH-8091 Zurich, Switzerland¹, Laboratory of Applied Mechanobiology, ETH Zurich, Vladimir-Prelog-Weg 1-5/10, 8093 Zurich, Switzerland², ab medica, Via Nerviano, 31, 20020 Lainate (Milan), Italy³, Uniklinik Balgrist, Department of Orthopedics, Forchstrasse 340, 8008 Zurich, Switzerland⁴

Introduction:

The healing of ruptured tendons often leads to scar formation, implying a mechanically weaker tissue. Therefore, one problem after tendon rupture repair is re-rupture. Early active motion might stimulate and accelerate healing. Nevertheless, the application of growth factors in a controlled manner to the wound site might improve the healing and strengthen the tendon tissue.

Methods:

A polymer tube fabricated from emulsion electrospun DegraPol with incorporated PDGF-BB [1] was placed around a 4-strand sutured fully transected rabbit Achilles tendon. Three weeks post-operation, the tendons were extracted and histological analyses were performed for tendon core tissue, the interface to the implanted tube and within the electrospun fibers of DegraPol. Total cell density as well as cell densities of tenocytes, tenoblasts, lymphocytes and macrophages were assessed. Collagen fiber orientation was scored semi-quantitatively and tenocyte/tenoblast nucleus morphology was determined – and compared to contralateral not operated legs as control. Also Stoll scores were assessed, including a diverse set of characteristics in tendon healing. As for biomechanical analyses, elastic modulus and failure stress were measured.

Results:

While the elastic modulus of the Achilles tendon was not influenced by the growth factor, the failure stress increased significantly ($p = 0.04$). Histology revealed a higher cell density in the presence of PDGF-BB, however, not statistically significant. As for the inflammatory reaction towards the growth factor-loaded implant, no change was determined when compared to the same implant but without growth factor. Furthermore, neither collagen fiber orientation, nucleus morphology nor Stoll scores were significantly influenced by the delivery of PDGF-BB.

Conclusion:

Although the failure stress improved significantly, histological analyses did not reveal the clear reason for this finding. The parameters analyzed so far are probably not sensitive enough in order to show significant differences connected to improved tendon strength. Further immunohistochemical staining is planned and might resolve the cause of significant higher failure stress at three weeks post-operation as a result of PDGF-BB application.

DC. Benz¹, F. Mikulicic¹, C. Gräni¹, D. Moret¹, M. Possner¹, OF. Clerc¹, AA. Studer Bruengger¹, O. Gaemperli¹, RR. Buechel¹, AP. Pazhenkottil¹, PA. Kaufmann¹

CT-derived Corrected Contrast Opacification Decrease Predicts Long-Term Outcome in Patients With Coronary Stenosis

Department of Nuclear Medicine, University Hospital Zurich, Zurich¹

Introduction:

Estimation of hemodynamic relevance of a coronary stenosis by fractional flow reserve (FFR_{CT}) from coronary computed tomography angiography (CCTA) has raised substantial clinical interest. Since its calculation is a cumbersome process, the corrected contrast opacification (CCO) decrease across a stenosis has evolved as a faster and less complex alternative with promising diagnostic accuracy. The aim of the present study was to evaluate whether the diagnostic accuracy of CCO decrease translates into an added prognostic value in patients evaluated for coronary artery disease (CAD).

Methods:

The present retrospective study consists of 161 consecutive patients who were referred for evaluation of known or suspected CAD with prospectively ECG-triggered CCTA. Patients with a history of revascularization were excluded. Mean attenuation of the coronary lumen was measured before and after a stenosis and corrected to the aorta to calculate CCO. The difference between CCO before and after the stenosis was defined as CCO decrease. A threshold of >0.184 was considered abnormal. CCO decrease was unavailable at the time of decision-making and, thus, had no impact on patient management. The following major adverse cardiac events (MACE) were used as endpoints: death, myocardial infarction (MI), unstable angina requiring hospitalization, and coronary revascularization. Multivariate Cox regression was analyzed with covariates age, sex, ≥3 cardiovascular risk factors and stenosis severity.

Results:

CCO decrease was successfully assessed in all patients with a stenosis (n=72). During a median follow-up of 6.1 years (interquartile range, 5.8-6.9), 55 patients had a MACE. Among patients with a stenosis, the presence of an abnormal CCO decrease was associated with a higher annual MACE rate (13% vs. 8%) and a worse MACE-free survival (p<0.05). In multivariate Cox regression, CCO decrease was an independent predictor of MACE (HR: 2.27, 95% CI: 1.14-4.52, p<0.05).

Conclusion:

In patients with a coronary stenosis, CCO decrease predicts long-term prognostic value – independent of clinical characteristics and stenosis severity.

YT. Chang¹, M. Ziegler¹, D. Ignatova¹, P. Ivanov², R. Profanter², K. Kerl¹, R. Dummer¹, E. Contassot¹, F. French¹, A. Cozzio⁴, S. Misailovic³, W. Hoetzenecker⁴, M. Vechev², E. Guenova¹

Ineffective antibody-dependent cellular cytotoxicity in patients with late stage cutaneous T cell lymphoma

Department of Dermatology, University Hospital of Zürich, University of Zürich, Switzerland¹, Software Reliability Lab, Department of Computer Science, ETH Zürich, Switzerland², Computer Science Department Department, University of Illinois at Urbana-Champaign, USA³, Department of Dermatology, Kantonspital St. Gallen & University of Zürich, Switzerland⁴

Introduction:

Targeted therapies and immune modulators are currently changing our understanding for the treatment of solid tumors, and promise to open a new perspective in the management of cutaneous T-cell lymphoma (CTCL) as well. The mechanisms of action of therapeutic antibodies in vivo is not fully elucidated in all cases, antibody-dependent cellular cytotoxicity (ADCC) mediated by natural killer (NK) cells often being presumed to be a key mode of action. However, since progressive impairment of cellular immunity is a hallmark of CTCL, we questioned the fact that patients with late stage CTCL will still be in a possession of fully functional ADCC. Our objective is to investigate the mechanism of ADCC in CTCL patients.

Methods:

NK cells were isolated from patients with MF stage I-IV, Sézary Syndrom (SS) patients and healthy individuals. An aCella-TOX GAPDH assay was used to detect the amount of endogenous glyceraldehyde-3-phosphate dehydrogenase (GAPDH) and the level of ADCC in each individual patient.

Results:

In vitro ADCC in patients with MF stage I was comparable to that of healthy individuals, but severely abrogated in all MF Stage IV and SS patients included in the study. The percentage of NK cells in the blood of CTCL patients was within normal limits. Trogocytosis, a mechanism of cellular communication that can hamper ADCC by cleaving the surface of the tumor cells from the targeted molecule, seemed not to play an essential role in CTCL. However, overexpression of MHC I on the malignant tumor cells in CTCL was important factor in helping tumor cells escape NK-cell activity and MHC I blockade could restore impaired ADCC.

Conclusion:

Impaired ADCC may pose some problems when choosing a targeted drug therapy for the treatment of late stage CTCL. Understanding of the immunological mechanisms behind it will help improve NK cell activity in CTCL patients and overcome resistance to treatment.

Effects of peg-IFN α on the HIV-1 DNA levels in HIV-1/HCV co-infected individuals

UniversitätsSpital Zürich¹, UniversitätsSpital Zürich and Institut of Medical Virology, University of Zürich²

Introduction:

Studies exploring effects of PEG-IFN α (pIFN α) on total HIV-1 DNA levels in HIV-suppressed patients have varied; therefore in a retrospective longitudinal study we assessed the effects of pIFN α on HIV-1 DNA levels in PBMC from Swiss HIV Cohort Study patients.

Methods:

Patients inclusion criteria were: 1. HIV-1/HCV co-infected, 2. on ART, 3. virally suppressed (< 50 HIV-1 RNA copies/ml of plasma) for >6 months, and 4. treated with pIFN α for \geq 24 weeks. Samples were collected before, during, and post pIFN α treatment (all follow-up time points available). Patients were categorised into three groups: Chronic HIV infection (n=22), Acute HIV infection (n=8), and a control group of no ART during pIFN α treatment (n=10). Patients with >1 pIFN α treatment were also included in the chronic group (n=4). HIV-1 DNA from HIV-1/HCV co-infected patients was quantified by an in-house qPCR assay measuring the U3-R region of the HIV-1 LTR. Clinical data were assessed for the effects of IFN α on the HIV-1 viral load (VL), lymphocyte and CD4 cell populations. Wilcoxon matched-pairs signed rank test was applied to all data sets to investigate significance.

Results:

A total of 247 samples were quantified for HIV-1 DNA with a mean number of time points (range) of 6.6 (2-12) in chronic, 5.6 (2-10) in acute and 5.7 (3-9) in the no ART groups. Maximum follow-up time was 112 months post-pIFN α . Patients were all Caucasian, mainly male (90%) with a mean age of 42 yrs. (27-55) and infected with HIV-1 subtype B (92.5%). pIFN α treatment caused general and CD4-lymphopenia in all patients as previously described. All ART treated patients maintained an undetectable VL. In non-ART-treated patients, pIFN α treatment decreased the HIV viral load by 0.89 log on average. Pre-IFN α HIV-1 DNA levels were on average 0.66 log higher in the chronic vs. the acute group. Total HIV-1 DNA levels remained stable before, during, and after pIFN α treatment with no clear trend found to suggest an effect of pIFN α on HIV-1 DNA levels in PBMCs (Figure 1). Repeated IFN α administration did not have an additional effect on HIV-1 DNA levels in the four patients studied.

Conclusion:

In contrast to other studies, our large longitudinal study in a well characterized patient group did not reveal any effect of pIFN α on the latent reservoir as measured by a HIV-1 DNA qPCR assay in PBMCs. Notably, repeated pIFN α treatment did not affect HIV-1 DNA levels. Cumulatively, no discernible effect of pIFN α on HIV-1 DNA in HIV-1/HCV co-infected individuals was detected.

O. Lauk¹, M. Friess¹, M. Meerang¹, M. Kirschner¹, C. Bommeli¹, RA. Staehl², W. Weder¹, I. Opitz¹

Is toxicity increased by adding intraoperative chemotherapy to preoperative induction chemotherapy for mesothelioma patients?

Division of Thoracic Surgery, University Hospital Zurich, Switzerland¹, Department of Oncology, University Hospital Zurich, Switzerland²

Introduction:

Intracavitary application of chemotherapy after mesothelioma resection is intended to prevent local recurrence. In the present study, we compared hematological and renal toxicity of patients treated with or without additional intracavitary cisplatin-fibrin after (extended) pleurectomy/decortication ((e)P/D) and previous i.v. induction chemotherapy with cisplatin/pemetrexed (CTX).

Methods:

Hemoglobin values, platelet count as well as urea, creatinine, sodium, potassium and magnesium values of 32 patients treated with (e)P/D were compared to the first five patients receiving 44mg/m² BSA intracavitary cisplatin-fibrin in our INFLuenCe-Meso phase II trial ([www.clinicaltrials.gov NCT01644994](http://www.clinicaltrials.gov/NCT01644994)). The median time between last cycle of CTX and surgery was 6 weeks (1-14 weeks). The blood values were measured on postoperative day (POD) 1 to 5, 7, 10 and 14 if available. For statistical comparison Mann-Whitney U test was used.

Results:

No significant difference between the 2 groups was observed in the preoperative baseline blood samples. On POD3 hemoglobin dropped significantly more in patients with cisplatin-fibrin application. However, the use of blood transfusion was not significantly different in both groups. Also sodium, potassium and magnesium levels were significantly lower in the study patient group. Disorders in electrolytes were however never reflected in clinical symptoms and reached only in 3 patients a CTCAE level ≥ 3 . There was no significant difference in platelet count, urea and creatinine levels.

Conclusion:

The present analysis shows that additional intracavitary cisplatin-fibrin after eP/D and previous i.v. induction chemotherapy with cisplatin/pemetrexed can lead to electrolyte disorders and drop in hemoglobin concentration. However, none of the mentioned laboratory findings had a clinically significant impact on the patients' postoperative course.

E. Bellini¹, N. Valtcheva¹, P.J. Wild¹

Identification of the molecular drivers of endometrial cancer progression

Institut für Klinische Pathologie, UniversitätsSpital, Zürich¹

Introduction:

Endometrial carcinoma is the most common malignancy of the female genital tract. The characterization of tissue microarrays (TMAs) containing a very large cohort of human endometrial cancer tissues showed that, although PI3K-mTOR pathway activation and TP53 inactivation play different roles in the initiation of different endometrial cancer subtypes, cooccurring alterations in both signaling pathways represent a frequent unifying pathogenic feature of late stage tumors of all subtypes.

Methods:

Our aim is to identify and functionally assess the role of the proteins crucial for the survival of endometrial cancer cells with the aforementioned molecular signature. For this purpose, we designed a PI3K pathway-dependent synthetic lethality screen using RNAi technology and used TALEN (TAL-effector nuclease) genome editing tool to knock-out PTEN (an important inhibitor of the PI3K pathway) in TP53^{-/-} endometrial carcinoma cell lines.

Results:

The signaling pathways of the identified targets will be further investigated in cell culture and in vivo experiments targeting the corresponding proteins. To confirm the aberrations critical for disease progression and assign them to each step of endometrial cancer development, we will further investigate the obtained results using the samples of our large human TMA cohort.

Conclusion:

Ultimately, this approach aims at using the knowledge gained from the cell culture model to decipher mechanisms commonly involved in the progression of the endometrial cancer of patients. The final goal is to characterize new prognostic and potentially predictive markers for improving personalised molecular diagnosis and treatment.

D. Hinger¹, F. Grossmann², P. Ruiz Sanchez¹, C. Maake¹

The novel photoactive nano drug HypLip as early detection and treatment modality for gastric cancer

University of Zurich, Institute of Anatomy, Zurich¹, Orphanbiotec AG, Zurich²

Introduction:

Photosensitizers are inherently fluorescent and specifically accumulate in tumor cells, which is why they can be used for diagnostic purposes (PDD) or in photodynamic therapy (PDT) to destruct cancers. However, their limited solubility and stability hampers routine use, which may be overcome by encapsulation.

Several promising novel nanoparticulate drug carriers including polymeric nanoparticles, metallic nanoparticles and lipid nanocomposites have been developed. However, many of them contain components that would not meet safety standards of regulatory bodies and due to difficulties of the manufacturing processes, reproducibility and scale up procedures these drugs may eventually not reach the clinics.

Recently, we have designed a novel liposomal carrier, consisting of nontoxic and FDA approved ingredients as promising vehicle for the approved drug and photosensitizer Hypericin (HypLip). The nano drug will be used for diagnosis and treatment of stomach cancer, which requires the formulation to be stable in the gastric environment.

Methods:

We have established a rapid method for parallel assessment of HypLip uptake and toxicity in gastric cancer cells and a spheroid 3D cell co-culture system to investigate cancer cell specificity.

Results:

Our latest results indicate an increased uptake in gastric cancer cells of HypLip compared to free Hypericin. Furthermore photodestructive effects of Hypericin are not diminished upon encapsulation into the liposomal carrier. Most importantly the formulation is stable in the gastric environment for up to several hours, while free Hypericin is degraded rapidly.

Conclusion:

Our formulation will be tested in a gastric cancer model in rats. HypLip will be administered orally and PDD will be performed by endoscopy to identify early tumor lesions, which would otherwise not be visible. An early detection of these lesions might drastically reduce mortality in gastric cancer patients, as this cancer is typically only diagnosed at a very late stage.

I. Alecu¹, A. Von Eckardstein¹, T. Hornemann¹

Elucidating Novel Metabolic Pathways of the Cytotoxic 1-Deoxysphingolipids

Institute of Clinical Chemistry, University Hospital of Zürich, Zürich¹

Introduction:

Serine palmitoyltransferase (SPT) catalyzes the first step in the *de novo* synthesis of sphingolipids, typically condensing serine and palmitoyl-CoA. Under certain conditions SPT also uses alanine, resulting in the cytotoxic 1-deoxysphingolipids (1-deoxySLs). Pathologically elevated 1-deoxySLs cause the inherited neuropathy HSAN1, and have also been found to be increased in patients with metabolic syndrome and type 2 diabetes. Due to the missing C1-hydroxyl group, 1-deoxySLs cannot be degraded by the canonical pathways and therefore they are widely assumed to be “dead-end” metabolites that accumulate to toxic levels.

Methods:

We used a variety of metabolic labelling approaches in combination with high resolution high accuracy mass spectrometry and metabolic profiling workflows to identify novel downstream 1-deoxySL metabolites. We elucidated the order of the metabolic pathway by treating cells with each of the individually purified metabolites. The formation of these novel 1-deoxySL metabolites was modulated using specific chemical inhibitors and inducers, as well gene overexpression.

Results:

In this manner we identified 8 novel 1-deoxySL metabolites which form 3 branches of a downstream metabolic pathway. Furthermore, we found that inhibition of the CYP4F enzyme subfamily prevented the production of these downstream metabolites, while chemical induction and gene overexpression increased their formation and decreased the levels of the toxic upstream 1-deoxySLs.

Conclusion:

While cytotoxic 1-deoxySLs are not metabolized by the canonical pathways, we showed for the first time that they are in fact further metabolized by CYP4F enzymes to 8 novel downstream metabolites. A number of reports have suggested that this enzyme subfamily is down-regulated in mouse models of obesity and fatty liver disease. Therefore, in the future this metabolic pathway may be exploited as a novel therapeutic target to reduce 1-deoxySL levels in metabolic syndrome and type 2 diabetes patients.

R. Steiner¹, A. Von Eckardstein¹, T. Hornemann¹

Elucidating the metabolic pathway of atypical deoxymethylsphingolipids

Institute für Klinische Chemie UniversitätsSpital Zurich¹

Introduction:

1-Deoxymethylsphingolipids (1-DeoxymethylSL) are atypical sphingolipids which are devoid of the C1 and the C1-OH-group present in canonical sphingolipids. They are formed by the condensation of palmitoyl-CoA and Glycine, instead of Serine as for the canonical sphingolipids. The biological role of 1-DeoxymethylSL is so far unclear but they have been found in mammalian cells and human plasma. They were assumed to follow the same metabolic pathway as canonical sphingolipids, but as they are missing the C1 hydroxyl-group 1-deoxymethylSL cannot be converted to complex sphingolipids nor phosphorylated and therefore not degraded via the lyase pathway.

Methods:

HEK293 cells were fed with isotopic labelled D5-1-deoxymethylsphinganine. By using LC-MS it was checked for all downstream metabolites bearing the D5 label. The chemical structure of their downstream metabolites was checked by the use of LC-MS and chemical derivatization reactions to elucidate the position of hydroxylation and unsaturation. The enzymatic pathway was demonstrated by feeding of isotopic labelled D5-1-deoxymethylsphinganine to HEK293 cells with the inhibition or overexpression of suspected enzymes.

Results:

1-Deoxymethylsphingosine (1-deoxymethylSO) is the unsaturated downstream metabolite of 1-deoxymethylsphinganine (1-deoxymethylSA) and formed over the sphingolipid desaturase I. The position of unsaturation in 1-deoxymethylSO was confirmed by LC/MS to be at the (3E) position. Additionally 1-deoxymethylSA and 1-deoxymethylSO can get mono-hydroxylated by the sphingolipid desaturase II or di-hydroxylated over cytochrome P 450 enzymes.

Conclusion:

1-DeoxymethylSO was presumed to bear the same (4E) double bond as sphingosine, which is then a (3E) double bond because of missing C1. Further 1-deoxymethylSO can get mono or di-hydroxylated, whereas canonical sphingolipids cannot be converted to di-hydroxylated metabolites.

We could show a clear difference in the metabolic pathway of canonical sphingolipids and the atypical 1-deoxymethylsphingolipids.

Synthetic materials meet 3D cell biology: PEG hydrogels as blank slate to study ECM-formation in 3D*University Hospital Zurich, Departement for Obstetrics, Zurich¹***Introduction:**

The physiological material surrounding cells in our body is the extra cellular matrix (ECM). The ECM is made of a complex network of several structural and adhesive molecules that display a dense 3-dimensional layout and thereby provide form and function to tissues. Current in vitro methods that aim to decipher biological mechanisms involving the extra-cellular milieu require working with natural hydrogels that are based on ECM-proteins such as collagens or fibrinogen. In contrast, synthetic ECM-free hydrogels such as poly(ethylene glycol) (PEG) avoid biological interferences and enable the study of cells on a blank slate. Here, we present PEG hydrogels as synthetic in vitro platform for 3D tissue models. We illustrate the value of such minimal approach by focusing on the role of the endogenously expressed ECM while microvascular network formation.

Methods:

TG-PEG hydrogels are formed via FXIIIa-mediated transglutamination of 8-PEG-MMPsensitive-Lys and 8-PEG-Gln precursors [Ehrbar et al, 2007, Biomaterials]. The cell adhesion peptide Lys-RGD is cross-linked into the gel at the same time. Human mesenchymal stem cells (MSCs) alone or in 1:1 combination with human endothelial cells (EC) are 3D encapsulated in TG-PEG hydrogels during the gelation process and cultured. ECM expression and formation as well as the formation of microvascular networks were analyzed by various microscopy techniques including bright field, confocal fluorescence and TEM. To analyse the gene expression of ECM components, PEG hydrogels were digested and qRT-PCR was carried out after isolating RNA from retrieved cells.

Results:

In TG-PEG hydrogels MSCs remodel the synthetic environment by degradation and deposition of endogenous ECM components such as fibronectin, collagen type 1 or collagen type 3, thereby turning the blank starting conditions into a cell-customized environment. As a result, ECs together with MSC are able to form 3D microvascular networks that are stable and lumenized.

Conclusion:

We have established a 3D tissue model for the formation of the microvascular bed within synthetic PEG matrices. In this set-up MSCs and the endogenous ECM promote ECs to self-assemble into microvascular structures. Such well-defined tissue model will enable us to study the role of the ECM in microvessel formation without confounding influences from the scaffold material. Moreover, by combining ECs and MSCs from healthy or diseased tissues we will be able to investigate and compare the interplay between those cells and the appropriate ECM components.

M. Samardzija¹, B. Landfried¹, M. Barben¹, C. Grimm¹

Digoxin-induced photoreceptor toxicity in the mouse retina

Department of Ophthalmology, University Hospital Zurich, Zurich, Switzerland¹

Introduction:

Digoxin is a cardiac glycoside drug used to treat heart disease as it inhibits the sodium-potassium ATPase. Some patients, however, report visual disturbances after the treatment suggesting adverse effects of digoxin. Recently, digoxin was shown to suppress autoimmune uveitis in a mouse model, but the same study reported induction of retinal degeneration after digoxin treatment (Hinshaw et al. IOVS, 2016). Here, we aimed to characterize the functional and molecular response of the mouse retina to digoxin-induced toxicity.

Methods:

Mice received 1 to 3 intraperitoneal injections of digoxin (0.5, 1 or 2 mg/kg) administered on a daily basis. Retinas were analyzed at different time-points after the last injection (6 h to 10 days). Methods of analysis included TUNEL, OCT, funduscopy, ERG, light and electron microscopy, immunofluorescence, Western blotting and real-time PCR. Mouse strains used included wild type (*B6* and *129S6*), *Rpe65^{R91W}*, *Rpe65^{-/-}* and *Nrl^{-/-}* mice.

Results:

Three injections of digoxin using the 2 mg/kg dose were sufficient to induce retinal degeneration in *wt* mice. Degeneration was characterized by thinning of the photoreceptor layer, predominantly within the central retina while the retinal periphery was spared. Macrophage infiltration was clearly observed 5 days after the last injection within the zone of injured photoreceptors and persisted up to the 10-day time-point (last time-point analyzed). This was preceded by the activation of an inflammatory response as evidenced by increased *Tnfa* and *Casp1* expression levels peaking at 48 h after the last injection. No obvious adverse effects were seen on other retinal cell types. ERG responses were strongly suppressed even with a dose that did not induce photoreceptor degeneration. Interestingly, digoxin was not toxic to photoreceptors in retinas of *Rpe65^{-/-}*, *Rpe65^{R91W}*, or *Nrl^{-/-}* mice, all of which have reduced levels of the visual chromophore 11-*cis*-retinal.

Conclusion:

This study may be useful for the assessment of digoxin-induced visual disturbances and/or retinopathy and may contribute to the understanding of the special vulnerability of photoreceptors to drug-induced toxicity. The mechanisms of protection observed in mouse models with reduced chromophore levels are currently under investigation.

V. Eckhardt¹, B. Li¹, E. Schaper², J. Dauvillier², C. Tournaire¹, P. Goloubninoff³, A. Aguzzi¹

Elucidating the role of chaperones in prion biosynthesis and replication by siRNA mediated high throughput screening

Institute of Neuropathology, University Hospital Zurich, Switzerland¹, Swiss Institute of Bioinformatics², Department of Plant Molecular Biology, University of Lausanne³

Introduction:

Prion diseases are transmissible neurodegenerative disorders fatally affecting humans and animals. The infectious agent is assumed to consist of the scrapie prion protein (PrP^{Sc}), a misfolded and aggregation-prone isoform of the cellular prion protein (PrP^C). The molecular mechanisms behind PrP^C biosynthesis and the conformational alterations from PrP^C to PrP^{Sc} are still unknown. Chaperones can specifically prevent aggregation of aggregation-prone proteins by tight binding, unfold misfolded and aggregated proteins, and convert them into harmless native proteins or degraded peptides. We propose to identify chaperone genes that are involved in PrP^C biosynthesis and PrP^{Sc} replication in mammalian cells.

Methods:

We have established an RNAi high throughput screen (HTS) system that we will harness to knock down chaperone genes in neuroblastoma cells and subsequently measure PrP^C or PrP^{Sc} by homogeneous phase fluorescence resonance energy transfer (HPFRET). Because chaperones collaborate with one or two co-chaperones, we plan to simultaneously knock down two or three chaperone genes. With our cell-based siRNA HTS system on an acoustic dispensing platform and a robotic system cells are reversely transfected with small interfering RNAs (siRNAs) in 384 well plates and incubated for 72 hours. During incubation, the cell viability is assessed with RT-Glo. At the assay day, cells are lysed and PrP^C or PrP^{Sc} signals are measured with HP-FRET. Experimental data and numerical and graphical quality controls are automatically pulled together in RMarkdown documents.

After accomplishing PrP^C and PrP^{Sc} screens in CAD5 cells, the findings are validated with other libraries or in other cell types generated by CRISPR-Cas9 genome editing.

Results:

The PrP^C single knockdown screen in CAD5 neuroblastoma cells was successfully completed. Calnexin and Calreticulin, which are ranked as hits, are involved in ER processing of glycoproteins and GPI-linked proteins, which both applies for the prion protein and gives us confidence in having found meaningful hits. Validation of other hits is ongoing. A PrP^C double and triple knockdown screen will be performed soon. In order to gain mechanistic insight to PrP^{Sc} replication, we are currently establishing an automatized PrP^{Sc} screen.

Conclusion:

Results of the PrP^C single knockdown screen give evidence, that our RNAi HTS system provides an unbiased approach to identify chaperone genes involved in prion biosynthesis and replication.

J. Schneider¹, V. Lapierre- Fetaud², F. Fluri³, A. Luft¹, JC. Sanchez², M. Katan¹

Serum Amyloid A - a novel predictor of stroke associated infections

Department of Neurology, University Hospital Zürich, Zürich¹, Human Protein Science Department; Centre Medical Universitaire, Geneva², Department of Internal Medicine and Research, University Hospital Wuerzburg³

Introduction:

The use of novel blood biomarkers to identify patients, vulnerable for post-stroke infections, may help to implement treatment more rapidly thus eventually reducing mortality.

Methods:

In 283 prospectively enrolled acute stroke patients we assessed presence and time point of post-stroke infections. Blinded Serum amyloid A – Protein (SAA) measurements were done within 72 hours from symptom onset. To determine the magnitude of association with the development of infections, odds ratios (OR) were calculated. The incremental discriminatory ability of SAA was assessed, by calculating the improvement of the area under the receiver operating characteristic curve (AUC).

Results:

Of 283 patients, 59 (20.8%) developed an infection after onset of stroke. After full adjustment including all routine inflammatory markers (white blood cells, monocytes, C-reactive protein) SAA remained and independent (adj. OR 1.38 [95% CI, 1.0 – 1.9], $p < 0.05$) predictor. Adding SAA to the full regression model, the discriminatory accuracy improved, from 0.77 [95% CI, 0.70 – 0.84]; to 0.79 ([95% CI, 0.73 – 0.85] $p < 0.03$ (likelihood ratio test)).

Conclusion:

Among ischemic stroke patients, serum Amyloid A- Protein measured on admission is a novel predictor of infection after stroke. The combination of routine inflammatory markers with SAA improved the prediction of patients who developed an infection.

B. Weder¹, C. Mamie², M. Hausmann², G. Rogler²

Increased lymphocyte apoptosis in a mouse model of spontaneous colitis upon A-1211212 treatment

University of Zurich¹, Department of Gastroenterology, University Hospital Zurich²

Introduction:

In the pathogenesis of inflammatory bowel disease (IBD) inflammation is sustained by an exaggerated response of T-lymphocytes. Enhanced expression of anti-apoptotic BCL-2 and BCL-x_L is associated with a diminished turnover of mucosal T-cells. Standard medical therapies that regulate lymphocyte proliferation are directly linked to the BCL-2 family-mediated apoptosis. An imbalance in BCL-2 family proteins may cause a failure in the therapeutic response. Here we investigated the role of A-1211212 (AbbVie, USA), a potent inhibitor of BCL-2 in the cell death of lymphocytes in mice under inflammatory conditions.

Methods:

A-1211212 was administered orally by gavage at dosages of 0, 3, 10, 30 or 100 mg/kg/day. Spontaneous colitis developed in *IL-10*^{-/-} after 12 weeks under SPF conditions. Haematological analyses were performed with an ADVIA 2120 flow cytometer and treatment-related changes in the immune cell population were investigated using the CyTOF 2.1 mass cytometer.

Results:

According to the haemogram, treatment with A-1211212 led to reduced lymphocyte count compared to vehicle-receiving controls ($0.21 \pm 0.08 \times 10^3$ cells/ μ L vs. $1.15 \pm 0.71 \times 10^3$ cells/ μ L, respectively, $p < 0.05$). CyTOF analysis of peripheral blood leucocytes revealed both diminished CD8⁺ T and B cells upon treatment. This finding was further confirmed by the increased apoptosis upon A-1211212 in splenocytes and lamina propria mononuclear cells compared with controls. Upon treatment, increased apoptosis was accompanied by a decrease in *Tnf* (0.76 ± 0.55 vs 0.99 ± 0.60), *Il1 β* (0.71 ± 0.55 vs 1.23 ± 1.00), *Ifny* (0.78 ± 0.27 vs 1.23 ± 1.00) and *Il6* (1.38 ± 1.12 vs 2.17 ± 2.09) compared with controls. A-1211212 positively altered the colonic mucosa at a macroscopic and microscopic level and ameliorated intestinal inflammation as shown by colonoscopy and histology.

Conclusion:

Pro-apoptotic A-1211212 was efficacious in diminishing accumulated lymphocytes and ameliorating colitis in the *IL-10*^{-/-} animal model of spontaneous colitis. Regulating inappropriate survival of autoreactive lymphocytes by A-1211212 may provide a new therapeutic strategy in IBD.

T. Skaria¹, E. Bachli², G. Schoedon¹

WIF1 prevents WNT5A-mediated actin cytoskeleton remodeling and monolayer disintegration in human vascular endothelial cells

Medicine, University Hospital Zurich, Zurich¹, Medical Clinic, Uster Hospital, Uster²

Introduction:

Wnt5A, a lipid modified signaling protein of the non-canonical Wnt family is detected in high levels in sera and bone marrow of patients with severe systemic inflammation. Wnt5A, through Ryk receptor interaction, regulates cytoskeleton remodeling, thereby inducing monolayer disintegration and barrier dysfunction in human vascular endothelial cells (VEC). The present study aims to investigate the potential of two naturally occurring secreted Wnt antagonists, sFRP1, and WIF1 to inhibit Wnt5A-mediated cytoskeleton remodeling and monolayer disintegration in human VEC.

Methods:

Human coronary artery endothelial cells (HCAEC) were treated with recombinant human (rh) /mouse Wnt5A (250 ng/mL, R&D systems), rh WIF1 (15 µg/mL, R&D systems) or rh sFRP1 (10 µg/mL, R&D systems) for 1 h, 4 h, and 8 h. Total and phospho-protein levels of LIMK and CFL were determined by immunoblotting. Live cell imaging using a RFP-actin probe was performed to detect actin cytoskeleton remodeling. The assembly of endothelial β -catenin and VE-cadherin were examined by immunofluorescence (IF) staining.

Results:

Wnt5A treatment significantly enhanced the phosphorylation of LIMK and CFL in HCAEC. Combining Wnt5A with Ryk-specific WIF1 significantly suppressed Wnt5A-triggered phosphorylation of both LIMK and CFL, while combination with sFRP1, specific for Fzd or Ror receptors, was not effective. When activated by phosphorylation, LIMK phosphorylates the actin depolymerization factor CFL1 and prevents CFL's ability to depolymerize actin filaments leading to the formation of actin stress fibers. Live cell imaging showed that Wnt5A enhanced stress fiber formation as a consequence of reduced actin depolymerization. Stress fiber formation was notably decreased when HCAEC were treated with a combination of Wnt5A and WIF1 whereas the presence of sFRP1 had no inhibitory effect. In non-treated cells, β -catenin and VE-cadherin were aligned at the cellular periphery forming intercellular borders. Wnt5A-mediated stress fiber formation notably disrupted both β -catenin and VE-cadherin at intercellular borders, forming larger inter-endothelial gaps. Combining Wnt5A with WIF1 prevented Wnt5A-induced disassembly of both β -catenin and VE-cadherin while sFRP1 failed to exert any antagonistic effects.

Conclusion:

WIF1 or molecules with similar properties could be potent tools for the prevention of vascular leakage due to Wnt5A-mediated actin cytoskeleton remodeling in diseases associated with systemic inflammation.

T. Fedele¹, G. Ramantani², S. Burnos¹, P. Hilfiker², G. Curio³, T. Grunwald², N. Krayenbühl¹, J. Sarthein¹

Prediction of seizure outcome improved by fast ripples detected in low-noise intraoperative corticogram

University Hospital Zurich, Neurosurgery Department, Zurich, Switzerland¹, Swiss Epilepsy Centre Department, Zurich, Switzerland², Neurophysics Group, Department of Neurology, Campus Benjamin Franklin, Charité, Berlin, Germany³

Introduction:

Fast ripples (FR, 250-500 Hz) in the intraoperative corticogram have recently been proposed as specific predictors of surgical outcome in epilepsy patients. However, online FR detection is restricted by their low signal-to-noise ratio. Here we propose the integration of low-noise EEG with unsupervised FR detection.

Methods:

Pre- and post-resection ECoG (N = 9 patients) was simultaneously recorded by a commercial device (CD) and by a custom-made low-noise amplifier (LNA). FR were analyzed by an automated detector previously validated on visual markings in a different dataset.

Results:

Across all recordings, in the FR band the background noise was lower in LNA than in CD ($p < 0.001$). FR rates were higher in LNA than CD recordings (0.9 ± 1.4 vs 0.4 ± 0.9 , $p < 0.001$). Comparison between FR rates in post-resection ECoG and surgery outcome resulted in positive predictive value PPV = 100% in CD and LNA, and negative predictive value NPV = 62% in CD and NPV = 80% for LNA. Prediction accuracy was 67% for CD and 89% for LNA.

Conclusion:

Prediction of seizure outcome was improved by the optimal integration of low-noise EEG and unsupervised FR detection. Accurate, automated and fast FR rating is essential for consideration of FR in the intraoperative setting.

M. Bombardo Ayats¹, E. Saponara¹, H. Malagola¹, R. Chen¹, R. Graf¹, S. Sonda¹

Inhibition of Class I HDAC ameliorates chronic pancreatitis by reducing leukocyte recruitment, acinar-to-ductal metaplasia and fibrosis

Swiss HPB Center, Visceral & Transplantation Surgery, University Hospital Zurich¹

Introduction:

Epigenetic mechanisms regulated by the activity of histone deacetylases (HDACs) contribute to the pathology of many inflammatory diseases. In this study we analyzed whether HDACs are activated during chronic pancreatitis (CP) and whether pharmacological inhibition of HDACs has a beneficial effect during this disease.

Methods:

CP was induced by repetitive cerulein injections in wild type C57BL/6 mice. The expression and activity of HDACs and the effects of class I HDAC inhibition with the selective inhibitor MS-275 were evaluated using biochemical, qRT-PCR and imaging techniques. *In vitro* effects of MS-275 were evaluated using 3D cultures of primary acinar cells and macrophage cell line RAW 264.7.

Results:

Induction of pancreatitis resulted in increased expression of class I HDACs, increased nuclear HDAC activity and decreased acetylation of nuclear proteins. Inhibition of class I HDAC with MS-275 significantly reduced pancreatic inflammation in CP. Macrophage migration was limited and their activation was impaired. In addition, MS-275 treatment limited the severity of acinar cell damage and prevented the formation of acinar-to-ductal metaplasia, both *in vitro* and *in vivo*. Finally, MS-275 reduced the development of fibrosis by down-regulating TGF- β and EGFR signaling in the pancreas.

Conclusion:

Our investigation demonstrates that class I HDACs play a crucial role in chronic pancreatitis, promoting the development of inflammatory response, metaplastic lesions and tissue fibrosis. In addition, our results show that inhibition of class I HDACs could be a useful treatment for this severe disease.

DW. Lewandowska¹, R. Capaul¹, S. Prader², O. Zagordi¹, FD. Geissberger¹, M. Knorr¹, C. Berger³, T. G ng r⁴, J. Reichenbach², J. B ni¹, A. Zbinden¹, A. Trkola¹, J. Pachlopnik Schmid², M. Huber¹

Persistent Mammalian Orthoreovirus, Coxsackievirus and Adenovirus Co-Infection in a Child with a Primary Immunodeficiency Detected by Metagenomic Sequencing

Institute of Medical Virology, University of Zurich¹, University Children's Hospital, Division of Immunology, Zurich², University Children's Hospital, Division of Infectiology and Hospital Hygiene³, University Children's Hospital, Division of Stem Cell Transplantation⁴

Introduction:

Here we report on a unique combination of viral infections diagnosed by metagenomic sequencing in a child with combined immunodeficiency. Following a flu-like infection with cough, headache and fever, the child suffered from persistent diarrhea for 18 months. Stool samples tested regularly positive for Enterovirus in a PCR assay but a specific enterovirus could not be typed by cell culture and subsequent indirect immunofluorescence staining. To define the infecting virus, we used an unbiased metagenomic approach to sequence cell culture supernatants and stool suspensions from several time points.

Methods:

For metagenomic sequencing, virus particles were enriched by filtration, total nucleic acids extracted and randomly amplified. Sequencing libraries were prepared with NexteraXT and sequenced on a MiSeq Illumina (1x150 bp). Quality filtered reads were aligned with BLAST against a database containing > 40,000 viral sequences.

Results:

Metagenomic sequencing identified Coxsackievirus A22 in stool suspensions and, very surprisingly, Mammalian Orthoreovirus (MRV) 3 in supernatants of stool cell culture, respectively, over at least a 12-month period. Phylogenetic analysis of MRV showed high similarity to isolates from bats in Germany and from a child with acute gastroenteritis in Slovenia; to our knowledge, the only other reported case of MRV originating from European bats with clinical manifestations in humans.

Conclusion:

MRVs have a broad host range and can also infect humans often causing mild enteric and respiratory infections. More severe cases include hemorrhagic enteritis and encephalitis. Recently, novel MRVs have been isolated from various bat species in Asia, Australia and Europe. Zoonotic transmission is often implicated as the origin of human infection. As our patient is living in close contact to pets and in the vicinity of an animal farm, this is a likely possibility. In summary, cell culture combined with open metagenomic sequencing was crucial in identifying MRV, as no specific routine tests are available for these viruses. This highlights the potential of metagenomic sequencing in complex diagnostic settings for the identification of atypical virus infections.

Alcohol-induced effect on gaze holding mechanism

Neurology Department, University Hospital Zürich, Zürich¹, Department of electrical computer and biomedical engineering, University of Pavia, Pavia²

Introduction:

Gaze-evoked nystagmus (GEN) is an ocular motor finding commonly observed in cerebellar disease, characterized by abnormal centripetal eye drift with centrifugal correcting saccades at eccentric gaze. Acute alcohol intoxication, by temporarily inhibiting cerebellar function, also induces GEN. GEN has been extensively investigated in cerebellar patients, yet a detailed analysis of the influence of alcohol on gaze-dependent eye drift is missing.

Methods:

We examined gaze-holding in healthy human subjects before (baseline) and 30 minutes after intake of the estimated alcohol amount needed to reach a blood alcohol content (BAC) of 0.06%(n=15) and 0.10%(n=10), respectively. Changes in gaze holding were quantified by analyzing eye drift velocity as a continuous function of gaze position over a large range (± 40 deg) of horizontal gaze angles. The position-velocity relationship was described using a two-parameter tangent model.

Results:

Compared to baseline, eye drift velocity increased for all gaze eccentricities by a factor 2 at 0.06%BAC and by a factor >2.5 at 0.10%BAC. Five subjects tested at 0.10%BAC showed a further nonlinear increase of eye drift velocity at large gaze angles.

Conclusion:

Similar linear and nonlinear transformations were also described in patients affected by cerebellar degenerations. We suggest that alcohol-induced GEN could provide a model of GEN in cerebellar pathology. A subgroup of cerebellar patients, however, demonstrated nonlinear increases of drift velocity in absence of an overall scaling, a condition not reproduced by our experiment. We hypothesize that alcohol cannot reproduce this pattern because of its homogeneous effects on all structures for gaze holding in the cerebellum.

I. Opitz¹, M. Friess¹, M. Meerang¹, M. Kirschner¹, K. Berard¹, O. Lauk¹, W. Weder¹

Long Term Freedom from Recurrence after Induction Chemotherapy and Extrapleural Pneumonectomy in Mesothelioma Patients

Division of Thoracic Surgery, University Hospital Zurich, Switzerland¹

Introduction:

Treatment outcomes following multimodality treatment of mesothelioma are variable. There are patients with exceptionally long freedom from recurrence (FFR) following multimodality treatment consisting of induction chemotherapy (CTX) followed by extrapleural pneumonectomy (EPP). We aimed to determine clinical and biological prognostic factors associated with long term freedom of recurrence (≥ 3 years).

Methods:

Between September 1999 and July 2009 93 patients with malignant pleural mesothelioma (MPM) were treated with induction chemotherapy and extrapleural pneumonectomy. They were stratified into 2 groups: freedom from recurrence (FFR) less than 36 months (n=81) and FFR of 36 months and longer (n=12). Proliferation index (Ki-67 and Survivin) in the surgical specimen as well as clinical factors (age, gender, laterality, chemotherapy combination, response to chemotherapy, blood values (white blood cells, lymphocytes, neutrophils, hemoglobin, platelets, albumin, C-reactive protein (CRP)), histological subtype at surgery, IMIG stage) were analyzed using Mann-Whitney U test for continuous variables and Fisher's exact test for categorical variables.

Results:

Age at surgery was significantly higher in patients with long term FFR (median age 66 years vs. 60 years; $p=0.001$) and there were significantly more women in long term FFR group (33% vs. 6%, $p=0.02$). As expected there were more resected epithelioid MPM (67% vs. 56%) in the long term FFR group but also more sarcomatoid MPM (17% vs. 3%) ($p=0.05$). IMIG stage was lower in the long term FFR group that included no IMIG stage IV MPM patients. Neutrophil count and CRP values were significantly lower in patients with long FFR ($p=0.009$ and $p=0.04$, respectively). Ki-67 proliferation index ($p=0.001$) and Survivin staining index ($p=0.02$) were significantly lower in the tumor tissue of patients with long term FFR.

Conclusion:

Our analyses demonstrated that older age, female gender, low IMIG stage and low tumor proliferation indices are associated with long FFR after multimodality treatment. This study shows that biological differences exist between patients with long and short FFR, which could be the underlying reason for these differences in FFR and warrant further investigation.

Visual Reinforcement of Illusory Rotations during Centrifugation: A Novel Habituation Strategy to Motion Sickness

Department of Neurology, University Hospital Zurich¹, TNO, Soesterberg, Netherland², DLR, Linder Hoehe, Cologne, Germany³, AUREA, Antwerp, Belgium⁴

Introduction:

Artificial gravity (AG) is the only countermeasure providing an “Earth-like” solution to weightless health hazards. Head movements during centrifugation, however, cause motion sickness (Cross-coupling stimulus) due to conflicts between perceived, though illusory, rotations and sensed gravity direction. Existing habituation protocols successfully abate motion sickness. The reduction of the conflict supposedly occurs by decreasing vestibular responses to rotation (as quantified by reflexes), i.e. adapting the semicircular canals contribution to the multi-sensory integration generating self-motion perception. In outer space, however, perception of self-rotation has an important role in self-motion sensing, as astronauts are already deprived of gravity reference. The aim of this research is to evaluate if a different adaptation is possible, abating motion sickness without decreasing response to rotation.

Methods:

We tested 19 healthy subjects on the ESA Short Arm Human Centrifuge at DRL, Cologne. The control group (CG: 9 subjects, 3 f) performed a “standard” habituation protocol consisting of 30° clockwise head rolls during centrifugation at 100°/s (1 g at feet). The test group (TG: 10 subjects, 5 f) performed an identical protocol, with the addition of visual stimuli triggered by head movements providing optokinetic stimuli matching the predicted vestibular sensation. Motion sickness was measured using a 1-20 scale, while an eye tracker recorded the vestibulo-ocular reflex (VOR). Measurements were repeated after 24h.

Results:

Only 15 subjects (7 CG, 8 TG) completed the experiment. The same reduction of motion sickness from day 1 to day 2 was observed in both groups (median [MAD] CG: -4 [2]; TG: -4 [1], $p=0.78$). The CG had a significantly larger reduction of the VOR duration than the TG (CG: -4 [1] s; TG: -1 [2] s, $p=0.05$).

Conclusion:

Subjects habituate even if illusory self-rotation induced by head tilts is sustained by visual input. Visually reinforced habituation preserves vestibular reflexive responses to rotations and it is therefore a good candidate to achieve an alternative adaptation of multi-sensory integration that preserve rotation sensing but abate motion sickness in AG.

A. Bürgin¹, C. Bockisch², A. Tarnutzer¹

Increased uncertainty about the direction of gravity in bilateral vestibulopathy correlates with residual utricular function

Neurology Department, University Hospital Zurich, Zurich, Switzerland¹, Otorhinolaryngology, Neurology and Ophthalmology, University Hospital Zurich, Zurich, Switzerland²

Introduction:

Gait imbalance and oscillopsia are major complaints in BVD-patients, and has been linked to increased variability in the perceived direction of gravity due to deficient vestibular (otolithic) input. Here we aimed to compare the accuracy and precision of the perceived direction of gravity for vision-dependent and vision-independent tasks in patients with bilateral vestibular deficits (BVD).

Methods:

Adjustment errors and trial-to-trial variability for different psychophysical tasks were obtained in patients with BVD (n=10) and compared to healthy controls (n=10). Subjective visual vertical (SVV) and subjective haptic vertical (SHV) were measured in different roll orientations (0°, ±45°, ±90°) and subjective postural adjustments along perceived earth-vertical and earth-horizontal were collected. Patients with bilaterally absent ocular vestibular-evoked myogenic-potentials (oVEMPs) were compared to those with (partially) preserved oVEMP-responses.

Results:

While variability depended on roll-angle for both patients and controls, variability was larger in patients for both for the SVV (p<0.001) and the SHV (p=0.004). Patients with bilaterally absent oVEMP-responses had higher SVV (p=0.024) and SHV (p=0.006) variability compared to those with (partially) preserved utricular function. Self-positioning along earth-horizontal was more variable in BVD-patients compared to controls (p<0.001), while this was not true for adjustments along perceived earth-vertical (p=0.420). Again variability was higher in those subjects with bilaterally absent oVEMP responses compared to residual (partial) utricular function (p=0.032). There was a significant correlation in variability for patients for the SVV and the SHV (R²=0.61, slope=1.06 [95%-CI=0.80-1.54]). Differences in adjustment errors between patients and controls were minor.

Conclusion:

The discrepancy between significantly decreased precision but preserved accuracy of verticality-estimates in patients compared to controls is most likely due to the bilaterality of vestibular deficits. With variability correlating amongst all three paradigms and also with oVEMP-responses, this emphasizes the role of bilaterally intact utricular input for precise verticality perception.

M. Rudnik¹, M. Stellato¹, E. Pachera¹, B. Maurer¹, JC. Henes², K. Klingel³, K. Sotlar⁴, P. Blyszczuk⁵, O. Distler¹, G. Kania¹

Monocytes/Neurotrophins/Myofibroblasts As a Novel Axis in Systemic Sclerosis

Center of Experimental Rheumatology, Department of Rheumatology, University Hospital Zurich, Zurich, Switzerland¹, Department of Internal Medicine II, Division of Rheumatology, University Hospital Tuebingen, Tuebingen, Germany², Department of Molecular Pathology, University Hospital Tuebingen, Tuebingen, Germany³, Institute of Pathology, Ludwig Maximilians University, Munich, Germany⁴, Cardioimmunology, Center of Molecular Cardiology, University of Zurich, 8952 Schlieren, Switzerland⁵

Introduction:

Systemic sclerosis (SSc) is an autoimmune disease, which is characterized by inflammation, fibrosis and vasculopathy in multiple organs, mainly in the lung, heart and skin. Neurotrophins (NTs) are a family of proteins promoting neuron growth and survival; however, their profibrotic and proangiogenic actions were recently discovered in fibroblasts and endothelial cells. Elevated number of monocytes and their activation state has been already reported in SSc, but detailed roles of monocytes in multiorgan fibrogenesis in SSc remain unclear.

We aimed to determine the contribution and the role of circulating monocytes in the onset and progression of multiorgan fibrosis in SSc. Additionally, we investigated the involvement of neurotrophin-3 (NT-3) and neurotrophins receptors in the fibrogenesis in SSc.

Methods:

Endomyocardial biopsies from SSc patients and healthy controls were screened by immunohistochemistry. CD14⁺ monocytes isolated from peripheral blood of SSc patients and healthy donors were differentiated towards the myofibroblast phenotype by stimulation with TGFβ1, IL-4, IL-10 and IL-13. In addition, CD14⁺ monocytes were co-cultured with dermal fibroblasts originated from SSc patients and healthy subjects, and with adult cardiac fibroblasts. After 7 days, myofibroblast gene expression and cytokine secretion profiles were evaluated by qPCR, Western blot, protein array and ELISA. Healthy and SSc dermal or cardiac fibroblasts were stimulated with NT-3 and induction of profibrotic genes was analysed by qPCR and immunofluorescence.

Results:

Myocardium of SSc patients revealed the presence of CD45-expressing infiltrates, extended collagen I deposition and the presence of CD14-expressing elongated cells in the fibrotic tissue. Stimulated monocytes acquired myofibroblast-like phenotype with increased expression of collagen I ($p < 0.0001$), fibronectin ($p < 0.05$), and α smooth muscle actin (α -SMA) in comparison to untreated cells. Similarly, CD14⁺ monocytes exposed to dermal or cardiac fibroblasts acquired spindle shape and expressed higher levels of profibrotic genes. The process of monocyte to myofibroblast differentiation employed TGFβ/SMAD signalling. Blocking of the TGFBR1 receptor and canonical SMAD-dependent pathway with inhibitors resulted in the abrogation of extracellular matrix secretion by monocytes. CD14⁺ monocytes from SSc patients were characterised by higher secretion of CXCL10 ($p < 0.001$), CCL20, CCL22, Leukemia Inhibitory Factor (LIF) and NT-3. SSc fibroblasts revealed higher expression of TrkB and p75^{NTR} receptors. Moreover, elevated level of α -SMA was observed in SSc fibroblasts after stimulation with NT-3.

Conclusion:

Here we demonstrated the capability of peripheral blood monocytes to differentiate towards the functional myofibroblast phenotype, indicating these cells as one of the potential sources of pathological tissue myofibroblasts in SSc. Additionally, SSc monocytes secreted NT-3, which induced fibroblast to myofibroblast differentiation. Further studies of TGFβ induced NT-3 expression in monocytes and its effects on fibroblast to myofibroblast differentiation might lead to novel treatment strategies.

F. Renoux¹, M. Stellato¹, O. Boyman², D. Impellizzeri², J. Distler³, C. Dees³, A. Subramaniam⁴, G. Kania¹, O. Distler¹

The transcription factor Fra2 is playing a key role in the control of Treg development and autoimmunity

Department of Rheumatology, University Hospital Zurich, Zurich, Switzerland¹, Department of Immunology, University Hospital Zurich, Zurich², Department of Internal Medicine 3, University of Erlangen-Nuremberg, Germany³, Immune Mediated Diseases, Sanofi-Genzyme, Framingham, MA 01701 USA⁴

Introduction:

Methods:

Decreased numbers or altered functions of regulatory T cells (Tregs) have been reported in many inflammatory rheumatic diseases, and Tregs are considered promising therapeutic targets for autoimmune diseases. It is thus of high importance to delineate the pathways controlling Tregs biology and the onset of autoimmunity. Fos-related antigen 2 (Fra2) is a transcription factor belonging to the Fos family proteins which is part of the AP-1 transcription complex. Our aim is to characterize the potential role of Fra2 in controlling Tregs and autoimmunity. Fra2 transgenic (tg) mice were generated, in which the Fra2 transcription factor is ubiquitously overexpressed. T lymphocyte populations were analyzed by flow cytometry, and pathological manifestations in multiple organs by histology. Bone marrow cells were transferred into lethally irradiated recipients to create Fra2-wt chimeric mice. Purified CD4 T cells were transferred into Rag2^{-/-} mice lacking T and B cells.

Results:

At 3 weeks of age, Fra2 mice showed a striking decrease of the Treg population (CD4⁺CD25⁺FoxP3⁺ in wt and Fra2 littermates spleens: 11.35 and 5.75% of CD4⁺, respectively, p=0.0005, n=6). The strong decrease in Tregs was stable over time and also observed in CD4⁺ single positive thymocytes, indicating that Fra2 mice have a defect in natural Treg development. Interestingly, from 7 weeks on, we could also detect the appearance of activated T cells (CD4⁺ and CD8⁺, with CD62L^{high}CD44^{high}CD127^{low} profile) which represented up to 60% of total T cells by 16 weeks of age. While the phenotype of young mice was limited to decreased Tregs, macroscopic and histological observations in 16 week-old mice showed the presence of an extensive multi-organ autoimmune phenotype: Perivascular inflammatory infiltrates, containing T cells, B cells and numerous granulocytes were observed in the lung and liver. Vascular remodelling and fibrosis were present in the lung. Extensive inflammation and fibrosis were observed in the thymus. Spleens were also enlarged with pronounced extramedullary haematopoiesis. Fra2 tg mice also developed dermatitis on eyelids and back-skin, with an increase in dermal and epidermal thickness. Finally, duodenum was enlarged due to acute inflammation and reactive hyperplasia. To understand whether the effect of Fra2 is T cell intrinsic or extrinsic, we also performed bone marrow transfer experiments in which irradiated wt recipient mice received Fra2 tg bone marrow. Interestingly, chimera mice displayed a decreased percentage of Tregs confirming an intrinsic role of Fra2 in Treg development. Finally, we could show that transfer of purified CD4 T cells from Fra2 tg mice into lymphopenic host (Rag2^{-/-}) was sufficient to transfer the phenotype, demonstrating the ability of CD4 T cells to induce the phenotype.

Conclusion:

These data suggest that Fra2 overexpression inhibits natural Treg development, resulting in 1: diminished Tregs, 2: activation of effector T cells and 3: development of inflammation in multiple organs. This is the first evidence for a role of Fra2 in controlling Treg development and autoimmunity. This murine model also provides a unique opportunity to delineate the function of the Fra2 pathway in T cells and Tregs and its impact on autoimmunity

V. Chandrasekar¹, M. Einsiedler¹, U. Herrmann¹, H. Budka¹, A. Aguzzi¹

Human iPSC stem cell based in vitro modeling and characterization of OPRI genetic prion disease

Institute of Neuropathology, University Hospital of Zurich¹

Introduction:

Prion diseases are progressive, adult onset, fatal neurological diseases characterized by the conformational conversion of the cellular prion protein PrP^C into misfolded PrP^{Sc}. Extra octapeptide-repeat insertions (OPRI) in the prion protein gene causes autosomal-dominant familial Creutzfeldt-Jakob disease (fCJD), but the molecular mechanism behind the pathology is not known; no therapy is available to date. We have shown (Sonati et al., Nature 2013) that the octapeptide-repeat (OR) containing N-terminal tail of PrP mediates neurotoxicity suggesting a spontaneous neurotoxicity in cases of genetic prion diseases with OPRI. Using induced pluripotent stem cells (iPSC) expressing OPRI-PrP, we derived neurons and characterized the subtle pathophysiological correlates to underpin the molecular pathways leading to OPRI-PrP induced neurotoxicity.

Methods:

To establish the model system, we reprogrammed human primary fibroblasts to create iPSC cells and derived human neurons. We cloned human WT and OPRI mutant *PRNP* gene and expressed them in human neurons and cell lines for characterization. For validating the *in vitro* CJD model system, we used antibody mediated epitope mapping, protease sensitivity assays and toxicity induced dysregulated genes by using western blots. Infectivity assays were performed using prion inoculation assays in the mice.

Results:

Here we show proof of methodology for *in vitro* modelling of a complex human genetic disease like OPRI-CJD using iPSC stem cells.

Conclusion:

The three core tenets of prion diseases such as “protease resistance”, “toxicity” and “infectivity” were characterized in the OPRI-PrP expressing human neurons. These identified phenotypes will be tested for the therapeutic potential of anti-prion antibodies against amino terminus PrP and the rescue of affected phenotypes will inform on the feasibility of immunotherapy against hereditary prion diseases.

In-vitro model for drug-induced hepatic steatosis*Pharmacology and Toxicology, University Hospital, Zurich¹***Introduction:**

Drug-induced liver injury (DILI) is a potentially fatal adverse event with significant medical and economic impact. Steatosis is one of the phenotypic manifestations of DILI. The prevalence of hepatosteatosis will continue to increase with the rapidly growing prevalence of obesity and the metabolic syndrome. Drugs associated with steatosis include amiodarone, methotrexate, tamoxifen, valproic acid, and glucocorticoids, which cause mitochondrial damage by inhibition of fatty acid beta-oxidation, oxidative phosphorylation and mitochondrial respiration. Mitochondria are essential regulators of cellular energy metabolism, redox homeostasis and cell survival.

Recently, there is growing evidence that the farnesoid X receptor (FXR) exerts a protective effect against liver steatosis. Moreover, FXR protects mitochondria in the kidney from obesity induced renal damage. FXR is a nuclear bile acid receptor that plays crucial roles in bile acid, cholesterol, lipoprotein, and glucose metabolism in the liver and intestine.

Our aim, therefore, is to investigate whether FXR activation can prevent drug-induced steatosis.

Methods:

Initially an *in vitro* model of drug-induced steatosis in human hepatocyte derived Huh7 cells were established to study the potential therapeutic value of FXR. The influence of the FXR ligands was evaluated after 24 hours' treatment of obeticholic acid (OCA) and GW 4064 on the expression of FXR-regulated genes by real time PCR. Subsequently, LD₅₀ were determined by AlamarBlue assay, and possible protective effect with FXR ligand co-treatment. Finally, with Oil O Red staining was shown accumulation of lipid droplets.

Results:

Firstly, both OCA and GW4064 led to an increased expression of the FXR target genes short heterodimer partner (SHP), the transporters bile salt export pump (BSEP), the organic solute transporters alpha/beta (OST α/β), and the nuclear receptor peroxisome proliferator-activated receptor alpha (PPAR α). Secondly, with AlamarBlue assay we determined the LD₅₀ of Amiodarone, Nefazodone and Acetaminophen. Moreover, Oil O Red lipid droplet staining is suggested to be good steatosis model when Huh7 cells were treated with e.g. sodium-valproate.

Conclusion:

In conclusion, Huh7 cells are suitable as tools to assess a potential effect of FXR agonists on FXR signaling and thus, potentially, on cell damage induced by drugs. Whether FXR agonists could play a role in the prevention of drug-induced liver injury, for instance by protecting against mitochondrial toxicity, remains to be elucidated.

J. Schniering¹, S. Haller², M. Benesova², Z. Guo¹, C. Feghali-Bostwick³, R. Schibli², O. Distler¹, C. Müller², B. Maurer¹

Targeted Nuclear Imaging for the Early Detection of Lung Involvement in Systemic Sclerosis

Department of Rheumatology, University Hospital Zurich, Zurich.¹, Center for Radiopharmaceutical Science ETH-PSI-USZ, Paul Scherrer Institute, CH-5232 Villigen², Division of Rheumatology/Immunology, Medical University of South Carolina, Charleston, United States³

Introduction:

Interstitial lung disease (ILD) is one of the main causes of systemic sclerosis (SSc)-related deaths. Since routine diagnostics such as high resolution computed tomography and pulmonary function tests often only detect ILD at disease stages with already impaired organ function and/or damage, there is an unmet clinical need for the non-invasive diagnosis of ILD at earliest, still reversible stages. Here, we assessed new radiotracers for the detection of SSc-ILD specifically targeting integrin $\alpha\beta3$ and folate receptor β (FR- β) as molecular players of inflammation and inflammation-dependent fibrosis in the murine model of bleomycin-induced lung fibrosis.

Methods:

Expression of integrin $\alpha\beta3$ and FR- β was analyzed in lung sections from patients with SSc-ILD, idiopathic pulmonary fibrosis (IPF) (n=5-6), healthy controls (n=4-5) as well as from bleomycin-treated mice and respective controls (n=6) using immunohistochemistry. In vivo imaging was performed using a RGD peptide derivative and a folate derivative radiolabeled with the gamma-radiation emitting radionuclide Lutetium-17 (¹⁷⁷Lu). SPECT (single photon emission computed tomography) was performed using a dedicated small-animal SPECT/CT scanner. Animals were scanned at day 7 after intratracheal installation of bleomycin to visualize pulmonary inflammation and incipient fibrosis. The specific pulmonary accumulation of the radiotracer was confirmed by ex vivo SPECT/CT, bio distribution, and autoradiography studies.

Results:

In lung sections of patients with SSc-ILD and IPF, the expression of integrin $\alpha\beta3$ was significantly increased compared to healthy controls ($p < 0.009$, $p < 0.02$). In contrast, FR- β expression was only significantly upregulated in lungs from SSc-ILD ($p < 0.04$), but not in IPF patients. In line with the results obtained in SSc-ILD, lungs of bleomycin-treated mice, but not of controls showed a significant increase in integrin $\alpha\beta3$ expression and FR- β expression ($p < 0.03$, $p < 0.05$). Notably, at day 7 after intratracheal installation of bleomycin, SPECT/CT with ¹⁷⁷Lu-RGD targeting integrin $\alpha\beta3$, successfully visualized pulmonary inflammation and incipient fibrosis in the model of bleomycin-induced lung fibrosis. Similarly, SPECT/CT of FR- β targeting ¹⁷⁷Lu-folate showed a higher pulmonary uptake of the radiotracer in bleomycin-treated mice than in controls. Ex vivo SPECT/CT, bio distribution and autoradiography studies confirmed the in vivo results and validated the specific uptake of both radiotracers in lungs from bleomycin-challenged mice as compared to controls.

Conclusion:

The here presented data provide evidence that targeting molecular players of inflammation and inflammation-dependent fibrosis using nuclear imaging methods may lead to a novel promising non-invasive approach for the early detection of lung involvement in SSc.

M. Stellato¹, M. Rudnik¹, F. Renoux¹, E. Pachera¹, K. Sotlar², K. Klingel³, J. Henes⁴, P. Blyszczuk⁵, O. Distler¹, G. Kania¹

Heart dysfunction in systemic sclerosis: involvement of a novel fibrogenic stromal cell subset

Center of Experimental Rheumatology, Department of Rheumatology, University Hospital Zurich, Zurich, Switzerland¹, Institute of Pathology, Ludwig Maximilians University, Germany², Department of Molecular Pathology, University Hospital Tubingen, Germany³, Division of Rheumatology, University Hospital, Tubingen, Germany⁴, Cardioimmunology, University of Zurich, Switzerland⁵

Introduction:

Cardiac dysfunction is a significant cause of the high mortality in systemic sclerosis (SSc). Heart involvement in SSc patients resembles inflammatory dilated cardiomyopathy (iDCM) with inflammation and fibrosis. Myofibroblasts are the main players in cardiac fibrogenesis, but their origin remains unknown.

Here, we aim to determine the role of specific myocardial stromal cell subsets in myocardial remodeling in SSc.

Methods:

The Fos-related antigen 2 (Fra2) tg mouse model of SSc/iDCM was studied. Immunohistochemistry (IHC) and immunofluorescence (IF) were performed on endomyocardial biopsies (EMBs) from SSc/iDCM patients (n=10) and on hearts from Fra2 tg mice (n=5). Flow cytometry analysis was used to identify different subsets of myocardial stromal cells that were sorted, cultured and stimulated with TGF β 1. The differentiation potential was assessed by qPCR, IF, stress fiber staining, SIRCOL and contraction assay on sorted cells. Proliferation and apoptosis were assessed by BrdU incorporation and caspase 3/7 detection. The antisense oligonucleotide GapmeR was used to downregulate Fra2.

Results:

Fra2 tg mice showed increased CD45⁺ leukocyte infiltrates and massive collagen deposition in the heart tissue similarly to the myocardium of SSc/iDCM patients. Moreover, the myocardium of Fra2 tg mice revealed increased expression of pro-fibrotic markers such as α SMA, vimentin, collagen I and fibronectin compared to wild type mice.

Among cardiac stromal cells (Ter119⁻CD45⁺CD31⁻Sca1⁺CD29⁺) four specific stromal cell subsets were identified: gp38⁺CD90.2⁻, gp38⁺CD90.2⁺, gp38⁻CD90.2⁺ and gp38⁻CD90.2⁻. The frequency of gp38⁺CD90.2⁻ (single positive) cells and gp38⁺CD90.2⁺ (double positive) cells was significantly higher in Fra2 myocardium compared to control mice (p= 0.009; n=11).

Importantly, in the myocardium of Fra2 tg mice, the majority of gp38⁺ cells co-expressed α SMA, vimentin, collagen and fibronectin, indicating that myocardial gp38⁺ stromal cells might proliferate and/or differentiate towards the myofibroblast phenotype.

Myocardial single and double positive stromal cells were cultured *in vitro*. After TGF β 1 stimulation, both cell subsets up-regulated α SMA mRNA levels. Importantly, gp38⁺ stromal cells from Fra2 tg mice showed the presence of α SMA fibers and stress fibers, as well as a stronger contraction capability even without TGF β 1 stimulation. In addition, apoptosis and proliferation were increased in Fra2 cells compared to wild-type cells. These findings indicate that Fra2 overexpression might trigger the differentiation of these cells.

Accordingly, Fra2 silencing resulted in a decreased differentiation capability of gp38⁺ stromal cells: mRNA levels of the pro-fibrotic genes α SMA and collagen I were significantly downregulated (p=0.0075 and p=0.0073; n=5). Moreover, Fra2 downregulation impaired the secretion of collagens and the formation of α SMA fibers.

Conclusion:

Cardiac gp38⁺ stromal cells might serve as a cellular source of pathological myofibroblasts playing a pivotal role in TGF β /Fra2-driven myocardial remodeling in SSc.

A better understanding of the mechanisms triggering myocardial dysfunction in SSc might be helpful in developing effective therapies.

G. Karsai¹, T. Hornemann¹, A. Von Eckardstein¹

The role of 1-deoxy-sphingolipids in cell migration and wound healing

Institute for Clinical Chemistry, University Hospital Zurich, Zurich, Switzerland¹

Introduction:

1-Deoxysphingolipids (1-deoxySL) are atypical and cytotoxic sphingolipids which are formed by the enzyme serine -palmitoyltransferase due to an alternative activity with alanine over the canonical substrate L-serine. Pathologically elevated 1-deoxySLs are found in the rare inherited neuropathy HSN1 but are also seen in patients with diabetes type 2 (T2DM). Both conditions are associated with peripheral neuropathy, ulcers and impaired wound healing.

A key feature of the wound healing process in skin is the ingress of first, immune cells and later fibroblasts and keratinocytes into the injured tissues from the periphery. Coordinated and dynamic changes of cytoskeletal structures are essential for neurite formation but also for cell adhesion and migration. Previous reports indicated that 1-deoxySL affect cytoskeletal dynamics by interfering with stress fiber formation and cytoskeletal integrity.

We therefore hypothesized that the elevated deoxySL levels seen in HSN1 and T2DM contribute to the observed impairments in wound healing and other skin defects.

Methods:

We established a cell culture based wound healing assay to investigate the migration capacity of cells in response to 1-deoxySLs. A confluent layer of NIH-3T3 fibroblasts was wounded with a defined scratch and the time required for the cells to close this gap was analyzed as readout for cell migration (scratch assay). Cells were treated with increasing amounts of sphingosine (SA) or 1-deoxy-sphinganine (1-deoxySA) and cell migration analyzed by live microscopy for 72 hours.

Results:

The addition of 1-deoxySA and 1-deoxySO reduced the viability and the migration capacity of NIH-J2 Fibroblasts in culture. The addition of FB1 rescues the inhibitory effect on migration and partially also on cell survival.

Conclusion:

In conclusion, we observed that 1-deoxySL reduced the migration capacity of NIH 3T3 Fibroblasts in culture. This could provide a functional link to ulcer formation and wound healing defects as seen in patients with HSN1 and T2DM.

E. Malagola¹, R. Chen¹, M. Bombardo Ayats¹, K. Schlesinger¹, T. Reding¹, A. Von Eckardstein², R. Graf¹, S. Sonda¹

Role of Thyroid hormone T3 in acinar cell proliferation following cerulein induced acute pancreatitis

UniversitätsSpital Zürich, VIS, Zürich¹, UniversitätsSpital Zürich, Endocrinology Department²

Introduction:

Thyroid hormones (TH) play an important role during development as well as regeneration of several tissues. 3,5,3'-triiodo-L-thyronine (T3) is considered to be the active form of thyroid hormones. In the present study we asked whether acinar cell proliferation following acute pancreatitis is dependent on TH action.

Methods:

Wild type C57BL/6 mice received serial injections of cerulean to induce pancreatitis; TH levels were altered *in vivo* by either T3 supplementation or pharmacological hypothyroidism. A panel of selective inhibitors were injected *in vivo* in combination with T3 to investigate the molecular mechanism beyond T3 action. Levels of cell proliferation, inflammation and fibrosis were investigated through immunohistochemistry as well as gene expression analysis. Serum THs' levels were quantified by biochemical analyses.

Results:

Gene expression analysis revealed a pancreas specific regulation of TH pathway following acute pancreatitis. Hypothyroid mice showed significant impairment in acinar cell proliferation following cerulean treatment and T3 supplementation was able to rescue this phenotype by inducing acinar cell proliferation without increasing damage or inflammation. Gene expression as well as immune assays revealed upregulation of AKT, histone deacetylases (HDACs) and β -catenin following T3 supplementation; use of selective inhibitors for AKT and HDAC reduced T3 induction of proliferation unveiling their involvement in the pathway.

Conclusion:

Endogenous TH pathway is activated following acute pancreatitis and drives acinar cell proliferation. Moreover, we found that T3 driven acinar cell proliferation is dependent on AKT and HDAC action. All together our data define an important role of TH in pancreas homeostasis and regeneration.

F. Ugolini¹, F. Andreoni², N. Keller², A. Neff², V. Nizet³, A. Holland⁴, E. Marques-Maggio⁵, AS. Zinkernagel², RA. Schuepbach¹

Attenuation of streptokinase-mediated virulence in *Streptococcus disgalactiae* subsp. *equisimilis* necrotizing fasciitis by immunoglobulin

*Division Surgical Intensive Care Medicine, University Hospital Zurich, University of Zurich, Zurich, Switzerland*¹, *Division of Infectious Diseases and Hospital Epidemiology, University Hospital Zurich, University of Zurich, Zürich, Switzerland*², *Department of Pediatrics, Division of Pharmacology & Drug Discovery, San Diego, CA*³, *Skaggs School of Pharmacy & Pharmaceutical Sciences, San Diego, CA*⁴, *Division of Clinical Pathology, University Hospital Zurich, University of Zurich, Zurich, Switzerland*⁵

Introduction:

Streptococcus dysgalactiae subsp. *equisimilis* (SDSE or group C and G *streptococcus*) causes a wide spectrum of human diseases ranging from superficial to invasive infections, particularly in patients with underlying chronic disease or immunodeficiency. Invasive streptococcal infections such as necrotizing fasciitis (NF) have predominantly been associated with group A *Streptococcus* (GAS or *S. pyogenes*), however recent studies show SDSE as an emerging cause of invasive disease, making improved understanding of SDSE virulence essential.

Methods:

The virulence factors activity of SLO, Sda1, SpyCEP, SpeB and streptokinase expressed by SDSE was quantified in vitro by specific functional assays. Virulence caused by streptokinase and effect of exogenous commercial pooled human intravenous immunoglobulin (ex-IgGs) on disease severity and clinical outcome were tested in vivo in a NF mouse model.

Results:

We isolated an SDSE strain producing high levels of streptokinase from a patient presenting with NF and lacking endogenous streptokinase-blocking antibodies. In contrast, blood from most volunteers contained streptokinase blocking-antibodies. Ex-IgGs efficiently blocked streptokinase-mediated fibrinolysis by SDSE supernatants. Confirming an important role of streptokinase in SDSE virulence, we found that the SDSE NF-isolate produced more streptokinase than a well characterized GAS NF-isolate and that the streptokinase-deficient mutant of the clinical SDSE NF-isolate lost virulence in a murine NF model. Likewise, clinical severity in the murine NF model was equally attenuated by administration of ex-IgGs.

Conclusion:

In conclusion our data suggest a major role of streptokinase in SDSE-associated invasive infection. Lack of endogenous streptokinase-blocking antibodies resulted in more severe disease providing a rationale for ex-IgGs therapy as a potentially useful adjunction to antibiotics.

A. Papachristodoulou², K. Hasenbach¹, M. Janicot¹, M. Weller², P. Roth²

Inhibition of TGF- β 1/2 as a therapeutic approach in experimental gliomas

Isarna Therapeutics GmbH, Munich, Germany¹, Laboratory of Molecular Neuro-Oncology, Department of Neurology, University Hospital Zurich, Switzerland²

Introduction:

Activation of the transforming growth factor (TGF)- β / SMAD cascade correlates with poor prognosis in glioblastoma patients. Increased TGF- β signaling enhances the invasiveness of glioma cells and contributes to the immunosuppressive microenvironment. Although the pathogenic function of TGF- β in glioblastoma is well defined, therapeutic targeting remains a challenge. Here we examine an alternative therapeutic approach of TGF- β inhibition using two novel phosphorothioate locked nucleic acid (LNA)-modified antisense oligonucleotide gapmers, ISTH1047 and ISTH0047 that specifically target TGF- β ₁ and TGF- β ₂, respectively.

Methods:

We characterized the effects of two novel TGF- β ₁ or TGF- β ₂ specific antisense gapmers on TGF- β _{1/2} expression, downstream signaling and growth of human LN-308 and murine SMA-560 glioma cells *in vitro*. The effect on target inhibition and survival in orthotopic xenogeneic and syngeneic glioma models after TGF- β ₁ or TGF- β ₂ inhibition was assessed *in vivo*.

Results:

Both antisense oligonucleotides silenced their corresponding target specifically and abrogated SMAD2 phosphorylation. Moreover, inhibition of TGF- β ₁ or TGF- β ₂ expression by ISTH1047 or ISTH0047 reduced the migration and invasiveness of LN-308 and SMA-560 glioma cells. Systemic administration of ISTH1047 or ISTH0047 to glioma-bearing mice significantly suppressed TGF- β ₁ or TGF- β ₂ mRNA expression respectively, as well as the expression of the down-stream target *PAI-1* in intracranially growing gliomas.

Conclusion:

Our findings demonstrate that targeting TGF- β expression with the novel antisense oligonucleotides ISTH1047 or ISTH0047 results in strong anti-glioma activity *in vitro* and *in vivo* which may represent a promising approach to be examined in human glioma patients.

Identifying the determinants of spongiform phenotype in prion infections

Institute for Neuropathology, UniversitätsSpital Zürich, Zürich CH-8091¹, Medical University of Lodz, Lodz 92 216, Poland²

Introduction:

Prion disease is a protein misfolding and aggregating disorder (PMA) implicated in Creutzfeldt-Jakob disease (CJD) and several transmissible spongiform encephalopathies of humans and animals. It is characterized by the accumulation and deposition of an abnormal conformer (PrP^{Sc}) of the endogenous prion protein (PrP^C). In addition to generic neuropathological changes (astrogliosis, neuronal loss, deposition of amyloid plaques), prion-infected brains feature a characteristic "spongiosis" which is caused by the accumulation of intraneuronal/intraneuritic vacuoles containing membrane fragments and, sometimes, degenerating organelles which are of uncertain biogenesis and content. The etiology of such pathology is still unclear, but vacuolation is spatiotemporally concurrent with the accumulation and deposition of PrP^{Sc}, an aggregated, proteinase K-resistant conformer of the cellular prion protein PrP^C. Previous studies have documented the accumulation of PrP^{Sc} in multivesicular bodies after prion infection, suggesting impairment of the endo/lysosomal machinery. Depletion of PIKfyve and FIG4, which are involved in synthesis of phospholipid PI(3,5)P₂ a key cog of endo/lysosomal machinery, induces vacuolation similar to spongiosis. We therefore decided to investigate whether the breakdown of the endolysosomal fusion machinery is the cause of spongiosis in prion infections.

Methods:

To address mechanistic details of spongiosis, we plan to use animal models (mice), organotypic slice cultures and cell lines. Techniques such as immunohistochemistry, electron microscopy and *in vitro* biochemical assays will be utilized in all these model systems identify determinants of vacuolation. Rescue experiments will be performed using osmotic minipumps to deliver a water-soluble version of PI(3,5)P₂ to the brains of prion-infected mice and we will monitor the survival and evaluate the neuropathology of brain.

Results:

We monitored the protein levels of PIKfyve and FIG4 in the brains of prion-infected *tga20* mice (overexpressing PrP^C) infected with Rocky Mountain Laboratory strain 6 (RML6) of prion. PIKfyve was significantly depleted at 90 days post-infection and profoundly depleted in terminally sick mice, whereas no change was observed in FIG4 levels. The mRNA levels of PIKfyve were unaltered, suggesting that posttranslational events led to destabilization. We identified that PIKfyve was deacylated in prion infected brain lysates obtained from *tga20* mice and deacylation led to the ubiquitination and degradation of PIKfyve. ER stress plays an important role in the toxicity in prion infections and time course analyses in N2A neuroblastoma cells revealed PIKfyve depletion upon ER stress induction. Treatment with GSK2606414, which alleviates the ER stress induced via the PERK pathway, restored acylation and steady state PIKfyve levels. Our time-course studies in *tga20* mice infected with RML6 prions showed that ER stress precedes the downregulation of PIKfyve.

Conclusion:

Our data suggests that spongiform change may directly result from the suppression of the PIKfyve kinase, resulting in the impairment of endolysosomal machinery and formation of progressively larger vacuoles. In our study, activation of ER stress preceded the depletion of PIKfyve, which was rescued by ER stress inhibitors. We propose to dissect the events leading to PIKfyve downregulation and investigate their importance for prion toxicity in a variety of models. Furthermore, the possibility that PIKfyve-dependent events may play a causative role in additional neurodegenerative disorders exhibiting vacuolation will be investigated.

R. Myburgh¹, J. Jonathan³, S. Surema¹, M. Michal², S. Isringhausen¹, E. Edo¹, AA. Müller¹, D. Neri³, B. Becher², M. Van den Broek², MG. Manz¹

Treatment of Acute Myeloid Leukemia (AML) with Immunotherapies

Hematology, University Hospital Zürich, Zurich ¹, University of Zurich², ETH Zürich³

Introduction:

Immunotherapies hold promise and have made major progress in the treatment of hematological malignancies in recent years. One particularly effective approach is the use of chimeric antigen receptor (CAR) T cells, consisting of high affinity single-chain monoclonal antibodies or single-chain variable fragments (scFv), linked to the signaling machinery of the T-cell receptor and costimulatory molecules. Recently, ground-breaking clinical responses to CAR T- cell therapy in CD19+ B-cell malignancies have been reported. Acute Myeloid Leukemia is a clonal disorder of the hematopoietic stem cell (HSC) and contains a subpopulation of leukemia-initiating cells (LIC) that can self-renew and give rise to the hierarchy of maturing blasts. While the proliferating mature blast pool is highly sensitive to chemotherapy, the more quiescent LICs are relatively resistant and can be a source of relapse. We postulate that the only way to lasting success in poor-risk disease is to radically eliminate LICs and accept collateral damage to HSCs that, subsequently, can be replaced by transplantation. We aim to create a platform for the generation of human CAR T-cells directed against leukemic and HSC antigens, the first of which will be c-Kit (CD117).

Methods:

We will use mouse AML models as well as humanized models carrying human AML cell lines and primary human leukemia to evaluate safety and efficacy of Chimeric Antigen Receptor (CAR) T-cell, Bispecific T-cell engaging (BiTEs) antibodies and monoclonal depleting antibodies. The capacity to eliminate LICs as well as bystander effects on healthy hematopoiesis will be assessed.

Results:

For the mouse AML model, we have generated a murine FBL3 cell line and murine AML TIB-49 cell line expressing murine c-Kit (CD117) and GFP. For the humanized model, the human AML cell line (Kasumi-1) has been characterized and naturally expresses c-Kit. Additionally, we have modified the Kasumi-1 cells to express human CXCR4 to facilitate *in vivo* homing and engraftment in immunodeficient mice. The design and synthesis of both fully murine and human CAR lentivector constructs consisting of an extracellular CD8 α sequence linking the scFv to the intracellular 4-1BB costimulatory and CD3zeta stimulatory domains have been completed. The design allows for insertion of different antigen targeting scFvs' without modification of the rest of the CAR construct. To generate our scFv targeting mouse CD117 we used phage display to identify a binder on soluble murine cKit protein. The novel binder scFv binding to cKit was verified by surface plasma resonance. The scFv was then re-formatted into a monoclonal antibody and binding to a murine cKit+ cell line and primary bone marrow mononuclear cells. The scFv was also expressed in context of an anti-mouse CD3 scFv as a BiTE antibody and binding cKit and CD3 was verified using a murine cKit+ cell line and primary mouse T cells respectively. A dual purpose positive selection and negative selection gene called RQR8 will be co-expressed on the CAR T cells, characterization of which is underway. Expression of RQR8 on a CAR T cell will allow for magnetic selection of CAR T cells using an anti-human CD34 antibody prior to administration of the cells. RQR8 also acts as a safety gene since it binds the B cell depleting antibody Rituximab. Administration of Rituximab resulted in the specific depletion of gene modified T cells *in vivo*.

Conclusion:

Our goal is to use these immunotherapies to radically eliminate both AML-LICs and HSCs by targeting non-tumor-selective HSC antigens and to subsequently deal with the life-threatening HSC depletion by allogeneic HSC transplantation.

Y. Zarb¹, D. Kirschenbaum², A. Aguzzi², A. Keller¹

Cerebral microvascular calcification in the mouse model for primary familial brain calcification is caused by ossification of capillaries.

Department of Neurosurgery, University Hospital Zurich, Switzerland ¹, Institute of Neuropathology, University Hospital Zürich, Switzerland²

Introduction:

Primary familial brain calcification (PFBC) is a rare neurodegenerative disease, which exhibits an autosomal dominant inheritance. Clinical manifestations are variable (e.g. parkinsonism, dementia, psychosis), however, all patients present with bilateral brain calcifications in the basal ganglia. The pathogenic mechanism of PFBC is unknown, but several autopsy studies point to microvascular insufficiency. Although PFBC is a rare disease, brain calcifications are a common CT finding, and vascular dysfunction is the second cause of dementia after Alzheimer's disease. Thus insights into PFBC will aid in better understanding vessel-associated calcification in the brain. Loss of function of platelet-derived growth factor-B (PDGFB) and its receptor, PDGFRB, are associated with PFBC, nonetheless the pathomechanism of vessel calcification due to their haploinsufficiency is not known. Previously we have shown that mouse PDGFB hypomorphs (*Pdgfb^{ret/ret}*) develop brain calcifications similar to PFBC patients and possess a strong pericyte-deficiency in the brain, as PDGFB/PDGFRB signaling pathway is crucial for pericyte recruitment to developing vessels. Interestingly, in *pdgfb^{ret/ret}* mice, brain regions prone to develop calcifications were reported to have a higher pericyte coverage of vessels than non-calcification prone regions. In this study, we have investigated the pathomechanism of cerebral microvascular calcification using *Pdgfb^{ret/ret}* mice, to understand if ectopic mineralization of tissue in this mouse model occurs either by precipitation of calcium phosphate on a permissive extracellular matrix, or by active deposition due to the presence of a bone forming cell.

Methods:

In this study, we employ *Pdgfb^{ret/ret}* mice, to investigate the mechanism leading to capillary mineralization in the brain. We investigate the presence of osteogenic markers and bone matrix proteins using various imaging techniques.

Results:

We find evidence that microvascular mineralisation in *Pdgfb^{ret/ret}* mice is a result of osteogenic calcification, where the presence of osteoblast, osteoclast and osteocyte markers together with bone matrix proteins, was observed.

Conclusion:

Brain calcifications in *Pdgfb^{ret/ret}* animals, a mouse model for PFBC, form via ossification. Future studies are directed towards elucidating how PDGFB hypomorphism and potential pericyte dysfunction lead to the development of bone forming cells along capillaries in the brain.

Refined buprenorphine treatment protocols for pain relief in mice

Center for Clinical Research, University Hospital of Zurich, Zurich ¹, Humanvet, Chemin des clochetons 8, 1004 Lausanne, Switzerland²

Introduction:

Buprenorphine is the opioid analgesic most commonly used in laboratory mice. However, to maintain therapeutically effective serum levels, repeated injections are required. To overcome negative aspects of repeated restraint and injection, sustained release formulations and oral-self administration are promising alternatives. Here we compare: 1) a sustained release formulation of buprenorphine (2.2 mg/kg), manufactured in-house, with a standard protocol of three injections of buprenorphine (0.1 mg/kg/8 hours; Temgesic) and 2) voluntary intake of buprenorphine via drinking water (0.009 mg/ml) with drinking water/injection (0.1mg/kg) combinations for their reliability to achieve effective drug supply and analgesia in C57BL/6J female mice.

Methods:

Buprenorphine serum concentrations were determined in healthy mice following injections of buprenorphine and/or administration via drinking water. Additionally, the pain relief properties were assessed following a mild impact surgery (sham embryo transfer) using physiological and ethological measures of pain, wellbeing and recovery.

Results:

In the injection protocols serum concentrations and analgesiometric tests (thermal sensitivity) indicate a duration of action of only 4-6 hours of standard buprenorphine and 24-48 hours in the sustained release buprenorphine formulation. All drinking water protocols resulted in mean drug serum concentrations assumed to be therapeutically effective throughout the dark phase. Nevertheless, sporadic drinking events and consequently highly variable individual serum concentrations during light phase suggest the need of a combination with several injections of buprenorphine.

Conclusion:

Standard buprenorphine applications provide clinically relevant serum concentrations, and therefore potential pain relief only for 4-6 hours after injection. Therefore, an application interval of 8 h, as commonly practiced, appears too long and might lead to periods with insufficient analgesia in animals undergoing lasting pain. While drinking water/injection combinations of buprenorphine (24h drinking water / 3 injections during the light phase) guaranteed continuous therapeutic serum concentrations for 24 hours, a single injection of the sustained release formulation decreased post-surgical pain for more than 24 hours and additionally minimized the need for restraint and manipulation of the mice. Both protocols offered effective pain relief in mice and resulted in the minimization of clinical and ethological pain signs after surgery.

J. Cosin-Roger¹, S. Bengs¹, S. Lang¹, M. Turina², A. Rickenbacher², K. Seuwen³, P. Ruiz¹, B. Misselwitz¹, G. Rogler¹, C. De Vallière¹

OGR1 (GPR68) expression is increased in intestinal inflammation and correlates with disease activity in patients with IBD

Division of Gastroenterology and Hepatology, University Hospital Zurich, University of Zurich, Zurich¹, Clinic of Visceral and Transplantation Surgery, University Hospital Zurich, Zurich², Novartis Institutes for Biomedical Research, Basel³

Introduction:

A family of pH-sensing G-protein coupled receptors (GPCRs), including ovarian cancer G-protein coupled receptor 1 (OGR1), T-cell death-associated gene 8 (TDAG8 or GPR65) and G-protein coupled receptor 4 (GPR4) play an important role in physiological pH homeostasis. Gut-wall inflammation in both forms of inflammatory bowel disease (IBD), Crohn's disease (CD) and ulcerative colitis (UC), is associated with extracellular tissue acidification. Recent studies reported a link between IBD and this family of pH-sensing receptors. TDAG8 has been identified as an IBD-risk gene. We previously reported that OGR1 is strongly regulated by TNF via a NF- κ B dependent pathway and is essential for intestinal inflammation and fibrosis. We showed that genetic ablation of OGR1 and GPR4 ameliorates colitis in different murine models. Further, we demonstrated that OGR1 regulates barrier function and epithelial restoration, and that OGR1 expression is enhanced by hypoxia.

Methods:

Expression of OGR1 in surgical specimens from non-IBD (n=5), CD (n=10) and UC (n=10) patients was determined by immunohistochemistry, RT-qPCR and Western blotting. Clinical disease activity was assessed by the Harvey Bradshaw Index and the Modified Truelove and Witts activity index (MTWAI) for CD and UC patients, respectively. Nonparametric Spearman's rank correlation analysis was performed.

Results:

OGR1 immunostaining of human surgical samples from non-IBD patients revealed OGR1 expression mainly in lamina propria cells, with weaker staining in epithelial cells. OGR1 staining in IBD patients was stronger compared to controls; however, in IBD patients OGR1 is highly expressed in both epithelial cells and cells in the lamina propria. Further, paired samples taken at the same time, from non-inflamed and inflamed intestinal tissue from IBD patients showed stronger OGR1 staining in the inflamed mucosa compared to the non-inflamed mucosa. Accordingly, mRNA and protein expression of OGR1 was significantly increased in patients with IBD compared to non-IBD patients. Additionally, a significant positive correlation was observed between OGR1 expression and the clinical score in both the non-inflamed (rs 0.5364, p=0.0218) and the inflamed mucosa (rs 0.6279, p=0.0053).

Conclusion:

OGR1 is significantly increased in IBD patients. OGR1 expression correlates with IBD disease activity, suggesting an active role of OGR1 in IBD pathogenesis.

YL. Kok¹, S. Schmutz¹, A. Inderbitzin¹, M. Shilaih¹, A. Kelley¹, C. Berens², HF. Günthard¹, KJ. Metzner¹

A Novel HIV-1-based Vector that Reproduces Features of Active and Latent HIV-1 Infections

Infectious Diseases and Hospital Epidemiology, University Hospital Zurich, Zurich¹, Institute of Molecular Pathogenesis, Friedrich-Loeffler-Institut, Jena²

Introduction:

The lack of phenotypic markers to identify *in vivo* latently HIV-1-infected cells that harbour replication-competent proviruses hampers the progress to understand factors that govern HIV-1 latency.

Methods:

We constructed a novel dual fluorescence HIV-1-based vector, containing a constitutively expressed fluorescent reporter gene to identify infected cells and another, driven by the HIV-1 LTR, to distinguish between productive and latent infections. Additionally, the constitutive fluorescent reporter gene cassette is flanked by a pair of genetic insulators, which protect it from position-effect variegation and alleviate promoter interference between the two gene cassettes. We infected Sup-T1 cells with the pseudotyped vector and analyzed the various profiles of bulk and clonal cell populations longitudinally.

Results:

We demonstrated the stability of our system; different variants and inputs of the vector consistently yielded the same infection phenotype and the initial phenotypes of both bulk and clonal cell populations remained the same during long-term culture of up to 12 months. The integration site patterns were similar to those of wild type HIV-1, and we showed the impact of differential integration sites, as well as vector intrinsic factors, on the reversal of silenced HIV-1 LTRs, i.e. an HIV-1 infection-dependent decrease in expression levels of vector-hosting genes and/or mutations in the vector genome correlated with a lower reactivation potential of the silenced HIV-1 LTR. The integration site repertoire of infected cells dwindled during long-term culture, suggesting the influence of integration sites on the selective propagation of certain cell clones. Our system was also responsive to a variety of latency-reversing agents, with the highest response induced with Romidepsin, Panobinostat, and SAHA in combination with TNF α . Most latently infected cell clones unresponsive to latency-reversing agents had large deletions within the integrated vector genome, similar to observations *in vivo*.

Conclusion:

In summary, we have developed a novel system that enables the identification and separation of cell populations accurately representing productive and latent HIV-1 infections.

Attenuation of Ischemia-Reperfusion Injury after ex vivo Preservation of Vascularized Composite Allografts by Subnormothermic Machine Perfusion with Hemoglobin-based Oxygen Carriers

University of Pittsburgh, Pittsburgh, United States¹, University of Zurich, Zurich, Switzerland², Gulhane Military Medical Academy, Ankara, Turkey³

Introduction:

Improving graft preservation techniques could reduce ischemia-reperfusion injuries (IRI), ameliorate immunological outcomes and allow better matching and graft allocation across wider distances in vascularized composite allotransplantation (VCA). We evaluated a protocol combining subnormothermic machine perfusion (SNMP) with a new hemoglobin-based oxygen carrier (HBOC) solution for *ex vivo* preservation in VCA.

Methods:

Swine vertical rectus abdominis muscle (VRAM) flaps were preserved for 14h with standard cold static preservation at 4°C (CSP; n=8) and SNMP at 21°C using an HBOC solution (n=8). Technical feasibility studies of *ex vivo* SNMP were followed by *in vivo* studies in heterotopic VRAM allotransplantation followed for 7 days under triple immunosuppression (n=8). In addition to recipient's clinical, histopathological and serum myoglobin monitoring, muscle tissue metabolomic analyses were performed.

Results:

SNMP provided constant low pressures (50-55 mmHg), steady flows (25-60 mL/min) and full oxygenation (FiO₂=60% @ 400mL/min) to flaps. SNMP stabilized perfusate's pH (7.55-7.6) while keeping lactate <4 mmol/L. Early contraction bands during *ex vivo* preservation were followed by moderate to severe IRI in the CSP flaps *in vivo*. Muscle fiber disruption and necrosis were significantly reduced in the SNMP group. Post-reperfusion myoglobin blood levels were significantly higher in the CSP flap recipients. Metabolites involved in pentose (nucleic acid back-bone) metabolism were significantly higher after SNMP: ribose (↑22-folds, p<0.001), ribonate (↑37-folds, p<0.001), and ribitol (↑10.5-folds, p<0.001). Glycolysis metabolites increased during SNMP: glucose-6-phosphate (↑23-folds, p=0.01), fructose-6-phosphate (↑12-folds, p=0.03), and phosphoenolpyruvate (↑8-folds, p=0.03). Antioxidant pathways were fully functional after SNMP: glutathione-cysteine disulfide (↑5.6-folds, p=0.01) and N-acetylcysteine (↑40-folds, p=0.007). Energy-related metabolites were significantly higher in SNMP flaps: cAMP (↑3.7-folds, p=0.02) and adenosine (↑129-fold, p=0.002).

Conclusion:

SNMP/HBOC provided effective *ex vivo* oxygenation of VRAM allografts over 14h while significantly decreasing IRI and post-transplant inflammation when compared to CSP. Metabolomic analysis suggests an anabolic state during SNMP with active energy metabolism and increased regenerative potential of the muscle tissue. SNMP/HBOC may enable long-distance graft sharing and improve immunological/functional outcomes in VCA.

R. Schweizer², JT. Schnider¹, PM. Fanzio¹, W. Tsuji¹, MG. Solari¹, KG. Marra¹, JP. Rubin¹, JA. Plock², VS. Gorantla¹

Systemic Application of Adipose Derived Stem Cells Accelerates Functional Peripheral Nerve Regeneration in A Rodent Transection and Repair Model

University of Pittsburgh, Pittsburgh, United States¹, University of Zurich, Zurich, Switzerland²

Introduction:

Complete disruption of peripheral nerves represents a severe injury leading to total loss of motor or sensory function and often results in unsatisfactory regeneration. The improvement of nerve regeneration after local application of adipose derived stem cells (ASCs) has been described lately. Possible mechanisms include transdifferentiation of ASCs into Schwann cells (SC) as well as paracrine effects. The aim of this study was to evaluate the functional outcome after systemic application of ASCs.

Methods:

Lewis rats underwent resection of the sciatic nerve (Res, n=6), transection and repair (TSR, n=10), TSR + ASCs (TSRA, n=12), or reconstruction with 15mm PCL conduits (CC, n=12) or 15mm PCL conduit + ASCs (CA, n=12). 10⁶ ASCs were administered intravenously on postoperative day one. Functional outcome was evaluated on a weekly basis with a swim test, static sciatic index (SSI), and CatWalk XT during 6 weeks (TSR, TSRA) or 8 weeks (CC, CA). Sciatic nerves and gastrocnemius muscles were harvested at 2 and 4 weeks, (n=2 per group) and at 6 weeks (Res, TSR, TSRA) or 8 weeks (CC, CA) for histological and histomorphometry analysis.

Results:

TSRA showed a clear improvement in SSI, as well as in the swim test compared to TSR. The swim test could detect improved functional recovery for TSRA already at week 2 followed by further improvement over 4 weeks. A superior outcome at 6 weeks endpoint could be observed compared to TSR. CC and CA did remain at the same levels as the Res and no functional recovery was monitored during 8 weeks. The CatWalk was only able to detect a postoperative decline due to the trauma, but did not exhibit sensitivity for differences between the treatment groups.

Conclusion:

We conclude that systemic application of ASCs after peripheral nerve transection and repair has the potential to enhance motor functional recovery and can be detected by static and functional tests. Systemic application of ASCs appears to be a promising approach in cases where multiple peripheral nerves are involved or in order to avoid direct access to the nerve as necessary in local application. Histology and MRI results may further clarify our findings.

M. Emmenegger¹, K. Frontzek¹, G. Meisl³, E. Schaper², K. Frauenknecht¹, N. Willemin⁴, J. Domange¹, K. Kleffel¹, L. Saleh⁵, T. Sonati⁴, S. Hornemann¹, I. Xenarios², A. Von Eckardstein⁵, A. Aguzzi¹

Large-scale screening for diagnostic and therapeutic autoantibodies in hospital cohorts

Institute of Neuropathology, University Hospital of Zurich, Zurich¹, Vital-IT, Swiss Institute of Bioinformatics, Lausanne², Department of Chemistry, University of Cambridge, Cambridge³, ImmunoQure Research AG, Schlieren⁴, Institute of Clinical Chemistry, University Hospital of Zurich, Zurich⁵

Introduction:

With an increasing average life expectancy of the world population and age as the strongest risk factor, neuronal protein aggregation diseases may assumingly reach epidemic dimensions in the coming decades. Yet, there is barely any treatment other than palliation available. Promising therapeutic candidates could be human-derived antibodies against endogenous antigens, as has been recently shown with Aducanumab in Alzheimer's Disease, an anti-A β -autoantibody extracted from a human B-lymphocyte. In the case of the prion protein (PrP) whose misfolded conformer, the scrapie prion protein (PrP^{Sc}), leads to prion diseases, epitope specificity of anti-prion-antibodies has been reported rendering them neuroprotective or neurotoxic. In order to exploit the possible therapeutic potential of neuroprotective anti-prion-autoantibodies, we intend to screen all USZ patients giving informed general consent to the utilization of *surplus blood samples*. Following titer determination by means of a high-throughput screen (HTS), hits will be correlated quantitatively to multidimensional matrices of encrypted clinical data including ICD codes and medication. Antibodies to therapeutically relevant targets will be cloned from buffy coats of high-titer patients, expressed *in vitro*, and their therapeutic potential will be assayed in preclinical disease models.

Methods:

To measure autoantibodies quantitatively and to enable subsequent clinical correlations, we have developed a fully automated HTS platform allowing screens of several thousand patients/day at the microliter scale within few hours. This is done by means of a microELISA where the recombinant prion protein is exposed in its natively folded state by site-specific biotinylation via a flexible *BirA* tag. The data collected in each experiment are processed with a custom algorithm to derive the EC₅₀. Since the HTS can be completed within <24 hours from drawing blood, viable memory B-lymphocytes can be isolated by FACS or microfluidics. Droplet-based PCR is used to sequence correctly paired V_L and V_H complementarity-determining regions, and recombinant antibodies are produced in appropriate expression systems and characterised *in cellula*, *ex vivo* and *in vivo*.

Results:

Proof-of-principle screens were carried out in order to address replicability and specificity. Several patient cohorts were repeatedly screened and available data for multiple targets was subjected to nonlinear dimensionality reduction. Preliminary data suggest both high replicability as well as specificity. Plasma samples from USZ have been routinely screened every day. We find anti-PrP-autoantibodies in approx. 0.1% of all tested patients. Correlation of high-titer patients with clinical data have so far revealed a heterogeneous picture without displaying a clear-cut disease association. Sorting of B-lymphocytes, cloning of antibodies and subsequent characterisation is ongoing. APECED patients known to harbour massive amounts of self-reactive antibodies due to a dysfunctional AIRE protein were tested for anti-PrP-autoantibodies: In contrast to the unselected patient cohort, reactivity was found in most APECED patients.

Conclusion:

Upon establishment of the HTS, plasma from USZ patients are now routinely obtained and screens run overnight. Moreover, selected cohorts such as genetic prion disease and neurology patients are assessed. On the long run, we intend to screen approx. 50000 plasma and to extend the scope of antigens including other proteins involved in neurodegenerative diseases. This unbiased quantitative approach may potentially reveal novel disease associations and biomarkers that could not be identified using cohorts of smaller sizes. Lastly, cloning of autoantibodies may provide safe therapeutics to treat so far incurable diseases.

R. Chen¹, T. Hornemann², S. Camargo³, R. Graf¹, S. Sonda¹

1-Deoxy-sphingolipids, novel biomarkers of diabetes, are cytotoxic for exocrine pancreatic cells

Swiss Hepato-Pancreatico-Biliary(HPB) Centre, Division of Surgical Research, Department of Visceral & Transplant Surgery, University Hospital Zurich¹, Institute for Clinical Chemistry, University Hospital Zurich², Institute of Physiology, University of Zurich, Switzerland³

Introduction:

Exocrine pancreatic insufficiency and dysfunctions are frequently associated with diabetes mellitus (DM), which also constitutes a risk factor to develop pancreatitis. We recently discovered that deoxy-sphingolipids (1-deoxySLs) increase during DM and are cytotoxic for beta cells. Knowing the anatomical and functional relationships between endocrine and exocrine pancreatic tissues, we hypothesize that elevated 1-deoxySLs levels observed in DM directly damage the exocrine compartment, thus increasing its predisposition to develop (exocrine) pancreatic diseases.

Methods:

DM was induced with streptozotocin injections in C57BL/6 mice and Wistar rats. Reduction of 1-deoxySL synthesis was obtained by oral L-serine supplementation. Disease severity was evaluated with biochemical and immunohistochemical methods. Molecular mechanisms of 1-deoxySL-dependent toxicity were evaluated *in vitro* in pancreatic acinar cells and primary pancreatic fibroblasts.

Results:

DM induction resulted in increased 1-deoxySL levels but also atrophy and fibrosis of pancreatic parenchyma. Reduction of 1-deoxySL synthesis by oral L-serine supplementation ameliorated the damage of the exocrine pancreatic tissue, without restoring insulin production in beta cells. This suggests that elevated 1-deoxySLs rather than insulin deficiency contribute to the exocrine damage in DM. *In vitro* studies showed that treatment with 1-deoxysphinganine at low micromolar concentration reduced replication and promoted cytotoxicity in pancreatic acinar cells and fibroblasts. Moreover, 1-deoxySL-mediated cytotoxicity was associated with ER stress and ROS production.

Conclusion:

Our work revealed that 1-deoxySLs are cytotoxic for exocrine pancreatic cells, suggesting a role for these lipids in the exocrine dysfunctions observed following DM. Oral L-serine supplementation could be an option for ameliorating exocrine pancreatic diseases in diabetic patients.

R. Chen¹, E. Malagola¹, G. Mosca¹, M. Dietrich², E. Saponara¹, K. Grabliauskaite¹, R. Zuellig², O. Tschopp², R. Graf¹, S. Sonda¹

Akt1 regulates the development of inflammation and tissue regeneration during acute pancreatitis

Swiss Hepato-Pancreatico-Biliary (HPB) Centre, Division of Surgical Research, Department of Visceral & Transplant Surgery, University Hospital Zurich¹, Division of Endocrinology, Diabetes and Clinical Nutrition, University Hospital Zurich²

Introduction:

The serine/threonine kinase Akt/PKB plays a key role in the conserved phosphoinositide 3-kinase signaling pathway. In mammals, activation of Akt is implicated in the regulation of divergent cellular processes, including proliferation, survival and cell size. Recently, Akt has also been implicated in the regulation of inflammation through activation of the NF- κ B pathway. Three Akt isoforms (Akt1, Akt2, and Akt3) are found in mammals and, despite being highly related and sharing the same structural organization, they show non-redundant physiological functions. In this study we investigated whether the Akt1 isoform plays a critical role during the development of acute pancreatitis (AP).

Methods:

AP was induced by repetitive injections of cerulein in wild type (WT) and Akt1^{-/-} mice. The onset and progression of the disease were evaluated in the two mouse strains by serum enzyme quantification, immunohistochemistry and qRT-PCR analyses.

Results:

Following AP induction, WT and Akt1^{-/-} mice showed comparable initial damage of acinar cells. However, during disease progression, Akt1^{-/-} mice displayed reduced infiltration of inflammatory cells in the pancreas. In addition, lack of Akt1 resulted in reduced acinar cell proliferation and de-differentiation into acinar-to-ductal metaplasia. Molecular analyses revealed a down-regulation of TGF- β signaling in Akt1^{-/-} mice.

Conclusion:

Our results revealed that Akt1 signaling does not mediate the initial acinar cell damage observed at the onset of AP. However, Akt1 signaling promotes both the inflammatory response and the regeneration of the pancreatic tissue. These findings provide novel insights into the molecular pathways governing pancreatic inflammation and tissue regeneration, with potential therapeutic implications.

Discovery of miRNA-Regulated PrP Synthesis Pathways via a Genome-Wide Human miRNA Screen*Institut für Neuropathologie¹, UniversitätsSpital Zürich***Introduction:**

A host of microRNAs, many of which have been implicated in cell death, innate immune responses, synaptic function and neurogenesis, have previously been reported to become de-regulated following induction of scrapie in mice, BSE infection in macaques or during onset of sporadic Creutzfeldt-Jakob disease in humans. Deep sequencing of exosomes has also revealed the presence of distinct miRNA signatures in prion-infected versus non-infected neuronal cells, implying that miRNAs expression profiles may serve as potential diagnostic markers for prionopathies. Moreover, the octapeptide repeat domain of human PrP^C has previously been shown to bind Argonaute thereby promoting formation and stabilization of the miRISC complex. Yet despite the ostensible role PrP may play in regulating miRNA-induced silencing, it remains unknown whether and to what extent miRNA may have an effect on PrP expression and its conversion to PrP^{Sc}. While multiple miRNA target prediction algorithms exist which, amongst several other parameters, calculate likeliness of miRNA binding to transcripts through assessing seed region complementarity in the 3' UTR, these estimates remain tentative as many cannot be confirmed biologically. Cell-based genome-wide miRNA screens address the limitations of *in silico* predictions and allow a further specific advantage, namely the assessment of cell type-specific miRNA-elicited effects, contingent upon endogenous miRNAome expression profiles. The current project seeks to assess whether, and to what extent, the microRNAome may post-transcriptionally modify PrP^C levels through direct or indirect pathways by means of an exploratory genome-wide human miRNA mimic screening approach.

Methods:

We have developed a robust robotic high-throughput cell-based screening platform in which U-251 MG or CHP-212 cells are reverse-transfected with a human miRNA library encompassing 2019 mimics in a randomized 384-well plate format. Following a 72-hour incubation period, PrP^C quantification is performed via TR-FRET, using Eu and APC fluorophores conjugated to the monoclonal antibodies POM2 and POM1 respectively. Convergent hits with SSMD scores above 3 or below -3 were selected for further validation in iPSC-derived human neurons. Hit regulatory pathways will be characterized by ribosome profiling to elucidate potential regulatory networks.

Results:

Screening of U-251 MG cells was successfully completed, yielding a mean technical triplicate linear regression R^2 of >0.65 with 9 and 22 hits displaying extremely stringent SSMD scores over 5 or under -5 respectively. Clustering of miRNA hits into families as well as assessing changes in cellular viability and PrP^C modulation specificity is now being performed to select the most relevant hits for further validation in iPSC-derived neurons. In congruence with the top 5 pooled *in silico* miRNA target prediction algorithms, all members of the miR-148/152 family were found to significantly down regulate (SSMD <-5) PrP^C levels. The majority of the other miRNA hits however, many of which possess only sparse or no previous investigation in the scientific literature, were not predicted as targeting the PRNP transcript, thus potentially indicating a secondary interaction pathway.

Conclusion:

A highly robust high-throughput platform has been established allowing the arrayed screening for effects of miRNA mimics on PrP^C levels. Results gained during these experiments will not only help infer regulatory roles of miRNAs in PrP^C homeostasis, but may also ordain the endogenously expressed miRNAs as potentially potent therapeutic targets for multigenic diseases involving complex pathways.

Validation of Dynamic Treatment-Couch Tracking for Motion Compensation during Prostate SBRT

*Department of Radiation Oncology, University Hospital Zurich and University of Zurich, Zurich¹,
Department of Radiation Oncology, University Hospital Zurich, Zurich²*

Introduction:

In stereotactic body radiation therapy (SBRT) of prostatic cancer, a high dose per fraction is applied to the treated region with steep dose gradients. Intrafractional prostate motion can occur unpredictably during the treatment and lead to target miss. Missing the target results in high doses to nearby organs which can cause complications. It is essential for a prostate SBRT treatment to observe and mitigate this motion. Dynamic treatment-couch tracking is a real-time adaptive therapy technique, compensating the prostate displacement by counter-movement with the treatment couch. This work investigated the dosimetric benefit of couch tracking for prostate SBRT treatments in the presence of prostatic motion.

Methods:

Ten previously treated prostate cancer patients with one index lesion were selected. Treatment target volumes (prostate and index lesion), and organs at risk (OAR: bladder, rectum and urethra) were contoured using the patient's treatment CT and MRI scans. SBRT treatment plans with integrated boost were prepared with a prescribed radiation dose of 5x7 Gy to the prostate and 5x8 Gy to the index lesion. The treatment plans were applied with a linear accelerator to a cylindrical dosimetric phantom, which measures radiation dose in a biplanar diode array. Each treatment plan was applied three times, while the phantom was either

- i) in static position,
- ii) moved according to five prostate motion curves without motion compensation or
- iii) with real-time compensation using couch tracking.

Electromagnetic transponders for position detection were mounted on the phantom surface. Their signal was used as position feedback for the couch tracking and their motion traces were evaluated to compare the tracked and untracked situation. The measured radiation dose was used to compare the dosimetric performance of couch tracking against no compensation: Gamma agreement and other dose parameters were evaluated within the biplanar array, as well as target- and organ-specifically.

Results:

The root-mean-square error of the motion traces (range: 0.8-4.4 mm) was substantially reduced with couch tracking (0.2-0.4 mm). Spikes (>1 mm) in the compensated motion curve were only observed at steep motion gradients with high velocity (>7.5 mm/s). The dose measurements with the phantom showed on the 1%/1 mm level significantly better gamma agreement with tracked motion (range: 83.4%-100%) than with untracked motion (28.9%-99.7%). Also with the 2%/2 mm criterion, gamma agreement was significantly superior for the tracked motion (98.4%-100%) compared to the untracked (52.3%-100%). The organ specific evaluation resulted in significantly better target coverage with tracking, however the dose to the rectum and bladder showed a dependency on the motion direction of the phantom.

Conclusion:

Couch tracking was able to mitigate the prostate motion and improved the dosimetric accuracy of prostate SBRT. The treatment couch was able to compensate the prostatic motion with only some minor residual motion at steep motion gradients. Therefore, couch tracking combined with electromagnetic position monitoring for prostate SBRT is feasible and improves the accuracy in treatment delivery when prostate motion is present.

K. Oehl¹, B. Vrugt¹, U. Wagner¹, M. Meerang², M.B. Kirschner², W. Weder², I. Opitz², P.J. Wild¹

Tracking the Clonal Origin and Chemotherapy Resistance of Malignant Pleural Mesothelioma

Institute of Surgical Pathology, University Hospital Zürich, Zürich¹, Division of Thoracic Surgery, University Hospital Zürich, Zürich²

Introduction:

Malignant Pleural Mesothelioma (MPM) is a rare but aggressive neoplasm with a median life expectancy around 12 months, despite widely used multimodal treatment efforts including chemotherapy followed by surgery. So far, no effective second-line treatment could be established. To investigate the mechanisms of MPM development leading to treatment resistance, the objective of this study was to track the clonal origin and to find genetic markers that predict resistance to chemotherapy.

Methods:

A cohort of 23 MPM patients undergoing treatment with Cisplatin and Pemetrexed followed by surgery were chosen for analysis. DNA was isolated from FFPE samples taken at the treatment-naïve biopsy, at surgery after combined induction chemotherapy and at relapse. Afterwards, we performed targeted amplicon sequencing. For this purpose, based on a systematic literature review, a custom-designed MPM sequencing panel was established, targeting the 30 most frequently mutated genes in MPM. Analysis was conducted following internal guidelines for diagnostic sequencing.

Results:

Sequencing revealed a high frequency of mutations occurring in *BAP1* and *NF2*. In most cases, these alterations are already present at a high allele frequency in the diagnostic biopsy, indicating an early clonal origin and potential roles as driving mutations. Additionally, most of the mutations lead to a premature termination of or frameshift in the respective protein, therefore probably exhibiting a high impact on protein function. Correlation of the sequencing data with the response of the patients to chemotherapy showed that *BAP1* mutations showed a strong positive correlation with resistance to treatment with Cisplatin.

Conclusion:

Our sequencing analysis revealed a high inter- and intratumoral heterogeneity in MPM. Most of the mutations were found in *BAP1* and *NF2*; they occurred early in tumor evolution and are therefore possible drivers of MPM. Especially *BAP1* seems to be involved in the innate resistance of MPM to chemotherapy. Analysis of the involved pathways could help to elucidate the role of somatic *BAP1* mutations in MPM and might reveal some new targets for alternative therapy options.

S. Velagapudi¹, L. Rohrer¹, A. Von Eckardstein¹

VEGF-A regulates endothelial HDL transcytosis

Institute of Clinical Chemistry, University Hospital Zürich¹

Introduction:

High density lipoproteins (HDL) have to pass the endothelial layer to exert their anti-atherogenic activities within the vascular wall. However the rate limiting factors that mediate HDL transcytosis in endothelial cells are yet little known. Therefore, we performed a high-throughput screen with kinase drug inhibitors to identify modulators involved in HDL endothelial transcytosis.

Methods:

High-throughput screening was performed, incubating human aortic endothelial cells (HAECs) with 141 kinase inhibiting drugs and Atto-594 fluorescent labelled HDL. Fixed cells were imaged using fluorescence wide-field microscope. Processing of microscopy acquired data using cell profiler and principle component analysis yielded several preliminary hits. We then applied RNA interference and pharmacological means to HAECs, to verify and further characterize screening hits towards their impact on binding, internalization and transport of radio-iodinated HDL.

Results:

In the screen, only inhibitors of VEGF receptor (VEGFR) consistently decreased HDL uptake. Our *in vitro* biochemical validation studies of silencing VEGFR2 showed significant decrease in ¹²⁵I-HDL cellular binding and association as well as transport of ¹²⁵I-HDL through endothelial cells cultured in trans-wells. RNA interference with VEGFR1 or VEGFR3 had no effect. Our results demonstrated that supplementation of VEGF-A to the cells grown in the VEGF depleted growth medium restored ¹²⁵I-HDL cellular binding, association and transport, whereas silencing SR-BI or drugs inhibiting PI3K and p38MAPK activation but not Raf/MEK/ERK pathways abolished this effect. Moreover, these dramatic changes in the VEGF-A mediated ¹²⁵I-HDL cellular binding, association and transport were modulated by SR-BI subcellular localization in the endothelial cells.

Conclusion:

The identification of VEGF as a regulatory factor of transendothelial transport of HDL supports the concept that the endothelium is a specific and hence druggable barrier for the entry of HDL into the vascular wall.

J. Cosin-Roger¹, C. Stanzel¹, A. Terhalle¹, L. Wolfram¹, K. Atrott¹, PA. Ruiz¹, H. Melhem¹, MR. Spalinger¹, S. Lang¹, I. Frey-Wagner¹, M. Scharl¹, M. Hausmann¹, G. Rogler¹

Gp96 deficiency partially affects TLR4 functionality due to an impaired ERK and p38 phosphorylation

Division of Gastroenterology and Hepatology, University Hospital Zurich, University of Zurich, Zurich, Switzerland¹

Introduction:

Gp96 is an endoplasmic reticulum chaperone which plays an important role in innate and adaptive immunity. The loss of tolerance against the host gut flora in patients with inflammatory bowel disease (IBD) is correlated with its absence in intestinal macrophages (iMACs). They are essential for pathogen recognition at the mucosal surface of the gastrointestinal (GI) tract through different receptors, among others, Toll-like receptors (TLRs). TLR activation leads to the phosphorylation of NFκB and kinases such as ERK, p38 and JNK. Our previous studies revealed a strong expression of TLR2 and 4, and a specific loss of gp96 in inflammatory iMACs of patients with CD. Hence, we aim to study the role of gp96 on TLR function in macrophages.

Methods:

MM6 were stably transduced with a lentiviral gp96-knockdown vector using Fugene Transfection Kit. Cells were treated with LPS (100ng/ml) for 2 hours. To study the relevance of gp96 *in vivo*, conditional LysMcre-gp96knock-out (cKO) mice were generated. Peritoneal macrophages were isolated from wild-type (WT) and cKO mice, and were treated with LPS (100 ng/ml) for 2 hours or with M-CSF 10 ng/ml for 3 days prior to restimulation with M-CSF 10ng/ml for 10 min. In all cases, TLR2 and TLR4 expression was analyzed by flow cytometry and the expression of NFκB, IκB-α, ERK, p38, IL-8, IL-6 and TNF-α was analyzed by Western blot, qPCR and ELISA.

Results:

Flow cytometry analysis revealed that the number of TLR4+ and TLR2+ gp96 shRNA cells was slightly decreased vs mock-transduced cells. In line with this, the number of TLR4+ and TLR2+ macrophages showed a slight decrease in cKO mice compared with WT mice. The functionality of TLR4 was analyzed and LPS induced a significant increase in the ratio p-IκB-α/IκB-α and in p-NFκB, but not in p-ERK/ERK and p-p38/p38 in both gp96 shRNA and in cKO macrophages compared with non-treated mock-transduced cells or WT cells. Moreover, LPS induced a significant increase in IL-8 expression and secretion in gp96 shRNA vs mock-transduced. LPS also induced a significant increase in the expression of IL-8, IL-6 and TNF-α in cKO macrophages vs non-treated WT macrophages. Moreover, M-CSF treatment induced a significant increase in the ratio p-p38/p38 and in the ratio p-ERK/ERK in WT macrophages compared with non-treated macrophages, whereas no significant increase was detected in treated cKO macrophages pointing to an impaired functionality of CSF1R.

Conclusion:

Loss of gp96 in macrophages affects the functionality of TLR4 through a reduction in the phosphorylation of kinases downstream this receptor. This impairment has a direct impact in several receptors such as CSF1R.

M. Barben¹, C. Schori¹, M. Samardzija¹, C. Grimm¹

Progressive cone degeneration in a chronic hypoxia-like situation can be rescued by targeting Hif1a

Dept. Ophthalmology, Lab of Retinal Cell Biology, Zurich¹

Introduction:

Human vision largely depends on cone photoreceptors which are responsible for color and high resolution vision. Patients suffering from cone degenerative diseases including age-related macular degeneration (AMD) lose this central vision, which severely affects their quality of life. Since hypoxia and hypoxia-inducible factors (HIFs) have been postulated to be important in the etiology of AMD, we mimicked chronic hypoxia by stabilizing HIFs in cone photoreceptors to further investigate the role of hypoxia on cone pathophysiology.

Methods:

To induce a chronic hypoxia-like response, we ablated the von Hippel Lindau (VHL) protein from cone photoreceptors of the all-cone *R91W;Nrt^{-/-}* mice using the Cre-loxP system (*BPcre;R91W;Nrt^{-/-};Vhl^{fl/fl}* (=cone^{ΔVhl})). We analyzed cone^{ΔVhl} mice at 4, 6, 8, 12 and 26 weeks of age and evaluated retinal function and morphology by ERG, OCT and light microscopy. Western blotting and real-time PCR were used to test differential regulation of several molecular pathways. Additionally, we analyzed *BPcre;R91W;Nrt^{-/-};Vhl^{fl/fl};Hif1a^{fl/fl}* (cone^{ΔVhlHif1a}) mice at 4, 8 and 12 weeks of age to test the effect of selective inactivation of *Hif1a*.

Results:

Cone-specific ablation of *Vhl* resulted in stabilization of HIF1A and in increased expression of HIF1A target genes such as *adrenomedullin* and *vascular endothelial growth factor*. Additionally, expression levels of genes associated with glycolysis (*Glucose transporter 1* and *pyruvate dehydrogenase kinase 1*) and mitochondrial autophagy (*BCL2/adenovirus E1B interacting protein 3; Bnip3*) were increased. Progressive cone degeneration as shown by severe reduction of the outer nuclear layer at 12 weeks of age was paralleled by reduced retinal function in cone^{ΔVhl} mice. Importantly, additional deletion of *Hif1a* in cone^{ΔVhlHif1a} mice rescued the observed phenotype.

Conclusion:

Here, we showed that activation of a chronic hypoxia-like response in cone photoreceptors leads to severe cone degeneration, a feature that may play an important role in AMD pathology. Differential regulation of genes involved in metabolic energy balance suggests a potential shift from oxidative phosphorylation to glycolysis. The observed vision loss in cone^{ΔVhl} mice can be rescued by selective inactivation of *Hif1a* in cone^{ΔVhlHif1a} mice. In summary, our results identify HIF1A as a potential therapeutic target to rescue hypoxia-mediated retinal degeneration in patients. Therefore, we are currently testing a gene therapy approach using an AAV-mediated expression of an shRNA directed against *Hif1a* in photoreceptors.

Optimizing STI Screening Among HIV positive MSM using a Simple Risk Evaluation

Division of Infectious Diseases and Hospital Epidemiology, University Hospital Zurich, Zurich, Switzerland¹

Introduction:

The increasing rates of sexually transmitted infections (STIs) among HIV-infected men who have sex with men (MSM) are of a growing concern. There is a scarcity of empirical data on whether a risk-tailored as opposed to a flat 3-monthly screening, is useful in optimizing screening.

Methods:

Between January 2015 and June 2016 we offered repetitive STI screenings to all patients from the Zurich Primary HIV-1 Infection (PHI) study who attended a clinical visit. Patients were tested for gonorrhoea, chlamydia and herpes simplex virus by polymerase chain reaction (PCR) obtained from the rectum, pharynx and urethra, and for syphilis by serological assay. Patients presenting with elevated liver enzymes were tested for hepatitis C by PCR. Mixed-effects logistic regression model with a random (per subject) intercept was used for the multivariable analysis. The model predictions were used for AUC ROC calculation and were also stratified for upper and lower risk quartiles.

Results:

Of 214 patients who attended a clinical visit and were offered a screening, 174 (81%) agreed to be screened at least once, resulting in a total of 334 screens. Most patients were male (96.6%), MSM (87.4%) and had a suppressed HIV viral load (88.5%) (Table 1). Fifty-eight of the 174 patients (33%) had at least one STI in the examined period, contributing to overall 79 detected STIs. Sixty-five percent (51/79) of the detected STIs were asymptomatic. The most frequent STI was chlamydia (n=40, 50.6%), with the rectum being the most prevalent site (n=20/40, 50%). For 84 MSM with a baseline negative test, the overall STIs incidence rate was 62.6 (C.I 40.5-92.4) per 100 person years. In a multivariable analysis, condomless sex (OR 2.2, 1.2-3.9), reporting symptoms of an STI (OR 3, 1.5-5.9) and shorter time since HIV diagnosis (OR 0.88, 0.81-0.96) were associated with higher odds of having an STI. The ROC AUC for a model with these predictors showed a fair performance (0.73), with the lower quartile of the predictions exhibiting a high negative-predictive value (93%).

Table 1. Selected variables examined in this study and the multivariable logistic regression mixed model (for MSM only).

	Overall (Screenings)	No STI	STI	p-value	Multivariable Model (MSM only) OR (95% C.I.)
N	334	263	71*		305
Age (median [IQR])	39.25 [34.05, 46.08]	41.44 [34.46, 46.42]	37.62 [31.62, 42.32]	0.006	-
Years since diagnosis (mean (sd))	5.30 (3.58)	5.62 (3.62)	4.07 (3.17)	0.001	0.88 (0.81-0.96)
Diagnosis year (mean (sd))	2010 (3.6)	2009 (3.6)	2011 (3.2)	0.002	-
History of psychiatric treatment (%)	81 (24.3)	70 (26.6)	11 (15.5)	0.074	-
Heterosexual (%)	29 (8.7)	28 (10.6)	1 (1.4)	0.027	-
Stable partnership (%)	181 (54.2)	150 (57.0)	31 (43.7)	0.061	-
Condomless sex (%)	131 (39.2)	89 (33.8)	42 (59.2)	<0.001	2.21 (1.32-3.96)
STI Symptoms (%)	52 (15.6)	27 (10.3)	25 (35.2)	<0.001	3.06 (1.57-5.99)
Number of sexual partners (median [IQR])	2 [1.00, 4.75]	2 [1.00, 4.00]	3 [2.00, 6.50]	<0.001	-
Closest CD4 (median [IQR])	686 [514, 876]	697 [518, 886]	608 [474, 836]	0.160	-
BMI (median [IQR])	23.57 [21.9, 25.5]	23.77 [21.9, 26]	22.61 [21.6, 24.6]	0.024	-

* A total of 79 STIs were detected, in 8 screens two STIs were found at the same screen

Conclusion:

We report a very high incidence and period-prevalence of STIs among MSM who initially presented with a PHI and received early antiretroviral treatment. Thus, a regular STI screening including asymptomatic individuals should be strongly considered in this population. We demonstrate that a simple risk evaluation may help to identify a sub-group of low-risk MSM that can postpone screening, thus optimizing resource allocation.

L. Ahnen¹, H. Stachel¹, S. Kleiser¹, C. Hagmann¹, J. Jiang¹, A. Kalyanov¹, S. Lindner¹, M. Wolf¹, S. Sanchez¹

Near-Infrared Image Reconstruction of Newborn's Brains: Development and Validation of the Light Sensor Prototype

Klinik für Neonatologie, UniversitätsSpital, Zurich¹

Introduction:

Imaging brain oxygenation is crucial for a better understanding of how lesions develop in prematurely born infants. In these patients, cerebral ischemia is known to be related with significant damage on white matter, often resulting in long-term neurodevelopmental impairments. We develop a novel multimodal hybrid diagnostic imager that will allow quantitative monitoring of structural and functional information of the brain. The novel imager will integrate an opto-acoustic (OA) device and a near-infrared optical tomography (NIROT) sensor in a single system. Our aim was to build a prototype of the NIROT sensor for the head of neonates. Since the head of a newborn is very small and fragile much care has to be taken in order to produce a mechanically friendly device in a compact format in which a sufficient number of light sources and detectors can be implemented. Further spatial constraints result from the combination with the OA probe that necessarily uses the fontanel aperture for measurements.

Methods:

The NIROT sensor was designed using 3D-printing technology, biocompatible silicone casting and highly flexible micro-fiber bundles. A 3D-printed rigid inner ring ensures a fixed relative position of the sensor's sources and detector fibers, which is crucial for a successful image reconstruction. The protective silicone casing prevents damage on the delicate infant's skin, ensures correct light coupling and integrates optical windows in a black substrate to avoid optical piping. The flexible sensor fibers keep the sensor light and easy to use in a clinical setting. Heterogeneous silicone phantoms were produced to validate data acquisition, data processing, and image reconstruction.

Results:

The new NIROT sensor prototype is compact and light. The ease of handling makes it very suitable for the clinical application at the bedside, where space is limited. The elevated optical windows of the sensor enable moderate adaption to the head's surface, ensuring good light coupling. No light piping between the source and detector fibers was detected during the measurements on the silicone head phantoms. The shape and location of the inclusion was accurately reconstructed.

Conclusion:

Reconstructed optical properties agree well with target values and the mechanical performance of the new NIROT sensor confirm its suitability for the clinical application.

P. Zanoni¹, S. Velagapudi¹, M. Keel¹, R. Meier², S. Stoma², S. Nørrelykke², L. Rohrer¹, A. Von Eckardstein¹

A genome-wide siRNA screen as a tool to unveil new players in hepatic High Density Lipoprotein metabolism

Institute of Clinical Chemistry, University Hospital, Zürich¹, ScopeM, ETH Zürich, Zürich²

Introduction:

Atherosclerosis is characterized by the progressive accumulation of cholesterol in the intima of the arteries. Plasma levels of high density lipoproteins (HDL)-associated cholesterol are inversely associated with cardiovascular disease in the general population. Many mechanisms have been proposed to explain the atheroprotective effect of HDL. The best described one is the ability of HDL to extract cholesterol from peripheral tissues, including macrophages in the intima of the arteries, and to deliver it to the liver for biliary excretion. Part of the delivery of cholesterol to the hepatocyte is made possible by the Scavenger Receptor Class B type I through selective cholesterol uptake. SCARB1 mutations that induce a complete loss of SR-BI function are associated with increased cardiovascular risk in humans. In addition to selective cholesterol uptake and similar to LDL, some HDL particles are endocytosed by hepatocytes as whole particles. This holoparticle uptake has not only been described for liver cells but also for macrophages, endothelial cells, enterocytes, and renal tubular epithelial cells but its molecular basis is little understood.

Methods:

To discover new genes involved in holoparticle uptake of HDL we performed a microscopy-based genome-wide siRNA screen. In our screen, we tested the effect of approximately 68000 different siRNAs (3 siRNAs per gene) on the uptake of HDL fluorescently labelled in their protein moiety (fl-HDL) by the human hepatocarcinoma cell line Huh-7.

Results:

The analysis of the screening data revealed a list of approximately 150 genes involved in fl-HDL uptake. Interestingly, when functional interaction networks were generated with these hits, many of the top hits display a high degree of functional interrelation. Furthermore, a Gene Ontology analysis revealed a significant enrichment for endocytosis and intracellular trafficking.

Conclusion:

In conclusion, we consider the data obtained to be a reliable source of novel players in HDL hepatic uptake.

SF. Stämpfli¹, T. Özkartal¹, N. Hagenbuch², B. Bernhart¹, AJ. Flammer¹, A. Vecchiati¹, GM. Fröhlich¹, F. Ruschitzka¹, L. Held², FC. Tanner¹

Small pericardial effusions predict outcome in heart transplant recipients

Department of Cardiology, University Heart Center Zurich, Switzerland¹, Department of Biostatistics; Epidemiology, Biostatistics and Prevention Institute, University of Zurich, Switzerland²

Introduction:

Hemodynamically irrelevant pericardial effusion (PE) is a known predictor of negative outcome in heart failure patients. In contrast, the clinical relevance of non-surgery related PE in heart transplanted patients remains unknown. This study was designed to assess the prognostic value of PE occurring later than one year after heart transplantation.

Methods:

All 313 patients who underwent heart transplantation in Zurich between August 1989 and July 2012 were retrospectively assessed for PE in our echocardiography database. Exclusion criteria were death within the first year after transplantation (64 patients), age <16 years at heart transplantation (8 patients), and lack of echocardiography follow-up (89 patients, mostly due to transfer to a different clinic after transplantation). Cox proportional hazard models were performed to analyze both mortality and unscheduled hospitalization for patients with and without PE. For analysis of mortality, the data was adjusted for gender and age at transplantation. Statistical analysis of not normally distributed parameters at baseline vs. time of PE was performed using Wilcoxon signed-rank test.

Results:

A total of 152 patients was included, of which 25 developed PE. The median follow-up was 11.9 years with a PE incidence of 14.4 per 1000 patient-years. Absolute number of deaths was 6 in the PE group and 46 in the non-PE group. The occurrence of PE was associated with an increased risk of death (HR 2.49, 95%-CI 1.02 - 6.13, $p < 0.05$). Cause of death was cancer (28.8%), infections (15.4%), heart failure (13.4%), cardiovascular events (11.5%), and transplant rejection (3.8%). Absolute number of unscheduled hospitalizations was 306. In patients with PE, the risk of hospital admission was increased (HR 2.53, 95%-CI 1.57 - 4.1, $p = 0.0002$). The main reason for hospitalization was infection in 47.6% followed by cardiovascular events (10.4%) and cancer (6.9%). Comparison of baseline characteristics as compared to the time point of PE suggested multifactorial etiologies of PE.

Conclusion:

This study reveals that the echocardiographic finding of PE in heart transplanted patients is associated with a 2.5 times higher risk of either death or hospitalization as compared to patients without PE. Thus, small PE which may be observed during routine echocardiography – even though hemodynamically irrelevant and of multifactorial origin – are associated with a negative outcome.

Electrophysiological changes in mice devoid of cellular prion protein*Institute of Neuropathology, University Hospital of Zurich, Zurich, Switzerland¹***Introduction:**

Prion protein (PrP^C) is a highly conserved cell surface protein that has been implicated in several cellular functions based on studies carried out in different lines of PrP^C knockout mice. However, the mixed genetic background of most of those mouse lines renders the results of these studies hard to interpret. Therefore, a new coisogenic PrP^C knock out mouse line (ZH3) has recently been generated in a pure Black-6 (C57Bl6/J) genetic background. This project is aimed at investigating the validity of a published phenotype of PrP^C knockout mice; a reduction of the slow afterhyperpolarization (sAHP), in the ZH3 mouse and to elucidate underlying molecular mechanisms.

Methods:

We analyzed 4-6 weeks old *Prnp* ablated and wild-type male littermates from heterozygous ZH3/C57Bl6/J breedings. Visually guided whole-cell patch clamp recordings in current clamp mode of pyramidal neurons in the CA1 area of the hippocampus of acute brain slices *in vitro* were performed. Medium (mAHP) and slow AHP were induced by a train of 50 short current injections and the amplitude of the sAHP was measured 200ms after stimulus cessation. Additional parameters assessed were: amplitude of the medium AHP (mAHP), resting membrane potential, input resistance, cell capacitance, action potential (AP) threshold, AP amplitude, AP rise time, AP half-width and fast AHP. Statistical significance was assessed using Student's t-test and two-way ANOVA with Bonferroni post-hoc correction where appropriate. P-values < 0.05 were considered significant.

Results:

CA1 pyramidal neurons of ZH3 mice show a significant reduction of the sAHP at 50 and 100Hz train frequency ($p < 0.0001$, two-way ANOVA, Bonferroni corrected). Interestingly, this difference could be rescued when slices were pretreated with MPEP, an antagonist of metabotropic glutamate receptor 5 (mGluR5). PrP^C has been suggested to interact with mGluR5 and mGluR5 activation is considered to induce a reduction of mAHP and sAHP. There was no significant difference in the other parameters.

Conclusion:

Our results show that CA1 pyramidal neurons of PrP^C knockout mice have a significantly reduced sAHP. This result reproduces several studies that have shown a reduced sAHP in PrP^C knockout mice of different genetic backgrounds indicating that the reduction of sAHP arises from a loss of physiological function of PrP^C and not due to genetic polymorphisms of mouse models used. Furthermore, we could rescue the phenotype by blocking mGluR5, indicating that ZH3 mice have a hyperactive mGluR5 signalling.

SF. Stämpfli¹, L. Erhart¹, N. Hagenbuch², BE. Stähli¹, C. Gruner¹, M. Greutmann¹, M. Niemann³, BA. Kaufmann⁴, R. Jenni¹, L. Held², FC. Tanner¹

proBNP is strong predictor of outcome in left ventricular non-compaction cardiomyopathy

Department of Cardiology, University Heart Center Zurich, Switzerland¹, Department of Biostatistics; Epidemiology, Biostatistics and Prevention Institute, University of Zurich, Switzerland², Faculty Mechanical and Medical Engineering, Furtwangen University, Germany³, Department of Cardiology; University Hospital Basel, Switzerland⁴

Introduction:

Left ventricular non-compaction cardiomyopathy (LVNC) is a potentially life threatening disease of the left ventricular myocardium characterized by a thin, compacted, epicardial layer and a thick endocardial layer with deep recesses between prominent trabeculations. While left ventricular ejection fraction, heart failure symptoms, and exercise capacity are known to correlate with clinical outcome in LVNC patients, the role of proBNP has never been assessed.

Methods:

A total of 153 patients with isolated LVNC were identified from the clinical databases at the University Hospitals Zurich and Basel (1988 and 2015). After a median follow-up of 6.6 years 23 (15%) patients reached the composite endpoint of all-cause mortality and heart transplantation. All available values for proBNP, left ventricular ejection fraction (LVEF, biplane Simpson's method), NYHA functional class, and exercise capacity by bicycle ergometer (percent of target performance) were analyzed using unadjusted and adjusted (for age and gender) Cox regression models as well as a combined covariate analysis.

Results:

Time to event analysis (death or transplantation) revealed a highly significant positive correlation for proBNP levels (adjusted HR 2.44 for every doubling, 95%-CI 1.45-4.09, $p=0.0007$) and a negative correlation for LVEF (adjusted HR 2.57 for 10% decrease, 95%-CI 1.67-3.59, $p<0.0001$). Using proBNP and LVEF as combined covariates, a very strong influence of proBNP on the hazard ratio was revealed (adjusted log₂ HR 2.89, 95%-CI 1.33-6.26, $p=0.007$), whereas LVEF was no longer significant (adjusted HR 1.02, 95%-CI 0.95-1.09, $p=0.66$) indicating a favorable prognostic power of proBNP over LVEF. The prognostic power of proBNP was underscored by the finding that no event was recorded in patients with normal proBNP levels whereas proBNP levels >2000 ng/l were associated with a 40 times higher risk of death or transplantation as compared to proBNP <2000 ng/l. A higher NYHA functional class was associated with a worse outcome (adjusted HR 3.58, 95%-CI 1.57-8.15, $p = 0.002$). Exercise capacity revealed a trend in the same direction.

Conclusion:

This study provides evidence that proBNP is a strong predictor of outcome in patients with LVNC. The prognostic power of proBNP was even stronger than that of LVEF, indicating a particularly high prognostic relevance in this patient population. Hence, proBNP measurement may improve clinical risk assessment in patients with LVNC.

HA. Mbunkah¹, S. Schmutz¹, A. Marzel¹, NN. Ndi², E. Mbu², LM. Besong³, BA. Sama⁴, E. Orock⁵, M. Shilaih¹, NK. Campbell¹, R. Kouyos¹, HF. Günthard¹, KJ. Metzner¹

Prevalence of transmitted HIV-1 drug resistance in Cameroon in the years 2014/15

Division of Infectious Diseases and Hospital Epidemiology, UniversitätsSpital Zürich¹, HIV Treatment Centre, Regional Hospital Bamenda, Cameroon², HIV Treatment Centre, District Hospital Kumba, Cameroon³, HIV Treatment Centre, District Hospital Ndop, Cameroon⁴, HIV Treatment Centre, Regional Hospital Ngaoundere, Cameroon⁵

Introduction:

The benefits of combination antiretroviral therapy can be compromised by the development of drug resistance. In resource-limited settings many patients receiving first-line drugs develop virological failure and may transmit drug resistant viruses to newly infected persons. In Cameroon, second-line therapy is often chosen without a genotypic resistance test. In order to determine the most recent prevalence, types and transmission patterns of resistance-associated mutations, we monitored HIV-1 drug resistance using next-generation sequencing.

Methods:

We developed an HIV-1 protease and reverse transcriptase drug resistance genotyping assay applicable to dried blood spot samples (DBS) and also universal - genotyping all heterogeneous HIV-1 subtypes of at least group M. DBS samples were collected from 200 newly diagnosed and drug-naïve HIV-1 patients in four hospitals in semi-urban to urban areas with some of the highest HIV-1 prevalence rates in Cameroon. RNA was extracted and a 1.4kb fragment of the *pol* gene was amplified using two overlapping nested RT-PCRs. Successful amplicons were sequenced with next-generation sequencing and the Stanford HIV Sequence Database was used to interpret resistance mutations. Subtyping was performed using the REGA Subtyping Tool.

Results:

All major group M HIV-1 subtypes were detected using the assay developed with an overall analytical sensitivity of 10^3 RNA copies/mL. The overlapping split strategy used in the PCRs showed a high sensitivity for the DBS: An 80% (160/200) amplification success rate was obtained with the DBS. These 200 patients had no viral load records but a mean CD4 count of 308.1 ± 192.7 cells/ μ L (Table 1). A significantly higher mean CD4 count was observed with unsuccessful patients' samples ($p = 0.0019$). HIV-1 subtype diversity was quite high with the commonest subtypes being: CRF02_AG (78%), G (5%), D, A, F (3% each), as well as other circulating and unique recombinant forms. Major resistance-associated mutations to Nucleotide Reverse Transcriptase Inhibitors was 3%, resistance to Non-Nucleoside Reverse Transcriptase Inhibitors was 8.1% and no major resistance mutations to Protease Inhibitors (Table 1). The drugs Zidovudine, Nevirapine and Efavirenz were most affected.

TABLE 1: Baseline characteristics of study population

Number of samples per site ^a	
Site A	50
Site B	85
Site C	31
Site D	34
Gender ^a	
Male	39.5%
Female	60.5%
Age (Mean \pm SD) ^a	35.2 \pm 8.4 years

CD4 Count (Mean ± SD) ^a	308.1 ± 192.7 cells/μl
WHO Clinical Staging ^a	
<i>Primary</i>	27.2%
<i>Stage 1</i>	30%
<i>Stage 2</i>	26.3%
<i>Stage 3</i>	14.5%
<i>Stage 4</i>	2%
Marital Status ^a	
<i>Single</i>	41.2%
<i>Married</i>	40.5%
<i>Widow(er)</i>	13.5%
<i>Divorced</i>	4.8%
Major NRTI Mutations ^b	
M184I	0.6%
M41L	0.6%
T215Y	1.2%
L210W	0.6%
Major NNRTI Mutations ^b	
E138G	1.3%
G190A	1.9%
E138K	0.6%
K103N	0.6%
E138A	2.5%
Y181C	0.6%
Y188H	0.6%
Major PI Mutations ^b	0%

^a Information for 200 patients

^b Information for 160 patients

Conclusion:

Transmitted HIV-1 drug resistance in Cameroon is low to moderate but has increased compared to previous reports in 2009. This evidence depicts a public health problem with possible implications on prevention, treatment and monitoring of HIV-1 infections in the country.

DL. Braun¹, R. Kouyos¹, B. Hampel¹, C. Grube¹, HF. Günthard¹, J. Böni², JS. Fehr¹

A Systematic HCV-RNA Sree in HIV+ MSM Reveals High Number of Potential Transmitters

Division of Infectious Diseases and Hospital Epidemiology, University Hospital Zurich, Zurich, Switzerland¹, Institute of Medical Virology, Swiss National Center for Retroviruses, Zurich, Switzerland²

Introduction:

The prevalence of sexually transmitted incident hepatitis C virus (HCV) infections among HIV-positive men who have sex with men (MSM) has increased worldwide, including an epidemic in Switzerland in MSM. The Swiss HCVree Trial (ClinicalTrials.gov NCT02785666) aims to implement a targeted HCV-RNA based assessment of the prevalence of replicating HCV infections in HIV-positive MSM participating in the Swiss HIV Cohort Study (SHCS), and thereafter to treat all HCV-RNA positive MSM with newest anti-HCV direct acting agents. Here we report on preliminary data from the screening period.

Methods:

Between October 1st 2015 and May 31th 2016 we offered a systematic, intensified HCV-RNA polymerase chain reaction (PCR) based screening to all MSM participating in the SHCS, which is estimated to represent 75% of all HIV-infected MSM living in Switzerland. Participants were screened at least once at the occasion of the regular clinical HIV visit. Liver transaminases were measured simultaneously, considering >50 U/l as above the upper limit of normal. HCV-RNA testing was done centralized at a single lab using the Abbott RealTime HCV assay with a limit of detection of 12 IU/ml.

Results:

Overall, 3'792 individuals are recorded as MSM in the SHCS database, of them we screened 3'620 (95%) by HCV-RNA PCR. Hundred-seventy-eight (4.9%) out of these 3'620 MSM harbored a replicating HCV infection (Figure 1). Mean age of MSM was 49 years and 94% had suppressed HIV viremia, without differences between replicating and non-replicating HCV. Genotype (GT) 1 was the most prevalent GT (72%), followed by GT 4 (22%), GT 3 (5%), and GT 2 (1%). Of the 178 MSM with replicating HCV, 32 individuals (18%) had an incident HCV infection, without prior positive HCV test (e.g. HCV antibodies, HCV-RNA) recorded in the SHCS database. Eight of the MSM with an incident HCV (25%) presented with normal liver enzymes during the screening period.

Figure 1: Proportion of MSM in the SHCS with a HCV-PCR screen, stratified by HCV replicating status and by newly detected (incident) and previously known HCV infection.



Conclusion:

We identified a high number of replicating HCV infections among HIV positive MSM participating in the SHCS, resulting in 5% prevalence in this population. A substantial proportion of MSM with replicating HCV presented with non-elevated liver enzymes. Thus, an intensified HCV-RNA based screening strategy among sexually active HIV-coinfected MSM is worth to detect potentially transmitters, and to offer universal treatment with DAAs in order to end the epidemic and to achieve a reduction of disease burden on a population level.

MS. Silginer¹, SN. Nagy¹, CH. Happold¹, HS. Schneider¹, MW. Weller¹, PR. Roth¹

Autocrine activation of the IFN signaling pathway modulates the immunogenicity of glioma cells

University Hospital Zürich, Department of Neurology, Zurich¹

Introduction:

Interferons (IFN) are cytokines that are typically induced upon viral infection, but can be constitutively expressed also in the absence of acute infection to regulate various processes. Alterations in IFN signaling have been observed in numerous malignancies, however the physiological role of autocrine and paracrine IFN signaling remains poorly understood.

Methods:

Here, we aimed at characterizing autocrine IFN- β signaling and its functional impact in glioma cells *in vitro* using RNA interference-mediated gene silencing.

Results:

Exposure to recombinant IFN- β led to the induction of the classical IFN-response gene Myxovirus A (MxA) in a panel of glioma cell lines, whereas some glioma-initiating cells showed basal MxA protein expression even in the absence of exogenous IFN- β , indicating the presence of constitutive IFN signaling. Silencing of the type I IFN receptors IFNAR1 or IFNAR2, or the ligands IFN- α or IFN- β , decreased MxA levels, providing evidence for the existence of an autocrine type I IFN signaling loop. On a functional level, we observed reduced PD-L1, MHC class I and class II expression and increased susceptibility to NK cell-mediated lysis upon IFNAR silencing, suggesting that constitutive IFN signaling in glioma cells plays an immunomodulatory role.

Conclusion:

Our findings point to an important role of constitutive IFN signaling in the immune evasion of glioma cells.

Molecular Pharmacology of Colistin Sulfate

University Hospital Zurich, Department of Clinical Pharmacology and Toxicology¹

Introduction:

Colistin is a polycation antibiotic used for the treatment of multidrug-resistance (MDR) gram-negative infections; nevertheless, its use is often limited by the high incidence of renal damage. The mechanism underlying colistin-induced nephrotoxicity is not known but perhaps related to its accumulation in the renal cortex upon extensive reabsorption from the nascent urine. The purpose of the present study was to better characterize the molecular mechanism of colistin-induced nephrotoxicity in order to define possible protective strategy.

Methods:

HEK293 cells stably transfected with the main organic cation transporters expressed at the apical membrane of proximal tubule were employed to characterize the transport system involved in colistin renal handling and to understand the impact of membrane transport in colistin toxicity. Freshly isolated, intact mitochondria, were used to study the direct mitotoxic effect of colistin and its molecular determinants.

Results:

[¹⁴C]Colistin was transported by carnitine/organic cation transporter 2 (OCTN2, SLC22A5) but not by the organic cation transporter 1 (OCT1) and N1 (OCTN1). Non-labeled colistin could inhibit in a non-competitive manner the OCTN2-mediated transport of [³H]L-carnitine ($K_i = 22.7 \pm 0.9$ mM). HEK293 stably transfected with OCTN2 were more sensitive than WT-HEK293 to colistin, suggesting that the toxicity was dependent on its intracellular accumulation. When the endogenous OCTN2-mediated colistin transport was inhibited by co-incubation with L-carnitine, primary mouse proximal tubular cells were fully protected from colistin toxicity. In summary, OCTN2 contributes to the transport of colistin across the plasma membrane and intracellular colistin accumulation and toxicity decreased along with the increasing extracellular L-carnitine, the main OCTN2 substrate.

Colistin intracellular accumulation is determinant for colistin toxicity. Because kidney from mouse exposed to colistin showed signs of mitochondrial stress we tested the hypothesis that colistin directly targets mitochondria. In isolated mitochondria from HEK293 cells or from mouse kidney, colistin induced a rapid shrinkage of the mitochondria and a collapse of the mitochondrial membrane potential.

Conclusion:

OCTN2 contributes to the transport of colistin across the plasma membrane. Colistin intracellular accumulation and toxicity negatively correlated with the extracellular concentration of L-carnitine, the main OCTN2 substrate, indicating that colistin toxicity depended on its intracellular level and carnitine protection was, at least in part, due to the inhibition of the OCTN2-mediated colistin uptake. Intracellular colistin directly targets mitochondria. Because carnitine plays an important role in the energy state of mitochondria it is possible that carnitine can exert its protective effect also at the mitochondrial levels.

Carnitine, as an endogenous, well-tolerated molecule, represents an intriguing candidate for protection against colistin nephrotoxicity and is now under evaluation in a preclinical, in vivo, study.

Calcium channel subunit $\alpha 2\delta$ -1 as a genetic modifier of prion toxicity*Institute of Neuropathology, University Hospital Zürich, Zurich¹***Introduction:**

Prion diseases are rare and inexorably lethal neurodegenerative diseases which can arise spontaneously, be inherited or acquired by infection. The pathogenic agent, the prion, consists of neurotoxic multimeric assemblies of misfolded, host-encoded prion protein (PrP^C). PrP^C expression is essential for prion propagation and for prion-induced neurodegeneration. How do prions cause neuronal demise? This question is still unanswered and this constrains our possibility of treatment. Since the central role of PrP^C in the pathogenesis, several approaches aimed at targeting PrP^C have been demonstrated to have therapeutic potential and are currently pursued. Complementary to this, the identification of PrP interacting partners may shed light on the cellular pathways which are perturbed in the case of prion infection and are relevant for the development of the disease.

PrP^C interacts with the $\alpha 2\delta$ -1 subunit of voltage-gated calcium channels (VGCC). $\alpha 2\delta$ proteins are glycosylphosphatidylinositol (GPI)-anchored VGCC-associated subunits that promote VGCC cellular transport and modulate presynaptic function by setting synaptic VGCC abundance and promoting efficient coupling of Ca²⁺ entry to drive neurotransmitter release. Genetic disease associated PrP mutants, which are prone to misfolding and intracellular retention, affect $\alpha 2\delta$ -1 cellular localization and VGCC function and compromise glutamate release and synaptic transmission in the cerebellum of transgenic mice. These findings pointed to $\alpha 2\delta$ -1 as the molecular partner by which PrP possibly exerts at least part of its biological activity in neurons, and by which misfolded and disease associated PrP produces neuronal dysfunction.

Methods:

We used a biochemical approach to identify the PrP domain that is involved in the binding with $\alpha 2\delta$ -1. To test if $\alpha 2\delta$ -1 acts as a relevant modifier of prion toxicity, we used a genetic and a pharmacological strategy both *ex vivo*, in cerebellar organotypic cultured slices (COCS), and *in vivo* by assessing the development of the disease in $\alpha 2\delta$ -1 overexpressing and $\alpha 2\delta$ -1 knock-out mice upon prion infection.

Results:

We have now characterized the PrP- $\alpha 2\delta$ -1 interaction further. By using transgenic mice that express PrP deletion mutants and testing the ability of these PrP truncated versions to co-immunoprecipitate with co-expressed $\alpha 2\delta$ -1, we have obtained an insight into the PrP domain that is involved in the binding with $\alpha 2\delta$ -1. The interaction could also be competed by anti-PrP antibody Fab fragment targeting the amino acid stretch involved in the interaction with $\alpha 2\delta$ -1. Upon intracerebral inoculation with two different doses of RML6 prions, $\alpha 2\delta$ -1 knock-out mice displayed shorter survival times. Thus genetic ablation of $\alpha 2\delta$ -1 significantly accelerated prion disease progression. *In vitro*, pharmacological blockade of $\alpha 2\delta$ -1 by gabapentin, did not prevent neuronal loss in RML infected COCS. Mice which overexpress $\alpha 2\delta$ -1 in neurons, succumbed to RML with attack rates and incubation times similar to wild-type mice and developed the classic histologic and biochemical features of prion diseases. *In vitro* however, COCS from $\alpha 2\delta$ -1 overexpressing mice tended to be less susceptible to prion induced neurodegeneration and to the neurotoxic prion mimetic POM1 antibody.

Conclusion:

Our results boosted our understanding of the prion-triggered pathogenic mechanisms and pointed to at potentiating $\alpha 2\delta$ -1 function as potential therapeutic approach for prion diseases.

ZL. Song¹, E. Maurizio¹, B. Humar¹, N. Borgeaud¹, R. Graf¹, PA. Clavien¹, YH. Tian¹

Exogenous Melatonin Rescues Small-for-Size Liver Graft Failure

Department of Visceral & Transplantation Surgery, University Hospital of Zurich, Switzerland¹

Introduction:

Live donor liver transplantation increases the liver donor pool, but it is impeded by small-for-size syndrome. Pharmacological dose of melatonin (MLT) has been shown to protect the liver grafts in several aspects. The aim of the study is to investigate whether MLT enhances liver regeneration and rescues small-for-size liver graft failure in mice models.

Methods:

Male C57BL6 mice were divided into 3 groups: (I) I/R+PH group: 60 min liver ischemia plus 2/3 hepatectomy; (II) I/R+exPH group: 60 min liver ischemia plus extended (86%) hepatectomy; (III) Partial liver transplantation (POLT) group: arterialized 30% liver transplantation. IL-6 knockout mice were used in the model of group I, some of the mice were treated with recombinant IL-6 30 min before surgery. Each group was subdivided into MLT treated and control groups. Hepatic injury was determined by AST, ALT and histology. The cytokines and histological evidence of liver regeneration were examined by PCR and immunostaining. Serum HMGB1 was measured by ELISA. The expression of gp 130 and STAT3 was performed by western blot. Survival rate was monitored in I/R+exPH and POLT groups.

Results:

Group I disclosed less hepatic injury, improved hepatocyte regeneration and promoted regenerating cytokine release in MLT treated group than controls. HMGB1 was reduced significantly in mice treated by MLT. Improved hepatocyte regeneration was lost in IL-6 KO mice even with the treatment of MLT, and it was restored with the treatment of recombinant IL-6. In group II, 7 day's survival rate was 0% in control mice in comparison with 50% in MLT treated mice. In POLT group, the treatment of MLT increased the survival rate of recipient mice from 0% to 57% and the expression of gp 130 and STAT3 was significantly upregulated by MLT treatment.

Conclusion:

MLT rescues small for size liver graft failure by reducing graft ischemic reperfusion injury and promoting liver regeneration through IL-6/gp130 dependent STAT3 pathway.

A. Bopp¹, P. Wolint¹, J. Buschmann¹, MY. Emmert¹, Y. Tian¹, O. Evrova³, M. Hilbe⁴, P. Giovanoli⁵, F. Maisano⁶, SP. Hoerstrup²

Effects of hcpMSCs seeded as single cells or as 3D-microtissues onto vascularization of a collagen Matricel® scaffold on the CAM assay

Division of Surgical Research, University Hospital of Zurich, Zurich, Switzerland¹, Institute for Regenerative Medicine, University of Zurich, Zurich, Switzerland², Laboratory of Applied Mechanobiology, ETH Zurich, Zurich, Switzerland³, Institute of Veterinary Pathology, Zurich, Zurich, Switzerland⁴, Plastic Surgery and Hand Surgery, University Hospital Zurich, Zurich, Switzerland⁵, Heart Center Zurich, University Hospital of Zurich, Zurich, Switzerland⁶

Introduction:

Neovascularization is one of the most important issues in tissue repair and regenerative medicine. Due to the lack of efficiency in previous single cell-based concepts, the strategy of 3D cell culture techniques is gaining interest. In this context, scaffold free 3D microtissues have been suggested as a promising alternative, as they were shown to have a greater angiogenic potential than their single cell counterparts. The chorioallantoic membrane (CAM) assay offers the option to compare the angiogenic effect *in ovo* between different cell types, not only in a morphological manner by histological analysis of the vessel ingrowth but also to measure precisely the functional perfusion capacity of vascularized biomaterials grown on the CAM *in vivo* by MRI.

The objectives of this study were (i) to get insight into potential inter-donor variability in terms of angiogenic potential, (ii) to study the differences of MTs and single cells in this experimental setting and (iii) to compare functional vessels as determined by the perfusion capacity (MRI) with the capillary density (histology).

Methods:

A commercially available collagen scaffold, Matricel®, was seeded with either MTs or single cells of cardiopoietic precursor cells of two human donors and placed onto the CAM. We analyzed the vessel ingrowth histologically by assessing the density of visually identifiable vessels in the border zone of the scaffold with the CAM after 2, 4 and 7 days. Furthermore, the perfusion capacity related to functional vessels was assessed by MRI *in ovo* at 7 days (control cell-free scaffolds).

Results:

MRI analysis showed no significant difference in perfusion capacity between the cell-free, control scaffolds and the samples seeded with either single cells or MTs at day 7. However, histological evaluation showed a significantly higher number of vessels in the scaffolds seeded with MTs compared to the ones loaded with single cells and the controls. Donor variability was only present in the single cell samples. Furthermore, the tissue composition within the scaffolds differed substantially between the groups. We found the pores of the MT-seeded scaffolds to be filled with newly produced tissue to a much higher extend compared to the other samples.

Conclusion:

There was no benefit in seeding the scaffolds with cells to improve its ability to induce functional tissue perfusion. However, our experiment showed a remarkably higher angiogenic potential of the MTs on a morphological level. This is probably due to their stronger influence on the formation of microvessels, which are not yet completely functional and therefore not detectable in the MRI analysis. Moreover, the MTs seem to have a greater capacity to induce tissue remodeling processes leading to enhanced tissue formation within the graft, which could be of considerable benefit in multiple regenerative approaches.

S. Sorce*¹, M. Nuvolone*¹, G. Russo², P. Schwarz¹, A. Aguzzi¹

Temporal transcriptional changes induced by prions in mice

Institute of Neuropathology, University Hospital Zurich, Switzerland¹, Functional Genomics Center Zurich (FGCZ), Zurich²

Introduction:

Transmissible Spongiform Encephalopathies (TSEs) are a group of neurodegenerative diseases caused by the accumulation of infectious prion deposits and characterized by the presence of spongiform vacuoles in affected brain regions. Although some of the molecular mechanisms underlying prion neurotoxicity have been identified, so far it is not possible to definitively arrest the course of the disease. Therapeutic treatment of TSEs remains therefore challenging; but clarifying all the components involved in prion neurotoxicity can be instrumental for novel possible therapeutic approaches.

Methods:

Mice challenged with prions or normal brain homogenate have been sacrificed at different time points after injection and RNA have been extracted from hippocampi and cerebella, which are the brain areas most affected by the disease. In order to better understand the toxicity pathways related to prion replication and accumulation in the brain, we have performed a transcriptional profile analysis by RNA-sequencing.

Results:

As expected, the results show a temporal pattern of changes linked to the progressive exacerbation of the disease, and mainly related to glial reactions. However, certain disease-related molecular changes could be already detected at the earliest time points, despite the known absence of obvious neuropathological or neurological hallmarks. In addition, we have noticed that these alterations in gene expression largely overlap with changes induced by the normal aging process: the brain of a 2.5 month-old mouse injected with prions presents features of the brain of an 8 month-old control mouse. These profiles were observed in both analyzed brain areas. Further analyses are ongoing to validate these results, identify the underlying molecular mechanisms and understand the clinical relevance of this process.

Conclusion:

These findings uncover a completely different perspective to understand and analyze the progression of prion diseases since they would implicate a premature, accelerated aging effect on the brain of young individuals in the presence of small amounts of seed prion aggregates. In light of the similarities with other common neurodegenerative diseases, it could be then imagined that such an early aging process could occur in the brain of young individuals that will eventually develop neurodegeneration in advanced age. Understanding this premature brain aging process during the initial disease stages would therefore mean that novel targets of early diagnosis and intervention could be identified in order to prevent/delay neurodegeneration.

** equal contribution*

The role of the prion protein in the development of muscular pathology

Institute of Neuropathology, University Hospital Zurich, Switzerland¹, Institute of Laboratory Animal Science, University of Zurich, Zurich²

Introduction:

The prion protein (PrP^C, encoded by the *PRNP* gene) is best known for its involvement in the development of transmissible spongiform encephalopathies. However, it is also physiologically expressed in many tissues and organs, other than the nervous system, where its role remains unknown.

Methods:

We have recently generated a new transgenic mouse line, which allows for conditional overexpression of PrP^C in specific cell types thanks to the cre-lox system, in order to study the effect of specific PrP^C overexpression in particular experimental settings. In addition to selective cellular overexpression, we were also interested in producing a new model to assess the ubiquitous effects of PrP^C overexpression. To achieve this aim we have therefore used the ZP3-cre line, which allows for germline recombination of the floxed stop cassette and consequent broad overexpression of PrP^C.

Results:

In the generated mice (termed ZP3-PrP211) we have noticed that broad increased PrP^C expression is particularly associated with the development of skeletal muscle degeneration. ZP3-PrP211 animals present reduced body weight, kyphosis and gait abnormalities, as compared to their transgene-negative littermates. Histological analyses show signs of centronuclear myopathy affecting skeletal muscles. No evident pathological signs are present in other organs. These data are confirmed by biochemical analysis indicating a significant increase in creatine kinase, which is a marker of muscular damage. The clinical relevance of these data is suggested by early reports of enhanced PrP^C expression levels in samples of human muscular diseases, and confirmed by our re-analysis of published transcriptomic profiles of human muscle samples from several independent studies. From these data, it appears that *PRNP* expression is elevated in skeletal muscle upon aging and in pathological conditions, such as Duchenne muscular dystrophy.

Conclusion:

Our results are in line with an involvement of PrP^C in muscular pathology. Further analyses are ongoing to better investigate the mechanisms underlying the induction of myopathy following PrP^C overexpression. In light of the translational potential of these findings, it would be important to validate whether PrP^C, or related molecular mediators, could be used as novel alternative pharmacological targets for muscular diseases.

U. Siler¹, S. Romao¹, E. Tejera¹, O. Oleksandr¹, E. Kuzmenko¹, R.G. Valencia¹, V. Meda Spaccamela¹, B.H. Belohradsky², O. Speer⁵, M. Schmutz⁵, E. Kohne³, M. Hoenig³, J. Freihorst⁴, A.S. Schulz³, J. Reichenbach¹

Severe glucose-6-phosphate dehydrogenase deficiency leads to susceptibility to infection and absent NETosis

Division of Immunology, University Children's Hospital Zurich and Children's Research Center, Zürich¹, Division of Infectious Diseases and Immunology, Dr. von Haunersches Kinderspital, University Children's Hospital, Ludwig-Maximilians-University, Munich², Department of Pediatrics and Adolescent Medicine, University Medical Centre Ulm³, Children's Hospital Ostalbklinikum, Aalen⁴, Division of Hematology, University Children's Hospital Zürich and Children's Research Center, Zürich⁵

Introduction:

Glucose-6-phosphate dehydrogenase (G6PD) deficiency is the most common enzymatic disorder of red blood cells in human subjects, causing hemolytic anemia linked to impaired nicotinamide adenine dinucleotide phosphate (NADPH) production and imbalanced redox homeostasis in erythrocytes. Because G6PD is expressed by a variety of hematologic and nonhematologic cells, a broader clinical phenotype could be postulated in G6PD-deficient patients. We describe 3 brothers with severe G6PD deficiency and susceptibility to bacterial infection. Objective: We sought to study the molecular pathophysiology leading to susceptibility to infection in 3 siblings with severe G6PD deficiency.

Methods:

Blood samples of 3 patients with severe G6PD deficiency were analyzed for G6PD enzyme activity, cellular oxidized nicotinamide adenine dinucleotide phosphate/NADPH levels, phagocytic reactive oxygen species production, neutrophil extracellular trap (NET) formation, and neutrophil elastase translocation.

Results:

In these 3 brothers strongly reduced NADPH oxidase function was found in granulocytes, leading to impaired NET formation. Defective NET formation has thus far been only observed in patients with the NADPH oxidase deficiency chronic granulomatous disease, who require antibiotic and antimycotic prophylaxis to prevent life-threatening bacterial and fungal infections.

Conclusion:

Because severe G6PD deficiency can be a phenocopy of chronic granulomatous disease with regard to the cellular and clinical phenotype, careful evaluation of neutrophil function seems mandatory in these patients to decide on appropriate anti-infective preventive measures. Determining the level of G6PD enzyme activity should be followed by analysis of reactive oxygen species production and NET formation to decide on required antibiotic and antimycotic prophylaxis.

The Metastatic Role of SOX9 in Neuroblastoma

Oncology, University Hospital, Zurich¹

Introduction:

Approximately 50% of neuroblastoma patients suffer from metastatic disease at diagnosis and require intensive treatment. Despite intensive therapy, the vast majority of patients still have a poor clinical outcome (5-year survival rate of 30% to 40%). Investigating the molecular basis of neuroblastoma metastasis is crucial to develop more effective therapies. The similarities between neural crest development and neuroblastoma progression have been recognized. Transcription factor SOX9 is involved in cell migration during neural crest delamination, and has also been implicated in formation and growth of various tumors. Currently, we know little about the role of SOX9 in neuroblastoma pathogenesis. Our hypothesis is that SOX9 plays a crucial role in neuroblastoma metastasis, and the goal is to investigate the function of SOX9 and to find out its dysregulation of downstream genes.

Methods:

To understand whether SOX9 promotes metastasis in neuroblastoma, low and high SOX9 expression neuroblastoma cell lines were chosen to generate overexpression and knockdown clones individually. Cell migration, invasion and colony formation assays were subsequently performed to determine metastatic and tumorigenesis abilities of SOX9 overexpressing and knockdown clones *in vitro*. Orthotopic model were used to evaluate tumorigenicity and metastasis ability *in vivo*. Implantation of SOX9 overexpressing and knockdown cells in mouse adrenal gland respectively were executed by collaborator Annick Mühlethaler-Mottet's lab. The growth of tumor was followed by echography. For further analysis of metastasis, HE staining and immunohistochemistry were applied to examine metastatic cells in distant organs.

Results:

Expression level of SOX9 in neuroblastoma cell lines was examined by western blot analysis. Low SOX9 expressing cell line: IMR-5 was chosen to overexpress SOX9, while high SOX9 expressing cell: SK-N-AS was used to knock down SOX9. In *in vitro* study, overexpression of SOX9 in IMR-5 significantly enhanced cell migration, invasion and tumorigenicity. On the other side, reduction of these abilities was observed in SOX9 knockdown SK-N-AS. The result of tumorigenicity was also confirmed in *in vivo* orthotopic model: implantation of SOX9 overexpressing IMR-5 had more rapid tumor growth than its control, while tumor formation largely reduced in mice injected SOX9 knockdown SK-N-AS.

Conclusion:

Taken together, these results clearly indicate that SOX9 positively involves in cell motility and invasive ability of neuroblastoma cells *in vitro*, and promotes tumorigenesis both *in vivo* and *in vitro* model. *In vivo* metastasis is now under analysis. Moreover, to support clinical relevance, SOX9 expression in patient's tumor will be analyzed. Base on our study, we expect to further figure out the molecular mechanism how SOX9 boost metastasis which eventually provides more therapeutic targets in metastasis prevention of neuroblastoma.

Systematic Profiling of Molecular Changes during Prion Disease Progression*Institute of Neuropathology, University Hospital Zürich, Switzerland¹***Introduction:**

Prion diseases are fatal neurodegenerative diseases and are caused by proteinaceous infectious particles termed prions. While the infectious agent of prion disease has been identified decades ago, the actual cellular processes that subsequently cause neurons to degenerate remain poorly understood. Importantly, different cell types show remarkable differences in their susceptibility to prion clearance, replication and toxicity, yet what determines these differences is entirely unknown. This highlights the importance of studying individual cell types rather than entire tissues. Of particular interest to prion disease are microglia and astrocytes, which are activated during prion disease progression, as well as neurons, which are especially vulnerable to prions.

Methods:

Using ribosome profiling, we will analyze translation rates in a genome-wide and unbiased manner, specifically in prion disease-relevant cells. Mice will be injected intraperitoneally with either non-infectious brain homogenate or rodent-adapted scrapie prions, and analyzed at 2, 4, 8, 16, and 24 weeks after inoculation and at the terminal stage of the disease (approximately 32 weeks post inoculation).

To quantitatively measure protein synthesis rates specifically in disease-relevant cells we will utilize a combination of two previously published techniques, ribosome profiling and TRAP (tandem ribosome affinity purification). Taking advantage of the binary Cre/lox system, GFP tagged ribosomes will be expressed in specific cell types in a Cre recombinase dependent manner. Ribosome protected fragments (RPF) will be recovered by partial nuclease digestion followed by the immunoprecipitation of tagged ribosomes. RPF libraries will be cloned and submitted for high-throughput sequencing.

Results:

We have generated mice that express GFP-tagged ribosomes specifically in either excitatory or inhibitory neurons, microglia, or astrocytes. These mice will be subjected to prion injection. The above-mentioned techniques to assess protein synthesis rates have successfully been established, and will be applied to analyzing prion-infected mice.

Conclusion:

The outlined approach will identify a comprehensive list of genes that are differentially regulated during the progression of prion disease and that are important for different aspects of disease pathogenesis. The investigation of different cell types at multiple time points after prion infection, allows the dissection of the dynamics of disease progression and will shed light on the role and interplay of different cell types in pathophysiology. This project will not only yield novel and important insights into prion disease pathophysiology, but also will also contribute to our understanding of other neurodegenerative diseases and provide potential starting points for the development of targeted therapeutic interventions.

HJ. Klein¹, F. Lehner¹, R. Schweizer¹, N. Fuchs¹, P. Steiger², P. Giovanoli¹, R. Graf³, JA. Plock¹

The Role of Pancreatic Stone Protein as Early Marker for Infection and Mortality in Burns

Klinik für Plastische Chirurgie und Handchirurgie, UniversitätsSpital Zürich, Zürich¹, Chirurgische Intensivmedizin, UniversitätsSpital Zürich, Zürich², Klinik für Viszeral- und Transplantationschirurgie, UniversitätsSpital Zürich³

Introduction:

In patients with major burns, early diagnosis of infection/sepsis is paramount as mortality increases by 7.6% for each hour delay of appropriate antimicrobial therapy. Pancreatic stone protein (PSP) has recently emerged as a promising diagnostic and prognostic marker in the clinical field. However, PSP time course and its predictive value regarding infection and mortality have not been studied in severely burned patients so far.

Methods:

In a prospective cohort of burn patients we analyzed blood samples to elucidate diagnostic/prognostic accuracy of serum PSP levels over a 14 days time course. In addition, we investigated whether PSP levels were influenced by age and total body surface area (TBSA).

Results:

Preliminary data of 26 burn victims (mean age: 48±20 years, median TBSA: 25% (IQR 21.7), median ABSI: 7 (IQR 3)) showed PSP levels not to be influenced by age and TBSA at admission to hospital. Receiver Operating Characteristic (ROC) curve demonstrated PSP to have significant predictive power at day 3 after trauma to delineate patients with infections from those with an uneventful course (AUC: 0.83, 95%-CI: 0.61-1.0). Non-survivors as opposed to survivors showed significantly higher PSP serum levels at admission. Currently, more samples are being analyzed and will be incorporated in the results for presentation.

Conclusion:

Serum PSP levels were significantly associated with the presence of infection and mortality irrespective of the patients' age and TBSA. In that way, PSP might serve as helpful biomarker for timely identification of patients in need of anti-infectious treatment. Likewise, PSP may serve as a predictive marker for fatal outcome leading to early ethical considerations.

D. Lenggenhager¹, J. Gouttenoire², M. Malehmir¹, M. Bawohl¹, H. Honcharova-Biletska¹, S. Kreutzer¹, D. Semela³, J. Neuweiler⁴, S. Hürlimann⁶, P. Aepli⁵, M. Fraga², R. Sahli⁷, L. Terracciano⁸, L. Rubbia-Brandt⁹, B. Müllhaupt¹⁰, C. Sempoux¹¹, D. Moradpour², A. Weber¹

Visualization of hepatitis E virus RNA and proteins in the human liver

Department of Pathology and Molecular Pathology, University Zurich and University Hospital Zurich, Zurich, Switzerland¹, Division of Gastroenterology and Hepatology, Centre Hospitalier Universitaire Vaudois, University of Lausanne, Lausanne, Switzerland², Division of Gastroenterology and Hepatology, Cantonal Hospital St. Gallen, St. Gallen, Switzerland³, Institute of Pathology, Cantonal Hospital St. Gallen, St. Gallen, Switzerland⁴, Gastroenterology and Hepatology Unit, Cantonal Hospital Lucerne, Lucerne, Switzerland⁵, Institute of Pathology, Cantonal Hospital Lucerne, Lucerne, Switzerland⁶, Institute of Microbiology, Centre Hospitalier Universitaire Vaudois, University of Lausanne, Lausanne, Switzerland⁷, Department of Pathology, University Hospital Basel, Basel, Switzerland⁸, Service de Pathologie Clinique Geneva University Hospitals Faculté de Médecine Geneva, Switzerland⁹, Clinics of Hepatology and Gastroenterology, University and University Hospital Zurich, Zurich, Switzerland¹⁰, Institut Universitaire de Pathologie, Centre Hospitalier Universitaire Vaudois, University of Lausanne, Lausanne, Switzerland¹¹

Introduction:

Although hepatitis E constitutes a substantial disease burden worldwide, surprisingly little is known about the localization of hepatitis E virus (HEV) in the human liver. We therefore aimed to visualize HEV RNA and proteins in situ.

Methods:

Antibodies against HEV open reading frame (ORF) 1-3 proteins were evaluated for immunohistochemistry (IHC) and two probes for *in situ* hybridization (ISH) in formalin-fixed, paraffin-embedded (FFPE) Huh-7 cells transfected with HEV ORF1-3 expression vectors. IHC (and partly ISH) were then applied to Hep293TT cells replicating infectious HEV and liver specimens from patients with hepatitis E (n=19) and controls (n=134).

Results:

Whereas ORF1-3 proteins were all detectable in transfected, HEV protein-expressing cells, only ORF2 and 3 proteins were traceable in cells replicating infectious HEV. Only the ORF2-encoded capsid protein was also unequivocally detectable in liver specimens from patients with hepatitis E. IHC for ORF2 protein revealed a patchy expression in individual or grouped hepatocytes, generally stronger in chronic compared to acute hepatitis. Besides cytoplasmic and canalicular, ORF2 protein also displayed a hitherto unknown nuclear localization. Positivity for ORF2 protein in defined areas correlated with HEV RNA detection by ISH. IHC was specific and comparably sensitive as PCR for HEV RNA.

Conclusion:

ORF2 protein can be reliably visualized in the liver of patients with hepatitis E, allowing for sensitive and specific detection of HEV in FFPE samples. Its variable subcellular distribution in individual hepatocytes of the same liver suggests a redistribution of ORF2 protein during infection and interaction with nuclear components.

F. Storti¹, J. Fingerle³, C. Maugeais², E. Nogoceke², L. Rohrer⁴, A. Von Eckardstein⁴, C. Grimm¹

Lipoprotein genes in the retina: a local role in the development of age-related macular degeneration (AMD)?

Laboratory for Retinal Cell Biology, Department of Ophthalmology, University Hospital Zurich, Switzerland¹, F. Hoffmann-La Roche Ltd, Research and Early Development, Neuroscience, Ophthalmology and Rare Diseases, Basel, Switzerland², Natural and Medical Sciences Institute, University of Tübingen, Germany³, Department of Clinical Chemistry, University Hospital Zurich, Switzerland⁴

Introduction:

We aim to investigate the role of selected genes involved in lipid transport and metabolism in healthy and diseased retinal pigment epithelium (RPE). Genes involved in lipid handling have been linked to age-related macular degeneration (AMD) in genome-wide association studies and lipids and lipoproteins are among the most abundant components of drusen and subretinal drusenoid deposits, the histological markers of AMD. Moreover, RPE cells need to phagocytose a massive load of lipids shed daily from photoreceptor outer segments. These facts, together with the lack of an association between AMD and systemic plasma lipoprotein levels, prompted us to hypothesize that lipid metabolism-related genes may have a local role in the development of retinal pathologies.

Methods:

We assessed the expression of a number of genes relevant for lipid metabolism in human and mouse eyecup tissue, as well as in human ARPE-19 cells. We focused primarily on the ATP-binding cassette A1 and G1 (*Abca1/Abcg1*) genes, which mediate cholesterol and phospholipid efflux from cells to extracellular acceptors, and we generated a transgenic mouse that lacks both genes specifically in the RPE to investigate the effect of gene inactivation for the retina *in vivo*. To assess our concept mechanistically, we investigated directional transport of labelled cholesterol in polarized RPE cells *in vitro*.

Results:

Nearly all investigated genes involved in lipoprotein metabolism were found to be expressed in human and mouse RPE/choroid tissue and in ARPE-19 cells. Importantly, mice lacking *Abca1* and *Abcg1* specifically in the RPE showed a pronounced altered morphology with a strong accumulation of lipid droplets in the RPE. This was accompanied by cellular vesiculation and hypertrophy of the RPE already at 6 weeks of age and resulted in inflammatory cells infiltration in the outer retinal layers and areas of retinal degeneration in 8 months-old mice. The functionality of the ABCA1/ABCG1 efflux pathway was confirmed in ARPE-19 cells, which were able to export cholesterol to the apical side of the polarized epithelium in an apolipoprotein A1 (APOA1)-dependent manner.

Conclusion:

Our results support an important and local role for lipoprotein genes in the retina. The ABCA1/ABCG1 cholesterol efflux pathway may be rate-limiting for lipid transport and metabolism in the RPE as indicated by the apical cholesterol efflux from RPE cells, by the very rapid lipid accumulation in RPE-specific *Abca1/Abcg1* knockout mice and by the subsequent retinal inflammation/degeneration occurring at older age. We suggest that the ABCA1/ABCG1 pathway, which has been extensively described as a key aspect of atherosclerosis, might also be crucial for the pathology of AMD.

SOX10 as a therapeutic target in clear cell sarcoma*Onkologie, UniversitätsSpital Zürich¹***Introduction:**

Clear Cell Sarcoma (CCS) is a very rare and aggressive subtype of soft tissue sarcoma, associated with a high tendency to relapse locally, metastasize distantly and with a poor overall survival. Most cases affect young adults between 20 and 40 years of age. CCS often arises next to tendons, aponeuroses and fascia on distal extremities. CCS is considered to be resistant to conventional chemotherapy. Neither targeted therapeutic options nor immunotherapeutic approaches have been successful, yet. The cells of origin of CCS are neural crest derived. The defining molecular feature of CCS is caused by either the recurrent translocation t(12;22) (q13;q12) or, in rare cases, t(2;22) (q34;q12), resulting in expression of EWSR1-ATF1 or EWSR1-CREB1 fusion genes, respectively. These fusion proteins are the transforming oncogenic event in CCS.

SOX10 is a transcription factor, which is essential in neural crest development, the self-renewal of neural crest stem cells and for the formation of melanocytes arising from the neural crest. Previous research showed that SOX10 plays also a very important role in the maintenance of melanoma and it might represent a therapeutic target. SOX10 is required for the cAMP-mediated activation of the M-MITF gene promoter in CCS by cooperating with CREB1 and ATF1 and it is therefore conceivable that SOX10 is a therapeutic target in CCS.

Methods and Results:

We first analyzed, whether SOX10 is expressed in CCS. We cultured primary cultures of melanoma as a positive control and a panel of CCS cell lines and assessed levels of SOX10 mRNA and protein. Both were readily detectable and expressed to similar levels as in melanoma. In collaboration with the Institute of Surgical Pathology, USZ (Dr. P. Bode, Prof. H. Moch), we next analyzed biopsies from patients by SOX10 immunohistochemistry (IHC). 5/5 samples showed a strong nuclear SOX10 staining. We are currently expanding this analysis in a collaboration with the EORTC and Prof. P. Schöffski, University Hospitals of Leuven, who have generated a tissue-microarray from samples from a clinical trial on CCS, which will be stained for SOX10. Staining will be quantified, grouped and correlated with clinical characteristics, as well as with other IHC markers. This will establish, whether SOX10 serves as a biomarker in CCS.

In preliminary functional experiments, we have knocked down SOX10 in the human CCS cell line KAS using lentiviruses expressing short hairpin RNAs targeting SOX10. Two different shRNAs reduced SOX10 protein expression compared to uninfected parental cells, or to cells expressing a non-silencing scrambled control shRNA. Both SOX10-shRNAs significantly reduced colony formation in long-term proliferation assays in vitro.

In order to evaluate the therapeutic potential of silencing SOX10, we are currently expanding our in vitro experiments. Experiments, in which we knock down SOX10 using short hairpin RNAs in our panel of CCS cell lines and assess effects on proliferation by performing colony formation assays and MTT assays, as well as induction of apoptosis by Annexin-V / propidium iodide co-staining, followed by FACS analysis, are ongoing. To assess the effects of SOX10 knock down in vivo, we are currently also establishing a CCS xenograft model in nude mice.

Conclusion:

We have preliminary evidence that SOX10 might serve as a therapeutic target in CCS in vitro. In ongoing in vitro and in vivo experiments, we will now expand those analyses. This will firmly establish, whether SOX10 serves as a biomarker and is a preclinically promising therapeutic target in this aggressive orphan sarcoma.

D. Impellizzeri¹, ME. Räber¹, W. Jungraithmayr², O. Boyman¹

Characterization of human skin-homing T cells in health and disease.

Department of Immunology, University Hospital Zurich and University of Zurich, CH-8091 Zurich, Switzerland¹, Klinik für Thoraxchirurgie, UniversitätsSpital Zürich²

Introduction:

The skin and lungs are among the largest organs of our body that are continuously exposed to foreign stimuli, including a diverse range of pathogens. Under normal conditions, these organs need to be able to rapidly sense and control tissue infection, which, at least in part, relies on the presence of non-circulating antigen-experienced (memory) T lymphocytes. These so-called tissue-resident memory T cells (T_{RM}) are phenotypically characterized by constitutive expression of certain markers, such as CD69 and the αE integrin CD103 in the case of skin-resident T_{RM} cells. Functionally, T_{RM} feature rapid and potent effector functions, including interferon-gamma production. T_{RM} cells have been implicated in the pathogenesis of chronic-inflammatory and autoimmune disorders where these cells might contribute to the chronicity and treatment resistance of disease. Thus, it might be interesting to target T_{RM} cell precursors before they home to tissues where they become difficult to target therapeutically. We here set out to characterize to determine phenotypic and functional properties of putative T_{RM} cell precursors.

Methods:

We performed phenotypic and functional characterization of human skin- and lung-derived T cells co-expressing CD69 and CD103 by flow cytometry, and compared these with circulating T cell subsets isolated from human peripheral blood of healthy donors (HD) and from patients affected by psoriasis.

Results:

T_{RM} -phenotype T cells were present in the skin and lung of HD. Notably, T_{RM} -phenotype T cells were not readily detectable in the peripheral blood of HD, and in psoriasis. However, we identified a subset of T cells that was significantly enriched for precursors of T_{RM} -phenotype T cells. Phenotypic and functional studies confirmed that this subset harbored cells that overlapped with T_{RM} -phenotype T cells in terms of function and antigen-specificity.

Conclusion:

We have identified a subset of circulating T cells that appears to harbor precursors of T_{RM} -phenotype T cells. Further in-depth analysis of this subset might help us gain insight into protective immunity of surface tissues, such as the lungs and the skin. Moreover, targeting of these cells might be an attractive means to treat T cell-dependent chronic-inflammatory disorders.

M. Malehmir¹, E. Kotsiliti², D. Pfister², V. Leone², C. Deppermann³, J. Volz³, D. Dauch⁴, B. Nieswandt³, L. Zender⁴, A. Weber¹, M. Heikenwälder⁵

Anti-platelet treatment for metabolically induced NASH and HCC

Department of Pathology and Molecular Pathology, University Zurich and University Hospital Zurich¹, Institute of Virology, Helmholtz Center Munich, TU Munich², Rudolf Virchow Center, University of Würzburg³, Division of Translational Gastrointestinal Oncology, University of Tübingen⁴, Department Chronic Inflammation and Cancer, German Cancer Research Center (DKFZ)⁵

Introduction:

By utilizing a long-term choline-deficient high-fat diet (CD-HFD), we recently have established a mouse model in which CD8+T- and NKT cells interact with hepatocytes to induce NASH and eventually NASH-to-HCC transition. Several studies have shown that platelet contribute to immunopathology of liver. Therefore, we aim to test whether platelet activation/aggregation is a driving force for liver recruitment of CD8+T- and NKT cells during disease progression. We hypothesize that accumulation of CD8+T- and NKT immune cells in the liver is mediated by activation/aggregation of platelets and anti-platelet therapy will reduce the conditions associated with NASH, hyperlipidemia and glucose tolerance.

Methods:

we are evaluating platelet deposition in NASH livers, long-term consequences of anti-platelet treatment with aspirin-clopidogrel as well as pharmacological inhibition of COX2 by sulindac and P2Y12 by Ticagrelor in the CD-HFD mouse model. Furthermore, different mouse models with genetically modified genes crucial for platelet activation/aggregation are studied. Different parameters including body weight, glucose metabolism, functioning of liver (serum ALT and AST levels), platelet phenotype, liver histology and HCC incidence are evaluated.

Results:

in this study we investigated the potential role of platelets during NASH development. We quantified the platelet numbers in mice which received CD-HFD compared to control mice which received normal diet (ND). Interestingly, the CD-HFD mice showed more platelets than ND group. To investigate whether this is also true in human NASH, we analyzed non-diseased compared to NASH human patients liver samples. In line with the results we observed in our mouse model, the NASH patient samples had significantly more platelets compared to non-diseased samples. Aspirin-clopidogrel and Ticagrelor treatment has reduced the intrahepatic accumulation of the CD8+T- and NKT cells. All of the parameters associated with NASH, including body weight, hyperlipidemia have decreased following treatment. Interestingly, the tumor incidence has been reduced significantly. Furthermore, we have identified genes that are involved in the pathogenesis of the disease and deficiency of which protects against the conditions associated with NASH, hyperlipidemia and improves glucose tolerance.

Conclusion:

we provide new insight into the role of platelets in driving the pathophysiology of the disease. We show, for the first time, that platelets are increased in both the murine model and human biopsies of NASH. We also provide rational for anti-platelet treatment which is capable of rescuing the inflammation-mediated phenotype associated with NASH. From these experiments, we expect to unravel how less platelet activation/aggregation in the liver leads to less NASH and NASH-driven HCC under high calorie environment. Understanding these mechanisms in a preclinical model is expected to provide the basis for developing an antiplatelet therapy against NASH and NASH-driven HCC in humans.

A. Zhakupova¹, N. Debeuf², M. Krois³, I. Alecu¹, A. Von Eckardstein¹, B.N. Lambrecht², S. Janssens², T. Hornemann¹

The Role of ORMDL Proteins as Regulators of Mammalian Serine Palmitoyltransferase

Institute of Clinical Chemistry, University Hospital Zurich, Zurich, Switzerland¹, Laboratory of Immunoregulation and Mucosal Immunology, VIB Inflammation Research Center, Ghent, Belgium², Department of Molecular Genetics, VIB-Antwerp University, Antwerp, Belgium³

Introduction:

Serine palmitoyltransferase (SPT) catalyzes the first step of the *de novo* sphingolipid synthesis. In yeast, SPT activity is tightly regulated by a metabolic feedback mechanism mediated by Orm1/2 proteins. Mammalian cells express three Orm orthologues (ORMDL1-3), but their role in regulating SPT activity is not clear, as the regulatory phosphorylation sites of Orm1 and 2 are not conserved in the mammalian forms. Several SNPs close to ORMDL3 (Chr 17q21) were found to be associated with increased ORMDL3 expression and a risk for early childhood asthma. However, the effect of ORMDL3 on SPT activity and sphingolipid formation, as well as its link to asthma remains elusive.

Methods:

In this study we investigated the association of ORMDL proteins with total sphingolipid levels and SPT activity using *in vitro* and *in vivo* models. We used ORMDL3 knock-out mice to study the effect of ORMDL3 on total sphingolipid levels.

Results:

Total C₁₈-sphinganine levels were found to be significantly elevated in plasma and tissues of ORMDL3 KO mice. However, C₁₈-sphingosine levels were not changed. Additionally, SPT activity was measured in MEF cells generated from ORMDL3^{+/+}, ORMDL3^{+/-}, ORMDL3^{-/-} mice. SPT activity was not altered in MEF cells from ORMDL3^{-/-} compared to ORMDL3^{+/+}. The role of ORMDL1, 2 or 3 on SPT activity was tested in HEK293 cells by overexpressing or silencing the respective ORMDL isoforms. The individual overexpression of ORMDL1, 2 or 3 did not alter cellular SPT activity. However, simultaneous knock-down of all three ORMDL isoforms significantly increased SPT activity compared to control cells.

Conclusion:

In conclusion, our experiments did not confirm a significant role of ORMDL3 in regulating SL *de novo* synthesis and SPT activity.

Retrospective analysis of pharmacokinetic interactions between Tizanidine and Ciprofloxacin

Clinical Pharmacology and Toxicology, University Hospital Zürich¹, Tox Info suisse, National Poisons Information Centre, Associated institute of the Zurich University, Zurich²

Introduction:

Tizanidine, an alpha-adrenergic substance with antinociceptive and antihypertensive effects, is extensively metabolized via cytochrome P450 (CYP) 1A2. Therefore, co-administration with potent CYP1A2 inhibitors such as ciprofloxacin is contraindicated. However, both drugs are broadly utilized in Switzerland.

Methods:

Several adverse drug interactions with clinical reactions after co-administration were reported to the Regional Pharmacovigilance Centre of Zurich. To analyse this possibly underestimated drug safety issue, we conducted a retrospective study of Individual Case Safety Reports (ICSRs) obtained from the World Health Organization (WHO) Global Database. All ICSRs of tizanidine registered in VigiBase™ until 3rd August 2015 were included. Demographic data, drug administration information, the course of the adverse drug reaction (ADR), its severity and outcomes were analysed for cases with ciprofloxacin co-medication.

Results:

3253 tizanidine-related ICSRs were identified. In 64 (2.0%) cases ciprofloxacin was reported as a concomitant drug. The majority of patients was female (n= 36, 56.3%), the median age was 53 years (range 13-83 years). Most reports were from the US (n=34; 53%) followed by Switzerland (n=11; 17%). Most of the reported ADRs were related to increased tizanidine effects on blood pressure and CNS. The patients receiving 12mg and more daily (n=14) had on average 5 other drugs in their medication besides ciprofloxacin and tizanidine. Patients with a dose regimen of less than 12mg received on average 8 other drugs. Two patients in each dosage group experienced fatal outcomes.

Conclusion:

Co-medication with ciprofloxacin increases the blood concentrations of tizanidine and consequently raises the risk for dose-dependent ADRs. This combination should be absolutely avoided. Especially combinations with large dosages of tizanidine ($\geq 12\text{mg/day}$) but also lower doses ($< 12\text{mg/day}$) combined with CNS- and blood pressure lowering drugs may result in serious adverse drug reactions and even fatal outcomes.

PW. Schreiber¹, SP. Kuster¹, B. Hasse¹, C. Bayard¹, C. Rüegg¹, P. Kohler¹, PM. Keller², G. Bloemberg², F. Maisano⁴, D. Bettex⁵, M. Halbe⁴, R. Sommerstein³, H. Sax¹

Reemergence of *Mycobacterium chimaera* in Heater-Cooler Units despite Intensified Cleaning and Disinfection Protocol

Division of Infectious Diseases, University Hospital Zurich¹, University Zurich, Institute of Microbiology², Division of Infectious Diseases and Hospital Epidemiology, University Hospital Bern³, Department of Cardiovascular Surgery, University Hospital, Zürich⁴, Institute of Anaesthesiology, University Hospital, Zurich⁵

Introduction:

Mycobacterium chimaera is an emerging pathogen associated with devastating infections of heart valve prostheses, vascular grafts, and disseminated infections after open heart surgery. Evidence indicates airborne transmission after aerosolization of *M. chimaera* from contaminated heater-cooler units (HCUs) used in cardiopulmonary bypass. We studied the colonization dynamics of *M. chimaera* in factory-new Sorin 3T HCUs initially testing negative.

Methods:

Due to repeated detection of *M. chimaera* and other nontuberculous mycobacteria (NTM) in HCU samples our center replaced a total of 5 HCUs in 2014 (2 in 01/14, 1 in 04/14, 2 in 09/14). HCUs were serviced according to manufacturer's recommendations until April 2014, when cleaning and disinfection was intensified. The protocol consisted of daily water changes with use of all-bacteria filtered (Pall-Aquasafe AQ14F1S; 0.2µm) tap water and addition of hydrogen peroxide (100ml of 3%) combined with disinfection performed every 2 weeks. Surveillance cultures composed of HCU water samples and exhaust air samples were obtained ~ every 4 weeks.

Results:

Overall, 134 water samples were taken from the study HCUs, 127 after implementation of the intensified protocol. Of all samples, 90 (67.2%) remained sterile for nontuberculous mycobacteria (NTM), 6 (4.5%) were contaminated by bacterial overgrowth, and 38 (28.4%) yielded NTM: *M. chimaera* (22; 57.9% of all NTM), *M. gordonae* (12; 31.6%), *M. chelonae* (1; 2.6%), *M. paragordonae* (1; 2.6%) and a combination of *M. chimaera* and *M. gordonae* (2; 5.3%). NTM were found in both HCU water circuits.

Out of 91 air samples, 90 remained without mycobacterial growth. One (1.1%) grew *M. chelonae*, but no mycobacteria were detected simultaneously in the corresponding HCU water.

NTM growth was recorded after a median of 174 days (range, 158–358) in HCU water samples. Regarding *M. chimaera*, one out of five HCUs remained permanently negative, whereas four HCUs became positive at a median of 250 days (range, 158–358).

Conclusion:

HCUs provide favorable environmental conditions for *M. chimaera* and NTM growth. Intensified cleaning and disinfection does not suppress growth completely, but may attenuate density and aerosolization. It remains unresolved when HCUs were contaminated, most probably during production. Our findings emphasize the need for a change in technology for temperature management during heart surgery to guarantee patient safety.

R. Grindberg¹, E. Schlaepfer¹, G. Schreiber³, V. Simon², S. Speck¹

Dose and subtype specific analyses of the anti-HIV effects of IFN-alpha family members

Infectious Diseases and Hospital Epidemiology, University Hospital Zurich, Zurich¹, Department of Microbiology, Icahn School of Medicine at Mount Sinai, New York², Department of Biological Chemistry, Weizmann Institute of Science, Rehovot, Israel³

Introduction:

Interferons (IFN) are cytokines that are fundamental to innate and adaptive immune responses and are named so by their ability to “interfere” with viral replication. The family of human IFN-alpha's (IFN- α) is encoded on chromosome 9 and comprises 13 different subtypes [1]. These molecules signal through the IFN- α receptors 1 and 2, prompting Jak/Stat activation and induction of interferon stimulated genes (ISGs) [2]. IFN- α 1 and 2 were the first two alpha subtypes characterized [3]. IFN- α 2 has a higher specificity and activity than IFN- α 1 and so became the prototype IFN for most subsequent studies. Data reporting the anti-viral effects of the other subtypes is sparse.

Methods:

Here we analyzed 12 IFN family members and 6 mutant IFN variants, engineered to have various binding efficiencies, for their ability to inhibit HIV-1 replication in primary human cells such as peripheral blood mononuclear cells, purified CD4+ T-cells as well as monocyte derived macrophages. We tested a range of concentrations (10 U/ml, 100 U/ml and 1000 U/ml) for each of the IFNs.

Results:

We found a significant difference in activities of the natural IFN variants at lower dosages, which was lost at higher concentrations. Similarly, at lower dosages, the IFN mutants with stronger (60x) binding affinity showed a higher inhibition than the mutants with lower (40x) affinity. However, this difference was also reduced with increasing concentrations, indicating that differential antiviral efficacies between IFN subtypes can be compensated for with higher amounts. These results are consistent with RNA-seq, differential expression and biological network analyses of IFN α -2, IFN α -14 and IFN mutant stimulated macrophages at high and low doses.

Conclusion:

Together, these observations bring into focus the importance of understanding putative differential IFN antiviral activity as a function of binding affinity, potency and dosage.

References:

1. Gibbert, K., et al., *IFN-alpha subtypes: distinct biological activities in anti-viral therapy. Br J Pharmacol*, 2013. **168**(5): p. 1048-58.
2. Hyrcza, M.D., et al., *Distinct transcriptional profiles in ex vivo CD4+ and CD8+ T cells are established early in human immunodeficiency virus type 1 infection and are characterized by a chronic interferon response as well as extensive transcriptional changes in CD8+ T cells. J Virol*, 2007. **81**(7): p. 3477-86.
3. Paul, F., S. Pellegrini, and G. Uze, *IFNA2: The prototypic human alpha interferon. Gene*, 2015. **567**(2): p. 132-7.

Low-dose IL-2 and improved IL-2 formulations for Treg-deficient immunopathologies*Klinik für Immunologie, UniversitätsSpital Zürich¹***Introduction:**

The prevalence of autoimmune diseases and chronic inflammatory disorders has been increasing in industrialized countries continuously in the past 50 years, reaching an all-time high during the last decade. The mainstay of current treatment is long-term application of immunosuppressive drugs, such as corticosteroids, cytostatics, calcineurin inhibitors, and biologicals. These drugs have in common to suppress the immune system often in a very unspecific manner, thus immunocompromising the patients and eventually resulting in a higher susceptibility for infections and malignancies.

Recently, low-dose interleukin-2 (IL-2) has emerged as a new therapeutic approach, which leads to the selective expansion of regulatory T (Treg) cells. By restoring the balance between Treg and effector T cells, low-dose IL-2 treatment improved clinical symptoms in Treg-deficient immunopathologies, such as chronic graft-versus-host disease, systemic lupus erythematosus, type 1 diabetes, and hepatitis C virus-induced vasculitis. However, IL-2 has a dual role in the immune system by stimulating not only Treg cells but also cytotoxic T cells and natural killer cells, which somewhat antagonize the immunomodulating action of Treg cells.

Methods:

We use pre-clinical murine transplantation models to assess efficacy and toxicity of novel IL-2 formulations. Furthermore, we are preparing investigator-initiated clinical trials to monitor clinical response and safety of low-dose IL-2 treatment in different autoimmune diseases and chronic inflammatory disorders.

Results:

Using so-called IL-2/anti-IL-2 monoclonal antibody complexes (briefly, IL-2 complexes), we were able to selectively stimulate Treg cells with even lower doses of IL-2, which also resulted in reduced side effects. Thus, IL-2 complexes made of murine IL-2 and the anti-mouse IL-2 monoclonal antibody JES6-1, expanded Treg cells in mice by 10- to 20-fold, without stimulating cytotoxic T cells or natural killer cells, thereby exerting strong immunosuppressive effects. In a mouse model of allogeneic pancreatic islet cell transplantation, use of IL-2/JES6-1 complexes led to long-term graft acceptance without the necessity of immunosuppressive drugs.

Conclusion:

Currently, we are thoroughly testing these IL-2 complexes in healthy mice as well as mice suffering from different autoimmune and chronic inflammatory diseases for general toxicity and detailed biological function on immune and non-immune cells. Furthermore, we are generating monoclonal antibodies that are directed towards human IL-2 and replicate the functional properties of mouse IL-2/JES6-1 complexes. Subsequently, we intend to humanize and develop these antibodies for an investigator-initiated clinical trial.

P. Baumgartner¹, M. El Amki¹, R. Steffen¹, H. Schneider¹, A.R. Luft¹, M. Weller¹, B. Imthurn², G.S. Merki-Feld², S. Wegener¹

Neuroprotective effects of new generation progestins in experimental stroke involve upregulation of GABA(A) receptor subunits

Department of Neurology, University Hospital Zurich, Zurich¹, Department of Reproductive Endocrinology, University Hospital Zurich, Zurich²

Introduction:

Progestins are synthetically produced steroid hormones derived from progesterone, predominantly used for contraception. Progesterone has been shown to exert neuroprotective effects in different disease models. Our goal was to test the effect of the new generation progestins desogestrel and drospirenone on infarct size and behavioral deficits in experimental stroke and characterize the mechanisms of such an effect.

Methods:

Different groups of C57/Bl6 mice were used: (1) males, (2) female ovariectomized mice modeling postmenopausal females, and (3) female non-ovariectomized mice pretreated daily (10 days), as in females taking a contraceptive pill. Transient middle cerebral artery occlusion (MCAO) was performed to induce ischemic stroke. Following MCAO, progestin, vehicle or progesterone 8 mg/kg bw (positive control) were administered at 1, 6 and 24 h post-ischemia. Two doses were tested for each progestin (desogestrel 1.5 and 3 mg/kg bw and drospirenone 2.1 and 4 mg/kg bw). Deficits were assessed using the sticky tape test and a composite neurological score and infarct size by triphenyl tetrazolium chloride (TTC) staining at day 3. In another group of mice, we evaluated the effect of progestins on the protein expression of the GABA(A) receptors $\alpha 4$ and delta subunits by Western blot.

Results:

Stroke size and neurological deficits were significantly reduced by treatment with both progestins compared to controls (sesame oil), similar to treatment with progesterone. The doses of 3 mg/kg for desogestrel and 2.1 mg/kg for drospirenone were most effective. The protection was most pronounced in males, intermediate in female ovariectomized and least pronounced in female non-ovariectomized mice, the latter having smaller infarctions even with vehicle treatment. Desogestrel and drospirenone increased the protein expression of GABA(A) receptor $\alpha 4$ and delta subunits within the whole brain.

Conclusion:

New generation progestins are neuroprotective in experimental stroke in male as well as female mice with and without progestin pretreatment. Our results suggest that GABA(A) receptors could be involved in the neuroprotective effect, most likely via increased tonic inhibition during ischemic injury. Our data support that the progestins desogestrel and drospirenone, already in clinical use as oral contraceptives, may be promising candidates for stroke applications.

Acknowledgements: Support was granted by the European Contraceptive Society (ESC), the P&K Pühringer Foundation and the UZH Filling-the-Gap Foundation.

Structural and Functional Characterization of Serine Palmitoyl Transferase in Mammals*Institute for Clinical Chemistry, University Hospital Zürich, CH-8952 Schlieren, Switzerland¹***Introduction:**

Sphingolipid levels in mammalian cells are regulated in response to growth, nutrient availability and various other biological and chemical stimuli. Given the magnitude of changes that sphingolipid species can manifest on physiological and cellular metabolism, differentiation, survival and fate, cells employ elaborate regulatory mechanisms to control their metabolism. The main target point for maintenance of the 'sphingolipid rheostat' is the rate limiting enzyme, serine palmitoyl transferase or SPT, an ER localized multimeric protein complex. We aim to elucidate, in detail the networks that govern the regulation of this complex and identify novel molecular/protein partners and pathways involved.

Methods:

To study determinants of sphingolipid *de novo* biosynthesis, we are using genetically modified cell lines for our experiments that are cultured with stable isotope labelled sphingolipids and substrates of SPT, followed by quantitative lipid mass spectrometry. Specifically, the subunits of the SPT core enzyme, SPTLC1, SPTLC2 and SPTLC3, as well as the anticipated regulatory factors such as ORMDL proteins are targeted. Knockout cell lines were developed with CRISPR-Cas9 technology to study the function of each of the core subunits in HEK293 cells. We also generated transgenic cell lines that express tagged versions of these proteins. Using epitope tagged proteins for co-immunoprecipitation studies and followed by protein mass spectrometry, we look for proteins that physically interact with the SPT complex and can variously alter its function. Furthermore, we challenge cells with pharmacological and biological stimuli to modulate sphingolipid synthesis to investigate the effect on the molecular and enzymatic properties of the SPT complex.

Results:

In HEK293 cells, SPTLC1 and SPTLC2 form a heteromeric protein complex which condenses L-serine and palmitoyl-CoA in a PLP dependent reaction. In this complex, SPTLC2 is the sole active enzymatic subunit whereas SPTLC1 does not possess any activity on its own, although, mutations in the SPTLC1 change the substrate specificity and lead to modulation of the *de novo* activity. We performed CRISPR-Cas9 mediated knockout of individual subunits of the enzyme. We show that the loss of SPTLC1 leads to a catalytically dead SPT complex, although the levels of SPTLC2 protein are essentially unchanged compared to the wild type cells. SPTLC1 is also essential for localization of the complex to the ER membrane. Also, SPTLC2 and SPTLC3 expressed alone or together do not rescue the SPT function, albeit when expressed together with SPTLC1.

Conclusion:

Mammalian SPT complex is regulated to influence both levels of sphingolipids and to maintain physiologically relevant sphingoid base spectrum. Protein factors, such as ORMDL proteins that are known to influence SPT activity in lower eukaryotes, do interact physically with the SPT complex, however, their function in mammalian cells is still elusive.

The presence of SPTLC1 is indispensable for assembly of the complex and any minimal *de novo* biosynthesis of the sphingolipids. SPTLC2 and SPTLC3 subunits generate a diverse class of sphingoid bases, SPTLC3, particularly is involved in producing atypical sphingolipids *de novo*.

Finally, SPT activity is mediated by direct modifications of SPT core-subunits and the association and dissociation with the inhibitory and activating proteins.

M. Meerwein¹, A. Tarnutzer¹, M. Hombach², A.S. Zinkernagel¹

Increased azithromycin susceptibility of multi-drug resistant Gram-negative bacteria in eukaryotic growth medium

*Division of Infectious Diseases and Hospital Epidemiology, University Hospital of Zurich, Zurich¹,
Institute of Medical Microbiology, University of Zurich, Switzerland²*

Introduction:

Antimicrobial susceptibility testing is routinely done on Mueller-Hinton medium to define the optimal treatment options in bacterial infections. In contrast to the rather scarce nutritional milieu found in the human body Mueller-Hinton medium provides the bacteria with optimal growth conditions. We therefore aimed to adjust testing conditions to match the patient's pathophysiological environment more closely.

Methods:

Twenty-four *Enterobacter cloacae*, 26 *Escherichia coli*, 27 *Klebsiella pneumoniae* and 29 *Pseudomonas aeruginosa* strains including carbapenemase-positive isolates were tested for antibiotic susceptibility (azithromycin, colistin, cefepime, tobramycin, clarithromycin, erythromycin, tetracycline, tigecycline) on Mueller-Hinton and RPMI 1640 medium using the Kirby-Bauer-disk diffusion test.

Results:

Azithromycin susceptibility increased in RPMI medium for *Enterobacteriaceae ssp.*, including carbapenemase-positive isolates, and for a subgroup of *P.aeruginosa*. Only 29% of all *Enterobacteriaceae* strains showed an inhibition zone diameter >13mm on MH medium in contrast to 90 % on RPMI medium.

Conclusion:

We showed that adapting the testing conditions using tissue culture medium might reveal additional antibiotic susceptibilities, such as we found for azithromycin, for multi-drug resistant bacterial infections.

J. Krayenbuehl¹, M. Di Martino¹, M. Guckenberger¹, N. Andratschke¹

Automated VMAT planning for whole brain irradiation with hippocampus sparing: improved target coverage while avoiding unnecessary hot spots in the brain

Radiation Oncology, Zurich University Hospital, Zurich¹

Introduction:

Whole-brain radiation therapy (WBRT) has been the standard treatment for patient with multiple brain metastases for decades. However, with broader application of stereotactic radiotherapy the use of WBRT has decreased in the past years to avoid possible adverse neurocognitive effects. With the advent of neuroprotective strategies such as hippocampus sparing (HS) the interest in WBRT has been revived. The gold standard constraints for HS WBRT were published by the RTOG 0933 in 2011. In this project, we used an automated treatment planning (aTP) approach aiming especially at reduced hot spots in the normal brain.

Methods:

Fourteen consecutive patients treated with HS WBRT were enrolled in this study. The planning target volume (PTV) was defined as the whole-brain excluding the hippocampal avoidance regions defined as the hippocampal expanded by 5mm in three-dimensions. 10 x 3 Gy was prescribed to 92% of the target volume. All patients were planned with volumetric modulated arc therapy (VMAT) technique using four arcs and two couch kicks (300° and 60°). The plans were optimized for a Trilogy linac (Varian Medical System) with 5mm leaf width (Millennium MLC). Plan were optimized using Auto-Planning (AP) (Philips Radiation Oncology Systems) and using one single AP template. Plan results were compared to published dose volume histogram (DVH) parameters for HS WBRT. Dose to 2% (D2%) and 98% (D98%) of the target volume and homogeneity index (HI) were evaluated. The hippocampus dose was evaluated based on the minimal dose (D100%) and the maximal dose (Dmax). In addition to DVH parameters evaluation, the effective planning time defined as the working time required between the volumes definition and the end of the plan optimization was evaluated.

Results:

Target and hippocampus DVH parameters were evaluated. The D2% to the brain was reduced on average by > 3Gy (34 Gy vs. RTOG 37.5Gy) and the maximum hippocampus dose was reduced by > 1Gy. All the other parameters were similar to published data. The effective planning was kept below 10' for each patient.

Conclusion:

Automated TP for HS WBRT with VMAT achieved significantly decreased maximal brain dose and maximal hippocampus dose while fulfilling all other RTOG 0933 constraints. With this approach, hot spots > 115% could be significantly reduced in contrast to a maximal allowance of 130% in the RTOG protocol.

S. Suriyanarayanan¹, T. Hornemann¹, A. Von Eckardstein¹

Elucidating the pathomechanism of neurotoxic 1-deoxysphingolipids

Institute for Clinical Chemistry, University Hospital Zürich, CH-8952 Schlieren, Switzerland¹

Introduction:

Hereditary sensory and autonomic neuropathy type I (HSAN1) is a slowly progressing neurological disorder characterized by loss of pain and temperature sensation in feet and hands, often accompanied by lancinating pain attacks, skin ulcers, and bone infections. HSAN1 has been associated with several mutations in the enzyme serine palmitoyltransferase (SPT) which catalyses the condensation of palmitoyl-CoA and serine - the first and rate-limiting step in the de novo biosynthesis of sphingolipids. The HSAN1 mutations shift the substrate specificity of SPT from L-serine to L-alanine which results in the formation of atypical and neurotoxic 1-deoxysphingolipids (1-deoxySL). These metabolites lack the C1 hydroxyl group of sphinganine, and can therefore neither be converted to complex sphingolipids nor degraded by the classical pathway. Consequently, they accumulate in the cells. 1-deoxySL are found to be pathologically elevated in the plasma and lymphoblast of HSAN1 patients. However, the pathomechanism underlying the 1-deoxySLs mediated neurotoxicity is unknown. This study aims to identify and characterize downstream pathways of 1-deoxySLs mediated toxicity.

Methods:

Downstream signaling pathways involved in 1-deoxySLs mediated cyto and neurotoxicity were identified by screening a commercially available kinase inhibitor library in Hek293 cells, SH-SY5Y cells and primary DRGs. Hek293 cells were used to study the cytotoxicity, cultured cells were treated with 1-deoxySA together with various kinase inhibitors to identify and cytotoxicity were assessed by cell viability assay. SH-SY5Y cells derived from neuroblastoma origin were used to study the neurotoxicity. Cells were cultured and differentiated under specific condition to neurons. Then treated with 1-deoxySA together with various kinase inhibitors for 24 hours and neurotoxicity were assessed by quantifying neurite outgrowth using Neuron J.

Results:

1-deoxySLs caused significant cytotoxic and neurotoxic effects in different cells in dose dependent manner. Results from live cell imaging and immunofluorescence analysis clearly showed 1-deoxySLs significantly affect cell morphology and reduced the number and length of neurites. The kinase inhibitor library screen identified several compounds which were capable to maintain cellular morphology and to block 1-deoxySLs mediated cyto- and neurotoxicity.

Conclusion:

The 1-deoxySLs were shown to be toxic to a variety of cells including neurons. This toxicity appears to be related by specific cellular signalling pathways which are involved in cytoskeleton remodeling.

RR. Reimann¹, L. Caffisch¹, Ah. Varol¹, V. Chandrasekar¹, M. Hermann¹, S. Hornemann¹, As. Senatore¹, Asv. Lakkaraju¹, Ma. Nuvolone¹, Be. Schneider², Aa. Aguzzi¹

Depicting the role of the FT functional domains in antiprion mediated neurodegeneration

Neuropathology, University Hospital of Zurich, Zurich¹, Brain Mind Institute, Ecole Polytechnique Fédéral de Lausanne, Lausanne²

Introduction:

Expression of the cellular prion protein (PrP^C) is a prerequisite for neurodegeneration in fatal transmissible spongiform encephalopathy (TSE) (1, 2). PrP^C is encoded by *Prnp* and structurally consists of a globular domain (GD) hinged to an amino-proximal tail (FT, amino-acids 23-125) (3). Neurotoxicity induced by antiprion antibodies is triggering converging pathways as in bona fide TSE (4). By using this paradigm, we have identified the FT as the executive domain in prion mediated neurodegeneration (5). In order to identify well-defined therapeutic targets, we now address the relation between the known functional domains of the FT and its pathological function. These domains comprise the charged cluster 1 (CC1, amino-acids 23-27), the octarepeat (OR, amino-acids 50-90), the charged cluster 2 (CC2, amino-acids 95-110) and the hydrophobic core (HC, amino-acids 111-120) (6).

Methods:

Cerebellar organotypic slice cultures (COCS) from PrP deficient mice (*Prnp*^{ZH3/ZH3}) are infected at day zero in culture with Adeno Associated Virus (AAV), resulting in a transient expression of a bicistronic construct. Different constructs under the synapsin promoter were assembled with Golden Gate cloning (7). By the use of a 2A side (8) the fluorescent reporter NeonGreen is simultaneously expressed with unaltered or mutated PrP^C (synthetic DNA). After two weeks in culture neurotoxicity is induced with the Fab fragment of the antiprion antibody POM19 (FabPOM19, binding the GD). The read out is based on NeonGreen morphometry.

Results:

COCS of *Prnp*^{ZH3/ZH3} are resistant towards neurotoxicity induced by prions or antiprion antibodies. Antiprion antibody mediated neurodegeneration is restored in neurons from *Prnp*^{ZH3/ZH3} COCS after infection with AAV expressing murine wild type PrP^C. In contrast neurotoxicity is not restored if expression of the deletion mutant PrP_{Δ32-93} (lacking larger part of the FT including the OR) is induced at a similar expression level. The OR comprises five tryptophan residues possibly contributing to a membrane integration of the FT upon binding of antiprion antibodies. However, antiprion antibody-mediated neurodegeneration is restored when these tryptophan residues are replaced by alanine. Equally non-essential are the four histidine residues of the OR which have a known interaction with copper ions. Further the alteration of a known SH3 binding motive in the CC2 region is not affecting antiprion mediated neurodegeneration

Conclusion:

COCS of *Prnp*^{ZH3/ZH3} are resistant towards neurotoxicity induced by prions or antiprion antibodies. Antiprion antibody mediated neurodegeneration is restored in neurons from *Prnp*^{ZH3/ZH3} COCS after infection with AAV expressing murine wild type PrP^C. In contrast neurotoxicity is not restored if expression of the deletion mutant PrP_{Δ32-93} (lacking larger part of the FT including the OR) is induced at a similar expression level. The OR comprises five tryptophan residues possibly contributing to a membrane integration of the FT upon binding of antiprion antibodies. However, antiprion antibody-mediated neurodegeneration is restored when these tryptophan residues are replaced by alanine. Equally non-essential are the four histidine residues of the OR which have a known interaction with copper ions. Further the alteration of a known SH3 binding motive in the CC2 region is not affecting antiprion mediated neurodegeneration.

1. S. Brandner et al., Nature 379, 339-343 (1996).
2. G. Mallucci et al., Science 302, 871-874 (2003).
3. R. Riek et al., FEBS Lett 413, 282-288 (1997).
4. U. Hermann et al., PLOS Pathogens (2015).
5. T. Sonati et al., Nature 501, 102-106 (2013).
6. A. Aguzzi et al., Annu Rev Neurosci 31, 439-477 (2008).

7. T. Cermak et al., *Nucleic Acids Res* 39, e82 (2011).
8. M. L. Donnelly et al., *J Gen Virol* 82, 1027-1041 (2001).

S. Bender¹, A. Sharma¹, A. Brogini-Tenzer¹, M. Pruschy¹

Role of SUV39H1 in ADAM17-mediated radioresistance

Laboratory for Molecular Radiobiology, Department of Radiation Oncology, University Hospital Zurich, Zurich¹

Introduction:

The therapeutic response of ionizing radiation (IR) is imparted by genomic instability and DNA damage. However, IR also triggers multiple intracellular signaling processes as part of IR-induced stress responses that lead to the secretion of various para- and autocrine factors. Here we investigated treatment-dependent secretion of these factors, which drive acquired rescue mechanisms and determine the overall radiation sensitivity of the tumor.

Methods:

Secretome analysis was performed using antibody arrays. Secretion kinetics of selected factors were determined using ELISA across different established tumor cells and in murine blood serum, derived from irradiated tumor xenograft-carrying mice. Clonogenic survival and xenograft tumor growth delay assays were performed in response to IR in siRNA- or inducible shRNA-targeted tumor cell lines or in combination with small molecular agents.

Results:

We identified amphiregulin and ALCAM as top hits of the IR-dependent secretome analysis in lung carcinoma cells. These factors are shed by the common upstream metalloprotease ADAM17 (A Disintegrin and metalloprotease domain 17). Irradiation induced a dose-dependent increase in the activity of ADAM17, which correlated with subsequent substrate shedding. siRNA- or inducible-shRNA-mediated silencing of ADAM17 or targeting of ADAM17 with the small molecular inhibitor TMI-005 suppressed IR-induced shedding of these factors, downregulated ErbB-signaling in target cells and enhanced IR-induced cytotoxicity *in vitro* and *in vivo*. Recently, we identified that targeting of ADAM17 also interferes with epigenetic mechanisms. It decreased the basal level of the histone methyltransferase SUV39H1 and abolished a short-term increase of the SUV39H1 protein in response to irradiation. Interestingly, SUV39H1 was downregulated to almost non-detectable levels in irradiated ADAM17 knockdown cells 24 hours after irradiation in comparison to irradiated control cells. Surprisingly decreased amounts of residual γH2AX were detected in ADAM17-depleted cells after irradiation despite their increased radiosensitivity in comparison to wildtype cells, implying a defect in the DNA repair machinery and pointing towards a potential mechanism of radiosensitization by ADAM17 targeting.

Conclusion:

Our findings demonstrate that IR significantly activates ADAM17, which results in shedding of survival factors, growth factor pathway activation and contributes to treatment resistance in NSCLC cells. Additionally, our data point towards a novel link between ADAM17, regulation of the cancer cell epigenome and the DNA damage response. We demonstrate that the impact of targeting ADAM17 is more pleiotropic than just diminishing ErbB signaling and provide a sound rationale for positioning ADAM17 inhibitors as radiosensitizers to improve the treatment of NSCLC.

E. Boran¹, S. Burnos¹, F. Fedele¹, N. Krayenbühl¹, P. Hilfiker², T. Grunwald², J. Sarnthein¹

Test-retest reliability of the spatial distribution of high frequency oscillations (HFO) in intracranial EEG

University Hospital of Zurich, Switzerland¹, Swiss Epilepsy Center, Zurich, Switzerland²

Introduction:

High frequency oscillations (HFO 80-500 Hz) are recognized as biomarkers for epileptogenic brain tissue to be resected in epilepsy surgery. We analysed here the test-retest reliability of HFOs recorded at different times.

Methods:

We analyzed long-term invasive night recordings of 11 patients who subsequently had an area of the brain resected and achieved seizure freedom. Four patients had mesial temporal lobe epilepsy (TLE) and seven extratemporal epilepsy (ETLE). For each night, 30-minute recordings were extracted during slow wave sleep, artifacts were removed and recordings were segmented into 5-minute intervals. HFOs were detected by a fully automated algorithm and contacts with the highest rate designated the HFO area for each interval.

Results:

The resected area included the HFO area for all intervals in 3/4 TLE and 5/7 ETLE patients. The scalar product of the normalized rate vectors significantly exceeded a random distribution for every night pair for 4/4 TLE and 3/5 ETLE patients with multiple nights and for all interval pairs for 3/4 TLE and 5/7 ETLE patients. When averaging over all intervals, the resected area included the HFO area for 10/11 patients.

Conclusion:

While the intervals have to be selected carefully from slow wave sleep, the test-retest reliability of the HFO analysis was sufficiently stable within and between nights.

M. Waldner¹, W. Zhang², IB. James², K. Allbright², R. Schweizer¹, JA. Plock¹, K. Marra², MG. Solari², VS. Gorantla², JP. Rubin²

Comparison of the immunomodulating effects of human bone marrow derived mesenchymal stem cells and adipose derived stem cells in vitro across different HLA barriers

UniversitätsSpital Zürich, Department of Plastic Surgery and Hand Surgery, Zürich¹, University of Pittsburgh, Department of Plastic Surgery, Pittsburgh, United States²

Introduction:

Mesenchymal stem cells derived from bone marrow (BMSC) and adipose tissue (ASC) have clinically useful immunomodulatory effects and low immunogenicity. Their ability to suppress innate and adaptive immune cells makes them ideal candidates for immunomodulative cytotherapy to reduce alloreactivity. The aims of this study were to assess and compare the immunomodulatory capacities of BMSCs and ASC across defined HLA barriers. This is the first study to compare paired ASCs and BMSCs isolated from the same human donors.

Methods:

Tissue samples of omental fat, s.c. fat and bone marrow aspirate from 10 human organ donors were retrieved and MSCs isolated. Cells were characterized and tested for tri-lineage differentiation. In mixed lymphocyte reactions (MLR), the capacity of ASCs and BMSCs to suppress immune response was assessed and compared within individual donors. Supernatants of MLRs were analyzed for cytokine via Multiplex assay.

Results:

All three cell types demonstrated a significant inhibition of CD3+ cell proliferation in MLR. Inhibition was dose dependent and more efficient on CD3+, CD4+ cells than on CD8+ cells. The combination of ASC with BMSC resulted in a synergistic effect with strong immunomodulative effect. Cytokine profiling demonstrated a significant increase of IL-6 and HGF.

Conclusion:

Human ASCs and BMSCs both showed effective immunomodulation across a defined HLA barrier. The combination of both cell types is an exciting possibility to modulate the immune response. Further mechanistic experiments are necessary to discover differences between MSC types.

Y. Yamada¹, D. Impellizzeri², T. Maeyashiki¹, K. Bruestle¹, L. Dubs¹, JH. Jang¹, U. Karakus², J. Woytschak², I. Inci¹, W. Weder¹, O. Boyman², W. Jungraithmayr¹

Induction of persistent tolerance to lung transplants by IL-2 complex-stimulated regulatory T cells in vivo

Division of Thoracic Surgery, University Hospital Zurich, Zurich, Switzerland¹, Department of Immunology, University Hospital Zurich, Zurich, Switzerland²

Introduction:

Transplant (Tx) tolerance is, by definition, a state of unresponsiveness of a recipient to Tx-related alloantigen. Treatment protocols of tolerance induction have been proposed in the past, however, with incomplete or short-term success only. Allo-Tx of the lung is an established procedure in patients with terminal pulmonary failure. However, lung allo-Tx shows the poorest allograft survival compared to other transplantable solid organs due to the lung's dual exposure to circulatory and airborne antigens. We have previously shown that the immunomodulatory cytokine interleukin-2 (IL-2) in complex (cx) with a particular neutralizing anti-IL-2 antibody induces potent expansion of regulatory T (Treg) cells. Here, we evaluated whether Treg cell-selective IL-2cx could induce allo-Tx tolerance in a fully MHC-mismatched mouse model of lung Tx.

Methods:

Single lung Tx was performed from BALB/c to C57BL/6 mice. Recipients received intraperitoneal injections of either PBS (control) or IL-2cx with anti-IL-2 antibody clone JES6-1 on three consecutive days before Tx. The outcomes of transplants were analyzed on day 5, 14, 28 and 56 by flow cytometry, lung functionality (compliance) and histology.

Results:

Acute allo-Tx rejection (AR) was virtually absent macroscopically and histologically in IL-2cx-treated animals on day 5, 14, 28 and even 56 compared to controls. AR scores, based on ISHLT guidelines, of allo-transplant of IL-2cx-treated mice were significantly lower vs. control (day 5, $p=0.04$; day 14, $p=0.01$; day 28, $p=0.02$). The population of Foxp3⁺CD4⁺CD25⁺ Treg cells in IL-2 cx-treated mice was significantly higher within allotransplants and contralateral naïve lungs on both day 5 and 14, and in spleens on day 14 ($p<0.05$, all). Transplant compliance of all IL-2cx-treated grafts on day 14 and 28 were preserved compared to controls (20 mbar airway pressure vs. none in controls; $p=0.01$ and $p=0.02$, respectively).

Conclusion:

Treatment of recipients using IL-2cx before lung Tx leads to intragraft Treg expansion, prevents from acute rejection and maintains a viable engrafted lung up to 28 days in a fully MHC-mismatched mouse model. These data provide insight into the mechanism of adaptive tolerance induction in Tx and may have implications for immune protocols for Treg modulation in human lung transplantation.

M. Langiewicz¹, A. Schlegel¹, E. Saponara¹, M. Linecker¹, P. Borger¹, R. Graf¹, B. Humar¹, PA. Clavien¹

Indian hedgehog mediates early acceleration of liver regeneration induced by ALPPS two-staged hepatectomy

Department of Visceral and Transplant Surgery Research, University Hospital Zürich, Zürich¹

Introduction:

Occlusion of one liver section by portal vein ligation (PVL) induces compensatory liver regeneration in the remaining part. PVL-induced liver growth is being exploited for the surgical removal of large/multiple liver tumors. A novel approach coined ALPPS (Associating Liver Partition and Portal vein ligation for Staged hepatectomy) combines PVL with parenchymal transection and massively accelerates compensatory growth, enabling much faster and more extensive tumor removal. Regenerative acceleration following ALPPS seems to be mediated by plasma factors, which we sought to identify.

Methods:

We compared a mouse model of ALPPS against PVL and additional control surgeries. Gene expression profiling was performed to identify candidate molecules unique to ALPPS liver. Recombinant protein and neutralizing antibody combined with appropriate surgeries were used to explore candidate function in ALPPS.

Results:

ALPPS in mouse confirmed formidable acceleration of liver regeneration relative to PVL. Ihh, a secreted ligand inducing hedgehog signaling, was uniquely upregulated in ALPPS liver. Ihh plasma levels rose 4h after surgery, along with hedgehog pathway activation and subsequent cyclin D1 induction in the liver. When combined with PVL, Ihh alone was sufficient to induce ALPPS-like acceleration of liver growth. Conversely, blocking Ihh markedly inhibited the accelerating effects of ALPPS. In human plasma, IHH was elevated early after ALPPS surgery.

Conclusion:

Ihh and hedgehog pathway activation provide the first mechanistic insight into the acceleration of liver regeneration triggered by ALPPS surgery. The accelerating potency of recombinant Ihh and its elevations in human ALPPS suggest clinical potential for this morphogenic protein.

J. Drazen¹, M. Töteberg-Harms¹

Micro-pulse Cyclophotocoagulation reduces IOP faster compared to G-probe-Cyclophotocoagulation

University/Hospital Zurich, Dept. of Ophthalmology, Zurich¹

Introduction:

The aim was to evaluate efficacy of standard G-Probe transscleral cyclophotocoagulation (TS-CPC) in patients with advanced glaucoma in comparison to Micro Pulse P3 (MP3-CPC) cyclophotocoagulation.

Methods:

A retrospective chart review was conducted. Efficacy, i.e. reduction of intraocular pressure (IOP) and number of anti-glaucoma medication (AGD), was evaluated with a follow-up of 6 month. Data was collected at baseline, 1, 3, and 6 month after the cyclophotocoagulation procedure.

Results:

34 eyes were included (16 eyes after MP3-CPC). Median age was 70.8±17.1years. IOP at baseline was 28.8±7.8 in the TS-CPC group and 29.0±8.2 in the MP3-CPC group, respectively ($P=0.493$). For the TS-CPC group IOP was reduced to 23.3±14.9mmHg at 1 month ($P=0.114$), to 14.9±6.7mmHg at 3 month ($P<0.001$), and to 19.1±8.5mmHg at 6 month ($P=0,048$). At baseline 3.2±1.6 AGD were administered with a change to 2.3±1.8 ($P=0,055$) at 1 month, to 2.9±1.6 ($P=0,052$) at 3 month, and to 3.6±1.1 ($P=0,048$) at 6 month follow-up. For the MP3-CPC group IOP was reduced to 15.8±4.3mmHg at 1 month ($P<0.001$), to 19.7±6.4mmHg at 3 month ($P<0.001$), and to 21.0±7.0mmHg at 6 month ($P=0,048$). AGD were reduced from 2.1±1.5 at baseline to 1.1±1.2 ($P=0,004$) at 1 month, to 1.6±1.7 ($P=0,151$) at 3 month, and to 3.0±0.7 ($P=0,311$) at 6 month follow-up.

Conclusion:

Both cyclodestructive procedures, TS-CPC and MP3-CPC, reduced IOP and AGD simultaneously. MP3-CPC was non-inferior to TS-CPC regarding IOP and AGD reduction. However, MP3-CPC reduced IOP significantly faster (at 1 month already), whereas TS-CPC reduced IOP not before 3 month. Analysis of data with longer follow-up and larger sample size is ongoing.

D. Kirschenbaum¹, F. Voigt³, D. Laptev², A. Sahin², O. Bichsel¹, F. Helmchen³, J. Buhmann², A. Aguzzi¹

CRYSTAL & HITS: quantifying Alzheimer's disease pathology in the whole-mount mouse brain

Institute of Neuropathology, University Hospital Zurich¹, Institute of Machine Learning, Department of Computer Science, ETH Zurich², Brain Research Institute, University of Zurich³

Introduction:

The backbone of classical histology in the last centuries was slicing and staining of tissue followed by microscopic detection. Slicing of tissue is necessary, since tissue is not transparent and as such not accessible to microscopy past a shallow depth. In order to avoid slicing, tissue clearing addresses this problem by homogenizing the refractive indices between cell membranes and water. This process of tissue transparentization enables deep imaging without slicing. Recently, multiple methods were published providing tissue clearing approaches. Clearing techniques either require a long time, quench fluorescence, or are difficult to implement. A further challenge is to achieve a uniform and specific molecular labelling in whole-mount tissue.

Methods:

We developed a method termed CRYSTAL, for clearing tissue of unprecedented rapidity and user-friendliness based on the CLARITY method. We further developed a technology for rapid staining of whole-mount tissue, which we termed HITS.

Results:

Combining these methods allowed us to transparentize and stain whole mouse brains within a matter of hours. We imaged whole brains with light-sheet microscopy within minutes. Here we present the power of this method by rapidly clearing and staining the brains of APP/PS1 transgenic mice. These mice develop β -amyloid plaques (A β P), resembling one of the pathologic hallmarks of Alzheimer's disease (AD). We were able to count the total amount of A β P with a custom-designed computer algorithm. Additionally, we segmented the images into microanatomical regions and provided exact numbers of A β P frequencies in various brain regions. We could describe the kinetics of plaque accumulation in these model mice.

Conclusion:

In summary, we present a methodology for high-throughput whole-mount tissue clearing, staining and imaging and show the applicability of this method in a disease model.

K. Frauenknecht¹, M. Emmenegger¹, A. Kerschenmeyer¹, C. Schiavi¹, R. Moos¹, S. Hornemann¹, A. Aguzzi¹

Evaluation of human antibodies against microglia related receptors as potential novel biomarkers and immunotherapeutics for targeted therapy in neurodegeneration and neuroinflammation

University Hospital Zurich, Institute of Neuropathology, Schmelzbergstrasse 12, 8091 Zurich¹

Introduction:

Microglia are part of the brain's innate immune system and mainly responsible for CNS protection against various types of pathogenic factors. Phagocytic action of microglia is important for proper brain development but also in many neurological diseases and during regenerative conditions. Once microglia are activated, they tend to accumulate at the site of a lesion to remove damaged cells and cell debris. In the case of misfolded protein aggregates such as Amyloid β in Alzheimer's Disease (AD) or pathologic factors such as myelin antigens in demyelinating diseases like Multiple Sclerosis (MS), microglia exert their function pivotal for the maintenance of a healthy brain. In recent studies, deficiency in TREM2 was shown to downregulate phagocytic activities of microglia and the R47H substitution in the TREM2 gene denotes the second highest risk allele to develop AD after APO ϵ 4. The therapeutic modulation of TREM2 but also of other microglial transmembrane proteins may offer a way to overcome the attenuated phagocytic activity of microglia. To exploit possible therapeutic windows and to uncover pathogenic links that may not be found using small-scale approaches, we aim to investigate human antibodies against TREM2, its associated receptor protein DAP12 as well as against CD33 by means of a high-throughput screen (HTS) established in this lab.

Methods:

In a first attempt to assess whether autoreactivity against the full-length human TREM2 could be detected, 1500 irreversibly anonymized plasma were tested in a fully-automated microELISA which is run in 1536-well plates. Subsequently, recombinant expression of TREM2 as well as DAP12 and CD33 in *E. coli* and, in order to obtain the glycosylated proteins, mammalian cells was established. Since we focus on conformational antibodies that may be therapeutically administered, the use of linker systems such as avitags is currently exploited. Concomitant to screening > 50000 fresh plasma from an unselected hospital cohort, buffy coats of the high-titer patients will be isolated and memory B-lymphocytes will be cloned. Moreover, these complex datasets will be mined in order to assess so far unknown disease associations.

Results:

In the preliminary study, approx. 0.07% of anonymized samples showed distinct reactivity which could be replicated in many follow up experiments. Apart from few high reactive samples, around 1% of patients displayed moderate reactivity while the vast majority did not evoke any measurable titer.

Conclusion:

Our results indicate that ~1% of the unselected hospital cohort displays moderate to marked reactivity against TREM2, hinting at the presence of anti-TREM2-autoantibodies. Thus, we propose to screen USZ patients - which agreed to the utilization of surplus blood samples - for the presence of autoantibodies against TREM2, DAP12 and CD33. Recombinant proteins produced in-house will be used for these assays. Positive hits will then be correlated to clinical data and antibodies will be cloned from buffy coats of high-titer patients and expressed in vitro. Function and immunotherapeutic potential will be tested in established disease models in vitro and in vivo. With this study, we hope to contribute to a better understanding of the immune regulations underlying neurodegenerative and neuroinflammatory diseases, in particular the role of microglial components. Lastly, human monoclonal antibodies targeting endogenous microglia receptors may yield a potential as novel disease biomarkers or even as safe and effective biological therapeutics.

Geriatric Assessment May Reduce Re-Visits in the Emergency Department in Older Patients with Positive Identification of Senior at Risk (ISAR) Screening*Klinik für Geriatrie¹, Institut für Notfallmedizin²***Introduction:**

Older patients often present with atypical symptoms, co-morbidities and cognitive impairment in the emergency department (ED). Therefore, their emergency care is complex and associated with an increased risk for re-visits to the ED, readmission and death. The "Identification of Seniors at Risk" (ISAR) screening is a tool to identify patients at risk for adverse outcomes. The aim of this study was to investigate whether older patients with a positive ISAR screening have an increased risk for adverse outcomes including re-visits and increased health service costs when admitted to the ED of the University Hospital Zurich.

Methods:

In a pilot study, we included 96 patients aged ≥ 70 yrs who received an ISAR screening at the ED of our tertiary care hospital between June 2015 and February 2016. We compared adverse outcomes within three months (re-visits to the ED, mortality rate, and hospital readmission) and in-hospital costs between patients with a positive (≥ 2 pts) and negative ISAR screening (< 2 pts). A single geriatric consultation (GC) was performed by a geriatric physician during the stay in the ED to identify medical, psychosocial, and functional limitations and resources of the elderly frail patient. Statistical analysis was performed using a uni- and multivariate logistic or linear regression model by controlling for age, sex, Charlson co-morbidity index and the emergency severity index.

Results:

Of 96 ED patients aged 70+ who were enrolled in this pilot study, 50 patients (52%) had a positive ISAR screening. Patients screening positive showed a significantly increased risk for a re-visit to the ED (adjusted RR 6.5, 95% CI 2.1-20.1, $p=0.001$) compared with those screened negative. In 29 patients (30%) a single GC was performed during the stay in the ED, of which 18 patients had a positive ISAR screening. In this sub-group of patients who received a single GC, the incidence of re-visits to the ED decreased in patients with a positive ISAR screening and was no more significant compared to those with a negative ISAR screening (unadjusted RR 2.2, 95% CI 0.4-13.9, $p=0.38$). Despite additional examinations by the geriatric physician during the single GC in the ED, patients with a positive ISAR screening did not have significantly higher in-hospital costs than those patients with a negative ISAR screening (9'202 vs. 14'733 CHF, adjusted difference -3'606 CHF, 95% CI -45'197-37'984, $p=0.85$). Mortality and the rate of readmissions did not show any significant difference between positive and negative ISAR screened patients.

Conclusion:

Older patients with a positive ISAR screening have an increased risk for re-visits to the ED so that an early and single GC by a geriatric physician during the ED visit may already reduce the incidence of re-visits to the ED. Regardless of additional examinations by the single GC in the ED, in-hospital costs were not increased in older patients with a positive ISAR screening. Based on this study, we plan to establish a comprehensive outpatient geriatric assessment in ISAR positive older patients in the local geriatric department to identify and address relevant risk factors for re-visits (i.e. falls) to the ED and to recommend preventive strategies.

I. Tcymbarevich², N. Obialo², J. Cosin-Roger², K. Seuwen¹, G. Rogler², B. Misselwitz², C. De Vallière²

The role of the rs8005161 polymorphism on pH-sensing G protein-coupled receptor GPR65(TDAG8) signaling in intestinal inflammation

Novartis Institutes for Biomedical Research, Basel¹, Division of Gastroenterology & Hepatology, University Hospital Zurich (USZ), CH-8091 Zurich²

Introduction:

Inflammatory bowel diseases (IBD), Crohn's disease (CD) and Ulcerative colitis, are typically associated with a decrease in local pH. Genome-wide association studies (GWAS) revealed a strong genetic impact on IBD, identifying over 200 non-overlapping single-nucleotide polymorphism (SNP) genetic risk loci. The proton-sensing G-protein-coupled receptor T-cell death associated gene 8 (TDAG8 or GPR65) has been identified to be a risk gene for IBD in recent GWASs. Thereby, the T genotype of the SNP rs8005161 within the GPR65 gene confers increased IBD risk. In response to extracellular acidification GPR65 activates second messengers: cAMP via the G_s signalling pathway or G_{12/13}/Rho signalling. In this study we aim to analyze the association of the SNP rs8005161 in the IBD cohort of patients with increased IBD risk, and its functional relevance.

Methods:

1138 individuals (591 non-IBD, 203 UC, 344 CD) were genotyped for risk SNPs, GPR65 (rs8005161, rs3742704) and GALC (rs1805078), with Taqman SNP Genotyping Assays. Additionally, more than 2064 IBD patients from the Swiss IBD Cohort Study (SIBDCS) were genotyped by Illumina sequencing. Ten patients with the genotype rs8005161 TT/CT and CC from the IBD cohort and ten non-IBD controls (CC) were recruited for the functional study. Human CD14+ cells were isolated from blood samples and subjected to an extracellular acidic pH shift (pH 6.6 vs. pH 7.6) in functional assays: cAMP, RhoA GTPase activation.

Results:

We showed that rs8005161 was more frequent in UC patients (Minor allele frequency (MAF) 14.53% vs 10.05% in non-IBD group), whereas no statistically significant association with IBD, UC or CD was shown for the other variants GPR65 rs3742704, GALC rs1805078 by Taqman genotyping. Sequenced genotype frequency of rare homozygote rs8005161 in the SIBDCS was 1.17%, MAF - 10.3%. No significant differences were observed in the cAMP production between IBD (TT, CT, WT/CC) and non-IBD (WT/CC) genotype carriers upon pH shift from 7.6 to 6.6. However, a decreased activation of GTPase RhoA was shown by IBD rs8005161 (TT) variant carriers after an acidic pH shift.

Conclusion:

No differences in cAMP signalling in IBD TT/CT/CC subjects compared to healthy CC subjects were observed. In contrast, TT IBD patients showed impaired activation of RhoA upon an acidic pH shift. Our results support the role of GPR65 in the intestinal inflammation in genetically predisposed individuals, emphasizing the link between acid-base homeostasis and IBD pathogenesis.

The role of TopBP1 in the cellular response to DNA double-strand breaks*Klinik für Gynäkologie, UniversitätsSpital Zürich¹***Introduction:**

The Topoisomerase II beta binding protein 1 (TopBP1) is a DNA damage protein accumulating in ionizing radiation induced foci (IRIF) upon treatment of cells with ionizing radiation (IR). TopBP1 contains multiple, evolutionary conserved, BRCT domains, which are characterized best for binding to phosphorylated proteins. The structure of TopBP1 suggests that it serves as a highly dynamic hub for protein-protein interactions. TopBP1 plays many important roles in DNA metabolic processes such as the initiation of DNA replication, DNA damage signaling, DNA repair and transcriptional regulation. So far, TopBP1 has predominantly been implicated in the DNA damage response during S phase, especially through its role in the activation of the ATR kinase. However, accumulating evidence describes that TopBP1 may also play a role in the repair of DSB. For instance, TopBP1 was found to act as a Rad51 loading factor in the homologous recombination repair pathway. Moreover, TopBP1 had been implicated to function in response to DNA damage in other phases of the cell cycle, such as G1 and mitosis. In G1, TopBP1 was found to form IRIF that colocalize with γ H2AX and 53BP1 at sites of DSB. However, the exact mechanism of recruitment and the function of TopBP1 at sites of DSBs in G1 is still elusive.

Methods:

To address the mechanism of TopBP1 IRIF formation in G1, we use biochemical methods as well as standard immunofluorescence (IF) and high-content microscopy including quantitative image-based cytometry (QIBC) in order to quantitatively assess the dynamics of TopBP1 IRIF formation in wild type cells and in cells that were genetically manipulated by CRISPR/Cas9. Immunoprecipitation and pulldown approaches are used to investigate the effect of site-directed mutagenesis of potential interaction partners of TopBP1.

Results:

TopBP1 accumulates at sites of DNA damage in G1 showing a cell cycle-dependent IRIF pattern. IRIF formation is dependent on MDC1 and 53BP1 in G1 but not in S/G2. Furthermore, we mapped a new TopBP1 interaction site in MDC1. We also observed an effect of TopBP1 depletion on ATR activation in G1 synchronized cells.

Conclusion:

In this study we investigate the role of TopBP1 in the cellular response to DSBs. First results show a direct role of the adaptor proteins MDC1 and 53BP1 for TopBP1 IRIF formation in G1. This suggests a distinct mechanism of TopBP1 recruitment in G1 as compared to other cell cycle phases. The physiological role of TopBP1 in the response to genotoxic stress in G1 will be further investigated as first results indicate a potential role for TopBP1 in ATR activation in G1.

Synergistic activity of NKG2D-based chimeric antigen receptor (CAR)-T cells and radiotherapy against glioma

University Hospital Zurich, Department of Neurology, Zurich¹, Department of Microbiology and Immunology, Geisel School of Medicine, New Hampshire, USA², Department of Radiation Oncology, University Hospital Zurich³

Introduction:

Glioblastoma is the most common primary brain tumor in adults and virtually always lethal despite a multimodal treatment regimen including surgery, chemotherapy and radiotherapy. Therefore, novel treatment modalities are needed. Adoptive immunotherapy with genetically engineered T cells that express a chimeric antigen receptor (CAR) to recognize and eliminate tumors in a MHC-independent manner is an emerging strategy that has led to remarkable responses in hematologic malignancies. CARs that target the natural-killer group 2-member D (NKG2D) system elegantly use the promiscuous binding properties of the NKG2D receptor that binds to several tumor-associated ligands. NKG2D-based CAR T cells have never been investigated against glioma and it is unknown if this strategy can overcome the challenges of this tumor entity and if it could even be implemented in established conventional treatment regimens.

Methods:

CAR T cells were generated by retroviral transduction of splenocytes derived from C57BL/6 or VM/Dk mice to express a synthetic receptor with the extracellular domain of NKG2D, a transmembrane domain and the intracellular CD3 ζ domain. As a control, splenocytes were transduced with wildtype-NKG2D (wtNKG2D). For *in vitro* studies, murine glioma cells (GL-261, SMA-560, SMA-540, SMA-407) were co-cultured with chNKG2D or wtNKG2D T cells and we assessed the cytolytic activity and IFN-g production by flow cytometry. For *in vivo* studies, we used GL-261 cells syngeneic to C57BL/6 mice and monitored tumor growth by magnetic resonance imaging. For *in vivo* tracking of CAR T cells, we used fluorescence molecular tomography (FMT), flow cytometry and immunohistochemistry. Long-term survivors were re-challenged with another tumor implantation and tumor-infiltrating and peripheral lymphocytes were analyzed by flow cytometry. To study the combination of radiotherapy with CAR T cells, mice received a single subtherapeutic dose of local irradiation.

Results:

In all murine glioma cell lines, chNKG2D T cells had a significantly higher specific cytolytic activity compared to wtNKG2D T cells. Furthermore, chNKG2D T cells produced more IFN-g. *In vivo*, intravenously injected chNKG2D T cells migrated to the orthotopic tumor site, were tolerated without toxicities, prolonged the survival and cured a fraction of tumor-bearing mice. This anti-tumor effect was even more pronounced in case of intratumoral CAR T cell administration. Survivors were long-term protected against tumor re-challenge. Mechanistically, this was not the result of a classical immune memory response, but rather due to local persistence of chNKG2D T cells. Radiotherapy, as part of the standard treatment regimen against glioblastoma, augmented the effect of chNKG2D T cell therapy already after a single application of a subtherapeutic dose. We identified two underlying mechanisms for this synergistic activity. First, a direct tumor-cell related effect as demonstrated by an increased cytolysis and IFN-g production after co-culture of low-dose pre-irradiated GL-261 cells with chNKG2D or wtNKG2D T cells and second an indirect migration-related mechanism as demonstrated by increased accumulation of CAR T cells within irradiated tumors *in vivo*.

Conclusion:

We provide the first systematical preclinical assessment of NKG2D-based CAR T cells against glioma. This strategy was effective, tolerated without toxicities, conferred long-term protection and was synergistic with radiotherapy. These findings could provide a rationale to test this immunotherapeutic strategy also in human glioma patients.

Functional and morphological outcome analysis of pediatric cataract surgery

Eyeclinic, University Hospital, Zurich¹, Children's University Hospital, Department of Pediatrics, Steinwiesstrasse 75, CH-8032 Zürich²

Introduction:

Development of glaucoma after pediatric cataract surgery is depending on multiple factors such as age at surgery, associated ocular pathologies, and intraocular lens implantation. Analysis of these factors associated with glaucoma development is warranted for improved patient management and better parental support.

Methods:

Retrospective chart review of consecutive cases which underwent cataract surgery until 10 years of age, during a 10-year period from 2004 to 2014 at the University Hospital Zurich, Switzerland. Analysis included functional and morphological data at initial presentation and last follow up as well as management of glaucoma. The study was approved by the local Ethics committee.

Results:

63 children (28 female, 94 affected eyes) with bilateral (68/94) or unilateral (26/94) cataracts were identified. Diagnosis of cataract were: congenital (82/94), juvenile (12/94), acquired (8/94, 3 of these post retinopathy of the premature treatment, 2 due to juvenile rheumatic arthritis, 3 due to trauma). Surgery was performed at a median age of 22 months: 49 of 94 eyes received an intraocular lens (median age 50.7 months at surgery) and 45 of 94 eyes were left aphacic (median age 1.5 months at surgery). At the last follow up visit (22 days - 8.6 years, median 31 months) visual acuity was ≥ 0.4 decimal Snellen equivalent in 23 patients (34/94) and ≤ 0.2 in 10 patients (12/94). Aphacic glaucoma was diagnosed in 12 of 45 eyes (9/28 patients) at a median of 6.8 months after surgery. Microcornea (5/12), anterior segment dysgenesis (1/12), aniridia (1/12), or Lowe Syndrome (1/12) were associated with glaucoma development.

Conclusion:

Congenital cataracts are the main cause of surgical intervention in our pediatric cataract group. In agreement with previously published data, aphacic glaucoma is one of the main postoperative complications and is often associated with abnormal ocular development.

C. Schori¹, M. Barben¹, M. Samardzija¹, D. Barthelmes², C. Grimm¹

The vitreous proteome of chronic hypoxic response mediated retinal degeneration.

Lab for Retinal Cell Biology, Department of Ophthalmology, University of Zurich, Zurich, Switzerland¹,
Department of Ophthalmology, University Hospital Zurich, Zurich, Switzerland²

Introduction:

Chronic hypoxia in the retina is a major risk factor for the development of wet AMD and may also be relevant for the dry form of the disease. Although dry AMD affects a large number of patients, a therapy is still an unmet medical need. Here, we use vitreous samples from genetically modified mice and human patients to identify biomarkers that may be involved in hypoxia-induced degenerative processes of the retina. Identification of such markers may help to define patient cohorts that might benefit from a therapy targeting the hypoxic response of the retina.

Methods:

To mimic chronic hypoxia in the mouse retina, we excised the *von Hippel-Lindau (Vhl)* gene specifically in photoreceptors using the Cre-LoxP system. The Vhl knockdown was performed either in rods of the typical rod-dominant mouse retina ($rod^{\Delta Vhl}$) or in cones of mice with an “all-cone” retina ($R91W;NRL^{-/-}$) ($cone^{\Delta Vhl}$).

The vitreous of these mice was isolated by an adapted method of *Skeie et al. (PlosOne; 2013)* and its protein composition analyzed by a discovery proteomics approach using an LC-MS/MS Orbitrap system and relative label-free quantification. Proteins with a minimal fold change of 2 and a pValue below 0.01 were considered to be differentially regulated.

To determine whether identified proteins may be relevant for human pathology, we will use vitreous samples from patients suffering from dry AMD and appropriate controls. These samples have been collected and are currently being prepared for proteomic analysis as described above.

Results:

Retinas of both $rod^{\Delta Vhl}$ and $cone^{\Delta Vhl}$ mice showed normoxic activation of *hypoxia inducible transcription factors* (HIFs), sustained expression of hypoxia responsive genes, and a slowly progressing age-dependent degeneration. The vitreous proteome of these mice revealed distinct protein compositions depending on the time point of analysis. The early time point of 10 week old $rod^{\Delta Vhl}$ mice, shared only two (*alpha-2 macroglobulin & guanylate binding protein 2b*) upregulated proteins with the late time point at 6 months. In the $cone^{\Delta Vhl}$ mice no differentially regulated protein was identified at 4 weeks of age. But already at 6 weeks, a time point at the beginning of degeneration, 50 proteins were identified to be upregulated. Several of them are known HIF target proteins, such as *heterogeneous nuclear ribonucleoprotein H1*, or *lectin galactoside-binding soluble 3*. Interestingly none of these proteins were found to be differentially regulated at 8 or 12 weeks when retinal degeneration and morphological changes were strongest.

Conclusion:

A chronic hypoxia-like response in photoreceptors alters the vitreous proteome in a time dependent manner. The distinct protein compositions present at early or late time points, suggest a well-regulated process in our models. We hypothesize that some of the proteins identified at early time points may serve as biomarkers for dry AMD caused by chronic hypoxia. The analysis of the vitreous proteome of AMD patients may provide further evidence for this hypothesis.

Rational design of anti-PrP antibodies to block prion induced neurodegeneration

Institute of Neuropathology, University Hospital Zürich, Zurich¹, Novartis Institutes for BioMedical Research, Novartis Pharma, Basel²

Introduction:

In prion diseases, neurodegenerative disorders of sporadic, genetic or infectious origin, the conformational conversion of the cellular prion protein (PrP^C) into the misfolded scrapie form (PrP^{Sc}) is the key pathogenic event leading to neuronal dysfunction and death. PrP^C is a glycosylphosphatidylinositol (GPI)-anchored membrane protein, highly abundant in the nervous system and conserved among species. PrP^C consists of two moieties: the C-terminal globular domain (GD) and the N-terminal flexible tail (FT), which includes the octapeptide repeat (OR) region, two regions enriched in positively charged residues (CC1 and CC2) and a hydrophobic core.

Since PrP^C function in the CNS is dispensable, as the protein can be safely knocked out, while the presence of PrP^C on the neuronal surface is essential for prion replication and toxicity, targeting PrP^C represents a rational approach to cure prion diseases. Whether antibody-based therapy for prion diseases is a valuable strategy has been highly debated. By testing our own series of monoclonal antibodies (mAb) for toxicity in vitro and in vivo, we demonstrated that the biological effect of anti-PrP antibodies strongly depends on the targeted PrP epitope: binding of the FT was always innocuous, whereas binding of epitopes within the GD was toxic. Thus, in-depth structural and molecular studies are needed to identify epitopes of PrP that can be pursued for a safe immunotherapy.

Methods:

With the goal to establish a preclinical pipeline for discovering therapeutic anti-PrP mAbs, we executed a high-throughput screen for saturation coverage of the PrP surface in collaboration with Novartis Institute for Biomedical Research. Novel anti-PrP Fabs were generated by using phage display technology coupled with Next Generation Sequencing (NGS) analysis of the panning output pools. This enables to identify rare, otherwise invisible epitopes in complement to the classical ELISA screening technique. A synthetic human Fab phage display library was selected by sequential biopanning rounds against PrP protein and peptides, in order to identify a broad range of Fabs binding to PrP in different regions. These Fabs were purified and characterized by several assays (surface plasmon resonance (SPR), ELISA, western blot) and tested for their ability to prevent neuronal loss in vitro in prion infected cerebellar organotypic cultured slices (COCS). Selected clones, the CC1 binder Fab3 and the OR binder Fab71, were further improved by phage display affinity maturation campaign.

Results:

We selected a panel of anti-PrP Fabs with known sequence and definite binding profile: CC1, OR, CC2 and GD binders. Additional clones with diverse epitopes were rescued by PCR from the output pools, based on the HCDR3 sequence frequency in NGS. Epitope mapping at amino acid level was determined by competition ELISA experiments using 12-mer PrP sequential peptides spanning the entire FT and confirmed in western blot by testing brain homogenates from mice expressing PrP deletion mutants. The binding affinity, as determined by SPR, was within the nM as order of magnitude and, upon affinity maturation phage selections of Fab3 and Fab71, novel clones with the same specificity as the parental but 2-log higher affinity were obtained. By flow cytometry, most of the Fabs detected native PrP on the surface of neuronal cell. Different OR binders proved to block prion induced neuronal degeneration in COCS.

Conclusion:

We have provided a more exhaustive anti-PrP antibody repertoire based on a rational design for the discovery of effective immunotherapeutics against prion diseases.

The role of SOX10 in melanoma resistance

Onkologie, UniversitätsSpital Zürich¹

Introduction:

Malignant melanoma is the most aggressive skin cancer and its incidence is steadily rising. Despite the recent success in treatment of melanoma patients with a variety of targeted inhibitors of RAS-RAF-MAPK signaling pathways the vast majority of patients develop resistance and succumb to the disease eventually.

Methods:

It has been hypothesized that stem cells are often responsible for tumor relapse and recently this hypothesis has been confirmed using genetically engineered mouse models. Here, we aim to address this hypothesis in melanoma using tissue biopsies, patient-derived primary cultures as well as genetically engineered mouse models of melanoma (*Tyr:Nras^{Q61K}Ink4a^{-/-}* model and *Braf^{V600E}Pten^{fl/ml}Tyr-CreERT2* model). We have obtained several sensitive and resistant cell lines (in collaboration with the Department of Dermatology, USZ). We have decided to select *NRAS*-mutated as well as *BRAF*-mutated patient-derived melanoma cell lines. Majority of *BRAF*-mutated cell lines acquired resistance due to the treatment with vemurafenib (*BRAF* inhibitor), while some of *NRAS*-mutated cell lines are resistant to binimetinib (*MEK* inhibitor).

Results:

Sox10 is a transcription factor playing a crucial role in the self-renewal of neural crest stem cells as well as in the maintenance of giant congenital nevi and melanoma. Using Western blot analysis, we have compared the levels of SOX10 expression between sensitive and resistant melanoma cell lines. Our preliminary data demonstrate that SOX10 is expressed at higher level in sensitive cell lines as compared to the resistant melanoma cells. Moreover, we show that upon treatment with inhibitors the expression of SOX10 is downregulated in sensitive cell lines. On the contrary, the resistant cell lines decrease the levels of SOX10 expression upon treatment with inhibitors.

To dissect the cellular mechanisms of resistance *in vivo*, we have generated xenografts from both cohorts of melanoma cell lines, sensitive and resistant. As a first step, we have analyzed the expression of melanoma-specific markers as well as the expression of SOX10. Surprisingly, based on our preliminary results, we do not observe any heterogeneity with respect to SOX10 expression. Furthermore, we have analyzed the expression of MART1 (melanoma antigen recognized by T cells 1) and TYR (Tyrosinase), markers often used to diagnose melanoma in clinics. The expression of MART-1 in xenograft tissue obtained from sensitive melanoma cell lines is distributed in a homogeneous manner. Interestingly, the xenograft tissue of resistant cell lines is characterized by completely different pattern of MART-1/TYR expression, with either patches of tissue showing positivity or only single cells expressing these markers.

Conclusion:

To further investigate the possible reasons underlying our observations, we plan to establish several clonal cultures of patient-derived melanoma cell lines. We aim to generate xenografts from these cultures and to analyze the expression of the above mentioned markers. Moreover, we are currently establishing mouse models, which will mimic the acquisition of resistance *in vivo* and therefore, will allow us to more precisely understand the molecular and cellular mechanisms of melanoma resistance.

M. Pfammatter¹, M. Andreassen², G. Meisl², R. Mezzenga³, T. Knowles², A. Aguzzi¹, S. Hornemann¹

Absolute quantification of amyloid aggregates using a digital amyloid amplification assay

Institute of Neuropathology, University Hospital of Zurich, Zurich, Switzerland¹, Department of Chemistry, University of Cambridge, Cambridge, United Kingdom², Department of Health Sciences and Technology, ETH Zurich, Zurich, Switzerland³

Introduction:

Amyloid aggregates are a pathological hallmark of protein misfolding and aggregation diseases, such as Alzheimer's, Parkinson and Creutzfeldt-Jakob disease. Despite their high abundance in diseased brains, the ante-mortem detection and quantification of amyloid aggregates remains challenging. However, sensitive detection assays would enable early diagnosis and therapeutic intervention and would provide new insights into the processes underlying amyloid aggregation. To address these challenges, we have developed an innovative digital amyloid amplification assay that allows the detection and precise quantification of amyloid fibrils using microfluidics technology.

Methods:

Based on the inherent autocatalytic amplification properties of amyloid fibrils we established a conversion assay, in which selective amplification of preformed amyloid fibrils enables the sensitive detection of fibrils. Therefore, monomeric substrate protein is mixed with the sample to be analysed for the number of "propagons" (defined as the minimal propagating unit of amyloid fibrils) and partitioned into several parallel reactions for propagon-catalysed amplification. Endpoint amplification leads to *de novo* formation of aggregates in the propagon-containing reactions, which can be followed by Thioflavin T fluorescence. By combining the digital readout with limiting dilutions of the original sample the total number of aggregates in the original sample can be calculated using Poisson statistics.

Results:

In a first step, we established an insulin amyloid amplification assay in a 384-well microplate format. We found conditions under which propagon-catalysed aggregation is promoted while spontaneous aggregation of insulin monomers is suppressed. Under those conditions the assay is capable to detect single propagating units of insulin fibrils in the test sample. To further improve the amplification assay, we transferred it to a droplet-based microfluidic platform. On-chip encapsulation of individual amplification reactions inside microdroplets allowed running several 1000 separate amplification reactions in parallel. This high number of replicate reactions led to a significant increase in precision and accuracy of aggregate quantification. In analogy to the microplate insulin assay, we developed an amyloid amplification assay for the detection and quantification of recombinant α -synuclein aggregates.

Conclusion:

Our newly developed digital amyloid amplification assays allow the precise, absolute quantification of amyloid aggregates in a test sample. In a next step, we aim to validate the α -synuclein amyloid amplification assay for the detection and quantification of α -synuclein aggregates in biological samples. Reliable aggregate quantification in biological samples will allow us to investigate the correlation between aggregate number and clinical manifestation. In addition, the α -synuclein amyloid amplification assay has the potential of being the first digital assay for the diagnosis of α -synucleinopathies.

A. Okonska¹, R. Parrotta¹, W. Weder², R. Stahel³, L. Lorenza⁴, E. Felley-Bosco¹

A novel BRCA1-associated protein-1 isoform affects response of mesothelioma cells to drugs impairing BRCA1-mediated DNA repair

Laboratory of Molecular Oncology, Division of Thoracic Surgery, University Hospital Zürich, Zürich 8091, Switzerland¹, Division of Thoracic Surgery, University Hospital Zürich, Zürich 8091, Switzerland², Cancer Center Zurich, University Hospital Zürich, Zürich 8091, Switzerland³, Institute of Molecular Cancer Research, University of Zürich, Zürich 8057, Switzerland⁴

Introduction:

BRCA1-associated protein-1, BAP1, is a tumor suppressor involved in multiple cellular processes such as transcriptional regulation, chromatin modification and DNA repair by deubiquitinating histone 2A. BAP1 mutations are frequent in malignant pleural mesothelioma (MPM). Our aim was to functionally characterize a newly identified isoform of BAP1 and investigate the effects of its expression on drug sensitivity in MPM.

Methods:

Expression of BAP1 isoforms was detected in MPM and normal mesothelium cell lines, tumor and non-tumor samples by qPCR. Histone H2A ubiquitination levels were analyzed by western blot after acidic extraction of core-histones. Subcellular localization of BAP1 isoforms was examined by immunofluorescence. MPM cell survival in response to PARP- and to dual PI3K-mTOR- inhibitors was analyzed by *in vitro* assays.

Results:

We have identified a novel alternative splice isoform of BAP1 (BAP1delta) which misses part of the catalytic domain. Cells transfected with BAP1delta showed loss of deubiquitinating activity compared to full length BAP1. The expression of BAP1delta transcript is more abundant in non-tumor compared to tumor samples. MPM cell lines expressing higher level of endogenous BAP1delta are more sensitive to Olaparib, a poly(ADP-ribose) polymerase 1 (PARP1) inhibitor, and this sensitivity is enhanced when Olaparib treatment is combined with GDC0980, dual PI3K-mTOR inhibitor, which induces downregulation of BRCA1.

Conclusion:

These observations suggest that BAP1delta may regulate DNA damage response and drug sensitivity. It might therefore be relevant to investigate whether patients with high expression of BAP1delta may be responsive to PARP/PI3K-mTOR inhibitors.

S. Santos¹, S. Stantos², Ch. Haslinger¹, M. Hamburger², M. Mennet³, O. Potterat², M. Schnelle³, U. Von Mandach¹, A P. Simões-Wüst¹

In vitro effect of *Bryophyllum pinnatum* press juice combined with atosiban on myometrium contractility

Department of Obstetrics, University Hospital Zürich, Zürich, Switzerland¹, Department of Pharmaceutical Sciences, University of Basel, Basel, Switzerland², Clinical Research, Weleda AG, Arlesheim, Switzerland³

Introduction:

Preterm birth is one of the most common causes of infant morbidity and mortality, and often results from preterm labour. The oxytocin receptor antagonist atosiban is frequently used to inhibit uterine contractions in women presenting with preterm labour. The herbal medicine *Bryophyllum pinnatum* has been used as a tocolytic agent in anthroposophic medicine and, more recently, as an add-on medication to inhibit preterm contractions. However, the influence of *B. pinnatum* on the effect of known tocolytics has not yet been investigated. In the present *in vitro* study, we compare the tocolytic effects of *B. pinnatum* leaf press juice and atosiban, used alone and in combination, on the contractility of myometrium tissue obtained from pregnant women.

Methods:

Myometrial biopsies were collected during elective caesareans. From each biopsy, four strips of 15x2x1mm³ were trimmed. Strips were placed under tension in a myograph chamber, and spontaneous contractions were recorded. After a 30 min period of regular spontaneous contractions, *B. pinnatum* (0.08%), atosiban (0.53 µg/mL), or the combination of both was added to the chamber, and the contractility was recorded for 30 min. After a washout period, vitality of strips was observed for additional 30 min. Area under the curve (AUC) of contractions was determined for each period analysed. Contractility after addition of the test substances was expressed as percentage of the baseline contractility (before addition of test substances).

Results:

All test substances inhibited myometrium contractility, i.e. they led to significantly lower AUCs compared to control (Krebs solution, $p < 0.05$). Atosiban inhibited contractions by $53.7 \pm 20.8\%$, and *B. pinnatum* decreased contractions by $30.1 \pm 14.0\%$. The combination of *B. pinnatum* and atosiban lowered contractions by $47.9 \pm 14.8\%$, which was not significantly different from the activity of *B. pinnatum* or atosiban alone.

Conclusion:

B. pinnatum and atosiban, alone or combined, show inhibitory effects on spontaneous myometrial contractions. However, at the concentrations tested, the combination of both medications did not significantly increase the inhibition of spontaneous contractions in human myometrium strips.

JH. Jang¹, F. Janker¹, S. Arni¹, N. Borgeaud², Y. Yamada¹, W. Weder¹, W. Jungraithmayr¹

NK cell recruitment via CD26/DPP4 inhibition decreased lung cancer growth

Division of Thoracic Surgery, University Hospital Zurich¹, Visceral and Transplantation Surgery, University Hospital Zürich²

Introduction:

Lung cancer is the leading cause of death among cancers. There is broad evidence that immune cells are involved in the growth and development of these malignancies. CD26/DPP4 (dipeptidyl peptidase 4) is a transmembrane glycoprotein, that is constitutively expressed on hematopoietic cells, but also found on lung epithelial and endothelial cells. We found previously that the activity of CD26/DPP4 of lung cancer patients is four times higher than in normal tissue. Here, we tested if CD26/DPP4-inhibition is able to modulate lung cancer growth via NK cell activation in mice.

Methods:

An orthotopic lung tumor model was employed by sc. injections of the mouse lung cancer (Lewis Lung Carcinoma (LLC)) and a human lung adenocarcinoma cell line (H460). These were developed in mice C57BL6 (n=18) and CD1-nude mice (n=20) respectively. The CD26/DPP4-inhibitor Vildagliptin was given in drinking water of 50mg/kg daily dose. Tumor growth was evaluated by wet weight of tumor mass at 2 weeks. Histological assessments included TUNEL, immunohistochemistry (IHC) of CD3, B220, F4/80, NKp46, and γ H2AX. IL-10, Arginase, IL-12, NKp46, NK1.1, IFN- γ , TRAIL, Granzyme, and Perforin 1 were analyzed by RT-PCR and FACS. *In vitro* analysis of γ H2AX expression in the TRAIL treated LLC was performed by western blotting. For a proof of concept and as a gain of function experiment, macrophage ablation was performed by clodronate-liposome during Vildagliptin treatment and NK cells were deleted by IL-15 knockout.

Results:

Vildagliptin treatment significantly reduced the tumor growth of both, LLC and H460 in mice. IHC showed macrophages (F4/80) and NK cells (NKp46) to be significantly increased by Vildagliptin within tumors, while TUNEL stain and IHC of T- and B cell infiltration did not show any difference. Gene expression levels of anti-inflammatory markers (IL-10, and Arginase) were unchanged, while the pro-inflammatory cytokine TNF- α , IL-12, and IL-15 were significantly elevated. The NK cell markers NKp46, NK1.1, IFN- γ , TRAIL, Granzyme and Perforin 1 were significantly upregulated within the tumor by Vildagliptin, indicating that inhibition of CD26/DPP4 recruits NK cells into the tumor. Furthermore, we found enhanced γ H2AX expressions in lung cancer cell lines by TRAIL treatment *in vitro*. Macrophage ablation with clodronate-liposome in Vildagliptin treated mice reversed the tumor size significantly. Deletion of NK cell significantly increased the tumor size compared to control.

Conclusion:

The Inhibition of CD26/DPP4 decreased lung cancer growth in primary models of mouse and human lung cancer and increased inflammatory macrophages and NK cell cytotoxicity including TRAIL within those tumors. Furthermore, an increased expression of cellular stress marker γ H2AX by TRAIL treatment in lung cancer cell lines suggests that NK cell derived TRAIL inhibited the lung cancer growth.

MRS. Spalinger¹, HL. Hering¹, MR. Manzini¹, JBR. Riggs¹, GC. Gottier¹, AK. Atrott¹, TR. Raselli¹, AF. Fettelschoss², TMK. Kündig², GR. Rogler¹, MS. Scharl¹

PTPN2 controls intestinal inflammation and promotes colitis-associated tumour formation via control of inflammasome activation and IL-1alpha release

University Hospital Zürich (USZ), Department of Gastroenterology and Hepatology, Zürich, Switzerland¹, University Hospital Zürich, Clinic for Dermatology, Zürich²

Introduction:

Variants in the gene locus encoding protein tyrosine phosphatase non-receptor type 2 (PTPN2) are associated with Crohn's disease (CD) and ulcerative colitis (UC). We recently found that deletion of PTPN2 in macrophages promotes colitis severity, while protecting from colitis-associated tumours, but the molecular mechanisms underlying this phenotype are still elusive. IL-1a and IL-1b exert important, yet distinct, immune-modulatory function in the intestine, but their precise role during intestinal pathologies is still controversial. Here, we investigated whether IL-1a and/or IL-1b are involved in enhanced colitis and/or reduced tumour development observed in mice lacking PTPN2 in macrophages (PTPN2-LysMCre mice).

Methods:

Colitis was induced in 10-12 week old PTPN2-LysMCre and their wild-type (WT) littermates by administration of 2% DSS for 7 days (acute colitis), or by repeated treatment with 1.5% DSS for 7 days, followed by 10 days normal drinking water (four cycles in total, chronic colitis). For tumour induction, mice were injected with azoxymethan (AOM) at day one of each DSS cycle during chronic colitis induction. IL-1b and IL-1a were inhibited using a vaccine-based approach.

Results:

In vitro, PTPN2-deficient macrophages secreted more mature IL-1b, and levels of active caspase-1 were enhanced, indicating pronounced inflammasome activity. Responsible for enhanced inflammasome activation was increased phosphorylation of the inflammasome-adaptor molecule ASC. Further, PTPN2-deficient macrophages secreted increased levels of IL-1a, while surface-associated IL-1a was markedly reduced. As expected from our previous studies, PTPN2-LysMCre mice suffered from pronounced colitis, but reduced tumour load. In the serum, IL-1a and IL-1b levels were enhanced in PTPN2-LysMCre mice upon DSS or AOM/DSS treatment, but surface IL-1a on macrophages and intestinal epithelial cells was reduced. Inhibition of IL-1b during colitis induction/tumour formation protected PTPN2-LysMCre mice from pronounced colitis, but re-established the susceptibility to colitis-associated tumours. In contrast, inhibition of IL-1a did not affect colitis severity, while protecting WT mice from the induction of colitis-associated tumours.

Conclusion:

PTPN2 is a crucial regulator of inflammasome activation, and its loss in macrophages has important consequences for intestinal homeostasis. Further, our results demonstrate that the structurally related molecules IL-1a and IL-1b exert distinct roles during intestinal inflammation and tumorigenesis, and PTPN2 modulates secretion and surface expression of these two cytokines.

Microvascular changes after experimental subarachnoid hemorrhage in mice

*Department of Neurosurgery, University Hospital Zurich, Zurich*¹, *Department of Neuropathology, University Hospital, Zurich*², *Institute for Biomedical Engineering, ETH & Univ. Zurich, Zurich, Switzerland*³, *Brain Research Institute, Universität Zürich, Zürich*⁴

Introduction:

Aneurysmal subarachnoid hemorrhage (aSAH) is a form of stroke which occurs in 6 to 8 out of 100 000 people. The majority of all cases are caused by the spontaneous rupture of a cerebral aneurysm at the skull base. Although aSAH cases only comprise 5% of all strokes, the mortality rate is high (40%) due to delayed ischemic neurological damage (DIND). The ischemic stroke is 20 times more common in our society, but the potential loss of life caused by aSAH is comparable due to the relatively young age of aSAH patients.

Methods:

In order to characterize spatial and temporal changes in microvascular permeability and integrity, we use the filament perforation model to induce experimental SAH in mice. The temporal course of edema formation, ischemia and cerebral blood flow are analyzed using magnetic resonance imaging (MRI). Blood- brain barrier and vascular permeability alterations after SAH are investigated using tracer injection and whole brain clearing.

Results:

The MRI results show a variability of pathological changes after several timepoints. We detect a formation of vasogenic edema and ischemic lesions in SAH operated animals which are absent in control animals. Cerebral blood flow alterations occur already 30 min after the SAH induction. Additionally, a pathological permeability of the blood brain barrier after SAH can be detected. A strong extravasation of tracer fluorescence (70 kDa dextran) can be seen all over the brain after SAH.

Conclusion:

Subarachnoid hemorrhage causes microvascular deficiency in the brain parenchyma shortly after bleeding which manifests in the dysfunction of the blood-brain barrier, as well as edema and ischemia formation and impairment of cerebral blood flow. Further studies will be directed towards elucidating the cellular and molecular mechanism that leads to the pathological changes.

Identifying the cell of origin of neuroblastoma*Oncology, University Hospital Zurich, Zurich¹***Introduction:**

Neuroblastoma (NB) is a pediatric cancer of the peripheral nervous system, which occurs almost exclusively in infancy and early childhood. It is widely assumed that oncogenic mutations occur in the cells of sympathoadrenal (SA) lineage during prenatal and postnatal life, however, the exact cell of origin has not been yet characterized. *MYCN* amplification and activating mutations of ALK (anaplastic lymphoma kinase) are among the most common genetic alterations in human NB described so far. There have been a number of attempts to model NB development in mouse models. The targeted expression of *ALK^{F1174L}* and *MYCN* oncogenes driven by a tyrosine hydroxylase (*Th*) and dopamine beta-hydroxylase (*Dbh*) promoters resulted in NB development. However, these mouse models fail to faithfully recapitulate human NB, there is a lack of schwannian stroma, only minimal metastasis formation and most importantly, a failure of mimicking the spontaneous regression, one of the key features of NB in humans. Furthermore, the onset of disease is delayed and majority of mice develop NB at 2 months old, which does not correspond to the pediatric characteristic of this tumor. A possible explanation for these discrepancies might be the fact that the oncogene expression is induced in progenitor cells rather than stem cell population. Taken together, these data suggest that there is a strong need to develop more faithful mouse models of NB development and therefore, a comprehensive analysis of the cellular hierarchy within SA lineage is a first step to understand the origin of NB.

Methods:

In order to identify the cell of origin of NB, we first traced different markers of SA lineage to clarify the cellular hierarchy during embryonic development. We induced oncogenes expression in key cellular populations of SA development to assess whether these mouse models recapitulate better the features of human NB. We used several Cre mouse lines, where Cre expression is driven by promoters that are markers of different levels in SA lineage differentiation. Through recombination was allowed population-specific transcription of *rosa26/tdTomato* reporter, or oncogenes as *rosa26/MYCN* and *ALK F1174L*.

Results:

Here, we demonstrate lineage tracing of different cellular populations in adrenal medulla (AM) and sympathetic ganglia (SG). As expected neural crest stem cells, marked by *Sox10* expression, gave rise to nearly all cells in AM. The expression of either *MYCN* or *ALK^{F1174L}* in *Sox10+* cells resulted in embryonic lethality.

We proved that SA progenitors, marked by *Ascl1* expression, are actually multipotent as they give rise to both glial and chromaffin cells in AM and SG. Surprisingly, lineage tracing of glial progenitors, marked by *Dhh* expression, showed that some of the glial cells can give rise to chromaffin cells. While the induction of *MYCN* expression in *Dhh*-expressing cells did not result in developmental abnormalities, the expression of *ALK^{F1174L}* in the very same cellular population was lethal.

Lineage tracing of *Dbh+* progenitors demonstrated that this population gave rise to only chromaffin cells, confirming that *Dbh* gene is expressed in the committed progenitors of the SA lineage.

Conclusion:

First of all, we showed that oncogenic activation of *MYCN* and *ALK^{F1174L}* in NCSCs leads to the embryonic lethality at E13.5. Secondly, we described two interesting cellular populations marked by *Ascl1* and *Dhh* expression that are not committed in a specific lineage as *Dbh+* cells are. These findings indicate how glial and SA lineages are close differently than previously defined.

Modulation of tumor hypoxia for hypofractionated radiotherapy*UniversitätsSpital Zürich¹, NormOxys²***Introduction:**

Tumor hypoxia is associated with resistance to radiotherapy, an increased risk of metastases and poor clinical prognosis. Reactive oxygen species are generated in response to ionizing radiation (IR) and produce amongst others irreversible DNA double-strand breaks followed by chromosomal aberrations and cell death. This IR-induced cytotoxic effect is less abundant under hypoxia and thus hypoxic cells are more resistant to IR. Hence reoxygenation or a reduction of the hypoxic tumor fraction by a combined treatment modality with a pharmaceutical agent is of high interest to reduce the required dose of IR and thereby to further minimize normal tissue toxicity. Here we investigated the combined treatment modality of the novel anti-hypoxia compound *myo*-inositol trispyrophosphate (ITPP) in combination with IR.

Methods:

ITPP was developed as an allosteric effector of hemoglobin to lower the oxygen/hemoglobin affinity thereby resulting in an enhanced release of oxygen upon tissue demand e.g. in hypoxic tumors. The capability of tumor reoxygenation by ITPP was serially probed by a non-invasive hypoxia-directed ODD-luciferase-based bioimaging approach and by immunohistochemistry (pimonidazole, CAIX) in FaDu HNSCC- and A549-lung carcinoma derived tumor xenografts. Tumor growth delay was determined on treatment with ITPP and a single high dose of IR (10 Gy).

Results:

Using our *in vivo* bioimaging approach, we confirmed as part of pharmacodynamic-oriented *in vivo* studies increased pO₂ starting 2 hours after ITPP application. Dose-titration studies indicated a maximal dose of 3g/kg of ITPP that was administered on two consecutive days followed by immediate irradiation 2 hours after the second application of ITPP. Interestingly ITPP alone did not affect the growth of FaDu tumor xenografts but significantly sensitized the tumor to a single dose of irradiation (10 Gy). Immunohistochemical analysis of the hypoxic marker CAIX validated this rapid decrease of tumor hypoxia in response to ITPP. Furthermore, the IR-induced tumor hypoxia observed at 4 days after IR may well be associated with a decrease in tumor vascular density, which was apparently prevented by combinatorial treatment with ITPP.

Conclusion:

ITPP administration induces an immediate increase of oxygen availability that can be exploited by a combined treatment modality with IR as shown in our HNSCC tumor model. ITPP also seems to protect the tumor vasculature upon IR, which may positively impact on the hypoxia status. Overall our results support the strong rationale to combine ITPP with IR for hypoxic tumors, but also demonstrate the need for further pharmacodynamic studies to investigate the optimal combination regimen in view of hypofractionated radiotherapy.

Analysis of the accuracy of a calculation tool to predict the yield of hematopoietic stem cells after leukapheresis*Hematology, University Hospital Zürich, Zurich¹, Oncology, University Hospital Zurich²***Introduction:**

Autologous and allogeneic hematopoietic stem cell (HSC) transplantation (SZT) are well established treatment options for a variety of hemato-oncological diseases like leukemia or lymphoma. Prerequisite for a successful SZT is the harvest of a sufficient number of peripheral blood (PB) HSC after mobilization with chemotherapy and stimulation with granulocyte colony stimulating factor (G-CSF) in autologous patients (AP) or G-CSF alone in healthy allogeneic donors (AD). For AP and AD at least 2×10^6 and 4×10^6 CD34⁺ HSC per kg body weight (kgBW) of the recipient are demanded to ensure a successful engraftment, respectively. Depending on the number of circulating HSC within the PB before leukapheresis (CN) as well as the body weight of the recipient and the target cell number (TN), the blood volume that has to be processed (BVP) during leukapheresis can be calculated. In this study we now sought to investigate the accuracy of a standard calculation tool in our leukapheresis department.

Methods:

Between January 2015 and August 2016, 99 AP and 44 AD that underwent leukapheresis in our department and had a complete data set were analyzed. HSC numbers and basic cell counts were measured before and after leukapheresis. Additionally, clinical features like age, sex, chemotherapy-regimes and underlying disease in AP as well as cumulative G-CSF dose in both groups were determined. Technical data including calculated blood volume and net harvest time were noted. The BVP to reach TN was calculated using this formula: $BVP = (TN \times BW) / (CN \times 0.4)$. After leukapheresis the number of collected HSC was analyzed and compared to the HSC numbers calculated.

Results:

Average age of AP and AD was 55.4 ± 1.1 years and 37.3 ± 2.1 years ($p < .001$), respectively. The number of leukocytes and platelets as well as the hemoglobin level was significantly decreased after leukapheresis in both groups. Cumulative G-CSF dose was $355 \pm 15 \times 10^6$ IE for AP and $420 \pm 9 \times 10^6$ IE for AD ($p < .0001$), respectively. Circulating HSC numbers in the PB before leukapheresis were significantly lower in AP ($79.0 \pm 8.4 / \mu\text{l}$) than in AD ($108.2 \pm 7.5 / \mu\text{l}$; $p = .02$). Strikingly, the calculated average HSC yield per kgbw in AP and AD ($4.8 \pm 0.5 \times 10^6$ and $6.8 \pm 0.4 \times 10^6$) was significantly lower than the net HSC yield per kgbw after leukapheresis ($6.1 \pm 0.6 \times 10^6$ and $9.0 \pm 0.5 \times 10^6$; both $p < .0001$), respectively. However, 18.2% of AP and 11.3% of AD had a lower number of collected HSC than calculated.

Conclusion:

The used calculation tool to determine the BVP needed to reach target HSC numbers underestimates significantly the net HSC number collected. However, in a substantial number of AD and AP, the calculated cell number was not reached. We therefore propose that beside the variables included in the calculation tool there are additional, so far unknown factors - possibly total leucocyte count or cumulative G-CSF dose - that correlate with the yield of the leukapheresis. Based on our data a revised calculation tool is currently developed and will be prospectively tested. This revised tool hopefully improves the accuracy of the prediction of the HSC yield after leukapheresis. This is particularly important for the protection of healthy donors to avoid the collection of surplus HSC not needed for transplantation.

Antibody based anti-HIV-1 therapy*UniversitätsSpital Zürich¹, Centre Hospitalier Universitaire Vaudois (CHUV)², Universität Zürich³***Introduction:**

The gold standard in treating HIV-1 is combined anti-viral therapy (cART), leading to a successful reduction of viremia and risk of transmission. However, cART requires daily medication, associated side effects and the risk of emergence of resistance in patients with poor drug adherence make the development of new therapeutic strategies necessary. During the last past years, a number of broadly neutralizing antibodies (bNAbs) against the HIV-envelope (env) have been identified and are a promising tool for new treatment approaches based on passive immunization.

Here we aim to investigate the anti-HIV-1 effects of a number of bNAbs in humanized NSG mice, infected with a replication competent, CCR5 tropic HIV strain. The bNAbs we are exploring are targeting different regions of the HIV-Env, i.e., VRC07 the CD4 binding site, LN01 the membrane proximal region, PG9 the V1/V2 region and 10-1074 the glycan V3 region. The anti-HIV efficacy of those antibodies is determined by using only a single HIV-Env bNAb for the treatment as well as different combinations of HIV-Env Abs in mixtures of 2-3 Abs.

Methods:

Pharmacokinetics: The half-life of each HIV-Env bNAb was determined in NSG mice. A single dose of HIV-Env bNAbs was injected subcutaneously. Blood samples were collected prior to the injection (day 0) and on days 1,3,5 and 7 after the injection. HulgG plasma concentration was analyzed by ELISA.

HIV-Env bNAb treatment: HIV infected humanized NSG mice were treated every 3-4 days with a single HIV-Env bNAb or a mixture of 2-3 Abs. Treatment was started 5 weeks after infection. Mice receiving the single HIV-Env bNAb were treated for 5 weeks and mice receiving the Ab-mixtures for 12 weeks. Throughout the experiment blood samples were collected for determination of viral load by PCR, plasma concentration of hulgG by ELISA and characterization of the human compartment by flow cytometry.

Characterization of escape mutants: In case of escape, viruses were isolated by co-culturing mice splenocytes and human peripheral blood mononuclear cells (PBMCs) and neutralization capacity of treatment Ab was analyzed by the TZM-bl neutralization assay.

Results:

The half-life of the examined HIV-Env bNAbs ranged from 1.97-9.58 days in humanized NSG mice with a serum concentration between 20-140µg/mL. For the anti-HIV-1 treatment using only one bNAb a significant but temporally limited reduction of viremia 7 days after start of the therapy was observed. The viral rebound was most likely due to the development of escape mutants. Viral rebound was not seen when using a cocktail of 2 or 3 three HIV-Env bNAbs. Here we observed a complete suppression of viremia within 1-7 weeks after treatment start.

Conclusion:

Using two or more HIV-Env-bNAbs results in long-term suppression of viremia. This kind of treatment allows extended dosing schedules compared to conventional cART requiring daily intake. We will explore in the next experiments the best combination of HIV-Env-bNAbs for their strength and safety. We are convinced that the HIV-Env-bNAbs are a promising alternative to cART in particular for patients who do not tolerate cART.

R. Casanova¹, U. Rulle¹, H. Moch¹, A. Soltermann¹

Prognostic relevance of lung squamous cell carcinoma tumor fragmentation, a histologic marker of increased tumor invasiveness

Department of Pathology and Molecular Pathology, University Zurich and University Hospital Zurich, Zurich, Switzerland¹

Introduction:

Lung squamous cell carcinoma (SCC) is the second most frequent histologic type of non-small cell lung carcinoma (NSCLC). Next to pTNM staging, grading is also important for histomorphologic classification of tumors into relevant prognostic groups. Histologically, SCC forms cohesive tumor sheets of various sizes, ranging from large pushing boundaries to small detached clusters. The presence of small clusters such as single cells, tumor buds <5 cells or cell nests ≤ 15 cells has been shown to be prognostic. However, scoring such small structures may be hindered by topographic heterogeneity and may not reflect lung SCC micro-architecture complexity. In this study we propose computer-based morphometric approach to quantify tumor fragmentation, an alternate marker of tumor invasiveness.

Methods:

In total three patients' cohorts of surgically resected lung SCC tumors were investigated (tissue microarray cohort: n=208, whole sections cohort: n=99 and an external TCGA cohort: n=326, H&E stained). TMA and whole sections cohorts were immuno-histochemically stained with pan-cytokeratin. Color-based segmentation (tumor epithelia brown, stroma blue-grey) allowed to separate tumor from stroma and to compute the number of tumor fragments. Associations with relapse-free (RFS) and overall survival (OS) were assessed by univariate Cox regressions. Tumor fragments were defined as tumor clusters $>800\mu\text{m}^2$ (circa >5 cells) separated by stroma and were automatically computed on TMA and whole sections cohorts. TCGA cohort was scored by eye on 50x magnification fields of view.

Results:

Histopathologic correlations indicated a positive association of tumor fragmentation (number of tumor fragments) with blood vessel infiltration (VI). In addition, increasing number of tumor fragments was associated with shorter OS and RFS on all three patients' cohorts ($p < 0.01$). In addition, tumor fragmentation was an independent prognostic marker on multivariate cox regression including stage, grade and VI.

Conclusion:

We used an automated morphometric approach for unbiased scoring of tumor fragmentation on digitalized histological sections. Our analysis revealed that tumor fragmentation is a poor prognosticator for lung squamous cell carcinoma, e.g. due to increased likelihood of vessel infiltration. This parameter could be relevant for refining current tumor grading systems and could be potentially applied to other solid human carcinoma.

A. Schindler¹, A. Courtier², M. Goldinger¹, F. Jaberg-Bentele¹, M. Manuel², S. Perez², J. Mouret², T. Nguyen-Kim¹, I.G. Raaijmakers¹, P. Kvistborg³, N. Pasqual², B.A. Haanen³, R. Dummer¹, P. Levesque¹

The peripheral blood TCR repertoire might facilitate patient stratification for immune checkpoint blockade inhibition in metastatic melanoma

University Hospital Zurich, Dermatology, Zurich¹, ImmunID Technologies, Grenoble, France², Netherlands Cancer Institute, Amsterdam, Netherlands³

Introduction:

Anti-PD-1 and/or anti-CTLA-4 antibodies show durable responses in metastatic melanoma. Measuring the diversity of T-lymphocytes in pre-treatment liquid biopsies may help stratify patients for immunotherapy.

Methods:

In this retrospective blinded study, we used a multi-N-plex polymerase chain reaction assay to measure T-cell receptors (TCR) combinatorial diversity from genomic DNA in peripheral blood from melanoma patients treated with anti-CTLA-4 (n = 38) or anti-PD1 (n = 36). A receiver operating characteristic curve was used to determine the threshold for dichotomized analysis (i.e. low vs. high diversity) according to RECIST 1.1. Association with benefit in the low vs. high groups was assessed through a Fisher's exact test. OS, PFS, and ORR were tested with absolute lymphocytes count (ALC), absolute neutrophils count (ANC), lactate dehydrogenase (LDH), S100 levels, and TCR diversity evenness (DE50) in a univariate model. Significant ($p < 0.10$) candidate predictive factors from the univariate analysis were included in a multivariate regression to define the added value of each variable on OR, OS and PFS prediction.

Results:

A DE50 < 20.5% was associated with a poor response (progressive or stable disease) to anti-CTLA-4 treatment ($p = 0.016$). In contrast, in anti-PD-1 treated patients a DE50 < 20% was associated with a good response to the treatment (partial or complete response) in 5 of the 12 responders ($p = 0.0021$), receiving anti-PD-1, and all non-responders (n = 24) had a high DE50 > 20%. Patients with a low DE50 were all non-responders in the anti-CTLA-4 cohort (100% negative predictive value), and in the anti-PD-1 cohort they were all responders (100% positive predictive value). A multivariate analysis of commonly documented clinical factors (i.e. ALC, ANC, LDH, or age) identified DE50 ($p = 0.00014$), ANC ($p = 0.016$) and ALC ($p = 0.027$) as independent predictive marker of response to anti-PD-1 therapy. The same test also highlighted that DE50 ($p = 0.040$) and ANC ($p = 0.0071$) were also independently predicting progression free survival of patients treated with anti-PD-1.

Conclusion:

Patients with a low DE50 did not benefit from anti-CTLA-4 therapy. In contrast, in patients treated with anti-PD-1 a low DE50 was associated with a better response after a least 12 weeks of therapy. Thus, the diversity of the TCR repertoire represented by the DE50 is a predictive biomarker of response that might help physicians choose the best immune checkpoint modulators for each patient. Several studies are ongoing to validate these results.

Nucleolar localization of TOPBP1 in response to DNA double strand breaks*Gynecology, University Hospital Zurich, Zurich¹***Introduction:**

In response to DNA double-strand breaks (DSBs), cells activate a series of molecular cascades mainly orchestrated by the ATM/ATR kinases, in order to arrest cell cycle and initiate DNA repair. Although findings in the past decade have allowed detailed insight into the key players and mechanisms responding to DSBs, it has not yet been elucidated whether the DSB response is uniform throughout the cell nucleus or if it is differently regulated at specific subnuclear regions. Only recently studies have started to reveal unique aspects of how DSBs response is organized in the nucleoli. TOPBP1 is a nine-BRCT domain protein implicated in different cellular processes such as DNA replication initiation, checkpoint signaling and DNA repair, as well as transcriptional control. In G1 cells, TOPBP1 localizes to sites of DNA DSBs, and this localization depends on its interaction with the DNA damage response factor 53BP1. A recent study revealed that, when overexpressed, TOPBP1 induces ATR-dependent nucleolar segregation and silencing of rRNA synthesis. However, the potential role of endogenous TOPBP1 at nucleoli remains elusive.

Methods:

In this study we used X-ray irradiation to generate DSBs in HeLa cells. The subcellular localization of TOPBP1 was studied by indirect immunofluorescence analysis. Co-immunoprecipitation experiments and pull-down assays were used in order to investigate the physical interaction of TOPBP1 with TCOF1. For synchronization experiments, HeLa cells were blocked in G2-M by monastrol and then released to progress synchronously in G1 phase. Images of fluorescently labeled cells were acquired with a Leica SP8 confocal microscope.

Results:

Following DSBs, TOPBP1 translocates rapidly in the nucleoli in an ATM dependent manner. In addition, both nucleolar segregation induced by TOPBP1 overexpression and TOPBP1 recruitment into the nucleoli upon DSBs were dependent on the nucleolar phosphoprotein TCOF1/Treacle. Co-immunoprecipitation experiments confirmed that TOPBP1 and TCOF1 physically interact and that the main interaction sites are located within the C-terminal region of TCOF1 and on BRCT1 of TOPBP1. Interestingly, TOPBP1 nucleolar recruitment upon DSBs appears to be regulated during the cell cycle, being maximal in G1 and reduced in late S and G2. Moreover, we observed increased localization and longer persistence of TOPBP1 in the nucleoli upon DSBs in cells depleted of 53BP1. On the other hand, TCOF1 depletion, which abrogates TOPBP1 nucleolar recruitment upon DSBs, results in earlier localization of TOPBP1 at DNA damage-induced nuclear foci.

Conclusion:

Our results are consistent with an intracellular antagonism between TCOF1 and 53BP1 in recruiting TOPBP1 to nucleoli and DNA damage-induced nuclear foci, respectively.

Modulation of visual response after L-dopa treatment in zebrafish larvae*Neurology Department, University Hospital Zürich, Zurich¹*

Introduction:

1.L-Dopa and the L-amino acid decarboxylase (AADC) inhibitor carbidopa are the most popular dopaminergic medications for Parkinson's disease (PD) patients.

2.After long-term introduction of dopaminergic medications, PD patients can experience visual hallucinations (VH) commonly during the evening and night.

3.Introduction of additional L-Dopa induces deficit in visual function and circadian rhythm. In PD patients, long-term treatment using dopaminergic medication results in visual disturbances, including diplopia, reduced visual acuity and color discrimination, and sleep disturbances, including sleep fragmentations, nightmare and reduction of rapid-eye movement stage (REM) sleep. Both visual and sleep disturbances together with other morphological and physiological changes were proposed to be the multifaceted reason for the induction of the visual hallucinations (VH) during the night.

4.When exposing zebrafish in an environment with repeated 5 minutes light/5 minutes dark exchange cycles, they display seconds of startle response behavior immediately after light extinction or light-on. After the startle response, zebrafish maintained in general higher activity for around 5 to 10 minutes during the dark exposure, during light exposure their activity slowly decreased. This higher activity in the dark has been termed the visual motor response (VMR).

Methods:

Individual zebrafish larvae were put in 48-well plates from 5 to 9 dpf and placed in a recording chamber, in which camera and light source were housed inside. The swimming traces and activity were recorded and analyzed by using the ViewPoint recording system (ViewPoint, France). From 0 day post-fertilization (dpf) to 5 dpf, light was turned on between 8AM and 10PM and switched off between 10PM and 8AM. The 14 hours light - 10 hours dark cycle is defined as normal circadian condition. From 6dpf to 9dpf, zebrafish were raised in an environment with repeated 5 minutes light/5 minutes dark exchange cycles. The asterisk indicates the beginning of the recording.

Results:

1. L-Dopa and carbidopa treated zebrafish exhibit reversed visual motor response (VMR) during the night time.
2. Reversed visual motor response is light intensity-dependent in L-dopa and carbidopa treated fish.
3. L-Dopa and carbidopa pre-treated larvae displayed stronger reversed visual motor response than larvae in treatment

Conclusion:

We discovered a very peculiar behavior of zebrafish larvae that were treated with both L-Dopa and carbidopa: they displayed higher activity in the light than in the dark during a certain time period at night. Similar to VH in PD patients, we only observed such behavior during the night in drug-treated fish. Moreover, this reversed VMR was light intensity-dependent. The pre-treated larvae displayed stronger reversed VMR than larvae in treatment suggesting that VMR reversal was induced by chronic effect of drug treatments.

M. Nesteruk¹, O. Riesterer¹, K. Ikenberg², S. Stieb¹, H. Moch², G. Studer¹, M. Guckenberger¹, S. Tanadini-Lang¹

Pre-treatment CT radiomics predicts HPV status and local tumor control after definitive radiochemotherapy in head and neck cancer

Department of Radiation Oncology, University Hospital Zurich, Zurich¹, Department of Pathology and Molecular Pathology, University Hospital Zurich, Zurich²

Introduction:

This study aimed to predict local tumor control (LC) after radiochemotherapy of head and neck squamous cell carcinoma (HNSCC) and HPV status using CT radiomics.

Methods:

HNSCC patients treated with definitive radiochemotherapy were included in the retrospective study approved by local ethical commission (93 and 56 patients in the training and validation cohorts, respectively). 317 CT radiomic features, including shape-, intensity-, texture- and transform-based features, were calculated in the primary tumor region. A Cox and logistic regression models were built to predict LC and HPV status, respectively. The best performing features in the univariate analysis were included in the multivariate analysis, after exclusion of redundant features. The quality of the models was assessed using the concordance index (CI) for modelling of LC and receiver operating characteristics area under the curve (AUC) for HPV status prediction. The radiomics LC model was compared to model incorporating clinical parameters (tumor stage, volume and HPV status) and a mixed model.

Results:

A radiomic signature, comprising three features, was significantly associated with LC ($CI_{\text{training}}=0.75$ and $CI_{\text{validation}}=0.78$), showing that tumors with a more heterogeneous CT density distribution are at risk for decreased LC. Addition of clinical parameters to the radiomics model slightly improved the model in the training but not in validation cohort. Another radiomic signature showed a good performance in HPV status prediction ($AUC_{\text{training}}=0.85$ and $AUC_{\text{validation}}=0.78$) and indicated that HPV positive tumors have more homogenous CT density distribution.

Conclusion:

HNSCC tumor density heterogeneity is associated with LC after radiochemotherapy and HPV status.

Uncovering the link between gaze evoked and rebound nystagmus*Neurology, University Hospital Zurich, Zurich¹***Introduction:**

Cerebellar disease is most commonly associated with two types of nystagmus called gaze evoked nystagmus (GEN) and rebound nystagmus (RN). GEN is defined by a sustained increase of the normally weak centripetal eye drift, when the eyes are moved away from the primary position (straight ahead). RN on the other hand describes a transient ocular drift in direction of the preceding sustained gaze after return to the primary position. GEN is considered an essential clinical sign of a deficient brainstem neural velocity-to-position integrator or its modulatory structures, and is thought to be caused by an insufficiency thereof. The thereby caused impairment of extra-ocular muscle contraction subsequently leads to GEN in eccentric position. RN on the other hand, is thought to be due to an overactive response mechanism which is elicited in order to decrease GEN. As GEN has been extensively described in the past, this study aims to provide the first close description of RN. Also, we study any possible relationship between GEN and RN, providing essential insight needed to further decipher the functions of the brainstem neural integrator.

Methods:

We recorded horizontal eye positions of 10 patients with cerebellar neurodegeneration and clinically confirmed GEN. With their head fixed, patients were asked to fixate a laser generated dot at different eccentricities between $\pm 30^\circ$. At these eccentricities, GEN was measured before, and RN after a 20 s eccentric fixation of either plus or minus 30° . Both drift velocity of GEN and RN, as well as drop of velocity during eccentric fixation were measured and statistically compared. Furthermore, linearity and symmetry were assessed.

Results:

RN, at zero degrees, and after 20 seconds of eccentric fixation at 30° , was found to be $2.365 \pm 1.276^\circ/\text{s}$. RN velocities were symmetric across all eccentricities as well as on the left and right side. During eccentric fixation GEN drift velocity dropped by $1.791 \pm 1.535^\circ/\text{s}$, while RN drift velocity increased by $2.088 \pm 1.109^\circ/\text{s}$. We found a high correlation between these changes of RN and GEN drift velocity during eccentric fixation ($p=0.0012$, slope= 0.810). Also, similar as described before in GEN, we found two specific types of patterns within RN.

Conclusion:

The results of this study not only provide the first close description of rebound nystagmus in patients with cerebellar neurodegeneration. They also highlight the high correlation between GEN and RN. This is not only reflected in the highly correlated changes of GEN and RN velocity, but also in the distinct pattern found within both.

An in-depth study of the influence of gabapentin and memantine on the infantile nystagmus syndrome in zebrafish: implications for therapy of ocular motor diseases*Neurology, University Hospital Zurich, Zurich¹***Introduction:**

Infantile nystagmus syndrome (INS) is a disorder characterized by typical horizontal eye oscillations. Due to the uncertain etiology of INS, developing specific treatments remains difficult. Single reports demonstrated alleviating effects of gabapentin and memantine, however on limited measures. In the current study, we employed the zebrafish INS model *belladonna (bel)* to conduct an in-depth study of how gabapentin and memantine interventions alleviate INS symptoms which may further restore visual conditions in affected subjects. Moreover, we described influence of both medications on ocular motor function in healthy, evaluating possible iatrogenic effects.

Methods:

Ocular motor functions and INS symptoms were assessed by the optokinetic response, nystagmus and spontaneous saccades in light, and spontaneous saccades in dark in 5-6 days past fertilization *bel* larvae and heterozygous siblings as controls. Single larvae were recorded before and after a one-hour drug treatment (200mM gabapentin / 0.2mM memantine).

Results:

Both interventions significantly reduced nystagmus intensity (gabapentin: 59.98%, memantine: 39.59%). However, while the application of gabapentin led to impairment of all tested ocular motor functions, memantine solely reduced nystagmus amplitude and intensity, and thus left controls completely unaffected. Finally, both drug treatments resulted in specific changes of characteristic of nystagmus waveform.

Conclusion:

Our study not only provides deeper insight into gabapentin and memantine treatment effect, it also opens the door for identifying action mechanisms of therapeutic effect in zebrafish models, which will serve as the basis for future large-scale clinical studies in humans.

D. Heinzer¹, M. Avar¹, M. Pfammatter¹, V. Eckhardt¹, B. Li¹, B. Kuhn², S. Mauerhofer², U. Rosenberg², S. Hornemann¹, A. Aguzzi¹

Establishing Methods to Detect Surface-Bound Scrapie Prion Protein on Surgical Steel

Institute of Neuropathology¹, Borer Chemie AG²

Introduction:

The incredible resistance of prions, the infectious agents of prion diseases such as the Creutzfeldt-Jakob disease, to common decontamination procedures bears the risk of iatrogenic transmission of these debilitating diseases by the use of inefficiently prion-decontaminated medical instruments. To date, the development of effective mild decontaminating products applicable to common sterilization procedures was difficult, because the efficiency of new products could only be tested in low-throughput and long-lasting prion infectivity bioassays. To overcome these limitations, a novel in-house developed cell-based assay, termed the digital Prion Infectivity Cell Assay (dPICA), and the real time quaking induced conversion (RT-QuIC) assay were adapted for the detection of prions on metal beads used to mimic surgical steel carriers. The assays were then used to evaluate the decontamination efficiency of prion contaminated metal beads by commercial and novel anti-prion decontamination formula.

Methods:

316L steel type metal beads were treated with prion-infected mouse brain homogenates. For the cell assay, prion-contaminated beads were co-cultured with neuronal hyCAD5 cells for 10 days to allow the transfer of infectivity from the beads to the cells. Cells were lysed and the lysate was digested by proteinase K to detect the disease-specific protein PrP^{Sc} (scrapie prion protein) by a homogenous-phase Förster resonance energy transfer (HP-FRET) assay. For the detection of active prions in the RT-QuIC assay, prion-contaminated beads were administered to the RT-QuIC reaction mixture containing the fluorescent dye Thioflavin T used to monitor the amplification of active prions on the steel beads.

Results:

We found that hyCAD5 cells could be successfully infected by prion contaminated steel beads and the presence of PrP^{Sc} could be detected by HP-FRET in a 24- and 48-well microtiter plate format. Treatment of the prion-contaminated beads with the known anti-prion inactivating procedure (1 M NaOH for 2 h at room temperature) resulted in a reduction of prion infectivity below the detection limit of the assay and demonstrated the suitability of the assay for prion decontamination studies.

We also demonstrated that the RT-QuIC assay is suitable to detect active prions on metal beads and that treatment with 1 M NaOH for 2h completely abolished a positive signal in the assay. As the RT-QuIC turned out to be more rapid and less laborious than the cell-based assay, we used this assay for the primary screen of different anti-prion decontamination agents. 30 different formulations were tested for their efficiency to inactivate or even remove prions from the steel beads. We found that nine out of 30 formulations strongly reduce a positive signal in the RT-QuIC assay. These candidates will be next validated in the dPICA to confirm their decontamination properties.

Conclusion:

We were able to show that both assays can be applied as sensitive and fast methods for the detection of prions on metal surface and thus for the screening of prion decontamination agents. So far, we could identify several products that reduce prions on metal surfaces. Interestingly, some commercial products turned out to not be able to completely remove prion infectivity under the experimental conditions. Based on these data, further formula and conditions will be developed and tested to eventually identify an efficient anti-prion decontamination formula that can be used to eliminate the risk of iatrogenic transmission of prion diseases.

J. Madon¹, AG. Franchini¹, DM. Heuberger¹, W. Ruf², L. Asmis³, RA. Schuepbach¹

Prolonged incubation of endothelial tissue factor with recombinant clotting factor VIIa reduces tissue factor complex activity

Division of Surgical Intensive Care, University Hospital Zurich, Zurich, Switzerland¹, Experimental Hemostasiology, Centre of Thrombosis and Hemostasis, University Johannes Gutenberg Mainz, Mainz, Germany², Unilabs, Coagulation Laboratory and Centre for Perioperative Thrombosis and Hemostasis, Zurich, Switzerland³

Introduction:

Tissue factor (TF) is a transmembrane glycoprotein and a receptor for clotting factor VII (FVII) and enzymatically active FVIIa. The TF/FVIIa complex physiologically initiates blood clotting and pharmacologic concentrations of FVIIa allow boosting of TF/FVIIa complex activity to bypass otherwise required enhancing steps involving FIX and co-factor VIII. We wondered whether prolonged exposure of TF to rFVIIa would affect availability or function of TF/FVIIa complex.

Methods:

Endothelial cells (HUVECs) were incubated in the presence of tumor necrosis factor- α (TNF) to induce the expression of TF and to enhance the secretion of microparticles containing TF. Cells or microparticles presenting TF were incubated with rFVIIa and the TF/FVIIa complex activity in the generation of FXa was colorimetrically measured. In addition ELISA was performed to detect the cell surface TF. The alkaline phosphatase sequence was linked to the N-terminus of TF and this recombinant chimeric protein was incubated with rFVIIa to test for potential degradation of TF.

Results:

Incubation of tumor necrosis factor- α induced endothelial cells (HUVECs) with recombinant (r)-FVIIa reduced cell surface TF/FVIIa complex activity and apical TF antigen as quantified by cell surface ELISA. Similarly, incubation of rFVIIa with microparticles or synthetic phospholipids containing rTF abolished TF/FVIIa complex activity and TF antigen. In cellular systems, TFPI could not explain our observation. To test for potential degradation of cell surface TF we overexpressed N-terminally tagged TF. Incubation with rFVIIa resulted in removal of N-terminal tags from the cell surface and decreased cell surface tagged TF/FVIIa complex activity.

Conclusion:

We identified a potential novel direct interaction between rFVIIa and its cellular receptor TF. Prolonged incubation of endothelial TF with recombinant clotting factor VIIa resulted in the removal of TF's N-terminal domain. The observed reduced tissue factor complex activity resulted in loss of cell surface TF antigen and function.

MB. Kirschner¹, B. Vrugt², M. Friess¹, M. Meerang¹, P.J. Wild², N. Van Zandwijk³, G. Reid³, W. Weder¹, I. Opitz¹

Refinement of the prognostic miR-Score for use in diagnostic specimens from chemo-naïve malignant pleural mesothelioma patients

Division of Thoracic Surgery, University Hospital Zurich, Zurich, Switzerland¹, Institute of Surgical Pathology, University Hospital Zurich, Zurich, Switzerland², Asbestos Diseases Research Institute, Sydney, Australia³

Introduction:

A 6-microRNA signature (miR-Score, Kirschner et al 2015) was previously demonstrated to show high prognostic accuracy in a series of surgical specimens (with and without induction chemotherapy). In the present study we investigated these microRNAs in an independent cohort of MPM patients all treated with induction chemotherapy followed by extrapleural pneumonectomy (EPP). The main focus of the study was to evaluate the possible effects of induction chemotherapy on microRNA expression and to refine and validate the miR-Score for use in chemo-naïve diagnostic specimens.

Methods:

We identified a cohort of 120 MPM patients who received chemotherapy followed by EPP between 1999 and 2014 at University Hospital Zurich. At present microRNA analysis (RT-qPCR) has been carried out in 34 pairs of chemo-naïve (diagnostic biopsy) and chemo-treated (EPP) specimens. Paired-samples t-test was employed to determine differences in microRNA expression pre- and post-chemotherapy. Accuracy of the miR-Score in predicting a good prognosis (>20 months survival post-surgery) was evaluated by ROC curve analysis. In addition, binary logistic regression modelling was used to build a refined miR-Score.

Results:

Applying the miR-Score to chemo-naïve diagnostic specimens revealed an area under the ROC curve (AUC) of 0.65 (95% CI: 0.46-0.84), and the same analysis on the EPP specimens gave an AUC of 0.57 (95% CI: 0.37-0.77). Therefore, the accuracy of the miR-Score was lower than observed in the previous study. However, pairwise comparison of microRNA expression before and after chemotherapy showed that although not reaching statistical significance, the levels of several microRNAs were lower following induction chemotherapy. We next employed binary logistic regression modelling on microRNA levels in chemo-naïve tissue to determine whether a refined microRNA signature less susceptible to chemotherapy-induced changes could be created. A refined miR-Score consisting of miR-221 and miR-30e, the two microRNAs least affected by chemotherapy, achieved AUCs of 0.77 (95% CI: 0.61-0.94) and 0.80 (95% CI: 0.64-0.96) in diagnostic and EPP specimens, respectively. When applied to samples from the previous study, the refined score resulted in an AUC of 0.72 (95% CI: 0.54-0.90).

Conclusion:

This validation and refinement study has shown that the expression of several miR-Score microRNAs appears to be affected by standard chemotherapy. A refined miR-Score was generated which is less susceptible to the effect of chemotherapy and may have prognostic value when applied to diagnostic specimens. Further validation in additional paired samples and investigation of the effect of cisplatin, pemetrexed and gemcitabine on microRNA expression are ongoing.

J. Kresoja¹, S. Sulemani¹, M. Kirchner², M. Ronner¹, G. Reid³, S. Kao³, BW. Schwaller⁴, RA. Stahel⁵, W. Weder², E. Felley-Bosco¹

Post-Transcriptional regulation of mesothelioma marker calretinin

Laboratory of Molecular Oncology, Thoracic Surgery, University Hospital Zürich¹, Division of Thoracic Surgery, University Hospital Zurich², Asbestos Diseases Research Institute, Sydney, Australia³, University of Fribourg, Department of Medicine, Anatomy, Fribourg, Switzerland⁴, Clinic of Oncology, University Hospital Zurich, Switzerland⁵

Introduction:

Calretinin (*CALB2*, CR) is a diagnostic and prognostic marker in malignant pleural mesothelioma (MPM). We previously reported that calretinin is regulated at mRNA level. The presence of a medium size 3' untranslated region (3'UTR-573nt) and additional two non-coding alternative transcripts arising from *CALB2* gene suggest a possible post-transcriptional mechanism of calretinin expression regulation. The *CALB2* 3'UTR contains microRNA target sites and an A/U-rich element (ARE) putative *cis*-regulatory elements. Our aim was to investigate the role of the *CALB2* 3'-UTR in the post-transcriptional regulation of calretinin expression in MPM.

Methods:

Using the pmirGLO dual-Luciferase expression vector, the complete *CALB2* 3'-UTR fragment was inserted downstream of the firefly luciferase reporter gene. Activity of the *CALB2* 3'-UTR was quantified after transient transfection into mesothelioma cells. *In silico* analysis TargetScan and AREsite2 were employed to predict potential microRNAs binding site or ARE element, respectively. Site-directed mutagenesis was employed to mutate consensus sequence of the previously predicted functional *cis*-elements. Subsequently, luciferase activity and calretinin expression were evaluated after overexpression or inhibition of the predicted microRNAs. In addition, calretinin protein, assessed by immunohistochemistry, and miR-30 expression, were investigated in a cohort of MPM patients (N=60).

Results:

The addition of the *CALB2* 3'-UTR significantly downregulated the luciferase activity in MPM cells. Bioinformatic analysis predicted miR-30 family members, miR-9 binding sites and ARE element within *CALB2* 3'-UTR. Mutational analysis of ARE site resulted in further destabilization of the reporter and biochemistry assay detected cytosolic protein binding to ARE sequence. The mutation of two miR-30-binding sites abolished calretinin 3'UTR destabilization effect. Transient delivery of a miR-30e-5p mimics or anti-miR into MPM cells resulted in significant decrease/increase of the luciferase reporter expression and protein. However, overexpression of *CALB2*-3'UTR quenched the effect miR-30e-5p on the protein, most likely by sequestering the mimics, suggesting a possible ceRNA (competitive endogenous RNA) network. Finally, expression of miR-30e was found to negatively correlate with the calretinin expression in a cohort of MPM patient samples.

Conclusion:

Our data show for the first time the role of miR-30e in the post-transcriptional negative regulation of calretinin expression via interaction with its 3'-UTR. We also demonstrated a stabilization role for ARE sequences in calretinin 3'UTR and possible physiological role of calretinin alternative transcripts.

A. Gomariz¹, S. Isringhausen¹, P. Helbling¹, U. Suessbier¹, G. Paul², G. Szekely², O. Goksel², S. Stoma³, S. Nørrelykke³, C. Nombela-Arrieta¹

Applying 3D quantitative microscopy to study global topography and cellular interactions in the bone marrow

Experimental Hematology Division, University Hospital Zürich, Zürich¹, Computer Vision Laboratory, ETH, Zurich², ScopeM, ETH Zürich, Zürich³

Introduction:

During adulthood, the bone marrow (BM) is the primary site of generation of huge amounts of mature blood cellular components from a population of rare hematopoietic stem cells (HSCs). Within the BM a non-hematopoietic heterogeneous compartment, formed by endothelial, mesenchymal and neural cells and collectively known as stroma, is known to provide critical regulation and support for hematopoiesis. Historically, inherent difficulties associated to the imaging of bone enclosed tissues have largely limited the quantitative analysis of BM populations to flow cytometry studies, in which spatial information is not available. Recently developed protocols and advanced microscopy techniques currently enable the generation of extensive 3D datasets, which can be used to examine how different hematopoietic and stromal components are structurally organized into functional tissues. However, up until now, conclusions have been drawn based solely on visual inspection of these images. As of today, a major challenge resides in the development of computational tools which extract quantitative information from these images and provide information about the spatial context in an automatic and unbiased fashion.

Methods:

We here address these shortcomings by implementing image analysis and spatial statistics tools to study the global topography and spatial relationships at an organ-wide scale in the context of the BM. For this purpose, we produce and use a representation of 3D BM samples by automatically detecting isolated objects (cells) and spatially extended and connected structures (sinusoidal blood vessels). This representation is used to study the cells as point distributions, which allows the use of classical spatial statistics methods. We adapted these methods to 3D and also included special boundary conditions imposed by our biomedical datasets. This framework was used to create realistic simulations and compare the observed spatial patterns to biologically relevant phenotypes.

Results:

We have employed these newly developed tools to describe for the first time the spatial distribution and perivascular nature of the mesenchymal cells of BM stroma. Surprisingly, flow cytometry, hitherto considered the standard method for analysis of BM samples, fails to detect the vast majority of stromal cells when compared to the present image-based approach. Our data demonstrates that the sinusoidal network occupies in average 26% of the BM volume and subsequently constrains the space available for other cells to distribute. Rigorous spatial statistic analysis reveals that 95% of the BM space has a sinusoidal vessel closer than 22 μm . This network. These observations were used to model and simulate the distribution of mesenchymal cells, and the data suggested that they are spatially arranged following an avoidance pattern.

Conclusion:

The set of tools developed in this project provides a framework to characterize the topology and cellular interactions in real 3D biological images and can be applied to generic problems in biology. In the context of the BM, these tools provided a new way to quantitatively describe the phenotype of the spatial distribution of cells and vessels, which are key for a robust characterization of the system and the evaluation of spatial changes arising under different treatments. Besides, the caveats in flow cytometry revealed by applying the developed tools suggested that the frequency of stromal cells has been so far underestimated, which may have led to incorrect inferences of their functional contribution to the microenvironment and interactions in niches. This can be an incentive to increase the use of quantitative 3D microscopy.

S. Steiner¹, G. Wanner-Seleznik¹, T. Reding¹, A. Dittmann¹, A. Perren², E. Eliane², M. Heikenwälder³, R. Graf¹

Gastrokine as a novel potential biomarker for premalignant pancreatic lesions

Swiss HPB Center, Visceral & Transplantation Surgery, University Hospital Zurich, Switzerland¹, Institute of Pathology, University of Bern, Switzerland², Institute for Virology, Helmholtz-Centre Munich, Germany³

Introduction:

Pancreatic ductal adenocarcinoma (PDAC) has one of the most dismal prognoses of all cancer types. Diagnostic techniques for early malignant and potentially curable lesions are limited, which shows an evident need for early detection methods. Gastrokine 1 & 2 (GKN1 & GKN2) are secreted proteins found almost exclusively in the gastric epithelium, where they are involved in gastric epithelial homeostasis and tumor suppression. So far nothing is known about gastrokine expression and function in other organs. A whole genome microarray analysis of a mouse with predisposition to pancreatic cancer showed a striking upregulation of the two gastrokines in the pancreas during carcinogenesis.

Methods:

GKN1 & GKN2 mRNA expression was confirmed by qPCR in patient and mouse pancreas samples. The presence of GKN1 was verified by western blot and IHC in mouse pancreas. Pancreatitis in Gkn2^{-/-} mice was induced by cerulein injection. Mouse pancreatic juice was analysed by proteomic analysis.

Results:

Gastrokine was highly upregulated during the early stages of pancreatic carcinogenesis in the mouse and in peri-tumoral human pancreas tissue. Gastrokine was not found in the healthy pancreas nor in tissue with pancreatitis. Immunohistochemistry shows a specific GKN expression in tissue areas with premalignant PanIN lesions while it is absent in PDAC. ELISA and proteomic analysis in mice confirmed the secretion of GKN1 into pancreatic juice but not serum.

Conclusion:

We identified for the first time specific gastrokine expression in premalignant lesions in pancreatic tissue. The secretion into the pancreatic juice during carcinogenesis could make gastrokine a potential biomarker for the detection of early pancreatic premalignant lesions.

L. Wu¹, W. Blum², L. Pecze², T. Henzi², V. Serre-Beinier³, H. Rerhauer⁴, C. Aquino⁴, B. Vrugt⁵, M. De Perrot¹, B. Schwaller², E. Felley-Bosco⁶

Role of macrophages and mesothelial precursors accumulation in tumor development in asbestos-exposed mice

Latner Thoracic Surgery Research Laboratories, Division of Thoracic Surgery, Toronto General Hospital, University Health Network, University of Toronto, Toronto, ON Canada¹, Unit of Anatomy, Department of Medicine, University of Fribourg, Route Albert-Gockel 1, CH-1700 Fribourg, Switzerland², Department of Thoracic Surgery, University Hospitals of Geneva, Geneva, Switzerland³, Functional Genomic Center Zurich, 8057 Zurich, Switzerland⁴, Institute of Surgical Pathology, University Hospital Zurich⁵, Laboratory of Molecular Oncology, Lungen- und Thoraxonkologie Zentrum, University Hospital Zürich, Sternwartstrasse 14, 8091 Zurich, Switzerland⁶

Introduction:

Mesothelioma development is associated with asbestos exposure but early steps of carcinogenesis are unknown.

Methods:

To assess the role of loss of homeostasis in the mesothelial environment after asbestos exposures during tumor development, Nf2^{+/-} mice were injected intraperitoneally with crocidolite fibers every 3 weeks for 8 rounds and monitored for tumorigenicity at two different time points. Signaling molecules and population profiles were investigated in peritoneal lavage. Tissue was collected for RNA extraction and transcriptome profile. A syngeneic cell line generated from one of the tumor developed was used to perform functional experiments.

Results:

11% of mice developed mesothelioma within 33 weeks after first exposure. M2 macrophages and mesothelial precursors accumulated into the peritoneal cavity accompanied by a peak of IL-10, G-CSF, CCL2, IL-6, and VEGF, but tended to decrease 42 weeks after the first exposure, while CCL5, IFN γ , GM-CSF and CXCL1 increased levels remained stable. Transcriptomic profile of scraped mesothelium and tumor revealed that 1260 genes were commonly upregulated in tumor and inflamed tissue. One of the highest upregulated genes was *Arg1*. The presence of Arg1 positive cells and other markers associated with M2 macrophages was confirmed. Intraperitoneal injection of syngeneic mesothelioma cells reproduced this phenotype. Macrophage and mesothelial precursor accumulation and tumor growth were impaired by administration of clodronate liposome.

Conclusion:

Altogether, crocidolite-induced loss of homeostasis in mesothelial environment skewed toward accumulation of M2 macrophages and mesothelial precursors is an essential step in mesothelioma development.

R.S. Bruckner¹, N. Marsiano², E. Nissim-Eliraz², E. Nir², S. Lang¹, M.R. Spalinger¹, G. Rogler¹, S. Yagel³, M. Scharl¹, N.Y. Shpigel²

New human gut xenograft mouse model for intestinal fistulas

Division of Gastroenterology and Hepatology, University of Zurich c/o University Hospital Zurich, Zurich¹, Koret School of Veterinary Medicine, Hebrew University of Jerusalem, Rehovot², Department of Obstetrics & Gynecology, Hadassah University Hospital, Jerusalem³

Introduction:

Fistulas represent a frequent complication in Crohn's disease (CD) and surgical resection is often required. Despite some progress in the understanding and treatment of inflammatory bowel disease (IBD), more effective medical treatments are still required, especially for CD patients with fistula formation. Previously we demonstrated that epithelial-to-mesenchymal transition (EMT) plays a critical role for fistula development in CD patients. Preceding upregulation of TGF- β , IL-13, TNF & their receptors along fistula tracts in CD patients seems to orchestrate a number of events contributing to the onset of fistulas, by inducing EMT. Due to a lack of a reliable *in vivo* model, new drug developments are complicated. Here, we are describing a new xenograft (XGR) mouse model of intestinal fistula, resembling the human condition.

Methods:

12-18 weeks (w) old human fetal small intestine was transplanted subcutaneously onto the backs of SCID mice. After 12–16 w, ~15% of the mature xenografts spontaneously developed enterocutaneous fistulas. Using systemic LPS treatment followed by mild skin irritation adjacent to the transplant, we established a reproducible model system, resulting in enterocutaneous fistulas 2-4 w later. Tissue specimens were immunohistochemically stained (IHC) for EMT and immune cell markers.

Results:

Morphological analysis of the fistulating XGR samples revealed flattening of the intestinal epithelial cells lining the fistula tract, resembling transitional cells described in human patient samples. IHC stainings for various EMT markers (e.g. SLUG, β -6 Integrin) revealed similar expression patterns like for human fistulating CD patient samples. The expression of the mesenchymal marker alpha-smooth muscle actin confirmed the hypothesis that EMT plays a critical role for the fistula development in the XGR samples, as well.

H&E staining also showed inflammation in the gut XGR up- & downstream to the fistulous tracts. Most of this inflammatory response consisted of human CD45+ round cells and very few murine CD45+ cells, mostly polymorphonuclear. Collagen staining revealed these inflammatory regions were also associated with massive fibrosis, suggesting extracellular matrix remodeling.

Besides we observed many potential necroptotic paneth cells in the XGR samples and a loss of this cells in the crypts adjacent to the fistula. RNA sequencing showed significant upregulation of genes related to IBD, necroptosis, ripoptosome, and NF- κ B signaling in inflamed LPS-treated XGRs.

Conclusion:

Our data demonstrate that the *in vivo* model recapitulates both morphologically and mechanistically, the human disease. Necroptosis might be the underlying molecular mechanism driving inflammation, EMT and finally resulting in fistula formation.

M. Meerang¹, J. Kreienbühl¹, M. Friess¹, M. Kirchner¹, W. Weder¹, I. Opitz¹

Targeting cullin ubiquitin ligase leads to growths arrest in malignant pleural mesothelioma cells

Division of Thoracic Surgery, University Hospital Zurich¹

Introduction:

Mutation of the tumor suppressor gene *Neurofibromatosis type II (NF2)* was detected in 30-40% of malignant pleural mesothelioma (MPM) patients. NF2 suppresses tumorigenesis in part by inhibiting Cullin4 ubiquitin ligase. Cullin4A (CUL4A) gene amplification and its' overexpression has been detected in MPM cell lines and tumors. We hypothesized that cullin4 is a potential treatment target for MPM. Cullins' activity can be blocked by the inhibition of neddylation, a post-translational modification for cullins. In this study we assessed the efficacy of pevonedistat, an inhibitor of protein neddylation, in MPM cells.

Methods:

Thirteen MPM cell lines and 3 MPM primary cells grown in monolayer (2D) were employed to assess the efficacy of pevonedistat *in vitro* compared to normal mesothelial cells, using MTT assay. The expression of cullins was assessed by quantitative real time PCR and western blot. Cell cycle was analyzed by flow cytometry. Four cell lines were cultured in multicellular spheroid (3D) format and measured for viability by acid phosphatase assay.

Results:

Across 13 MPM cell lines, 5 cell lines (38%) were sensitive to the treatment with pevonedistat (IC₅₀<500nM). All sensitive cell lines overexpressed CUL4A in both mRNA and protein levels. The treatment induced G2 cell cycle arrest and accumulation of cells containing >4N DNA content, representing cells undergoing DNA re-replication. DNA re-replication is known to be mediated by the accumulation of a DNA replication licensing factor, CDT1. Indeed, higher CDT1 accumulation was detected in the sensitive compared to the resistant cell lines. All primary cells showed no CUL4A overexpression compared to normal mesothelial cells, nonetheless 2 of them were sensitive to pevonedistat. Interestingly, these cells exhibited higher levels of neddylated (activated) CUL4A and higher CDT1 accumulation following the treatment. Cell lines overexpressing CUL4A remained sensitive to pevonedistat when cultured in 3D spheroids.

Conclusion:

Inhibition of cullins by pevonedistat induced growth arrest preferentially in MPM cells overexpressing CUL4A in 2D and 3D cultures. The major mechanism seems to be mediated by DNA re-replication induced by CDT1 accumulation. More investigation into the role of cullin ubiquitin ligase in MPM is ongoing.

EP. Pachera¹, AS. Assassi², GS. Salazar², MFB. Frank-Bertoncelj¹, RD. Dobrota¹, FK. Kurreeman³, JVB. De Vries-Bouwstra³, TM. Messemaker³, CFB. Feghali-Bostwick⁴, JD. Distler⁵, GK. Kania¹, OD. Distler¹

Long Noncoding RNA H19X is a Master Regulator of Extracellular Matrix Production in Systemic Sclerosis and Other Fibrotic Diseases

Department of Rheumatology, University Hospital Zurich, Zurich¹, Department of Internal Medicine, University of Texas, Houston², Department of Rheumatology, Leiden University Medical Center, Leiden³, Division of Rheumatology, Medical University of South Carolina, Charleston⁴, Department of Internal Medicine 3, University of Erlangen, Erlangen⁵

Introduction:

Long noncoding RNAs (lncRNAs) are an emerging class of large noncoding transcripts involved in the regulation of gene expression in health and disease. We have recently identified a novel lncRNA, H19X, which is strictly regulated by TGF β in a dose and time dependent manner. Here we aim to characterize the expression of H19X in Systemic Sclerosis (SSc) and other fibrotic diseases as well as its function.

Methods:

Skin and lung biopsies from patients with SSc, idiopathic pulmonary fibrosis (IPF), and healthy controls (HC) were obtained from cohorts at four different expert centers. Expression of H19X was analyzed by RNA Sequencing Illumina HiSeq2000 and quantitative (q)PCR respectively. The function of H19X was investigated in skin fibroblasts transfected with locked nucleic acid oligonucleotides (LNA GapmeRs) by using the following methods: microarray analysis, qPCR, immunofluorescence, sircol and contraction assay, ELISA, and Western blot (WB). In situ hybridization of H19X in SSc dermal fibroblast was performed using Stellaris FISH probes.

Results:

H19X expression was consistently upregulated across all the four cohorts (SSc n=34, HC= 26), using different techniques. The upregulation was also consistent across different subsets of patients and between patients with different disease durations. H19X showed a similar expression profile in clinically non-fibrotic and clinically fibrotic skin biopsies indicating a role in early disease development. Moreover, H19X expression was also significantly increased in SSc interstitial lung disease patients versus HC (n=11 each, p<0.05). A significant H19X overexpression was also detected in IPF samples suggesting a broader role of H19X in fibrotic diseases (n=11 each, p<0.05). Microarray analysis after H19X silencing revealed a strong involvement in extracellular matrix production with collagens being the most downregulated genes. Accordingly, collagen catabolic process, extracellular matrix organization and extracellular matrix disassembly were among the pathways with highest number of enriched genes. Downregulation of collagen I α 1, fibronectin and α -smooth muscle actin (α SMA) after H19X knockdown was confirmed by qPCR (n=5, p<0.05). Sircol assay for pan-collagen production, ELISA for pro-collagen I α 1 and WB analysis for fibronectin confirmed the importance of H19X in the regulation of extracellular matrix components. Additionally, silencing of H19X significantly impaired α SMA fiber formation, stress fiber formation as well as cell contractility strongly suggesting an important role of H19X in the development of the myofibroblast phenotype (n=5-6, p<0.05). Cell fractionation showed that TGF β induced expression of H19X is localized mainly into the nucleus. In situ hybridization confirmed H19X localization as mainly nuclear and within a defined spot indicating that H19X could influence gene expression by interacting directly with the chromatin (n=4).

Conclusion:

This is the first study reporting a significant upregulation of H19X expression in SSc and across fibrotic organs. By focusing on this novel class of regulatory, noncoding RNAs new perspectives in the pathogenesis of fibrotic diseases are opened.

L. Hering¹, JB. Riggs¹, S. Lang¹, K. Atrott¹, B. Becher², G. Rogler¹, M. Scharl¹, MR. Spalinger¹

Loss of PTPN2 in dendritic cells affects expression of pro-inflammatory cytokines but has no major role in the intestine

Division of Gastroenterology and Hepatology, University Hospital Zurich¹, Institute of Experimental Immunology, University of Zurich, Zurich²

Introduction:

Variants within the gene locus encoding protein tyrosine phosphatase non-receptor type 2 (PTPN2) are associated with the development of inflammatory bowel disease (IBD) and other inflammatory disorders, including rheumatoid arthritis and psoriasis. The role of PTPN2 in T cells and intestinal epithelial cells has been investigated previously but its role in dendritic cells (DCs) remains unclear. Since DCs play an important role in T cell activation and immune responses, the DC-specific role of PTPN2 is of great interest. This study addresses how loss of PTPN2 in DCs affects the expression of pro-inflammatory cytokines and signal transduction as well as the effect on different organs and colitis severity.

Methods:

Mice with a LoxP flanked PTPN2 gene were crossed with mice expressing Cre-recombinase under control of the integrin alpha X (Cd11c) promoter in order to specifically delete PTPN2 in DCs (PTPN2-CD11cCre mice). Acute colitis was induced in 10-12 week old females by administration of 2.5% DSS for 7 days. Bone marrow-derived dendritic cells (BMDCs) were differentiated from bone marrow cells of 9 week old mice in presence of GM-CSF. For activation, BMDCs were stimulated with 2 µg/mL IFN-γ and 10 ng/mL LPS.

Results:

Even without any treatment, PTPN2-CD11cCre mice show symptoms of splenomegaly and dermatitis. In addition, inflammatory infiltrations in the liver and the lung can be observed in some PTPN2-CD11cCre mice. These symptoms start to develop around 10 weeks of age but onset and severity of the inflammation varies between individuals, and results in sudden, spontaneous death in some mice. Further, PTPN2-CD11cCre mice show increased numbers of effector/memory T cells within CD4+ and CD8+ T cells in the spleen. However, severity of DSS-induced acute colitis was not affected upon loss of PTPN2 in DCs. *In vitro*, PTPN2-deficient BMDCs show increased phosphorylation of nuclear factor κB (NFκB) p65, enhanced expression levels of the co-stimulatory molecules CD80 and CD86, and enhanced mRNA levels of TNF and ICAM-1 upon treatment with LPS. Upon treatment with IFN-γ, phosphorylation of signal transducer and activator of transcription 1 (STAT1) and mRNA expression of TNF and ICAM-1 was enhanced in PTPN2-deficient BMDC.

Conclusion:

PTPN2 in dendritic cells has an important anti-inflammatory role in the skin, lung and liver but it seems to be dispensable in the setting of acute intestinal inflammation. Increased expression of co-stimulatory molecules *in vitro* and increased numbers of effector/memory T cells *in vivo* indicate a role in T cell activation. Therefore, we will further study the effect of a loss of PTPN2 in DCs in more chronic and T cell mediated colitis models.

SOX10 as a therapeutic target in Clear Cell Sarcoma*Onkologie, UniversitätsSpital Zürich¹, Pathologie, UniversitätsSpital Zürich²***Introduction:**

Clear Cell Sarcoma (CCS) is a very rare and aggressive subtype of soft tissue sarcoma, associated with a high tendency to relapse locally, metastasize distantly and with a poor overall survival. Most cases affect young adults between 20 and 40 years of age. CCS often arises next to tendons, aponeuroses and fascia on distal extremities. CCS is considered to be resistant to conventional chemotherapy. Neither targeted therapeutic options nor immunotherapeutic approaches have been successful, yet. The cells of origin of CCS are neural crest derived. The defining molecular feature of CCS is either the recurrent translocation t(12;22) (q13;q12) or, in rare cases, t(2;22) (q34;q12), resulting in expression of EWSR1-ATF1 or EWSR1-CREB1 fusion genes, respectively. These fusion proteins are the transforming oncogenic event in CCS.

SOX10 is a transcription factor, which is essential in neural crest development, the self-renewal of neural crest stem cells and for the formation of melanocytes arising from the neural crest. Previous research showed that SOX10 plays also a very important role in the maintenance of melanoma and it might represent a therapeutic target. SOX10 is required for the cAMP-mediated activation of the M-MITF gene promoter in CCS by cooperating with CREB1 and ATF1 and it is therefore conceivable that SOX10 is a therapeutic target in CCS.

Methods:

We first analyzed, whether SOX10 is expressed in CCS. We cultured primary cultures of melanoma as a positive control and a panel of CCS cell lines and assessed levels of SOX10 mRNA and protein. Both were readily detectable and expressed to similar levels as in melanoma. We next analyzed biopsies from patients by SOX10 immunohistochemistry (IHC). 5/5 samples showed a strong nuclear SOX10 staining. We are currently expanding this analysis in a collaboration with the EORTC and Prof. P. Schöffski, University Hospitals of Leuven, who have generated a tissue-microarray from samples from a clinical trial on CCS, which will be stained for SOX10. Staining will be quantified, grouped and correlated with clinical characteristics, as well as with other IHC markers. This will establish, whether SOX10 serves as a biomarker in CCS.

In preliminary functional experiments, we have knocked down SOX10 in the human CCS cell line KAS using lentiviruses expressing short hairpin RNAs targeting SOX10. Two different shRNAs reduced SOX10 protein expression compared to uninfected parental cells, or to cells expressing a non-silencing scrambled control shRNA. Both SOX10-shRNAs significantly reduced colony formation in long-term proliferation assays in vitro.

In order to evaluate the therapeutic potential of silencing SOX10, we are currently expanding our in vitro experiments. Experiments, in which we knock down SOX10 using short hairpin RNAs in our panel of CCS cell lines and assess effects on proliferation by performing colony formation assays and MTT assays, as well as induction of apoptosis by Annexin-V / propidium iodide co-staining, followed by FACS analysis, are ongoing. To assess the effects of SOX10 knock down in vivo, we are currently also establishing a CCS xenograft model in nude mice.

Results:**Conclusion:**

We have preliminary evidence that SOX10 might serve as a therapeutic target in CCS in vitro. In ongoing in vitro and in vivo experiments, we will now expand those analyses. This will firmly establish, whether SOX10 serves as a biomarker and is a preclinically promising therapeutic target in this aggressive orphan sarcoma.

F. Largey¹, Iv. Jelcic¹, A. Czaplinski², R. Capaul³, M. Sospedra¹, R. Martin¹, Il. Jelcic¹

Fingolimod-induced peripheral lymphopenia leads to expansion of cytomegalovirus-reactive T cells and concomitant attrition of varicella zoster virus-specific immunity

Clinical Research Priority Program Project – MS (CRPPMS), Neuroimmunology and Multiple Sclerosis Research Section, Department of Neurology, University Hospital of Zurich, Switzerland¹, Neurozentrum Bellevue, Zurich, Switzerland², Institute of Medical Virology, University of Zurich, Switzerland³

Introduction:

Persistent latent infections with multiple herpesviruses are widespread in the human population and require life-long competent immune control. Varicella zoster virus (VZV) may escape immune control in healthy elderly people and immunocompromised individuals, but also in patients with relapsing-remitting multiple sclerosis (RRMS) treated with the immunomodulatory functional sphingosine-1-phosphate antagonist fingolimod (FTY). FTY treatment induces peripheral lymphopenia by modulating sphingosine-1-phosphate-mediated lymphocyte egress from secondary lymphoid organs and increases for yet unknown reasons only the risk for symptomatic reactivation of VZV but not of other co-infecting herpes viruses such as cytomegalovirus (CMV).

Methods:

In order to better understand herpes viral immune control during FTY therapy, we systematically assessed quantitative, phenotypical, functional and gene expression changes in CD4+ and CD8+ T cell immunity against CMV, VZV, other (herpes) viruses and recall antigens in multiple sclerosis patients before and during immunomodulatory therapy with FTY. We controlled also antiviral humoral immunity and gene expression changes in target cells of herpesvirus infection, such as monocytes for CMV infection.

Results:

Surprisingly, we observed an exclusive increase of the peripheral frequency of CMV-specific CD4+ T cells in CMV-seropositive donors during FTY therapy. As a possible reason for the expansion of CMV-specific CD4+ T cells during FTY therapy we found interferon signaling and other pathways critical for maintenance of CMV latency in monocytes impaired in FTY-treated donors, which might promote CMV reactivation and fuel CMV-specific CD4+ T cell immunity. However, no CMV reactivation or viremia was found, indicating effective immune T cell immune control of CMV. This was supported by the expansion of late-differentiated CD4+ and CD8+ T cells including NKG2D+ and CD244+ CD4+ T cells with high cytolytic potential, representing known hallmarks of CMV-reactive immunity. The number of peripheral VZV-reactive effector memory (EM) and effector memory RA (TEMRA) T cells, which are important for VZV control, decreased in HCMV-seropositive donors more than in HCMV-seronegative donors. Importantly, the FTY-associated expansion of HCMV-specific CD4+ T cells in HCMV-seropositive MS patients correlated inversely with reduced VZV-specific CD4+ T cell frequencies. No significant changes in T cell immunity against herpes simplex viruses type 1 and 2, Epstein-Barr virus were observed.

Conclusion:

FTY therapy differentially affects anti-herpesviral T cellular immunity in CMV-infected individuals by enhancing CD4+ T cell control of CMV and conversely compromising VZV-reactive CD4+ T cell immunity. Future studies should test for an association of CMV-seropositivity and/or peripheral frequency of CMV-specific T cells with increased risk to develop symptomatic VZV reactivation and evaluate these parameters for risk stratification in FTY-treated RRMS patients. The presented methodology offers a rapid and simple testing of phenotypical and functional immune response to various antigens, which could easily be applied to larger screens to monitor immune response and to identify novel biomarkers.

F. Largey¹, Iv. Jelcic¹, M. Sospedra¹, R. Martin¹, Il. Jelcic¹

Patterns of Intrathecal Antiviral Antibody Production During Natalizumab-Associated Progressive Multifocal Leukoencephalopathy

Clinical Research Priority Program Project – MS (CRPPMS), Neuroimmunology and Multiple Sclerosis Research Section, Department of Neurology, University Hospital of Zurich, Switzerland¹

Introduction:

Progressive multifocal leukoencephalopathy (PML) is a severe infectious brain disease caused by JC virus (JCV) and may occur in multiple sclerosis (MS) patients under immunomodulatory treatment with the monoclonal antibody natalizumab (NAT). Washing out NAT by plasma exchange causes a vigorous antiviral immune response in the PML lesions, which, in the vast majority of cases, again leads to an acute neurological worsening, called PML-immune reconstitution inflammatory syndrome (PML-IRIS). This antiviral inflammatory response is until now the only way to resolve JCV infection from affected brain areas. Recent reports show, that 55% of NAT-treated patients with newly diagnosed PML (NAT-PML) have intrathecal JCV-specific antibody production, but none of NAT-treated MS patients without PML (0%), and that recognition holes in intrathecal antibody responses against PML-causing JCV strains before and during NAT-PML were closed during PML-IRIS. It remains unclear, whether these increased intrathecal antibody responses are confined to JCV or may include other common viral antigens.

Methods:

We collected paired serum and CSF samples from 16 Swiss NAT-PML cases at time of PML diagnosis (PML), onset of PML-IRIS and/or after resolution of PML-IRIS (after IRIS). Samples were tested with capture ELISAs using antigens from measles-, rubella-, mumps-, influenza-, entero-, herpes- and polyomaviruses (JC, BK, KI, and WU viruses) with BKV being the nearest JCV homologue (70% sequence identity). The respective virus-specific CSF/serum antibody index (CAI) was calculated for each antigen. $CAI \geq 1.5$ indicated intrathecal production of virus-specific antibodies.

Results:

The prevalence of cases with intrathecal JCV-specific antibody production increased significantly from PML (31%) to IRIS (78%) and after IRIS (100%), paralleled by a significantly increased prevalence of intrathecal BKV-specific antibody production (13% of PML, 67% of IRIS cases and 88% after IRIS). Moreover, the strength of intrathecal production of antibodies against JCV and BKV increased significantly between PML, IRIS and after IRIS. In contrast, the prevalence and the strength of intrathecal antibody production against all other viral antigens remained unchanged. At onset of IRIS and after IRIS, BKV-reactive antibodies mainly cross-recognized JCV in serum and CSF, but only a minor fraction of JCV-reactive antibodies cross-recognized BKV.

Conclusion:

Intrathecal antibody responses to both JCV and BKV are increasing specifically during NAT-associated PML-IRIS. Cross-recognition of BKV indicates broadening of the antigen spectrum recognized by JCV-reactive antibodies during inflammatory resolution of PML. These findings underscore the role of broadly recognizing JCV-reactive antibodies in resolution of PML.

Ms. Irmisch¹, Ms. Freiburger¹, Mr. Cheng¹, Mr. Pornputtpong², Ms. Singer³, Mr. Thurnheer⁴, Mr. Stekhoven³, Ms. Halaban⁵, Mr. Beerenwinkel⁴, Mr. Dummer¹, Mr. Levesque¹

Whole exome sequencing and a novel gene panel as precision medicine tools for metastatic melanoma patients

Dermatologische Klinik, UniversitätsSpital Zürich, Zürich¹, Department of Pathology, Yale University School of Medicine, CT, 06511 New Haven, USA², NEXUS Personalized Health Technologies, ETH Zürich, Zürich³, Department of Biosystems Science and Engineering, ETH Zurich Basel⁴, Department of Dermatology, Yale University School of Medicine, 06520 New Haven, USA⁵

Introduction:

Novel immune checkpoint inhibitors and targeted therapies have remarkably improved progression-free and overall survival in patients with metastatic melanoma. Nonetheless, not all patients respond to these therapies and most responding patients eventually progress without further treatment options.

Methods:

To offer some of these patients personalized therapies instead of best supportive care, we have established a molecular tumor board based on fresh tumor biopsies that are used for whole exome sequencing (WES) and a novel melanoma-specific gene panel (MelArray), which was developed at USZ and Yale University. The MelArray is tailored to the detection of frequent alterations in melanoma and covers about 190 genes with over 3000 exons, including genes associated with FDA approved drugs, and drugs in clinical trials. Furthermore, the panel includes heterozygous SNPs across the genome for the accurate estimation of CNVs. Using the gene panel, we aim to achieve up to 1000x coverage to be able to analyze even small subpopulations of cells within the tumor, while WES covers the complete exome with approx. 100x coverage. A clinical report of these genetic aberrations, corresponding suggestions of potentially effective drugs (including off-label and compassionate use), and matching clinical studies is then generate.

Results:

The first rounds of MelArray have shown that the method reliably detects mutations, CNVs, gene fusions and tumor content. Currently, five end-stage melanoma patients have been prospectively analyzed within the Molecular Tumor Board Zurich to facilitate the integration of next generation sequencing data into clinical practice.

Conclusion:

Potentially targetable genetic aberrations could be detected in each of the first five patients. Further development of the MelArray panel for diagnostic application is currently ongoing.

Choroidal Melanoma and Fractionated Radiosurgery (fSRS) with Photons

Radiation Oncology, Dessau City Hospital, Germany¹, Radiation Oncology, Zurich University Hospital, Zurich²

Introduction:

Proton therapy has been the standard treatment for ocular melanoma for the last decades. Improvement of planning systems and beam application technologies allow photon therapies to be used in clinical settings for curative radiotherapy of primary ocular tumors and clinical data are promising.

Methods:

Since December 2014, we have treated 40 patients with choroidal melanoma at the Dessau City Hospital with photons. fSRS was used to treat a target volume of 0,5 to 1,9 ml with 5 fractions of 10 Gy using as treatment planning system HybridArc™ (HA) of iPlan® 4.5.3 (Brainlab™, Feldkirchen, D) which allows to combine five to eight arcs with five to eight intensity modulated fields (IMRT) as used in the present series. Positioning was ascertained after episcleral implantation of tantalum clips a week prior to radiotherapy planning. Planning based on a 3T magnetic resonance tomography in treatment position using clips and anatomical structures for image registration. The treatment was delivered by a linear accelerator (Novalis® on TrueBeam™STx, Varian™, Palo Alto, CA) using ExacTrac 6.0.6® (Brainlab™, Feldkirchen, D) for positioning verification. Treatment plans were subjected to external review. HA plans were compared to automatically generated plans obtained with volumetric modulated arc therapy (VMAT) using 6 arcs obtained with the treatment planning system Eclipse® (Varian, Palo Alto, CA). The model for automated planning was based on 28 HA plans. Seven patients treated with HA were re-planned with Eclipse® and compared. All plans optimized in Eclipse® used the same optimization template.

Results:

HA and VMAT fulfilled all the constraints criteria. Target coverage was 95,1 % ($\pm 2,5$) for HA, and 94,2 % ($\pm 2,0$) for VMAT, respectively. The mean dose given to the affected eye was 24,5 Gy ($\pm 6,4$) for HA and 28,3 Gy ($\pm 6,4$) for VMAT. For HA, $D_{0.03}$ delivered to the optic nerve was 21,2 Gy ($\pm 12,4$) and 26,8 Gy ($\pm 6,9$) for VMAT, respectively. The mean dose to the lens was 9,Gy ($\pm 12,5$) for HA and 17,2 Gy ($\pm 8,7$) for VMAT. The ipsilateral lacrimal gland received 12,7 Gy ($\pm 6,3$) with HA, and 12,7 ($\pm 4,0$) with VMAT.

Conclusion:

Manually generated HA plans compared very favourably with automatically generated plans, and HA plans seemed to perform slightly better in respect of dose delivered to organs at risk.

Relapsing Solitary Brain Metastases Treated with HybridArc™: ICRU 50/62 for Small Volumes

Radiation Oncology, Dessau City Hospital, Germany¹, Radiation Oncology, Zurich University Hospital, Zurich²

Introduction:

Isolated brain metastases predispose to disease progression in the brain during follow-up. Fractionated stereotactic Radiosurgery (fSRS) and Stereotactic Brain Radiotherapy (SBRT) are routinely used in first line as well as in case of relapsing brain metastasis. However, re-treatment may be compromised by precedent dose delivered to the brain and optimal sparing of normal tissue may compromise dose homogeneity of the target volume.

Methods:

We present a 67-year old male patient with stable metastatic renal cell carcinoma to the chest and lungs but with relapsing metastases of the brain. Six series of fSRS, SBRT or highly conformal fractionated radiotherapy were applied to treat singular brain lesions from February 2014 until November 2015 using the HybridArc™ technique of iPlan 4.5.3 (Brainlab, Feldkirchen, D). The treatment was delivered by a linear accelerator (Novalis powered by TrueBeam STx™, Varian, Palo Alto, CA) using ExacTrac 6.0.6® (Brainlab, Feldkirchen, D) for positioning verification.

Results:

The dose gradients achieved using a flattening-filter-free photon beam of 5.5 MeV ranged from 14 to 50 Gy/cm. The homogeneity index (HI) never exceeded 0.09 or 0.05 ± 0.02 . The conformity index (CI) at a minimum dose of 95% of the prescribed dose was ≤ 1.30 or 1.19 ± 0.07 . Maximum dose ranged from 101.9% to 106.6% in each irradiation series, not exceeding a cumulative dose of 138 % or $119\% \pm 12\%$ in relation to the local prescribed dose. Organ doses never exceeded 25% of recommended biological effective dose values. The gamma value remained < 1 in 99% of all voxels. Distance to agreement was 1.5 mm and dose errors within 1.5%. The patient remained without relapse to the brain at follow-up in November 2016. However, metastatic progress to the bones presenting a singular bone metastasis of the proximal right tibia resulted in a change of the systemic therapy from pazopanib (on therapy since February 2015 after one year sunitinib) to nivolumab in July 2016.

Conclusion:

Cumulative toxicity of radiotherapy to the brain is a major concern in patients with slowly progressive or treatable metastatic cancer disease. fSRS with HybridArc™ is highly reliable for repeated dose applications to small target volumes easily implementing ICRU standards (Reports No. 50 and 62) for coverage and maximal dose delivery avoiding heterogeneity within the target volume.

M. Dysli¹, M. Dysli², D. Rappoport¹, T. Schmückle Meier¹, C.J. Bockisch¹, C.J. Bockisch², C.J. Bockisch³, K. Landau¹, KP. Weber¹, KP. Weber²

Hess screen testing shows an exodeviation shift compared to the Harms screen test

Augenklinik, UniversitätsSpital Zürich, Zürich¹, Neurologische Klinik, UniversitätsSpital Zürich², Otorhinolaryngology Department, University Hospital Zürich, Zurich³

Introduction:

Manifest ocular deviation (tropia) is present in strabismus patients and latent ocular deviation (phoria) a common finding in normal subjects. Besides the prism cover test for near and far, Hess and/or Harms screen testing are often performed to objectively assess the amount of ocular misalignment. This study investigates the differences of the results from Harms and Hess screen test in combination with the prism cover test.

Methods:

Ocular deviation measures of 18 normal subjects and 41 adults and children with congenital or acquired paralytic or concomitant strabismus were assessed with a complete orthoptic examination including prism cover test for near (50cm) and far (3m) compared to objective measurement methods using the Hess screen (50cm) and the Harms screen test (3m), where both eyes are dissociated.

Results:

On average, subjects showed an exodeviation shift of 6.3° in the Hess test when compared to the Harms screen (3.6° for normals, 7.5° for patients). Subjects which were orthophoric in the prism cover test for near mainly showed an exodeviation in the Hess screen test, whereas in the Harms screen test they showed no horizontal deviation. Likewise, subjects with a small esophoria in the cover test for near showed no deviation in the Hess screen test.

Conclusion:

Hess screen testing for near records a relative exodeviation compared to the prism cover test for near and to the Harms screen test for far. This shift most probably is due to the difference in convergence effort during the various tests. This study emphasizes the importance to consider the convergence angle when comparing the Hess screen test with other methods, and to test ocular deviations for near and far distances separately to get a representative assessment of the ocular deviations.

U. Süssbier¹, HC. Wong¹, S. Isringhausen¹, A. Gomariz-Carillo¹, P. Helbling¹, T. Nagasawa², AM. Müller¹, MG. Manz¹

Functional and structural dynamics of the bone marrow stromal microenvironment after cytoreductive therapies

Hematology, University Hospital Zürich, Zurich ¹, Institute for Frontier Medical Sciences, Kyoto University, Kyoto, Japan²

Introduction:

Bone marrow (BM) cavities are the primary site of blood cell production during adulthood. Continuous hematopoiesis is sustained by the proliferation and differentiation of hematopoietic stem and progenitor cells (HSPCs), which are critically regulated by signals emanating from stromal cells that form the BM microenvironment. The BM stromal compartment comprises different non-hematopoietic cell types of mesenchymal, endothelial and neural origin. Cytoreductive treatments such as ionizing irradiation and chemotherapeutic agents are the treatment of choice for multiple different haematologic and non-haematologic malignancies as well as for myeloablative conditioning regimens in BM transplantations. The cytotoxic damage and rapid killing of cycling cells elicited by myeloablative therapies have been extensively characterized in what pertains to their direct effects on hematopoietic cells. However, whether and to what extent these treatments target stromal BM cells is largely unknown.

Here we have analyzed the dynamics of stromal cell populations upon myeloablation, the resulting microarchitectural effects on the BM microenvironment and the kinetics of regeneration of fully restored BM tissues post-injury.

Methods:

In our study we combine two approaches to investigate changes in the BM upon cytoreductive therapies. To provide a comprehensive analysis of quantitative changes of the hematopoietic but especially of the stromal compartment, comprising mesenchymal and endothelial cell populations, we employ advanced flow cytometric protocols. Structural effects on the murine BM microenvironment are visualized and quantified by using advanced 3D-confocal microscopy imaging of thick bone slices in combination with computational tools developed in our laboratory.

Results:

As previously reported, ionizing irradiation and 5-fluorouracil treatment led to a severe loss of HSPCs, Lin^c-kit⁺Sca-1⁻ and Lin^c-kit⁺Sca-1⁺ cells. Notably, a similar profound decrease in endothelial as well as mesenchymal cells, phenotypically defined as CD45⁻Ter119⁻Sca1⁺CD31⁺ and CD45⁻Ter119⁻Sca1⁻CD31⁻CD140b⁺ cells, was observed. Decline in stromal cell numbers was apparent 7 days after treatment and encompassed a major loss of structural integrity of the BM microenvironment. 3D imaging revealed massive sinusoidal dilation followed by the appearance of ruptures of the vessel walls. Both structural effects and decrease in cell numbers were partially reversed 14 days post treatment in a regenerative process that culminated at day 28 post treatment. In addition, massive *de novo* differentiation of mesenchymal progenitors into adipocytes lead to adipogenic infiltration of large regions of the BM, which were not hematopoietically active. Of note, this process was fully reversible and virtually almost all adipocytes were cleared from BM tissues 56 days after treatment. To compensate for the impaired function of the BM, reversible extramedullary hematopoiesis could be observed at the time points of maximal BM damage.

Conclusion:

Our observations demonstrate that the stromal BM microenvironment is highly sensitive to myeloablative therapies, which lead to massive alterations in the BM microstructure. Of note, our observations further highlight that BM tissues are endowed with an intrinsic regenerative and self-organizing capacity that enables rebuilding of a fully functional tissue microenvironment after severe damage. We are currently investigating the inflammatory mechanisms that trigger injury as well as regeneration of the BM stromal infrastructure.

Multidimensional analysis of the hematopoietic microenvironment during embryonic development and early postnatal life.

Experimental Hematology Division, University Hospital Zürich, Zürich¹, Kyoto University Hospital, Kyoto²

Introduction:

Hematopoietic stem and progenitor cells (HSPCs) continuously replenish all mature blood cell types in a demand-adapted and dynamic manner throughout life. During adulthood, HSPCs are maintained in a specialized microenvironment within the bone marrow (BM), called the stem cell niche, which has been studied in great detail. During embryonic development, HSPCs are generated and expanded in an elaborate process involving multiple anatomic sites including fetal liver and spleen before homing to the bone marrow. Exposure to different anatomic microenvironments is thought to play a fundamental role in adapting hematopoietic output to the changing physiological needs during development. Nonetheless, the cellular and molecular components of the niches through which HSPCs migrate, and how they regulate hematopoiesis are poorly understood to date. Our aim is to dissect the putative stromal cell subsets existing in fetal and postnatal liver and spleen, and determine their contribution to the hematopoietic microenvironment and HSPC maintenance.

Methods:

We have employed flow cytometry to analyze the identity and phenotypic characteristics of non-hematopoietic stromal components present in embryonic and postnatal hematopoietic organs. To study the anatomical distribution of the different hematopoietic and non-hematopoietic cellular components and quantify relevant cellular interactions we employ tissue-scale 3D imaging technology. Finally, an extensive analysis of gene expression profiles of the described stromal cell populations will inform on the mechanisms by which these cells regulate HSPC function.

Results:

BM mesenchymal stromal cells that form the BM HSPC niche secrete high levels of the chemokine CXCL12, and play a major role in HSPC cell retention and maintenance. Hence we have employed CXCL12-GFP knock-in reporter mice to investigate the presence of CXCL12 expressing stromal subsets in embryonic hematopoietic organs with putative HSPC supportive functions. At early stages of development (E12.5-14.5) evolving hepatoblasts, identified by expression of the marker DLK1 express CXCL12. Even higher expression of CXCL12 was found in stromal cells expressing the mesenchymal markers Pdgfr- β and Nestin and displaying fibroreticular morphology. Of major interest, these CXCL12+ mesenchymal-like cells are found scattered throughout fetal liver and splenic tissues predominantly during embryonic and postnatal development, vanishing from these organs as hematopoietic activity declines and transitions to the BM.

Conclusion:

Mesenchymal stromal cells in the BM have an imperative function in maintaining HSCs. We are currently investigating the identity and role of stromal cells in the regulation of hematopoiesis in late embryonic and early postnatal development. Our initial data describe a population of CXCL12+ stromal cells, potentially of mesenchymal origin, which is present in the fetal liver and spleen during the developmental window in which active hematopoiesis is established in these organs. On the basis of these observations and the fact that these cells express high levels of hematopoiesis-supportive factors, we postulate that fibroblastic mesenchymal cells critically contribute to establish the extramedullary hematopoietic microenvironment during development. We are currently conducting experiments to further characterize the developmental origin, potential heterogeneity and functional relevance of this poorly characterized cell type.

A. Eckhard¹, D. Bächinger¹, V. Wettstein¹, C. Brühlmann¹, T. Honegger¹, B. Schuknecht², A. Huber¹, A. Monge Naldi¹

MR-Imaging of the Vestibular Aqueduct in the diagnosis of Meniere's Disease

*Department of Otorhinolaryngology and Head and Neck Surgery, University Hospital Zurich¹,
Medizinisch Radiologisches Institut (MRI) Bethanien, Zurich²*

Introduction:

Meniere's disease (MD) is a syndromic disorder of the inner ear, which presents with episodic vertigo, sensorineural hearing loss, tinnitus, and aural fullness. Clinically, MD poses a significant diagnostic challenge, since (i) among MD patients the preponderance, frequency and intensity of symptoms ("phenotypes") differ widely, and (ii) the current diagnostic criteria for MD are rather unspecific, and are overlapping considerably with other vertigo-associated diseases. This study aims to establish magnetic resonance (MR) imaging-based criteria that allow to distinguish clinically (phenotypically) distinct "subgroups" of MD patients based on the trajectory and the MR-signal intensity of their vestibular aqueduct (VA) in the temporal bone.

Methods:

1) Retrospective analysis of MRI data from 95 patients with a clinical diagnosis of "certain" MD and endolymphatic hydrops (EH), as well as from 15 control cases with a clinical diagnosis of vestibular migraine (n=9) or sudden sensorineural hearing loss (n=6) and no EH, who underwent 3T MR imaging of the temporal bone (3D real inversion recovery (3D-IR) sequence performed four hours after intravenous contrast administration (Barath et al., Am J Neuroradiol, 2014)). In the MR image data sets from each case the angle "beta" of the proximal VA and the distal VA merging into the vestibule and the posterior cranial fossa, respectively, were determined. The MR signal intensities in the most distal segment of the VAs from both sides were compared semiquantitatively. 2) Retrospective chart review regarding clinical history and course of disease in MD patients.

Results:

Among the MD cases, four distinct subgroups of patients could be distinguished, based on significantly different (1) trajectories of their VAs, (2) interaural MR signal intensities in the VAs, as well as (3) the presence/absence of EH in the labyrinthine structures. Analysis of these imaging features in the control cases suggests that certain trajectories of the VA, as well as a significant loss of MR signal intensity in the distal VA were exclusively associated with certain subgroups of MD patients. Clinical chart review revealed significant clinical ("phenotypic") differences between MD subgroups, such as clinical laterality of the disease (uni- or bilateral affection).

Conclusion:

In summary, we have established a new strategy that allows us to isolate (patho-) morphologically distinct subgroups of MD patients using clinical imaging (gadolinium-enhanced 3T MRI). A preliminary retrospective analysis of clinical history in these patients suggests that these patients also exhibit significantly different phenotypic traits in the course of their disease. Future studies will show whether MR imaging-based sub-categorization of MD patients can be applied clinically, in order to improve clinical diagnosis and prognosticate certain features in the clinical course of the disease in individual MD patients.

DM. Heuberger¹, AG. Franchini¹, RA. Schuepbach¹

The thrombin-thrombomodulin complex cleaves protease-activated receptor 2 in a glycosylation dependent manner

Surgical Intensive Care Medicine, University Hospital Zurich, Zurich, Switzerland¹

Introduction:

Protease-activated receptors (PARs) are G-protein coupled receptors involved in a variety of biological processes ranging from platelet activation and vascular barrier regulation to chronic inflammation, metastasis and apoptosis. PARs are uniquely activated by protease cleavage of the N-terminus which allows the new unmasked tethered ligand to activate PAR intramolecular.

Thrombin is the prototypical activator for PAR1, PAR3 and PAR4 whereas PAR2, lacking the thrombin recognition site, was believed to uniquely be activated trypsin. We wondered whether thrombin could cleave PAR2 efficiently if PAR2 is co-localized with the co-receptor thrombomodulin that recruits and binds thrombin to the cell surface. We investigated the interaction of the three players and at which site PAR2 is cleaved by thrombin.

Methods:

To determine whether thrombin can cleave PAR2 in presence of the co-receptor thrombomodulin, PAR2 constructs containing an N-terminal alkaline phosphatase (AP) tag and thrombomodulin constructs were transiently overexpressed in HEK T293 cells. Cell surface expression and co-localization of PAR2 and thrombomodulin was shown by immunostaining. To determine the PAR2 cleavage by thrombin in presence of thrombomodulin the AP activity either in the supernatant or on the cell surface was measured with an established alkaline phosphatase assay (SEAP).

Results:

We showed that PAR2 was efficiently cleaved by the thrombin-thrombomodulin complex. Overexpression of truncated thrombomodulin constructs showed that full glycosylation and EFG-like domain 5 and 6 are required for thrombomodulin mediated cleavage of PAR2 by thrombin. The results showed that PAR2 is cleaved by the thrombin-thrombomodulin complex at aa R31 and/or aa R36. The cleavage of PAR2 at aa R31 is more efficient if the N-glycosylation of the N-terminus is changed to O-glycosylation.

Conclusion:

Our experiments showed that PAR2 is cleaved by the thrombin-thrombomodulin complex depending on the glycosylation pattern of the receptors. Whether the cleavage of PAR2 at aa R31 and/or aa R36 leads to the activation of the receptor and if the G-protein coupled activation would have biological relevance has to be investigated.

M. Schneider¹, A. Gupta¹, P. Borger¹, R. Graf¹, P-A. Clavien¹

Adipose tissue-derived mesenchymal stem cells for the treatment of small for size liver

Visceral and Transplant Surgery, University Hospital Zurich, 8091 Zurich, Switzerland¹

Introduction:

Mesenchymal stem cells (MSC) hold great promises for regenerative medicine their influence on promotion of liver regeneration (LR) after partial hepatectomy has been documented in various studies. However, the potential benefit of treatment with mesenchymal stem cells on the mitigation of SFSS has not been examined. Furthermore, various reports describe growth-stimulatory effect of MSC on cancerous cells. The influence of MSC on growth of tumor cells in vitro and in vivo in a murine model of colorectal liver metastases will be assessed.

Methods:

Adipose tissue derived mesenchymal stem cells were isolated from epididymal fat pads and cultured according to established protocols. Regular 68% and extended 86% hepatectomy (Hx) for induction of SFSS were performed as previously described.

Results:

No changes in LW/BW ratio were seen 48 hours after Hx, however, a significantly increased number of hepatocytes had entered cell cycle in MSC treated mice in 68%Hx as well as 86%Hx compared to control injections. Expression analyses revealed significant upregulation of FoxM1 and Cyclin B2 accompanying MSC treatment. Upregulation of p21, the cell cycle inhibitor responsible for delayed progression through cell cycle in SFSS, was reversed with MSC treatment. Analyses of Serum markers showed lower bilirubin levels in 86% Hx animals treated with MSC compared to controls, while serum levels of AST, ALT, AP, Albumin and NH3 did not differ significantly at 48 hours.

Conclusion:

MSC might depict a promising option for treatment and prevention of SFSS. However, before any clinical application potential pro-cancerous effects must be carefully assessed.

V. Lysenko¹, N. Wildner¹, RA. Flavell², MG. Manz¹, A. Theocharides¹

Establishment of a patient-derived myelofibrosis xenograft mouse model

Hematology, University and University Hospital Zurich, Zurich, Switzerland¹, Department of Immunobiology, Yale University, New Haven, Connecticut, USA²

Introduction:

A growing number of patient-derived xenograft (PDX) mouse models have been developed over the past few decades that allow engraftment of human hematopoietic stem cell (HSC) malignancies. This is a powerful tool for investigating the evolution of HSC and leukemic stem cells, as well as disease heterogeneity. However, engraftment is often limited due to potential lack of supportive factors in the bone marrow (BM) microenvironment. This limitation facilitated the development of more advanced mouse strains that express human cytokines and growth factors that are needed for efficient human hematopoietic development *in vivo*. Myelofibrosis (MF) is a HSC disorder characterized by bone marrow fibrosis that has the potential to transform into acute myeloid leukemia depending on the clonal evolution of MF stem cells (MF SCs). However, the engraftment of MF SCs in PDX models is poor. We hypothesized that the constitutive expression of human cytokines and growth factors in a PDX model may promote the development of the human MF clone *in vivo*. Therefore, we used next-generation mice that express human M-CSF, IL-3, GM-CSF, TPO, and SIRP α Tg (MISTRG) in order to develop a pre-clinical MF PDX model.

Methods:

Purified peripheral blood stem and progenitor (CD34+) cells were collected from MF patients and intrahepatically transplanted into sublethally irradiated newborn MISTRG mice. NSG mice (Standard PDX mouse strain) are used as controls. Each mouse strain is transplanted with the same patient sample. 5-9 weeks after transplantation mice are sacrificed and analyzed for human engraftment using flow cytometry and immunohistochemistry.

Results:

Most patient samples so far were transplanted into MISTRG mice. We are currently in the process of also transplanting NSG mice as a comparison. Preliminary results show that four out of seven samples engraft in the BM of MISTRG mice with a total median human CD45+ cell engraftment of 23%. Over 60% myelo-monocytic differentiation was observed in the mice that showed engraftment. The spleen weight was significantly increased in mice that engrafted in comparison to those that did not due to increased extramedullary hematopoiesis. Overall, preliminary results suggest that the next-generation MISTRG mice support robust human MF engraftment.

Conclusion:

MISTRG mice support unprecedented myelo-monocytic engraftment of human MF SCs in 57% of patient samples investigated so far. To further investigate the contribution of human cytokines to human MF engraftment in PDX models we are planning to use MISTRG mice that express human IL-6, a cytokine that may be involved in the pathogenesis of MF. In order to determine whether specific somatic mutations promote human MF engraftment in PDX models next-generation sequencing will be performed on transplanted patient samples. Moreover, clonal evolution *in vivo* will be tracked and correlated with disease progression in patients.

CM. Wilk¹, I. Weber², K. Seidl², AM. Müller¹, C. Rachmühl², A. Holzmann-Bürge², SP. Kuster², U. Schanz¹, AS. Zinkernagel²

Impact of oral gut decontamination on *Staphylococcus aureus* colonization in patients undergoing hematopoietic stem cell transplantation

Hematology, University Hospital Zürich, Zurich¹, Infectious Diseases and Hospital Epidemiology, University Hospital Zurich, Zurich²

Introduction:

Hematopoietic cell transplant (HCT) recipients are at increased risk for infections. *Staphylococcus aureus* (SA) colonizes 20-50% of healthy individuals and is a risk factor for subsequent invasive SA infections. Colonization rates in patients undergoing allogeneic HCT and clinical relevance for the time of aplasia and severely reduced immune function following HCT are not known. Only some retrospective data on methicillin-resistant SA infection rates are available. In this study, we prospectively assessed the prevalence of SA colonization in 110 consecutive patients before and during allo-HCT in a single-center observational study from June 2013 to January 2016.

Methods:

All included patients undergoing allo-HCT were screened for nasal and pharyngeal SA colonization weekly beginning at the time of admission to the transplant unit until neutrophil recovery. After swabs for the initial SA screening were taken all patients were put on oral gentamicin and vancomycin for gut decontamination until neutrophils had recovered. Quantitative stool analyses were performed weekly. In case of fever or increase of inflammatory laboratory parameters (C-reactive protein) blood cultures were drawn.

Results:

In our cohort we found a SA prevalence of 11.8% (13/110 patients) at the time of admission to the transplant unit. All SA strains detected were sensitive to methicillin. All patients colonized with SA in the nose (13/13), while pharyngeal colonization was found less frequently (5/13, 38.5%). Patients aged above 60 years (14/110) showed the highest SA carrier rate (4/14 patients aged above 60 years and 4/13 colonized patients, respectively). There was no correlation between SA colonization and sex, underlying disease or chemotherapeutic pretreatment. Prior systemic antibiotic treatments using SA effective drugs within six months before admission to the transplant unit did not have relevant impact on SA prevalence at the time of screening.

Within the group of the 13 SA-positive patients there were 2 patients (15.4%) who had received oral antibiotic gut decontamination (vancomycin and / or gentamicin) within twelve weeks prior to admission. In the SA negative group a similar proportion of patients had received oral gut decontamination (12/97; 12.4%).

Despite the severe immunosuppression and skin and mucosal lesions incl. indwelling catheters no systemic SA infections (including bacteremia) were found during hospitalization in any of the HCT patients. All SA positive patients became SA negative within three weeks. These observations imply that decolonization is achieved by the consistent oral gut decontamination that all patients received.

Conclusion:

In conclusion, the SA colonization prevalence in our cohort of patients undergoing allogeneic HCT was 11.8% which is lower than described previously in the literature. Of note, our cohort did not comprise patients with MRSA. We here demonstrate in a prospective study that oral gut decontamination with vancomycin and gentamicin in addition to strict hygiene measures resulted in eradication of SA colonization in all 13 colonized patients within three weeks.

T. Skaria¹, J. Vogel¹

α CGRP suppresses the proliferation and Angiotensin II induced myofibroblast differentiation of cardiac fibroblasts

Institute of Veterinary Physiology, University of Zurich¹

Introduction:

Chronic hypertension is associated with a pathological cardiac remodelling characterized by cardiomyocyte hypertrophy as well as increased proliferation and myofibroblast transformation of cardiac fibroblasts. α CGRP released from skeletal muscles appears to be an endocrine factor that “directs” the heart to develop a physiological hypertrophy and improves cardiovascular function during exercise. Exercise in absence of α CGRP results in pathological cardiac hypertrophy. In the present study, we tested α CGRP’s effects on the proliferation and profibrotic myofibroblast differentiation of cardiac fibroblasts.

Methods:

Adult murine cardiac fibroblasts isolated from C57BL6 (BL6) mice were cultured and treated with Angiotensin II (100 nM, Bachem), a hypertensive agent, and α CGRP (200 nM, 400 nM, Bachem). cAMP production was determined by ELISA. Fibroblast proliferation was measured using BrDU assay. The expression of α -smooth muscle actin, fibronectin and collagen-1 was assessed by immunofluorescence staining and immunoblotting. The animal experiments in this study were conducted in accordance with the EU and national guidelines.

Results:

α CGRP treatment significantly increased cAMP production, thereby indicating its potent biological activity and the presence of functional α CGRP receptors in cardiac fibroblasts. Proliferation of cardiac fibroblasts, a process contributing to fibrosis was effectively suppressed by α CGRP as indicated by significant reduction in the proportion of S-phase cells. Treatment with the potent hypertensive agent Angiotensin II notably increased stress fiber formation in cardiac fibroblasts. Moreover, the expression of α -smooth muscle actin, fibronectin and collagen-1, which are the molecular markers of myofibroblast differentiation were highly increased upon treatment with Angiotensin II. This profibrotic effect of Angiotensin II was significantly lower when cardiac fibroblasts were treated with a combination of Angiotensin II and α CGRP.

Conclusion:

α CGRP directly inhibits profibrotic myofibroblast differentiation of murine cardiac fibroblasts. Thus, α CGRP agonism might prevent fibrosis and pathological cardiac remodeling during chronic hypertension.

Co-housing DSS treated mice with healthy mice results in faster normalization of the intestinal microbiota and promotes recovery from colitis

University Hospital Zürich (USZ), Department of Gastroenterology and Hepatology, Zürich, Switzerland¹

Introduction:

The intestine is populated with myriads of bacteria, which form a complex ecosystem and have tremendous impact on our health. In inflammatory bowel disease (IBD), shifts in microbiota composition and a reduction in overall diversity have been described. There are attempts to therapeutically transfer the microbiota from healthy subjects to persons suffering from intestinal disease. While in case of *Clostridium difficile* infections, this approach proves to be very efficient; the therapeutic value of fecal microbial transfer (FMT) in IBD is still unclear. In mouse models of intestinal inflammation, the effect of FMT has been studied poorly and if so, germ-free or antibiotic-treated animals have been used – models that poorly reflect the situation in human IBD patients. Here, we addressed how transmission of microbiota from healthy to diseased mice affects recovery from acute colitis.

Methods:

Acute colitis was induced in 12-14 week old C57B6 mice by administration of 2% DSS in the drinking water for 7 days. Mice with colitis were co-housed with healthy mice after removal of DSS. Due to coprophagy, this results in fast transfer of the microbiota between co-housed mice. To analyse changes in the composition of microbiota over time, stool samples were taken every second day and sequenced for the V4 hyper-variable region in the bacterial 16S DNA.

Results:

As expected, DSS treatment resulted in severe weight loss, and even 7 days after withdraw of DSS (day 15), histology confirmed severe colitis. Intestinal inflammation was accompanied by an overall reduction of microbial diversity (decreased Shannon index, $p < 0.01$), and a marked shift in the composition of the microbiota (increased abundance of *Verrucomicrobia*, *Cyanobacteria* and some families of *Firmicutes* [mainly *Clostridiaceae*], although overall abundance of *Firmicutes* was decreased [$p < 0.01$ for all]). However, on day 15, these changes were less pronounced, indicating a normalization of the microbiota composition upon recovery. DSS-treated mice which were co-housed with healthy littermates after colitis induction, showed faster recovery (earlier weight gain, reduced histological scores, reduced levels of the infiltration marker myeloperoxidase (MPO), less pronounced shortening of the colon, $p < 0.01$ for all) and an earlier normalization of the microbiota composition.

Conclusion:

Our results indicate that co-housing of DSS-treated mice with healthy mice results in transfer of healthy microbiota to diseased mice, and promotes recovery from colitis. This indicates that introduction of a “healthy” microbiota might have beneficial effects during intestinal inflammation and opens the possibility to systematically study the effect of genetic alterations in donor and/or recipient on the efficacy of FMT.

Reduced inflammasome activation upon loss of PTPN22 is dependent on autophagy-mediated degradation of NLRP3

University Hospital Zürich (USZ), Department of Gastroenterology and Hepatology, Zürich, Switzerland¹

Introduction:

A variant in the gene locus encoding protein tyrosine phosphatase non-receptor type 22 (PTPN2) is associated with decreased risk to develop Crohn's disease (CD), but at the same time promotes autoimmunity. Presence of this variant results in altered target-specificity and altered function of the phosphatase. We have recently shown that loss of PTPN22 promotes NLRP3-tyrosine phosphorylation, ultimately resulting in decreased NLRP3-induced inflammasome activation. Autophagy is crucial for intestinal homeostasis, and we have previously shown that loss of PTPN22 promotes autophagy. Further, autophagy controls inflammasome activation. Therefore, the aim of this study was to investigate whether autophagy plays a role in reduced NLRP3-inflammasome activity observed upon loss of PTPN22.

Methods:

Bone marrow derived dendritic cells (BMDC) from wild-type and PTPN22-deficient mice, and human THP-1 monocytes were used for all studies. Non-targeting control-, or PTPN22-specific shRNA was introduced into THP-1 cells using lentiviral vectors for stable knockdown of PTPN22. The NLRP3 inflammasome was activated using MDP, MSU and ATP. Autophagy was inhibited using 3-methyladenine, Wortmannin and bafilomycin, or by transfection with siRNA specific for ATG16L1 or LC3B.

Results:

BMDC and THP-1 cells lacking PTPN22 showed a marked reduction of inflammasome activation, as observed by reduced levels of cleaved caspase-1 and mature IL-1b. However, when autophagy was inhibited using either chemical compounds (3-methyladenine, Wortmannin, bafilomycin) or LC3B and ATG16L1-specific siRNA, PTPN22-deficient cells secreted as much mature IL-1b as PTPN22-competent cells. Further, we found that tyrosine-phosphorylated, but not non-phosphorylated NLRP3 is recruited to autophagosomes upon inflammasome activation. Upon loss of PTPN22, NLRP3-phosphorylation was increased and more NLRP3 was present in autophagosomes. On the other hand, presence of the altered-function variant in PTPN22 diminished NLRP3 phosphorylation and abrogated its recruitment to autophagosomes. Of note, presence of the altered-function variant in PTPN22 enhanced cleavage of caspase-1 and secretion of IL-1b. NLRP3 that lacks the tyrosine-phosphorylation site was not found in autophagosomes.

Conclusion:

NLRP3 tyrosine phosphorylation promotes recruitment of NLRP3 into autophagosomes. PTPN22 dephosphorylates NLRP3 and in this way inhibits its autophagy-mediated degradation, allowing for efficient inflammasome activation. This helps to explain, how presence of several genetic variants in one individual, for instance variants in PTPN22 and in genes involved in autophagy, might affect relative disease risk.

KA. Airich¹, HS. Hornemann¹, YL. Liu¹, KL. Luk², AA. Aguzzi¹

Development of a cellular alpha-synuclein aggregation assay for high-throughput screens

Institute of Neuropathology, University Hospital Zurich, Schmelzbergstrasse 12, CH-8091, Switzerland¹, Department of Pathology and Laboratory Medicine, University of Pennsylvania, 3600 Spruce St. 1, PA 19104 USA²

Introduction:

The Aguzzi lab has previously developed a "digital prion infectivity cell-based assay" (dPICA) for screening large numbers of genes for their potential to influence prion replication and propagation. We adapted this technology to an automated, high-throughput cellular alpha-synuclein (α Syn) aggregation assay, which will be applied for a genome wide screening to identify novel biological pathways and druggable target genes relevant to Parkinson's Disease.

Methods:

For reliable and specific detection of α Syn aggregates we modified previously published protocols based on immunocytochemistry (ICC) and fluorescence microscopy. To that aim, we selected the antibodies MJFR1 (recognizing endogenous α Syn) and 81A (against phosphorylated α Syn found in aggregates) from a collection of different antibodies available in the Luk laboratory to establish the image-based readout in a 384-well plate. For that purpose, the IncuCyte® ZOOM System, which contains a microscope housed inside a cell incubator and the high-end MetaMorph Software from Molecular Devices was used. The cell based assay is being transferred to our robotic platform and the next step is to perform a genome wide high-content screen for the screening of large numbers of genes using RNAi libraries for their potential to influence α Syn aggregation and pathology.

Results:

We modified previously published protocols based on pre-formed-fibrils (PFF) transduction and our final protocol revealed uniform seeding across the wells and reliable detection of de novo formed hyperphosphorylated α Syn aggregates. For the detection in 384-well plates, an automated quantitative image-based-readout for the analysis of hyperphosphorylated α Syn aggregates at single cell resolution was established. This set-up enabled us to simultaneously scan several 384-well plates with uniform detection of the immunofluorescence-labeled hyperphosphorylated α Syn aggregates and also allowed a direct comparison to appropriate controls (e.g. knock-down of α Syn by siRNAs).

This automated image-based quantification of phosphorylated α Syn aggregates revealed an intense signal and a very high signal to noise ratio, which are prerequisites for accurate high content image analysis. To that aim, we established a nuclear staining protocol for fully automated cell counting. We are now in the progress of testing various technical, negative and positive controls to ensure their reliability in the assay and to establish appropriate RNAi transfection conditions.

Conclusion:

The effective adaptation of the cell-based model of α Syn pathology towards a homogenous-phase protocol is applicable for high-throughput screenings in 96- and 384-well plate formats and is convenient for high quality data acquisition in an unbiased manner. The successful development of an automated, quantitative image-based read-out for single cells containing de novo formed hyperphosphorylated α Syn aggregates is a prerequisite for our aim to identify crucial and actionable nodes and to formulate testable hypotheses on the pathways exploited for genes that control the crucial aspects of α Syn aggregation and propagation.

N. Arenas-Ramirez¹, C. Zou³, S. Popp³, D. Zingg², B. Brannetti³, E. Wirth³, T. Calzascia³, J. Kovarik³, L. Sommer², G. Zenke³, J. Woytschak¹, C.H. Regnier³, A. Katopodis³, O. Boyman¹

Improved cancer immunotherapy by a CD25-mimobody conferring selectivity to human interleukin-2

Department of Immunology, University Hospital Zurich, University of Zurich¹, Stem Cell Biology, Institute of Anatomy, University of Zurich, CH-8057 Zurich, Switzerland², Novartis Institutes for Biomedical Research, Novartis Pharma AG, CH-4002 Basel, Switzerland³

Introduction:

Interleukin (IL)-2, an essential cytokine for the homeostasis and activation of T cells, can stimulate cells expressing different levels of dimeric or trimeric IL-2 receptors (IL-2Rs). The administration of IL-2 at high doses proved its benefit for patients with advanced cancer through the stimulation of cells expressing high levels of dimeric IL-2Rs (CD8⁺ T cells and NK cells). Most of the IL-2-related side effects observed in patients treated with IL-2 have been associated to the binding of the cytokine to its IL-2 receptor α (CD25) subunit, preferentially expressed by immunosuppressive CD4⁺ T regulatory cells. Specific anti-IL-2 monoclonal antibodies (mAbs) have previously shown to lead to a vigorous activation of effector immune cells generating potent anti-tumor effects in mice. Currently, no mAb specific to human (h) IL-2 suitable for clinical development in cancer immunotherapy is available. In order to cover this clinical need, we developed a rational approach to generate a high affinity anti-hIL-2 antibody specifically blocking the CD25 binding site (termed NARA1).

Methods:

In order to screen anti-hIL-2 antibodies obtained after immunization and hybridoma generation, we developed a screening approach for the detection of specific anti-hIL-2 antibodies covering the CD25 binding site of the cytokine. The best monoclonal antibody, NARA1, was isolated and fully characterized *in vitro* using surface plasmon resonance (SPR) and x-ray crystallography in complex with hIL-2. We injected wild-type (*Wt*) mice with hIL-2/NARA1 complexes in order to check levels and kinetic proliferation of relevant immune cell subsets. Finally, we investigated the anti-tumor effect of hIL-2/NARA1 complexes in comparison to hIL-2 in two syngeneic (B16-F10) and in one spontaneous metastatic (Tyr::N-RasQ61K *Ink4a*^{-/-}) melanoma mouse models. In order to confirm which cells and mechanisms were responsible for the obtained anti-tumor response, we used hIL-2/NARA1 complexes for the treatment of *Tcrbd*^{-/-}, *Rag1*^{-/-} and *Wt* mice depleted of CD4⁺ or CD8⁺ T cells bearing B16-F10 tumor cells. Finally we checked the adverse effects using hIL-2/NARA1 complexes in comparison to hIL-2 by determining the aminotransferase levels (AST and ALT) and lung edema in mice.

Results:

Only 0.2% of all anti-hIL-2 mAbs found by our screening approach bind the target epitope. The SPR results showed that NARA1 was efficiently blocking the CD25 binding site of hIL-2 acting therefore as a high affinity CD25-mimobody. The crystal structure allowed us to identify the binding epitope of NARA1. The hIL-2's residues contacting NARA1 are clearly involved in the binding to CD25. *In vivo*, hIL-2/NARA1 complexes preferentially expand CD8⁺ T cells and NK cells, while the expansion of CD4⁺ T regulatory cells remain low. The immuno-stimulatory effect of hIL-2/NARA1 complexes leads to potent anti-tumor responses correlating with higher levels of CD8⁺ T cells in the tumor site. The anti-tumor effect observed was clearly dependent on CD8⁺ T cells that remain less exhausted than the ones generated upon hIL-2 immunotherapy. Moreover, hIL-2/NARA1 complexes lead to more favorable benefit to adverse effect ratios, as shown treating Tyr::N-RasQ61K *Ink4a*^{-/-} mice which developed less skin melanoma nodules and lung metastases while tolerating well several cycles of hIL-2/NARA1 complexes.

Conclusion:

We were able to generate and fully characterize the first anti-hIL-2 mAb able to potentiate the immunostimulatory properties of hIL-2, thus meriting further investigation for clinical development.

Dissecting mechanisms that drive HSC towards quiescence

Klinik für Hämatologie, UniversitätsSpital Zürich, Schmelzbergstrasse 12, 8091, Zürich Switzerland¹

Introduction:

Hematopoietic stem cells (HSC) are the source of lifetime supply of all blood cells. While in steady-state a substantial fraction of HSCs are dormant (>90% in G0 of cell cycle). However HSC turnover can rapidly change in response to systemic stresses, for instance bleeding, inflammation, infection and aging. Tight regulation of HSC turnover is therefore indispensable as both over-production (in the worst case myeloproliferative neoplasm, leukemia) as well as under-production (in the worst case aplasia) would endanger survival of the affected individual.

To study HSC cell cycle kinetics *in vivo*, our group recently developed a CFSE-based method. CFSE labels cytoplasmic proteins, is equally distributed to daughter cells and allows to study HSC divisional behavior with high resolution. Findings generated by using this tracking system suggest that drive to quiescence is more pronounced in aged HSC and HSC with high proliferative history. However, an in depth cell cycle analysis of HSC is necessary to clarify the exact stage of their replicative potential.

We hypothesize that steady-state fast-cycling or enhanced turnover with aging or transplantation-induced proliferation might activate an intrinsic HSC program that drives toward quiescence. Dysregulation of these pathways might cause bone marrow suppression and pancytopenia, which in turn impairs recovery from infections, or alternatively lead to accumulation of genetic alterations and blood malignancies, especially in aged HSCs.

Methods:

We successfully coupled the CFSE *in vivo* single cell tracking method with Ki-67 proliferative assay. This will allow us to examine HSC cell cycle status in distinct divisional clusters (i.e. from 0- to >5-divided cells) and determine their predisposition to fall into quiescence.

In addition, we will combine single cell RNA-sequencing with the CFSE-labeling approach. We will compare gene expression in young, old and experimentally aged HSC, with particular emphasis on cell cycle- and leukemia-associated genes.

Upon identification of possible targets from gene expression profiling, we will test effects of overexpression and deletion on HSC biology *in vitro* and *in vivo*.

Finally, we will compare expression of the newly identified factors in HSC from healthy individuals as well as from Leukemia-initiating cells (LICs) in acute myeloid leukemia (AML) samples available at University Hospital Zurich, by measuring mRNA levels using RT-qPCR and/or single cell transcriptomics.

Results:

We have so far shown that:

- CFSE *in vivo* tracking method can be coupled with Ki-67 proliferation assay. This assay does not affect divisional resolution.
- Aged HSC delay their entry into cell cycle, if compared to young HSC.
- Time-course experiments suggest that, after each cycle, a some cells slow down or enter quiescence, while other cells remain actively dividing.

Conclusion:

To understand the regulatory mechanisms involved in proliferative control of the HSC compartment, particularly the elements that drive HSC to quiescence, will allow to ultimately developing means for therapeutic intervention in HSC aging and/or pre-malignant HSC alterations that are observed in an aging population. Beyond, it might be speculated that these findings could apply to other somatic stem cell systems.

Deciphering hematopoietic stem cell niche factors in bioengineered human bone marrow models *in vivo*

Ehrbar Lab, Department of Obstetrics, UniversitätsSpital Zürich¹, Laboratory of Stem Cell Bioengineering, Institute of Bioengineering, École Polytechnique Fédérale de Lausanne, Switzerland²

Introduction:

Sufficient numbers of hematopoietic stem cells (HSCs) needed for bone marrow transplantations remains a major challenge in medicine today. HSCs expanded *in vitro* rapidly lose their regenerative capacity likely due to the lack of niche-derived signals comprising molecular and cellular components. Identification of critical hematopoietic niche components necessitates both the generation of more tractable *in vivo* models and, in parallel, novel approaches for heightened throughput in screening such systems *in vivo*. We have previously reported on a blank biomaterial that can be decorated with different growth factors and cell types known to be present in the niche *in vivo*. Here, we present a novel device, which allows the screening of multiple unique niche factor conditions in a single mouse with the aim to establish a minimalist human bone marrow model.

Methods:

Functionalized biomimetic polyethylene glycol (PEG) hydrogels were laden with human mesenchymal stem cells (hMSCs) and supplemented with or without bone morphogenetic protein-2 (BMP-2). These PEG gels were polymerized directly in the individual wells of novel multiplexing polydimethylsiloxane (PDMS) devices. Next, the screening devices containing PEG hydrogels were subcutaneously implanted in immunocompromised mice (4x per animal). At 8 weeks, the devices were explanted and analyzed for bone and bone marrow formation by microCT, histology and FACS.

Results:

Screening devices featuring 2mm diameter wells were shown to be the minimal size for niche formation allowing 8 conditions to be screened per implantable site (32 different conditions per mouse). MicroCT analysis revealed mineralization in all wells containing gels with hMSCs and BMP-2, but not in those lacking the growth factor. Histological analysis corroborated these findings. Hydrogels containing hMSCs and BMP-2 developed into bone marrow-like constructs including a typical bone shell filled with marrow and trabecular bone structures. Ultimately, long-term HSC enrichment in the constructs containing cells and BMP-2 was confirmed by FACS analysis on the recruited murine cell population. These results indicate the formation of a functional ectopic niche in BMP-2 and cells-laden gels.

Conclusion:

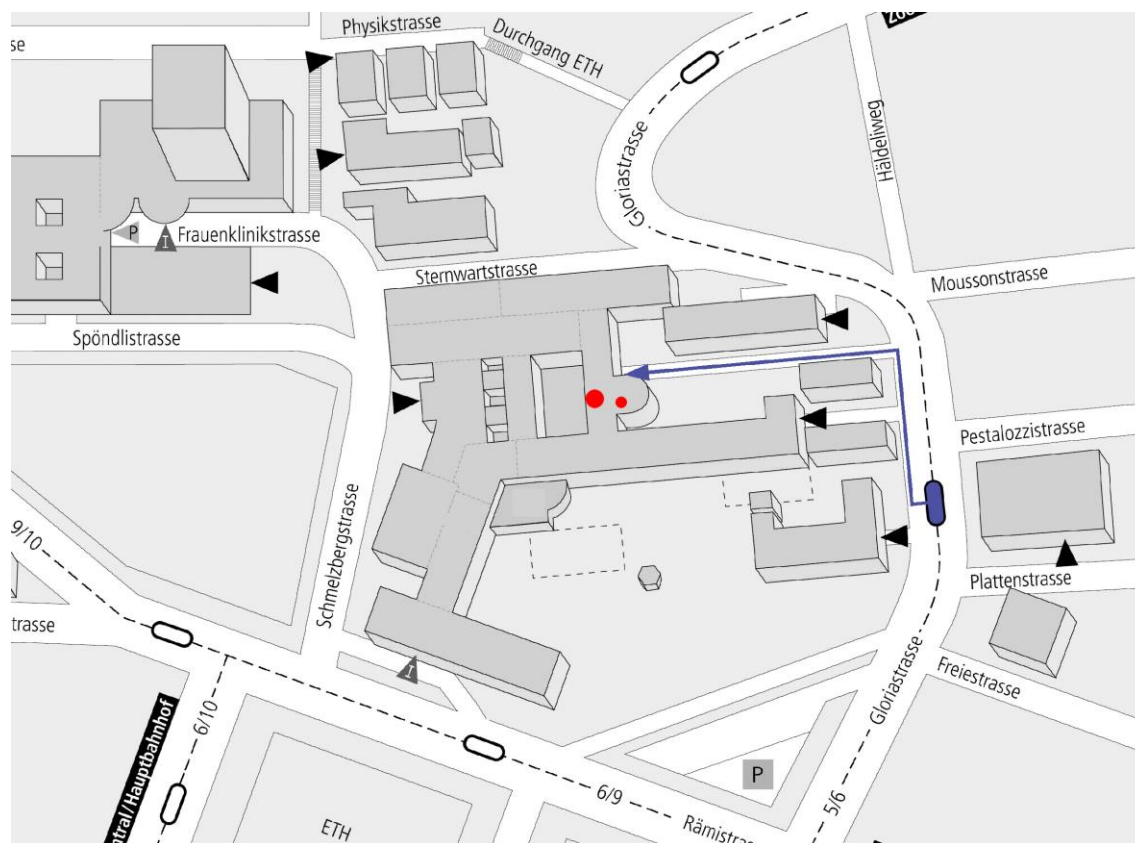
An implantable screening device was developed to optimize hydrogel conditions, cell type, and soluble factors to support bone marrow niche formation *in vivo*. Up to 32 unique conditions could be tested per mouse. Results indicated the need for hMSCs and BMP-2 in hydrogel constructs for recruitment of murine HSCs. This device represents a powerful new tool for heightened *in vivo* screening of tissue engineering constructs with a broad range of applications.

Conference Location

University Hospital Zurich
Grosser Hörsaal Ost
Rämistrasse 100
8091 Zürich

Contact Address

Prof. Dr. med. Gabriela Senti
Direktorin Forschung und Lehre
UniversitätsSpital Zürich
Rämistrasse 100 / MOU 2
8091 Zürich



**UniversitätsSpital
Zürich**